

**Characterising the Mechanical Loads
Acting on Nuclear Packages During
Rail Transportation**

Andrew Cummings

A Thesis submitted in partial fulfillment
of the requirements of Liverpool John Moores University
for the Degree of Doctor of Philosophy

August 2016

Abstract

The safe transportation of new and spent nuclear fuel is an essential part of the nuclear fuel cycle. The aim of this thesis was to obtain a more thorough understanding of the mechanical loading acting on heavy nuclear packages during rail transportation.

There were two motivating factors for this study. Firstly, the design of equipment used to tie down a package to its conveyance has become more challenging with the recent trend of increasing package mass; often exceeding 100 tonnes. This difficulty is due to the advisory acceleration factors recommended for design. Despite widespread acceptance that the factors ensure safety, it is also recognised that for heavier packages they can be prohibitive and result in over engineered tie down systems.

Secondly, transportation imparts complex dynamic mechanical loading on packages and the fuel assemblies within them. There have been no reported instances in the UK of problems caused by fuel vibrations. However international studies have prompted this investigation.

A rail wagon and tie down system for a 100 tonne package were instrumented with accelerometers and strain gauges. The measurements were taken during a routine rail journey from Barrow-in-Furness to Sellafield. Continuous data was digitally recorded with a sampling rate sufficient to capture shock and vibrations up to 100 Hz. Accelerometers were selected to measure very low frequencies to capture quasi-static loading.

Investigation of the frequency content of the accelerations indicated that digital filtering of the data is necessary to determine the magnitudes of the structural loading on tie downs. A method for designing a suitable filter has been developed. A sensitivity analysis of different filters indicated there is a possibility for over estimating loads based on measured data due to poor filter design.

Industrial design of tie downs using FEA requires pragmatic run times. This motivated a comparison of the measured strain time histories with the results of a linear static FEA model. The correlation between measured and predicted strains, was strong at frequencies < 3.5 Hz. A residuals analysis indicated that the model predicted the underlying strain process accurately.

The methods described are generic and adaptable. They will aid any future experimental work, to characterise shock, vibration and quasi-static loads acting on nuclear packages and their ancillary equipment.

Acknowledgements

I would like to express my gratitude to my director of studies, Dr. Glynn Rothwell, whose expertise, understanding, and support has helped me complete this thesis. In particular his assistance in writing reports and continual review of my work has been superb. The biggest acknowledgement is his response to my questions any time of day, weekend or evening has been hugely appreciated, he has gone out of his way to help.

I would like to thank Dr. Christian Matthews for his technical critique and appraisal of my work. His review and comments on my papers and thesis has been invaluable and his knowledge of my subject area has prompted some good discussions.

I also extend my thanks to Dr. Remy Krywonos whose encouraging words and enthusiasm for my research provided additional motivation early on.

I recognise that this research would not have been possible without the financial support of the company I work for; INS (International Nuclear Services Ltd). I express my gratitude to those within the company who have enabled my studies. In particular I would like to thank Peter Purcell and Ian Grainey for their encouragement to further my studies, present and publish my work.

I would like to make a special thanks to my wife Katy, without whose love and encouragement, I would not have finished this thesis. Since I'm forever indebted, I'll make a start on those jobs in the house this weekend...

To my children, Reiner and Sasha, as you get older I hope this inspires you to work hard, enjoy what you do and believe in yourselves. Love Dad.

Peer Reviewed Journal Publications

Some of the work described in this thesis has been previously published in different peer reviewed international journals and conferences.

Full copies of these publications can be found in the appendix to this thesis.

A. Cummings, J. Krywonos, P. Purcell, G. Rothwell and R. English

"An Experimental Procedure for Measuring Accelerations and Strains from a Tie Down System of a Heavy Nuclear Transport Package during a Rail Journey".

Packaging, Transport, Storage & Security of Radioactive Material, 23(3/4):167–177, December 2012.

A. Cummings, J. Krywonos, P. Purcell, G. Rothwell and C. Matthews

"Filtering and Analysis of Accelerations and Strains Measured on a Tie Down System of a Heavy Nuclear Transport Package during a Routine Rail Journey".

Packaging, Transport, Storage & Security of Radioactive Material, 24(1):23–35, March 2013.

A. D. Cummings, G. Rothwell and C. Matthews

"How well does a Linear Static Finite Element Analysis Predict Measured Strains from a Nuclear Package Tie Down System during Rail Transportation".

Proceedings of the Institution of Mechanical Engineers, Part F: Journal of Rail and Rapid Transit, Accepted July 2016

Table of Contents

Abstract	i
Acknowledgements	i
Peer Reviewed Journal Publications	iii
Table of Contents	iv
List of Figures	ix
List of Tables	xv
1 Introduction	1
1.1 Background	1
1.2 Scope of this Work	7
1.3 Synopsis	7
2 Background	9
2.1 Mechanical Loading of Structures	9
2.1.1 Normal Conditions	9
2.1.2 Accident Conditions	15
2.2 Normal Operating Loads during Rail Transportation	16
2.2.1 Quasi-Static	17
2.2.2 Shock and Vibration	18
2.3 Rules and Regulations	20

2.3.1	IAEA Regulations	20
2.3.2	Competent Authorities and Transport Modal Organisations	22
2.3.3	Codes of Practice	24
3	Experimental and Analytical Studies	25
3.1	Experimental Methods	25
3.1.1	Shock	29
3.1.2	Vibration	36
3.1.3	Structural	42
3.2	Computer Simulation Techniques	52
3.2.1	Shunting and Coupling	53
3.2.2	Vibration	64
3.2.3	Crashworthiness	66
3.2.4	Fatigue	69
3.2.5	Validation	71
3.3	Summary	75
4	A Method for Measuring Acceleration and Strain during a Routine Rail Journey of a Heavy Nuclear Package	76
4.1	Introduction	76
4.2	Aims and Objectives	77
4.3	Method	77
4.3.1	Selection and Positioning of the Accelerometers	79
4.3.2	Selection and Positioning of the Strain Gauges	82
4.3.3	Data Acquisition System and Transducers	89
4.4	Results	92
4.4.1	Loading Test	92
4.4.2	Journey Test	96
4.5	Discussion	102

4.5.1	Comparison of Results with Important Studies and Designer’s Guidance Documents	102
4.5.2	Benefits from the Measured Data	104
4.5.3	Limitations of the Data	105
4.6	Summary	105
5	Signals Analysis of the Measured Accelerations and Strains	107
5.1	Introduction	107
5.2	Aims and Objectives	108
5.3	Initial Visual Interpretation and Error Detection of the Measured Signals	108
5.4	Frequency Analysis	110
5.4.1	Power Spectral Density	110
5.4.2	Strain PSDs	111
5.4.3	Acceleration PSDs	111
5.5	Digital Filtering	116
5.5.1	Filter Requirements	117
5.6	Sensitivity of Acceleration Extrema due to Filter Design	121
5.7	Effect of Filter Cut-Off Frequency on Acceleration Extrema	126
5.8	A Quick Estimate of the Filter Cut-Off Frequency based on Displacement PSDs	128
5.9	Trends Observed in the Statistics of the Filtered Accelerations	130
5.10	Discussion	135
5.10.1	Frequency Analysis	135
5.10.2	Filter Design	135
5.10.3	Peak Analysis	136
5.11	Summary	137
6	Comparison of Strains Predicted with Finite Element Analysis and Measurements	138
6.1	Introduction	138

6.2	Aims and Objectives	139
6.3	Overview	139
6.4	Correlation between Measured Accelerations and Strains	141
6.4.1	Assessing the Strength of the Correlation	141
6.4.2	Data Cleansing	144
6.5	Tie Down System - General Arrangement	145
6.6	Finite Element Model	147
6.6.1	Materials Modelling	149
6.6.2	Boundary Conditions and Loads	150
6.6.3	Quality Checks	150
6.6.4	Calculating Strain Time Histories	152
6.6.5	Contact Modelling	154
6.6.6	Contact at the Trunnion Attachments	154
6.6.7	Lateral Restraint Bolts	154
6.7	Sensitivity Analysis	156
6.7.1	Non-Linear Effects during Longitudinal Loading	157
6.7.2	Non-Linear Effects during Lateral Loading	159
6.7.3	Vertical Load Application	161
6.8	Correlation between Predicted and Measured Strains	162
6.9	Cause of Lid End Anomaly	167
6.10	Analysis of Residuals	169
6.11	Discussion	172
6.12	Summary	173
7	Conclusions	174
8	Recommendations for Further Work	179
9	References	180

Appendices	192
A HyperMath Scripts	193
B Reduced Abaqus Input Files	197
C Residual Analysis	202
D Peer Reviewed Journal Publications	217

List of Figures

1.1	A Typical Tie Down System for a Heavy Nuclear Package	2
1.2	Modes of Transport	2
1.3	Examples of Packages used for Transporting Nuclear Material	4
1.4	Examples of Different Tie Down Systems	4
1.5	Examples of Nuclear Fuel Assemblies	6
2.1	An Example Standard Load History from an Offshore and Sea Application (Return Period of 3 years) <i>after</i> Li [34]	10
2.2	An Example of the Sea State Sequence Generated by the WASH Algorithm <i>after</i> Kam [48]	11
2.3	Normal Operational Loading Sequence of a Nuclear Package Transported by Rail	12
2.4	Uses for Experimental Field Data during Transportation	16
2.5	Categorised Loads Acting on Nuclear Packages, their Contents and Ancillary Equipment during Normal and Routine Conditions of Transport	17
3.1	An example of an Enveloping Procedure used to derive Classical Half Sine Shock Pulses from Measured Shock Response Spectra <i>after</i> Magnuson [82]	31
3.2	Bounding SRS for Rail Transportation of Nuclear Packages	33
3.3	Peak Longitudinal Acceleration due to rail wagon coupling <i>after</i> Singh [11]	34
3.4	Synthesised Time History based on a PSD and Probability Distribution <i>after</i> Rouillard [87]	34

3.5	Bounding Envelope Zero-to-Peak Vibration Amplitudes for Multiaxial Testing (the Specification is applicable for each axis) <i>after Sanders et al [16]</i>	37
3.6	Gaussian Distribution	38
3.7	Comparison of Measured Acceleration Spectral Densities with Test Specification provided in BS EN 61373 <i>after Hampshire [14]</i>	39
3.8	Experimental Configuration for Random Vibration Testing Non-Stationary Transportation Vibrations <i>after Rouillard et al [89]</i>	41
3.9	Level Crossings Counting Example [97]	43
3.10	Peak Counting Methods [97]	43
3.11	Rainflow Cycle Counting - Counts Closed Hysteresis Loops that Contribute to Fatigue Damage [97]	44
3.12	Comparison of Level Crossings and Range Pair Plots of the Wind Turbine SLH's WISPER and WISPERX, derived from Rainflow Cycle Counting [101]	45
3.13	Basic Design Methodology for Tie Down Systems	45
3.14	Triaxial Peak Acceleration Distributions Measured During a Long Haul Rail Journey <i>after Cory [84]</i>	47
3.15	Normalised Acceleration Frequency During Road Transport <i>after Dixon [85]</i>	48
3.16	Vertical Acceleration Histogram from Axle box of Passenger Rail Vehicle. Extrapolation Method Proposed by Curve Fitting <i>after Hampshire [14]</i>	49
3.17	Quasi-Static Load Spectra after the Damage Consistency Calibration <i>after Zhu et al [79]</i>	51
3.18	One Dimensional Dynamic Model of Rail Wagon for Assessing Low Velocity Impacts <i>after Magnuson [82]</i>	53
3.19	RICTL Rail Car Impact Cargo Tie Down Loads <i>after Bartholomew [25]</i>	54
3.20	Key Results of Rail Wagon and Package Impact Model <i>after Bartholomew [25]</i>	55
3.21	CARDS Computer Model <i>after Fields [32]</i>	56

3.22	Finite Element Model of Rail Wagon, Tie Down System, Package and Coupler <i>after</i> Elbestawi <i>et al</i> [23]	61
3.23	FEA Predictions of Fuel Bundles due to Rail Wagon Shock <i>after</i> Elbestawi [23]	62
3.24	FEA Model of Rail Wagon, Package and Tie Down System <i>after</i> Read <i>et al</i> [46]	63
3.25	Finite Element Prediction of Accelerations acting on a Heavy Package during Rail Impact under Regulatory Conditions <i>after</i> Read <i>et al</i> [46]	63
3.26	A 3 Degree of Freedom Road Vehicle, Package and Anti Vibration Mounts Model <i>after</i> Tartary [60]	64
3.27	Notching Method to Simulate Road Transportation of Package and assess effect of Anti-Vibration Mounts <i>after</i> Tartary [60]	65
3.28	FEA Model of a Leading Rail Cab Vehicle and a 40 tonne Deformable Object <i>after</i> Xue <i>et al</i> [63]	66
3.29	Crash Progress of a Vehicle Colliding with a 40t Object of Deformable and Rigid Structure <i>after</i> Xue <i>et al</i> [108]	68
3.30	Comparison of Calculated and Experimental Acceleration Time Histories from a Rail Wagon and Package Impact <i>after</i> Fields [22]	73
3.31	Autocorrelation function of the residuals between DADS Simulation and Experimental Data <i>after</i> Chaika <i>et al</i> [118]	74
4.1	Map of Rail Journey from Barrow-in-Furness to Sellafield Site, Cumbria	78
4.2	CAD Model of Rail Wagon, Package and Tie Down System	79
4.3	Accelerometer Positions	80
4.4	Accelerometer Positions on Transport Frame	81
4.5	Finite Element Model of the Transport Frame and Package	82
4.6	Principal Stress Contour Plots of Transport Frame (in units of MPa)	85
4.7	Principal Stress Hot Spot Locations (in units of MPa)	86
4.8	Strain Gauge Labels and Positions	88

4.9	Breakdown of the Strain Gauge Rosette Identification Number used to Measure Strain in this Experiment [130]	91
4.10	Example of Strains Measured during Loading of Package onto Tie Down System	94
4.11	Example of the Accelerations Measured during Loading of Package onto Tie Down System	95
4.12	Example of Strain Time Histories Collected during the Rail Journey	98
4.13	Example of the Acceleration Time Histories Collected from the Tie Down System during the Journey	99
4.14	Example of Acceleration Time Histories Collected from the Wagon Bed (Accel. C) and Bogie Frame of the Wagon (Accel. J) during the Rail Journey	100
4.15	Latitude, Longitude, Altitude and Vehicle Speed Time Histories	101
4.16	Schematic of Vertical Load Transmission and Attenuation	103
5.1	Typical Strain Time History Characteristics	108
5.2	Example Strain PSDs for Strain Gauge Rosettes 9 and 10	111
5.3	Acceleration PSDs at Wagon Bed and Bogie	112
5.4	Accelerometers Selected for Detailed Analysis	113
5.5	PSDs from Measured Accelerations at Wagon Bed, Saddle and Stanchion	113
5.6	Filters Designed to Minimise Time Domain Ringing	118
5.7	Filters Designed to Maximise Roll-off Rate	118
5.8	Pole-Zero Plot in Z-Domain of Five Low Pass Filter Designs, $f_c = 17.5$ Hz and $f_s = 1200$ Hz (O = Zeroes and X = Poles)	119
5.9	Level Crossing Histograms of Low Pass Filtered Lateral Accelerations at 17.5 Hz. Resulting Distributions from Various Filter Designs	125
5.10	Acceleration Extrema vs Filter Cutoff Frequency	126
5.11	Vertical Displacement PSD from Wagon Bed and Stanchion	128
5.12	Lateral Displacement PSD from Wagon Bed and Stanchion	129
5.13	Longitudinal Displacement PSD from Wagon Bed and Stanchion	129

5.14	Peak Vertical Acceleration Measured at Wagon Bed	132
5.15	Peak Vertical Acceleration Measured at Stanchion	133
5.16	Filtered Peak Vertical Acceleration Measured at Stanchion and Wagon Bed	134
6.1	Sources of Error	142
6.2	Example of Coherence between Measured Acceleration and Strain	143
6.3	An Example of Data Cleansing used on some of the Measured Strain Time Histories	144
6.4	Details of the Tie Down System Construction	145
6.5	Detail of Lid End Trunnion Bushes and Upper Stanchion	146
6.6	Finite Element Model of Tie Down System and Dummy Package	147
6.7	Details of Finite Element Mesh of Tie Down System	148
6.8	Finite Element Mesh of Lid End Trunnion Attachments and Restraint Bolts	149
6.9	Boundary Conditions Applied to the Model	150
6.10	3 x 1g Load Cases (Unit Loads)	151
6.11	Locations and Orientations of the Virtual Strain Gauges	153
6.12	Detailed Mesh of Package Required for Non-Linear Studies	157
6.13	Example of von Mises Stress Results from Virtual Strain Gauges during Combined Longitudinal and Vertical Loading	158
6.14	FEA Sensitivity Analysis, Non-Linear Lateral Load Case to Assess the Effects of Discontinuous Contact Behaviour between the Package Side Walls and Tie Down Lateral Restraint Bolts	159
6.15	Sensitivity Analysis, Example of Non-linear and Linear Load Case Stress Results	160
6.16	Preliminary Correlation Results	163
6.17	Correlation Results with Channels $< 10 \mu\text{m}/\text{m}$ Removed	164
6.18	Final Correlation Results	164
6.19	Effects of (f_c) on Correlation of Strain Gauge Rosette 12	166

6.20	Time History Slice Comparison of Filtered Base and Lid End Lateral Accelerations at the Tie Down Stanchions	168
6.21	Comparison between Predicted and Measured Strain Time Histories, Converted into PSDs, Log-Log Scale, Full Bandwidth	169
6.22	Comparison between Predicted and Measured Strain Time Histories, Converted into PSDs, 0 - 25 Hz	170
6.23	Correlogram of the Measured Strain Signal from the 90° Leg of Rosette 12	171
6.24	Correlogram of the Residuals between the Measured and Predicted Strain Signal from the 90° Leg of Rosette 12	171

List of Tables

1.1	Mass of Packages in Figure 1.3	3
2.1	Comparison of Rail Load Cases set by Rail and Nuclear Authorities for Tie Down System Design	23
2.2	Rail Load Cases for Fatigue Assessment of Tie Down Systems	24
3.1	Observed Impact Velocities during Rail Coupling, 4.5 tonne Surrogate Weapons <i>after</i> Magnuson <i>et al</i> [82]	30
3.2	Rail Shock Represented by a Single Half Sine Pulse (4.5 tonne and 13.5 tonne cargo) <i>after</i> Magnuson <i>et al</i> [82]	32
3.3	Half Sine Pulses for Rail Coupling Shock <i>after</i> Magnuson <i>et al</i> [17]	33
3.4	Rail Vibrations for 45 tonne Package <i>after</i> Magnuson [18]	37
3.5	Theil's Inequality Coefficients for Response Variables Determined using Calculated and Measured Coupler Forces <i>after</i> Fields [22]	72
4.1	Load Cases for Finite Element Analysis of the Tie Down System and Package used to Select the Position of Strain Gauges	83
4.2	Maximum Principal Stresses Converted from Measured Strains during Loading Test	92
4.3	Absolute Maximum Accelerations Measured during Loading Test	93
4.4	Maximum Principal Stresses Converted from Measured Strains during Journey Test	96
4.5	Absolute Maximum Accelerations Measured during Journey Test	97
4.6	Comparison of Raw Measured Acceleration Peaks vs Advisory Acceleration Factors	102

5.1	Frequencies at which Various Butterworth Filters Attenuate to -40dB	117
5.2	Statistics of Filtered Lateral Accelerations	122
5.3	Statistics of Filtered Vertical Accelerations	122
5.4	Statistics of Filtered Longitudinal Accelerations	123
5.5	Acceleration Extrema due to different Filter Cutoff Frequencies . .	127
5.6	Possible Filter Cutoff Frequencies	129
5.7	Statistics of Acceleration Signals Low Pass Filtered at 100 Hz	130
5.8	Statistics of Acceleration Signals Low Pass Filtered at Cutoff Frequencies from Table 5.6	130
5.9	Statistics of Acceleration Signals Band Pass Filtered, Lower Cutoff Frequencies from Table 5.6 and Upper Cutoff Frequencies at 100 Hz	130
5.10	Transmission of Peak Vertical Acceleration from Wagon Bed into Package	131
5.11	Comparison of Filtered Measured Accelerations Peaks vs Advisory Acceleration Factors	136
6.1	Material Properties applied to Finite Element Model	149
6.2	Run Times to Completion for Linear Model	151
6.3	Combination of Loading in Non-Linear Analysis	157

1. Introduction

1.1 Background

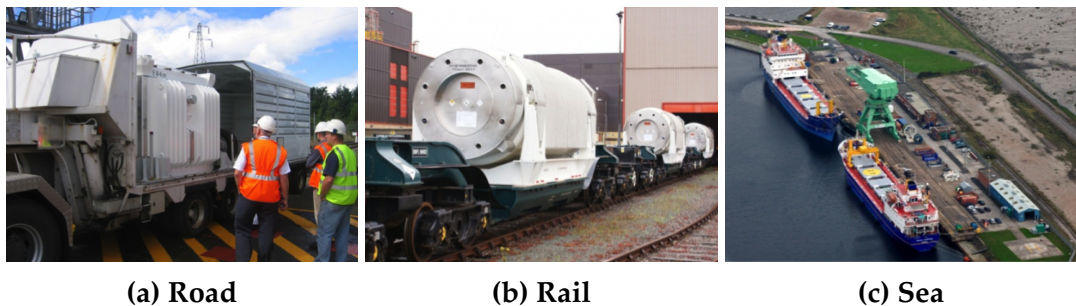
The safe transportation of new and spent nuclear fuel and irradiated waste is an essential part of the nuclear fuel cycle. As a consequence of existing design standards and procedural practices there have been very few safety related incidents or accidents during transport reported in the UK or elsewhere in the world. Nuclear transportation packages and their ancillary equipment are designed to meet stringent regulations for normal and accident conditions of transport [1, 2]. To ensure the quality of new fuel and the structural integrity of used fuel, a detailed knowledge of the mechanical loading during normal conditions of transport is required [3, 4]. Detailed knowledge exists only for a limited number of applications.



Figure 1.1: A Typical Tie Down System for a Heavy Nuclear Package

Tie down systems are used to constrain packages to their conveyance and they must withstand forces experienced during transport **Figure 1.1**. This is generally achieved by package operators around the world by adhering to a very limited set of design rules provided in [2]. However there is a concern that knowledge of the real operational loading is not complete. Recently several authors have either undertaken measurement programmes, literature reviews or analytical studies to test the appropriateness of the design loads [5–8].

There are four modes of transport for packages; road, rail, sea and air. For large mass Radioactive Material (RAM) packages the prevalent modes of transport used in the UK are rail and sea. A tie down system can therefore be mounted to the flat-bed of a trailer, to a rail wagon bed or in a ship or aeroplane cargo hold **Figure 1.2**.



(a) Road

(b) Rail

(c) Sea

Figure 1.2: Modes of Transport

The types of packages in existence vary in size and mass considerably **Figure 1.3**. The Safkeg is the smallest package shown, it weighs 146 kg and is 1 m in height with a maximum outer diameter of 0.425 m. The CASTOR HAW is the largest package shown, it weighs 116 tonnes when loaded and is over 7 m long with a 2.75 m diameter (including shock absorbers). **Table 1.1** summarises the mass of each of the packages in **Figure 1.3**.

Package	Mass [kg]
Castor HAW	116,000
Excellox 6	94,215
M2e Magnox	49,480
M4-12	12,990
Safkeg	146

Table 1.1: Mass of Packages in Figure 1.3

The different types of package in existence lead to a large variety of associated tie down systems **Figure 1.4**. As a consequence of the variability in the transportation system (package, tie down, conveyance, mode of transport) there is considerable uncertainty over mechanical loading during transport and more importantly over which loading factors should be applied in design [8–10].

Fourgeaud et al carried out a review of existing standards, norms and literature on the loading during transportation [8]. They concluded that the regulatory guidance for tie downs was not sufficient and made several recommendations to increase design loads. In the case of rail transportation, their argument was based on evidence from an experiment conducted by Singh [11]. In Singh’s experiment he measured acceleration at the base of engine racks transported by freight rail wagons in the US. His results indicate large peak accelerations occurred at very high frequencies. However his experimental results were intended to provide shock and vibration test specifications for engine racks and as such there isn’t strong justification to support a radical increase in quasi-static design loads for tie-downs.



(a) Castor



(b) M4-12



(c) Safkeg



(d) Excellox



(e) M2e Magnox

Figure 1.3: Examples of Packages used for Transporting Nuclear Material



(a) Stillage



(b) Twist-locks and Spigots



Desnoyers suggested that the existing regulatory guidance could be updated to include more current standards and norms [9]. He found that several alternative sources offer more flexibility in design methods for tie downs [12, 13]. In particular the use of measured loading data to verify designs allows for an alternative route of design justification. This could be used in special circumstances where the advisory load cases provided in the regulations become overly restrictive. Additionally the documents Desnoyers refers to provide a standard for design methodology across all European member states. This is particularly desirable where transportations are planned that cross the borders of several countries.

Apel [10] points out that with so many different parameters that vary in a transport system, there is a need to expand the current advisory material for the regulations. He suggests existing data published in standards and technical regulations could be used to supplement the IAEA Regulations to develop a table of acceleration loads that encompass many design variables. The table would then highlight any missing data that can guide subsequent use of experiments and computer simulation. Pragmatically he explains that experiments can provide additional data but it is impractical to rely on them for each design dependent variable. Therefore the role of experimentation is to provide a validation method for computer simulations. The rationale is that validated computer models can ultimately be used to acquire any missing data sets [14, 15].

On a more specific topic, Purcell [7] indicates that mechanical loading of tie downs for particularly heavy packages is limited by the mass of its conveyance. Stability assessments for both rail and road vehicles were carried out independently by both Purcell and Gleed-Owen for heavy packages [6, 7]. They concluded independently that lateral loading should be limited to the stability limit for toppling of the vehicle.

It is therefore of obvious importance to have accurate definitions of loading for structural design of tie down systems during rail transportation. Also of great significance to the nuclear industry is the effects of mechanical loading during rail transportation acting on nuclear fuel assemblies (sometimes referred to as fuel bundles). In **Figure 1.5** examples of Mixed Oxide (MOX), Pressurised Water Reactor (PWR) and Boiling Water Reactor (BWR) fuel assemblies are shown.

Historical research conducted throughout the 70's, 80's and 90's focused on understanding if the shock and vibration environment during transport caused damage to fuel assemblies [16–24]. The focus of the experimental and analytical studies frequently interchanged between tie down systems and fuel assemblies [25–32]. The majority of these studies were carried out in the United States with a strong empha-

sis on characterising shock and vibration levels. Extensive studies were also carried out on peak accelerations during longitudinal shunting of rail wagons loaded with nuclear packages.

More recent work has addressed the root cause of grid-to-rod fretting wear of fuel assemblies [33]. The influence of transportation vibrations was considered to be much less damaging than the operational environment within a reactor or loading rates of the individual rods during assembly of fuel bundles. In the UK very few studies of this type have been carried out, however fuel is transported all over the world from the UK with very few incidents of damage conclusively related to transportation.

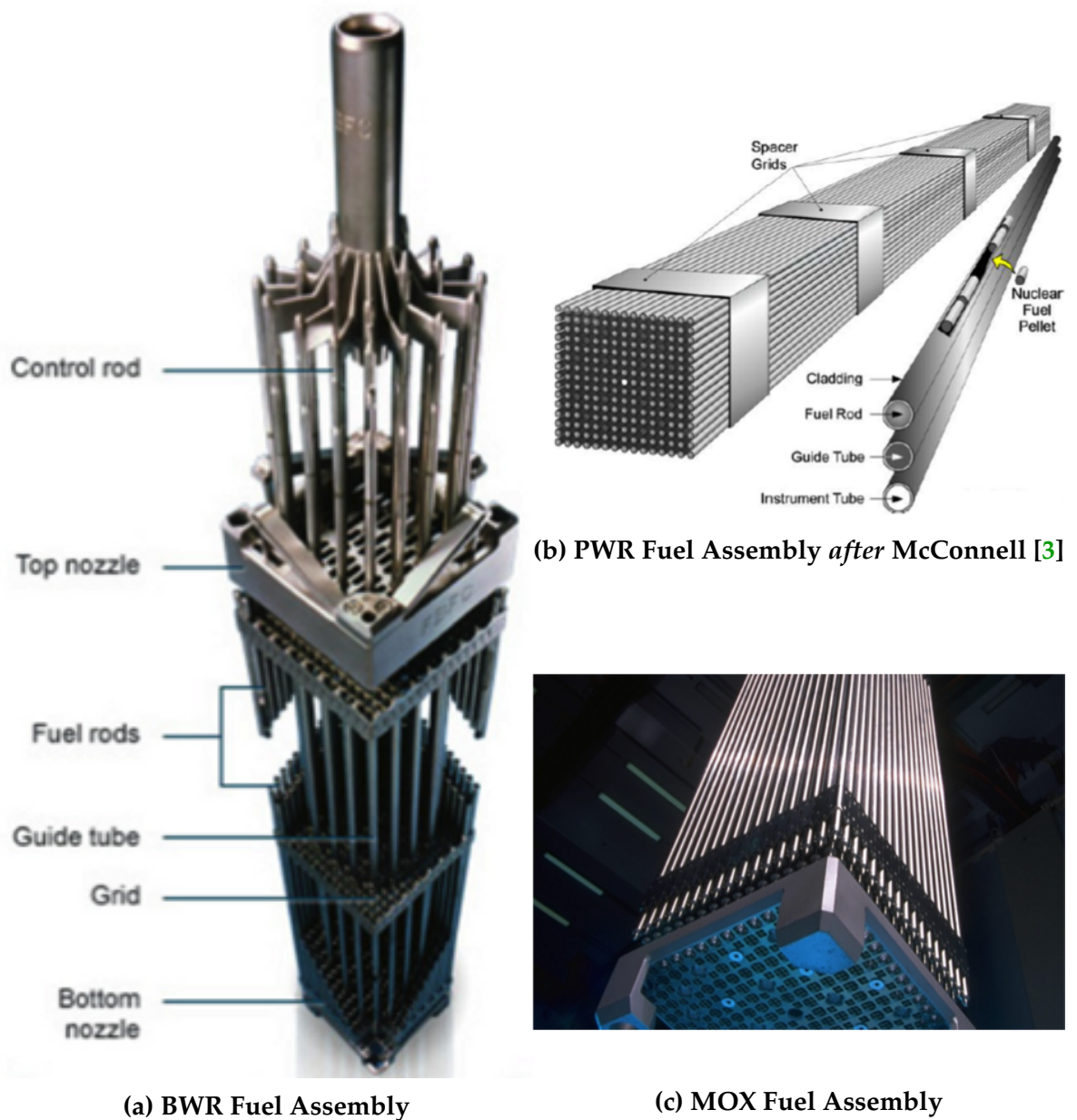


Figure 1.5: Examples of Nuclear Fuel Assemblies

1.2 Scope of this Work

The main objective of this work is to develop a clearer understanding of the loading imparted onto nuclear packages during rail transportation. The primary focus is on the loading experienced by a transport frame for a heavy nuclear package. The two requirements for better understanding of the transportation loading are for the purposes of tie down design and fuel quality/integrity. Therefore a secondary aim of the work is to gain more knowledge of the loading that fuel is subjected to. To achieve these objectives this thesis is split into three sections:

1. Carry out an experiment to measure accelerations and strains on a nuclear package tie down system and rail wagon during a routine rail journey.
2. Analysis of the resulting data collected from the experiment.
3. Comparison of a Finite Element model with the experimental results.

1.3 Synopsis

The research is structured into five main chapters. **Chapter 2** provides a broader perspective on the subject of mechanical loading, considering how other industries tackle the problem of defining suitable loads for design. The rail transportation environment is then categorised into quasi-static, shock and vibration loading. This chapter concludes with a brief overview of the current rules and regulations that are adhered to in the nuclear industry.

In **Chapter 3** both state of the art and historical experimental and computational studies are reviewed and critiqued. The chapter covers both rail and nuclear specific studies, detailing experimental work on vibration, fatigue and longitudinal coupling and shunting. The chapter also provides an in-depth review of techniques used by other researchers to compare their computer models with experimental data.

Chapter 4 describes the experimental procedure used in this work to acquire continuous strain and acceleration time histories from the rail wagon and tie-down of a heavy package during a routine rail journey. Details of the instrumentation and digital data acquisition are provided and the positioning of instrumentation is explained. A brief summary of the results is also presented.

Chapter 5 focuses on analysis of the measured time histories. Filtering of the acceleration data is necessary to remove spectral components of the signals not related to structural loading, therefore filter design is treated in detail. Spectral analysis of

the accelerations and strains is used to gain insight into the frequency characteristics of the measured loads. Methods for comparing the data with existing standards, specifications and norms are presented.

In **Chapter 6** a linear Finite Element Analysis is used to calculate strain time histories for comparison with the experimental results. The chapter considers how well a linear static analysis procedure can predict real time dynamic strain measurements. The correlation between computational and experimental results is assessed and both frequency and time domain methods are used to determine the degree of agreement between the two data sets.

Finally the results from the entire research are summarised and discussed in **Chapter 7**.

2. Background

2.1 Mechanical Loading of Structures

Defining representative mechanical loads is the first step in any detailed structural assessment. For many engineering applications it is also the most challenging aspect of design. In the automotive, aerospace, military, wind, offshore and sea industries, methods are continually improving to refine load spectra [34–39]. The majority of the literature related to nuclear packages transported by rail is focused on the mechanical loading acting on fuel assemblies. The literature available on the structural loading of tie down systems is sparse.

2.1.1 Normal Conditions

2.1.1.1 Fatigue

Because stresses and strains are directly related to loads, any small change to loading can have large effects on fatigue life estimations. Therefore the load spectra for fatigue assessment is critical. Many distinctly different approaches have been proposed to define suitable load cases. In general the derivation of loads relies upon a three part methodology:

1. Physical testing.
2. Development and validation of computer models for sensitivity analysis.
3. Data analysis and reduction.

In **chapter 3** a more detailed review of the derivation of fatigue loads for rail structures is presented. In the current chapter it is useful to introduce the ideas and some terminology adopted by other industries for obtaining suitable fatigue load spectra.

A common approach used is to derive equivalent static load cases [14, 40–42]. In this method complex loading histories are reduced to a single load case, which is applied for a given number of cycles, typically 10^7 . The amplitude of the design load is adjusted to ensure that the fatigue damage is equivalent to that experienced during the life of the structure. This is sometimes called the *principle of fatigue damage equivalence*. Halfpenny advises caution with the equivalent static load case method as it is heavily dependent on the choice of fatigue model and parameters. He also points out that it does not maintain the actual cycles, frequency, time or amplitude of the original load history [43]. However due to the simplicity of the method it is often used for design calculations [42, 44–46].

Another approach is to build up an operational load history profile that allows for the estimation of a fatigue life. This is sometimes referred to as a standard load sequence or standard load history (SLH) which is a compressed time history [43]. The idea is that by repeating the SLH a number of times a complete usage history (sometimes referred to as *mission profile* or *operating profile*) can be analytically reproduced [34, 37]. The length, or *return period* of the SLH is critical. For example if it is too short then larger more damaging cycles will be repeated more times, resulting in shorter fatigue life predictions [34, 37].

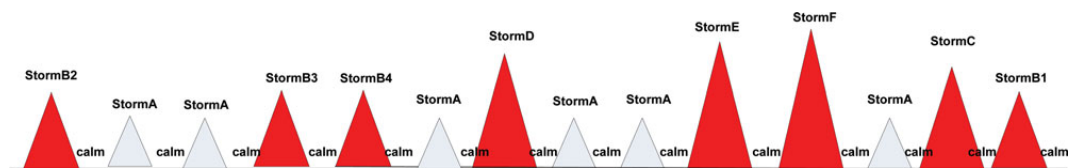


Figure 2.1: An Example Standard Load History from an Offshore and Sea Application (Return Period of 3 years) after Li [34]

An example SLH is shown in **Figure 2.1** for offshore and sea applications. Here the characterisation of ocean waves is carried out by measuring short term load histories and categorising them into 12 different sea states; calm sea ranging from 1 - 6 and storm sea ranging from 7 - 12 (A - F). To deal with the large amount of data that an SLH generates, Li [34] compresses the short term load measurements of each sea state into turning points and filters small, non-damaging cycles [47]. The SLH is then constructed by concatenating the compressed short term measurements based on the number of expected storms during the return period. Finally a full usage history is developed by repeating the SLH to match the anticipated life of the structure under assessment.

Kam [48] describes an alternative method for marine applications called the Wave Action Standard History (WASH) for testing offshore structures. WASH was developed in the UK in the 1980's for offshore oil platforms in the North Sea. It is essen-

tially an algorithm that generates a load sequence with a 1 year return period that includes all expected sea states. The WASH algorithm proceeds in two steps; in the first step a sea state sequence generator based on Markov chains is applied. Markov chains are a mathematical technique for linking random numbers together to form a sequence in a realistic way that results in continuous transitions between random sea states. The occurrence of a particular sea state does not affect the probability of occurrence of other states. Typical output of the sequence generator is shown in **Figure 2.2**. The second step implements a pseudo-random time history generator to match the spectral content of the generated load histories to those measured at each discrete sea state. By combining the two steps a complete loading sequence is obtained.

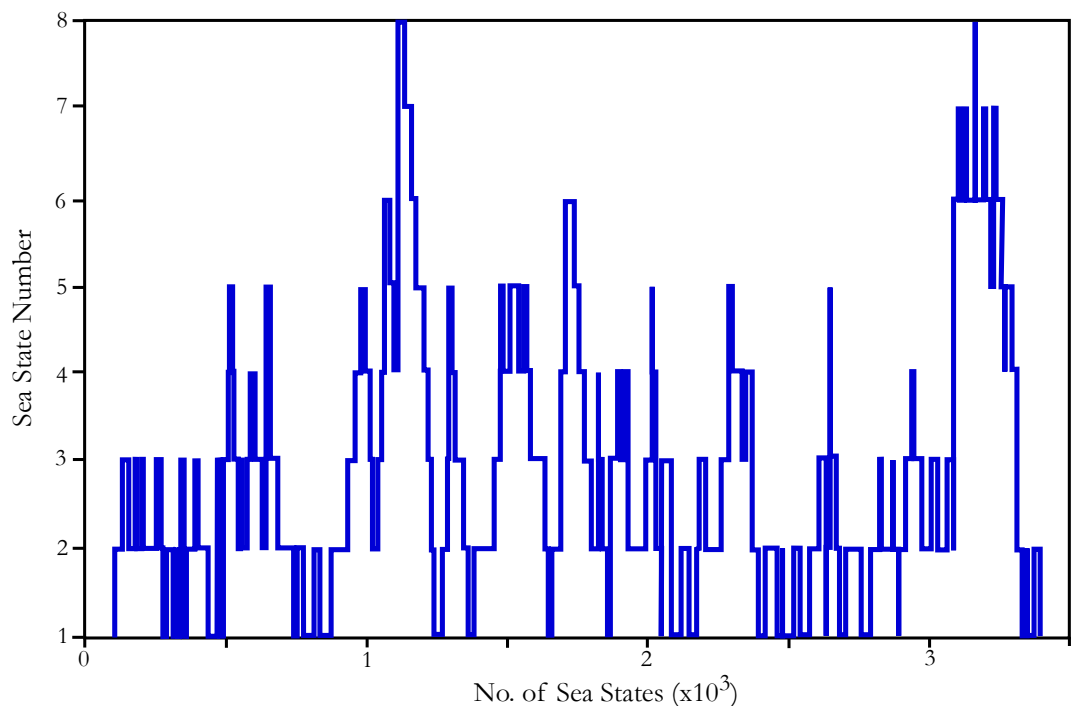


Figure 2.2: An Example of the Sea State Sequence Generated by the WASH Algorithm after Kam [48]

The spectral density functions underpinning the WASH method were assessed by Pook [39]. He reviewed the existing data measured in the North Sea, which were gathered over a twenty year period. Pook noted that records of filter frequencies and sampling rates used prior to spectral density calculations were incomplete. Despite this he was able to fit the existing data to analytical functions to enable regeneration of a selected set of spectral densities. These functions were used in the WASH load sequence program to generate lower/upper bound and typical sequences, with or without structural resonance affects. This flexibility offers engineers the opportunity to tailor a fatigue spectra for different applications [49, 50].

Comparing the two marine cases described above, the critical difference is that Li's approach discards the dynamic data in the short term load histories by converting the time series into turning points and filtering small cycles [47]. In contrast WASH was developed to maintain the frequency content of the experimental studies. Therefore the first method is more suitable for stiff structures such as ships but less appropriate for flexible structures such as tall offshore platforms.

A generic SLH for a nuclear package tie down system transported by rail is proposed in **Figure 2.3**. Here the return period is set to a single journey, from which a complete usage history can be constructed using the number of journeys expected in the operational life of the tie down system. The usage history could be used to screen new designs to determine if a detailed fatigue analysis is warranted.

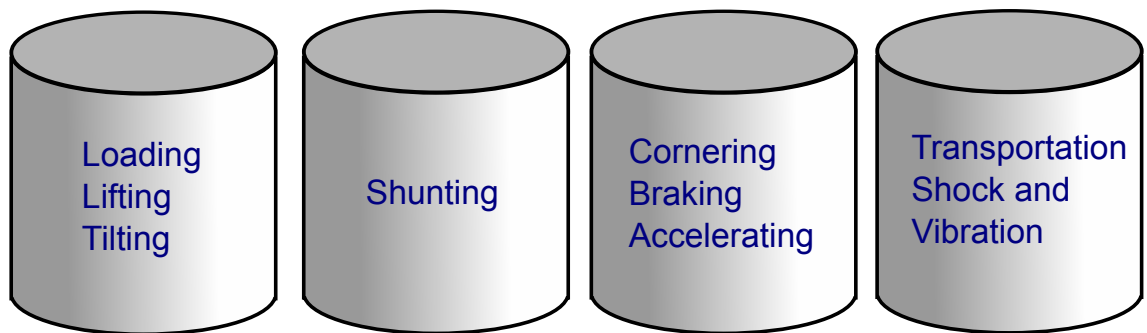


Figure 2.3: Normal Operational Loading Sequence of a Nuclear Package Transported by Rail

2.1.1.2 Transportation Shock and Vibration

The first step in a shock and vibration assessment requires the acquisition of loads from field experiments, similar to the type of data required for fatigue. However the subsequent data analysis and data reduction methods used are quite different. The influence of shock and vibration on fuel assemblies is assessed by physical testing, usually carried out on an electrodynamic or hydraulic shaker table. Shaker tests are used to assess the structural integrity of fuel assemblies that are exposed to shock and vibration transportation environments [3, 4, 51]. The development of test specifications used to reproduce transportation loading on a shaker table for nuclear fuel assemblies is discussed in more detail in **chapter 3**. This section focuses on the background and methods currently used by engineers to analyse the effects of shock and vibration environments on structures.

One particular technique that is used for characterising shock loading is the Response Spectrum or Shock Response Spectrum (SRS) [52]. By repeatedly calculating

the response of a single degree of freedom oscillator to an input signal and incrementally increasing the oscillators natural frequency for every calculation, a graph of response (typically acceleration) vs natural frequency can be constructed. The SRS was developed to provide a conservative method for assessing the severity of short term transients. However it can also be calculated with longer, random vibration time histories, which provides a useful tool for comparison of shock severity between different loading environments [38, 53, 54]. When used on longer time histories it is sometimes referred to as the response spectrum. Furthermore by synthesis of a transient pulse that satisfies the SRS, a test specification for a shaker table can be created.

Lalanne [54] used the principle of the SRS to develop the Fatigue Damage Spectrum (FDS) which calculates relative fatigue damage vs natural frequency of a single degree of freedom oscillator. He also developed an Extreme Response Spectrum (ERS), this provides essentially the same output as an SRS but the input used in its calculation is a Spectral Density (not a time history) [43]. These methods are particularly useful in developing accelerated fatigue tests. The FDS is used to ensure that the principle of damage equivalence is adhered to whilst the ERS serves as a monitoring tool to ensure that shock severity of an accelerated test specification is not likely to cause overload failures [38].

The Power Spectral Density (PSD)¹ and can be used as input to drive random vibration tests. A typical PSD test specification is presented in tabular form, consisting of paired data points that represent vibration level and frequency.

The methods described above are well suited to testing flexible structures that weigh significantly less than their foundation structure. However this is not the case when considering a tie down system for a heavy nuclear package. Fields [22] investigated this by analysis, considering the effects of dynamic coupling of a package, tie down and rail wagon during a marshalling yard procedure known as hump shunting. From his computer model he used the resulting transient acceleration signals to calculate an SRS. His studies indicated that a more severe SRS was obtained when a rigid rail wagon was assumed and that a more realistic SRS was obtained with a flexible model of the rail wagon. He also demonstrated that significant differences in SRS were obtained if the rotation of the rail wagon was not accounted for in sim-

¹Early spectral analysis was carried out using analogue bandpass filters to determine the mean square value of waveforms in a narrow frequency band of either voltage or current. Because v^2 and i^2 are proportional to electrical power the mean square of these waveforms was termed the power of the signal. Because it is not possible for any physical filter to isolate only one frequency the mean square was normalised by Δf and the resulting spectrum called the Power Spectral Density [41]. In practice today the Spectral Density, Power Spectral Density and Acceleration Spectral Density are often used interchangeably, see for example [41, 55, 56].

ulations.

In instances where heavier components are to be shock tested shaker tables are too light weight. Instead pneumatic hammer shock testing machines or floating platform testing machines are used. In the US this type of equipment is used for Naval shock analysis and design. A complete monograph on this subject has been published which describes the methods used for testing heavy, coupled, dynamic systems in isolation [57]. The basis of the approach is to modify a measured SRS by deleting the peak resonances due to the coupling effects of the tested structure and its foundation. The modified SRS is then used for testing and analysis.

NASA have developed similar methods to reduce random vibration test severity on ancillary equipment attached to spacecraft [58]. This is achieved by *notching* of the test specification at the natural frequency of the tested items. Notching is a means of eliminating or reducing resonances that occur during field testing due to structural coupling, by setting input PSD levels at the resonant frequencies to match the forces experienced during a flight [59]. This is necessary because the foundation structure, the spacecraft, is relatively flexible and therefore has low mechanical impedance i.e. the ratio of input force to response velocity is low. By comparison a shaker table has very high mechanical impedance which results in higher interface forces during testing than in a real flight. The over testing problem occurs, even if similar accelerations are measured between flight and test [53].

Although physical testing of heavy nuclear transportation equipment for random vibrations is generally considered impractical (at least on a shaker), the basic methods used by NASA have been theoretically applied in the design of anti-vibration mounts for a 13 tonne nuclear package tie down system, see **chapter 3** [60]. There is also an example of a servo-hydraulic shaker test rig for a full-size rail vehicle described by Smith *et al* [61].

2.1.2 Accident Conditions

In the rail industry some attention has been devoted to accident conditions for the purposes of passive safety. Xue [62–64] concentrates on crashworthiness assessments of passenger rail vehicles in high speed crashes. His emphasis is ensuring that finite element (FE) modelling is representative of real loading scenarios. In his studies he advocates the use of deformable impacted structures (as opposed to rigid targets) and raises concerns about the use of lateral symmetry conditions, which do not allow for realistic prediction of asymmetric, progressive crushing of impact zones. Sun [65] has also undertaken analytical work on frontal impacts of passenger rail vehicles using rigid body dynamics. Xue and Sun remark that designing crush zone members to static proof loads causes overly stiff behaviour in an impact and to optimise crush zones a more complex crash analysis is required.

Thomas *et al* [66] focused on another accident scenario; rail vehicle overturning due to excessive high cross winds or running speed. Thomas used measurements of the relative displacements between bogie frame and vehicle body to validate 2-D and 3-D rigid body dynamics models of a high speed train. Vehicle overturning has also been considered in the nuclear transport industry (albeit to far lesser extent) for the purposes of understanding limiting lateral accelerations when transporting very heavy payloads [6, 7].

2.2 Normal Operating Loads during Rail Transportation

Loading of nuclear packages is categorised into accident, normal and routine conditions of transport. Both physical testing and computer analysis are used to engineer structures during accident loading. However physical tests during normal and routine conditions of loading are not carried out as frequently. However operational experiments during these conditions offer the chance to validate and improve current designs and methodology. **Figure 2.4** shows how field testing plays a pivotal role in understanding and characterising the mechanical loading environment.

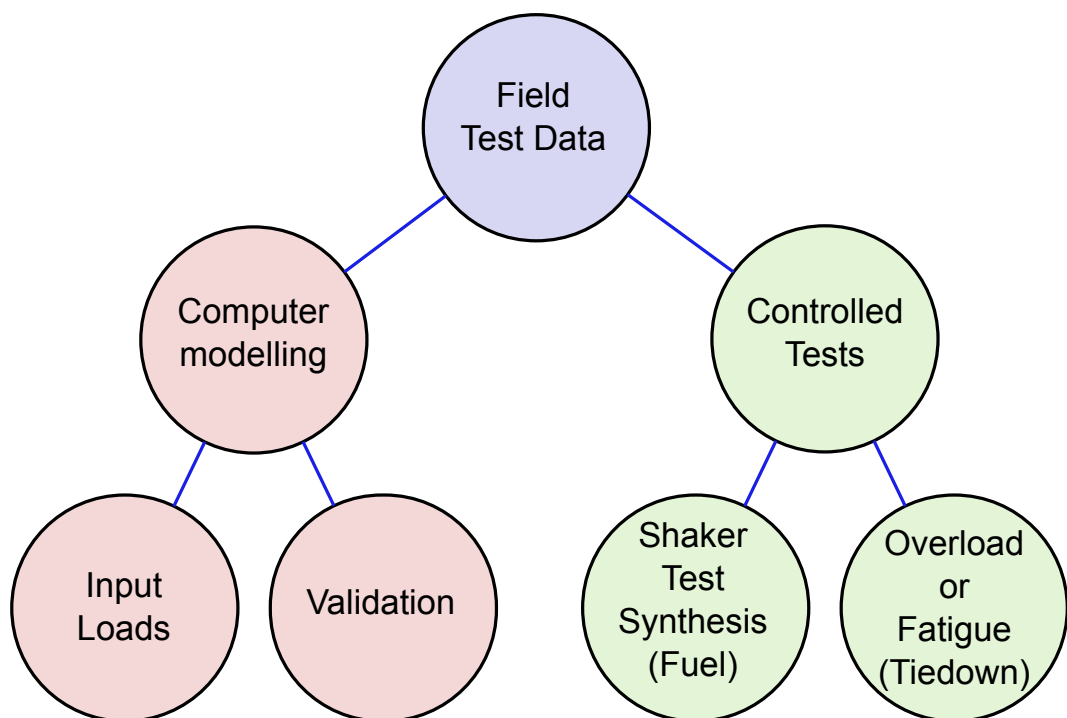


Figure 2.4: Uses for Experimental Field Data during Transportation

Loading during normal rail transport conditions can be categorised into three main types:

1. Quasi-Static.
2. Shock.
3. Vibration.

In **Figure 2.5** the categorised loads are attributed to the various components of the transport system of a nuclear package. The size of each box is used to indicate the possible influence of the categorised load acting on each particular member of the system.

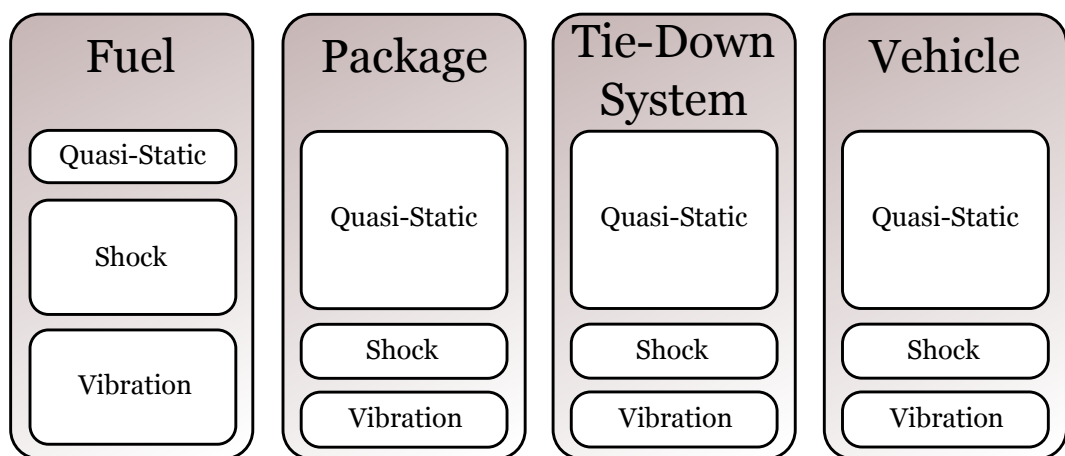


Figure 2.5: Categorised Loads Acting on Nuclear Packages, their Contents and Ancillary Equipment during Normal and Routine Conditions of Transport

2.2.1 Quasi-Static

Quasi-static loads are generally slowly applied and therefore tend to appear in the lower frequency range i.e. < 30 Hz [67]. The IAEA Advisory Material does not provide a specific definition for quasi-static loading, however it does offer guidance on filtering time histories to obtain quasi-static loading. It suggests that based on experience 10 – 20 Hz is a suitable cut-off frequency for a package of 100 tonnes. For the purposes of experimental and structural analysis two formal definitions are provided:-

1. Structural response is time dependent if loading is time dependent. However if loading is cyclic and of frequency less than roughly one-quarter of the structure's natural frequency of vibration, dynamic response is scarcely larger than static response [68].

2. For frequencies considerably below the first resonance or slowly varying time histories the response will be purely quasi-static and reasonable results can be obtained from a static analysis [69].

The definitions suggest that a filter cut-off frequency should be based upon prior knowledge of a tie down systems first natural frequency. For large mass packages (where the ratio of package mass to conveyance mass is >1) this is not a straightforward calculation [57, 58]. To obtain an accurate natural frequency estimate a more complex test of the complete system (i.e. vehicle and payload) is required [70]. Multi body dynamics tools may also provide good estimates but parameter identification and validation of these techniques is challenging [71].

2.2.2 Shock and Vibration

The nature of shock loading is a short transient burst of energy that occurs rapidly and involves a much larger frequency range [55]. A shock is characteristically defined as a transient response that is initially low, rises to a maximum and then decays as random vibrations. Shock loading will typically excite many natural frequencies of a structure. The resulting structural response consists of a weighted combination of the mode shapes, which can cause a significantly different response than that due to a quasi-static load [57, 72]. Examples of shock loads are longitudinal coupling of rail wagons or hump shunting operations. Snatch lifting and loading of packages may also cause shock due to their rapid occurrence. Short sections of a transport journey will involve uneven rail track, level crossings or points that may produce longer duration transients but are also considered as transportation shock and vibration.

Vibration is categorised into two types; deterministic and stochastic. Deterministic vibratory loads are generally created by rotating machinery such as piston engines, pumps and turbines. This kind of loading can be measured and relatively easily reproduced in a subsequent test. The loading on a tie down system during a rail journey cannot be reproduced exactly each time it is measured because it falls into the second class of stochastic or random vibration.

Random vibration can only be quantified using probabilistic methods, therefore a repeat test will produce the same statistical measures such as the root mean square (RMS) value of a signal. Depending on the modal characteristics of the structure and also the level of energy contained in the input signal, random vibrations can be treated in three different ways:-

1. If the highest frequency content of the loading is less than a quarter of the fundamental natural frequency of the structure or is slowly occurring then the loading can be treated as quasi-static.
2. If the vibration is of sufficient level and close to the fundamental natural frequency of the structure then resonance effects should be accounted for in structural integrity calculations.
3. If the level of vibration loading is insufficient to affect the structure or the lowest frequency of the loading is much higher than the fundamental natural frequency of the structure then the influence of random vibrations can be excluded from further assessment.

2.3 Rules and Regulations

2.3.1 IAEA Regulations

The IAEA Regulations Advisory Material stipulates the design of a tie down system should comply with the relevant competent authorities and transport modal organisations [2]. It provides some design guidance in the form of example calculation methods and includes suggested acceleration factors to apply for design. Specifically the advisory material states:-

"The inertial forces that act on the packages under routine conditions of transport can be derived from:-

- 1. Uneven road or track.*
- 2. Vibration.*
- 3. Linear accelerations and decelerations.*
- 4. Direction changes.*
- 5. Road skids in inclement weather that do not result in impact.*

The inertial forces that act on the packages under normal conditions of transport can be derived from routine conditions of transport plus the following less common occurrences:

- 1. Minor impacts with vehicles and obstacles.*
- 2. Rail shunting.*
- 3. Heavy seas.*
- 4. Turbulence or rough landings in air transport."*

According to [2] lower acceleration factors may be agreed by the relevant competent authorities. The following extract from [2] explains how the demonstration of a tie down system by experimental methods can be achieved by measuring loading conditions:

"It may be desirable to demonstrate, through testing, that a package and its retention system satisfies the acceleration factor requirements. When acceleration sensors are used to evaluate retention system behaviour, the cut-off frequency should be considered relative to defining equivalent quasi-static loads. The cut-off frequency should be selected to suit the mass, shape and dimensions of the package and the conveyance under consideration. Experience suggests that, for a package with a mass of 100 t, the cut-off frequency should be of the order of 10-20 Hz. For smaller packages with a mass of m t, the cut-off frequency should be adjusted by multiplying by a factor of $(100/m)^{1/3}$."

2.3.2 Competent Authorities and Transport Modal Organisations

2.3.2.1 Competent Authorities

The relevant competent authorities and transport modal organisations vary depending on country. In the UK the competent authorities for rail transportation of dangerous goods is the Convention Concerning International Carriage by Rail (COTIF) Appendix C – Regulations Concerning the International Carriage of Dangerous Goods by Rail (RID), 01/01/2013 [73], as stated in [74].

2.3.2.2 Transport Modal Organisations

The structural design of freight rail vehicles is carried out in accordance with the following documents:

1. CR WAG TSI, 2006, “Relating to the Subsystem Rolling Stock – Freight Wagons” [13].
2. GM/GN2688, 2010, “Guidance on the Design of Rail Freight Wagons (Including Tank Wagons)”, Rail Safety Standards Board [75].
3. BS EN 12663-2, 2010, “Rail Applications - Structural Requirements of Railway Vehicle Bodies. Part 2 Freight Wagons” [12].

Technical Specifications for Interoperability (TSI) were introduced by the European Commission in the 2000’s and are binding on all member states, including the rail industry in the UK [13]. A TSI has been produced which provides an over arching framework for the “*authorisation of sub-systems and vehicles for placing into service by a member state*”. The Euro norm is harmonised with the TSI which means that there is an assumption of conformity to the TSI provided BS EN 12663-2 is satisfied.

GM/GN2688 is a guidance document that supplements the TSI. Section 2.16 of [75] describes procedures for design of load restraints, in particular the following devices are considered; twist locks, Holland locks, spigots, winches and webbing. The document contains two sets of acceleration factors used for fatigue and proof strength assessment.

Reference	Longitudinal [g]	Lateral [g]	Vertical [g]
IAEA Regulations Advisory Materials SSG-26 Table IV. 1 [IV.8]	5	2	2(D); 2(U)
IAEA Regulations Advisory Materials SSG-26. Radioactive material packages in Europe by rail (UIC) Table IV. 2 [IV.8]	4 (1) ¹	0.5	1 ±0.3
TCSC 1006 Guide to the Securing/Retention of Radioactive Material Payloads and Packages During Transport, 2012	4 (1) ¹	1	2(D); 1(U)
RSSB – GM/GN2688 Guidance on the Structural Design of Rail Freight Wagons including Rail Tank Wagons	2	1	2(D); 1(U)
BS EN 12633-2 Railway Applications Structural Requirements of Vehicle Bodies	2	1	2(D);1(D)

¹ Lower acceleration factors are allowed if dedicated movements with special rail wagons are made. Additionally, higher acceleration factors are required if snatch lifting on the attachment points is likely to occur, or if the rail wagons are to be carried on certain roll-on/roll-off ferries

Table 2.1: Comparison of Rail Load Cases set by Rail and Nuclear Authorities for Tie Down System Design

Section 7.7 of [12] provides guidance on longitudinal and vertical resistance testing of special wagons for the conveyance of ISO containers. The test is intended to assess the securing device(s) of the containers by reproducing a shunting operation. The vehicle impact speed is adjusted until the measured acceleration on the containers is 2 g (low pass filtered at 16 Hz). **Table 2.1** provides a summary of the load cases provided in the nuclear and rail design documentation.

2.3.3 Codes of Practice

The Transport Container Standardisation Committee (TCSC) is chaired at Harwell, UK. The document TCSC 1006 is written specifically to provide design guidance for tie down systems of radioactive material payloads [74]. TCSC 1006 provides tables of acceleration factors to apply as design parameters for both normal and routine conditions of transport. These are referenced from various sources throughout the literature and standards. **Table 2.2** shows the fatigue design parameters in common use for body structures of rail vehicles including tie down systems in the UK.

Reference	Longitudinal [g]	Lateral [g]	Vertical [g]
TCSC 1006 and GM/GN 2688	± 0.2	± 0.2	± 0.4
BS EN 12633-2	± 0.2	$\pm 0.25^1$ ± 0.3	± 0.3

¹ For Freight Wagons with Double Stage Suspension

Table 2.2: Rail Load Cases for Fatigue Assessment of Tie Down Systems

3. Experimental and Analytical Studies

The main objective of the present work was to carry out a field experiment during a routine journey of a rail wagon laden with a heavy nuclear package. By analysis, data reduction and subsequent computer modelling advances in characterising the mechanical loading environment are possible. In this chapter a detailed review of the most pertinent experimental and analytical studies previously undertaken is provided.

3.1 Experimental Methods

The majority of nuclear related experimental studies on the mechanical loading during transportation have been carried out in the United States. Their focus has been on understanding the shock and vibration environment that nuclear fuel and tie downs are exposed to during transport. In 2013 a literature review of the studies in the US was undertaken by Maheras [76] of the US Nuclear Regulatory Committee (NRC) to understand whether sufficient knowledge of the loading environment exists. Maheras [76] concluded that there is a shortage of data for heavier packages (in excess of 85 tonnes) and also of data at the fuel rod or assembly level.

Recent research carried out in the rail industry has mainly involved studies on fatigue and vibration [14, 77–79]. Some experimental studies have been published that focus on heavy braking of long freight trains, and in-transit (*on-line*) coupling of vehicles [80, 81].

The pioneers of the experimental work carried out in the nuclear transport sector where based in the United States scientific research laboratories [17, 18, 26, 27, 82]. In 1978 Savannah River Laboratory (SRL) summarised a large testing programme on rail tie down systems of heavy nuclear packages [26]. Due to a request from the NRC the programme was expanded to support closely related programmes at the Sandia National Laboratories, Los Alamos Scientific Laboratory (LASL) and Hanford Engineering and Development Laboratory (HEDL). The programme ran for approxi-

mately a decade and the four laboratories where assigned roles to provide:-

Savannah River Laboratories: Test data as a basis for development of a tie down system design standard for radioactive shipments.

Sandia National Laboratories: A generic definition of the environment of the package/wagon interface for use in developing licensing guidelines.

Los Alamos Scientific Laboratory: Actual test experience to validate the Rail Car Impact Cargo Tie down Loads (RICTL) computer program.

Hanford Engineering and Development Laboratory: Data to calibrate and verify an analytical model of the rail wagon/package tie down system.

To characterise the mechanical loads by experiment Petry (SRL) and Lamoreaux (Sandia) independently stated the need to test different design variables within the transport system [26, 27]. Petry [26] reported a total of eighteen different test configurations assessed at SRL. The independent variables in those tests were:-

1. Rail wagon type.
2. Rail wagon coupling mechanism.
3. Package mass.
4. Impact speed.
5. Tie down configuration.
6. Natural frequency of the tie down system.

Lamoreaux *et al* [27] carried out a testing programme on packages transported by road and rail vehicles . Their report stated that a very large number of experiments were required to thoroughly describe the mechanical loading environment. They identified a similar set of unknown variables within the transport system:-

- | | |
|---------------------------------|----------------------------------|
| 1. Package mass. | 6. Vehicle suspension stiffness. |
| 2. Tie down stiffness. | 7. Vehicle suspension damping. |
| 3. Tie down damping. | 8. Speed. |
| 4. Vehicle mass. | 9. Tyre pressure (for trucks). |
| 5. Vehicle structure stiffness. | |

If maxima and minima were considered for each variable then 512 (2^9) configurations require evaluation. Furthermore if a mid-point value was considered, in addition to the extreme values, then 19,683 (3^9) configurations were necessary. On this basis

Lamoreaux suggested experimentation should be used to validate computer models which offer the flexibility of parameter sensitivity studies, thereby reducing the number of experiments required.

Recent studies carried out in the rail industry have adopted a different approach to experimental design. Belforte [80] conducted an experiment to understand the on-line coupling of long haul freight trains, consisting of 28 vehicles in total (including two locomotives) and weighing in excess of 1600 tonnes. He measured buffer forces, displacements and rail wagon accelerations to provide metrics for computer simulation validation. The vehicle was running on a straight track and passing over a switch whilst the measurements were taken. In a further study conducted by Cheli [81], rig testing of vehicle buffers was used to develop a computer model for the simulation of shunting and coupling load cases. Cheli's experimental approach provides input data for a computer model which offers the possibility of sensitivity analysis across a broad spectrum of load cases.

In the UK the Rail Safety Standards Board (RSSB) commissioned an extensive vibration research programme on passenger trains [14]. In this programme one of the key parameters varied between experiments was the running gear (bogies) of the vehicles. A considerable amount of acceleration data were collected during several thousand kilometres; representative of typical operational usage. The resulting time histories were converted to Power Spectral Densities and used to validate computer simulations. The validated models were subsequently used to perform sensitivity studies, varying parameters to assess the effects of ageing vehicle components (i.e. wheel out-of-roundness, suspension degradation) on the mechanical loading experienced by the bogies and vehicle body mounted equipment.

In the nuclear sector fatigue related studies have focused on the structural integrity of fuel assemblies during transportation [23, 24, 33, 83]. There are few studies that have attempted to describe fatigue loading spectra for tie down systems [84, 85]. On the other hand several studies in the rail industry have developed methods for establishing fatigue loading spectra of rail vehicle bogies and body structures [14, 44, 61, 79].

In the rest of this section, a summary of the key results, data reduction methods and conclusions on the shock, vibration and structural loading studies is presented.

3.1.1 Shock

During normal conditions of rail transport it is recognised that the most onerous event that occurs is due to shunting. It is understood that the practice of gravity (or *hump*) shunting is carried out routinely in freight transportation marshalling yards across the United States and Europe. A marshalling yard consists of many different tracks and sidings used to stow wagons. Gravity shunting is an automated process of releasing wagons into a marshalling yard, controlling their velocity with special retarders. They gain initial velocity by a hump engine which pushes them to the top of a hump in the yard and then releases them down the hump propelled by gravity. They stop by shunting into other stationary vehicles or end buffers (sometimes referred to as *fly shunting*). In the UK hump shunting is obsolete, due to the closure of hump yards, however during the formation of trains there is still a requirement to connect wagons loaded with nuclear packages by flat shunting.

Longitudinal coupling of rail vehicles is a dynamic interaction which occurs due to acceleration and deceleration. The severity of the resulting loads acting on the vehicle body and cargo depend on the draw gear (coupling mechanisms between wagons) and buffer configuration and type, number of vehicles in the train and position of the vehicle within the train. Buffers act under compression during braking whilst draw gear carry tractive loading, therefore the dynamic behaviour of rail vehicles under tractive or braking forces can be significantly different [80, 81].

Normal transportation without shunting or coupling can still produce shock loading as described in **chapter 2**. In North America the term superimposed shock on vibration is used to describe this kind of loading [82]. In general the severity of superimposed shock on vibration is anticipated to be less than coupling or shunting. Unlike the other two sources of shock that predominantly act in the longitudinal axis, superimposed shock on vibration can coexist in all three loading directions.

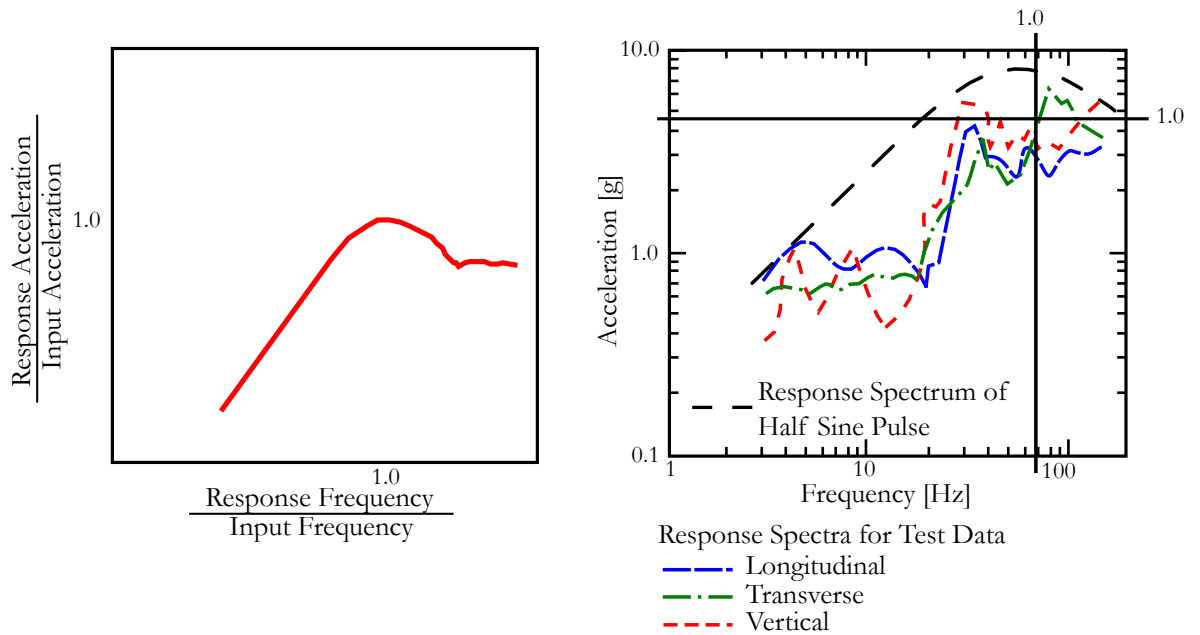
Magnuson [17, 18, 27, 82] (Sandia) authored a lot of research reports detailing the post processing and data reduction methods used to assimilate test results. In his earliest work he developed a method for characterising shock loading, focusing on the effects of longitudinal coupling of rail wagons laden with surrogate weapons; a relatively light cargo (4.5 tonnes). Observed impact velocities during rail coupling were reported (**Table 3.1**). The table shows that 63.5% of the observed impact velocities were below 5.25 mph, nearly 90% were below 6.7 mph, 98% were below 8.83 mph and 99.8% were below 11.05 mph.

For easy relative comparison of different experimental results he derived classical half sine time histories that satisfy an enveloping SRS. First a SRS was calculated for

a half sine pulse and then the response frequency and acceleration were normalised (**Figure 3.1a**). The normalised half sine SRS was then overlaid on the measured SRS and the half sine pulse magnitude and duration selected from the values corresponding to 1 on the normalised curve (**Figure 3.1b**).

Impact Velocity [km/hr]	Impact Velocity [mph]	Number Reported	Total [%]	Cumulative [%]
≤8.05	≤5	9936	63.5	63.5
9.66	6	2831	18.1	81.6
11.27	7	1331	8.5	90.1
12.87	8	748	4.8	94.9
14.48	9	492	3.1	98.0
16.09	10	208	1.3	99.3
17.70	11	73	0.5	99.8
19.31	12	1	0.01	99.8
20.92	13	20	0.1	99.9
22.53	14	3	0.02	99.9
24.14	15	3	0.02	99.9
25.75	16	0	0.0	99.9
27.36	17	2	0.01	100.0

Table 3.1: Observed Impact Velocities during Rail Coupling, 4.5 tonne Surrogate Weapons after Magnuson *et al* [82]



(a) Normalised Enveloping SRS to satisfy a Half Sine Wave Time History Pulse

(b) Test Data SRS overlaid with Normalised SRS of a Half Sine Pulse

Figure 3.1: An example of an Enveloping Procedure used to derive Classical Half Sine Shock Pulses from Measured Shock Response Spectra *after* Magnuson [82]

Magnuson's methods were used extensively thereafter on experiments involving packages weighing 13.5 tonnes, 36 tonnes, 45 tonnes and 64 tonnes [17, 18, 26, 27, 82]. In these experiments train lengths varied from 65 to 120 freight vehicles, the largest train weighed in excess of 4,000 tonnes. The tests captured several different events such as run in, run out, crossing rail switches, road crossings, bridges and highway underpasses. A summary of results for the lighter cargo is shown in Table 3.2. It is evident that the superimposed shock on vibration pulses are similar in duration but much lower in magnitude than those due to coupling or shunting.

Limited information on data acquisition methods was provided in the literature, although Lamoreaux [27] stated that in one particular study a sampling rate of 5 kHz and an anti-alias filter of 2 kHz was used. Measurements were collected by manually triggering data loggers at anticipated transportation events, something that is automated in modern data acquisition systems. This study directly fed into Magnuson's post-processing work.

Shock Source	Coupling Velocity [km/h]	Coupling Velocity [mph]	Axis	Peak Acceleration [g]	Pulse Duration [ms]
Superimposed Shock on Vibration	N/A	N/A	All	4.7	14
Coupling and Shunting	8.45	5.25	Longitudinal	33	11
			Vertical	15	8
	10.78	6.70	Longitudinal	38	10
			Vertical	18	7
	14.21	8.83	Longitudinal	51	12
			Vertical	20	10
17.78	11.05	Longitudinal	39	18	
		Vertical	36	9	

Table 3.2: Rail Shock Represented by a Single Half Sine Pulse (4.5 tonne and 13.5 tonne cargo) after Magnuson *et al* [82]

After completion of the programme Sanders *et al* [16] produced a summary report. Included was data analysis on heavy nuclear packages, weighing 36 tonnes and 64 tonnes [16–18, 27]. The results were again presented in SRS format, for the longitudinal, vertical and lateral axes and converted in to half sine pulses. **Table 3.3** provides the peak acceleration and pulse duration for these tests. Both the magnitude and duration of vertical and longitudinal accelerations are nearly the same, as expected the longitudinal accelerations are the largest. Lateral accelerations were also reported and found to be considerably lower than in the other axes.

Sanders *et al* proposed bounding SRS for all three axes for shunting and superimposed shock on vibration based on all the experimental data. He achieved this by taking the union of all three axes from each test SRS and then drawing a bounding envelope over the resulting SRS (**Figure 3.2**). From the enveloping SRS Sanders proposed a bounding half sine pulse of magnitude 2.4 g over a duration of 83 ms for superimposed shock and 33.2 g over a duration of 30.1 ms for shunting.

This approach essentially introduces two safety factors into the measured SRS. Firstly the union of the three axes increases the severity of the shock, which is potentially quite significant in the case of shunting, where lateral shock loading is low (**Table 3.3**). Secondly the enveloping procedure increases the shock content further. It is noteworthy that Sanders explicitly states that these values would be overly conservative if applied to linear dynamic or quasi-static analyses.

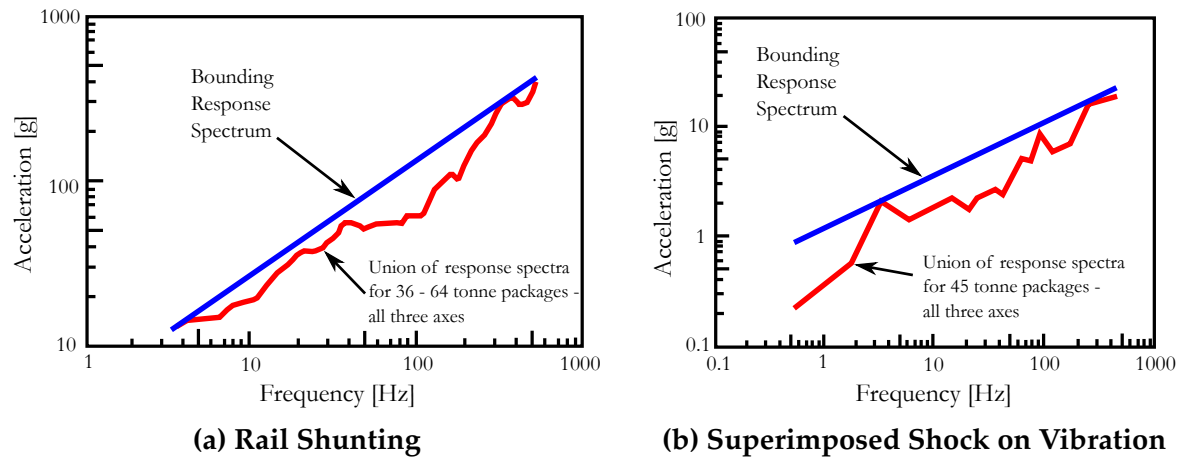


Figure 3.2: Bounding SRS for Rail Transportation of Nuclear Packages

Package Mass [tonnes]	Coupling Device	Axis	Peak Acceleration [g]	Pulse Duration [ms]
36	Standard	Longitudinal	34	14
		Transverse	8	11
		Vertical	31	13
64	Standard	Longitudinal	21	20
		Transverse	8	8
		Vertical		
		3 - 35 Hz	17	50
		35 - 90 Hz	17	10
36	Hydraulic end-of-car	Longitudinal	30	23
		Transverse	4.4	8
		Vertical	20	14
36	Sliding centre sill	Longitudinal	5.3	45
		Transverse	2.5	13
		Vertical	4.4	24

 Table 3.3: Half Sine Pulses for Rail Coupling Shock *after* Magnuson *et al* [17]

In a non-nuclear transportation study Singh [11] developed a method for characterising the shock and vibration environment during rail and road shipments of steel racks loaded with automotive engines for Ford Motor Company. The rail experimentation was carried out on a freight wagon during a 6 day journey from Windsor, Canada to Kansas City, Missouri, USA.

EDR-Model 3 environmental data recorders were positioned at the base of the engine racks. They were set to record 1 second of data every 5 minutes and measure all events over the minimum threshold of 0.1 g. A sampling frequency of 1000 Hz was selected and the recorders were set to overwrite mode which resulted in only the most severe events recorded in any 5 minute period and 185,000 samples to be collected.

A maximum longitudinal acceleration of 5.7 g was measured over a time period of 14 ms and was followed by a smaller secondary impact, caused by rail wagon recoil (Figure 3.3). Singh proposed that the steel racks be tested on a horizontal impact testing machine in the same configuration as they are loaded on the rail wagon. The measured peak acceleration and duration used as input to the testing machine program, carried out in accordance with ASTM-D4003 [86].

Fourgeaud *et al* [8] proposed that this acceleration should also apply in the design of tie down systems. This isn't a view shared by others; Sanders *et al* [16], Sczusso [57] and Scharon [58] all recognise the overly conservative nature of applying peak shock loads using quasi-static design methods.

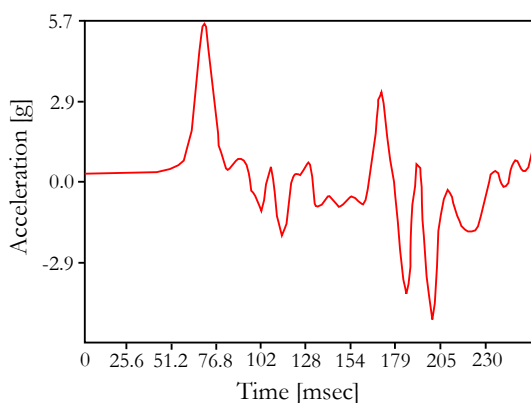


Figure 3.3: Peak Longitudinal Acceleration due to rail wagon coupling after Singh [11]

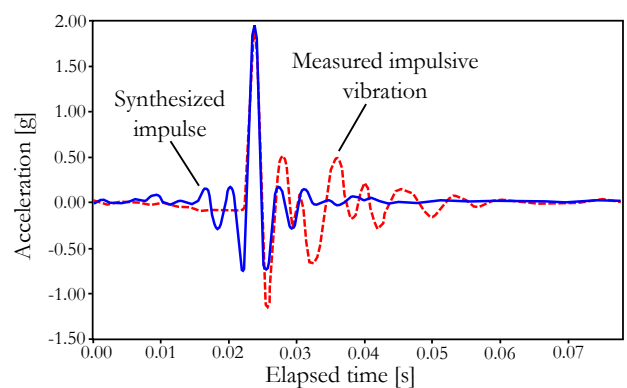


Figure 3.4: Synthesised Time History based on a PSD and Probability Distribution after Rouillard [87]

The hardware used to carry out shock testing may inherently limit Singh's [11] proposal and the ASTM method [86]. Programmable shock testing machines typically offer control over a limited set of input parameters such as pulse shape, magnitude

and duration. This may result in a different transient pulse during shock testing than actual measured data and therefore differences in shock severity.

Rouillard [87] developed an improved method for testing structures subjected to intermixed shock and vibration during rail transportation which improves the fidelity of the shock pulse applied during laboratory tests. He low pass filtered, continuous, measured accelerations from a rail wagon at 25 Hz, to separate the vehicle vibration modes from the higher frequency structural vibrations. Analysis of the separated time histories revealed that the high frequency shocks were intermittent. Rouillard proposed that an average PSD of the low frequency, *steady-state*, vibrations would suffice to characterise the vibrational aspects of the loading.

The shock definition was generated using the PSD of each intermittent transient, calculated with an inverse fast Fourier transform (IFFT), **Figure 3.4**. By superposing the steady-state and transient time signals a feedback system was developed to drive a shock-on-vibration shaker test.

3.1.2 Vibration

Vibrations during transportation can result in the degradation of nuclear fuel quality. There are three main methods for dealing with potentially adverse effects of vibration:-

1. Design of an anti-vibration system into the package or tie down.
2. Design of a special purpose vehicle suspension system.
3. Demonstration by shaker test and analysis of fuel quality.

A common approach is by demonstration of fuel quality by test and analysis; the vibration environment serves as input data for shaker tests and computer models [3, 51, 88]. The design of anti-vibration systems also requires knowledge of the vibration environment which is used to drive shaker tests and analytical models [4, 60]. In a vehicle dynamics approach an experimentally defined vibration environment provides a baseline response which vehicle dynamicists can use as a reference from which improvement can be judged. It is evident that each method relies extensively on a well characterised vibration environment.

Many of the early studies on vibrations during nuclear package transportation were interlinked with those described for shock loading, as part of the NRC programme [16–18, 24, 27, 82]. A software program was developed by Sandia National Laboratories to post-process test data. In keeping with the previous shock data analysis, each experiment was post-processed consistently. Vibration data reduction was achieved by extracting peak values in discrete frequency bands. Peaks exceeding 99% of the maximum values were omitted from the algorithm and treated as superimposed shock.

Magnuson [18] measured triaxial accelerations during a long rail journey of a 45 tonne package, he increased the frequency range of interest by using two types of accelerometers; piezoelectric (3 – 2500 Hz) and piezoresistive (0 – 750 Hz) [18]. The results indicate peak accelerations with similar magnitude exist throughout the frequency range 0 - 750 Hz (Table 3.4). Sanders *et al* [16] compared triaxial vibration data from several of the studies on nuclear packages, they concluded that the vertical axis of vibration contained the largest peaks in each frequency band. They calculated the union of each experimental data set to produce a bounding envelope vibration specification for the US NRC (Figure 3.5). In the absence of other data this specification provides a conservative envelope for a multiaxial test i.e. the same amplitudes are applied in each direction.

Frequency Band [Hz]	Longitudinal [g]	Lateral [g]	Vertical [g]
0-5	0.052	0.190	0.37
5-10	0.037	0.072	0.37
10-20	0.052	0.190	0.37
20-40	0.072	0.072	0.27
40-80	0.052	0.140	0.27
80-120	0.072	0.072	0.37
120-180	0.052	0.100	0.19
180-240	0.100	0.140	0.37
240-300	0.052	0.100	0.52
300-400	0.052	0.100	0.27
400-500	0.072	0.140	0.27
500-600	0.100	0.100	0.27
600-750	0.100	0.100	0.27

Measurements on Cargo Floor [g]
99% Level of 0 to Peak Amplitude

Table 3.4: Rail Vibrations for 45 tonne Package *after* Magnuson [18]

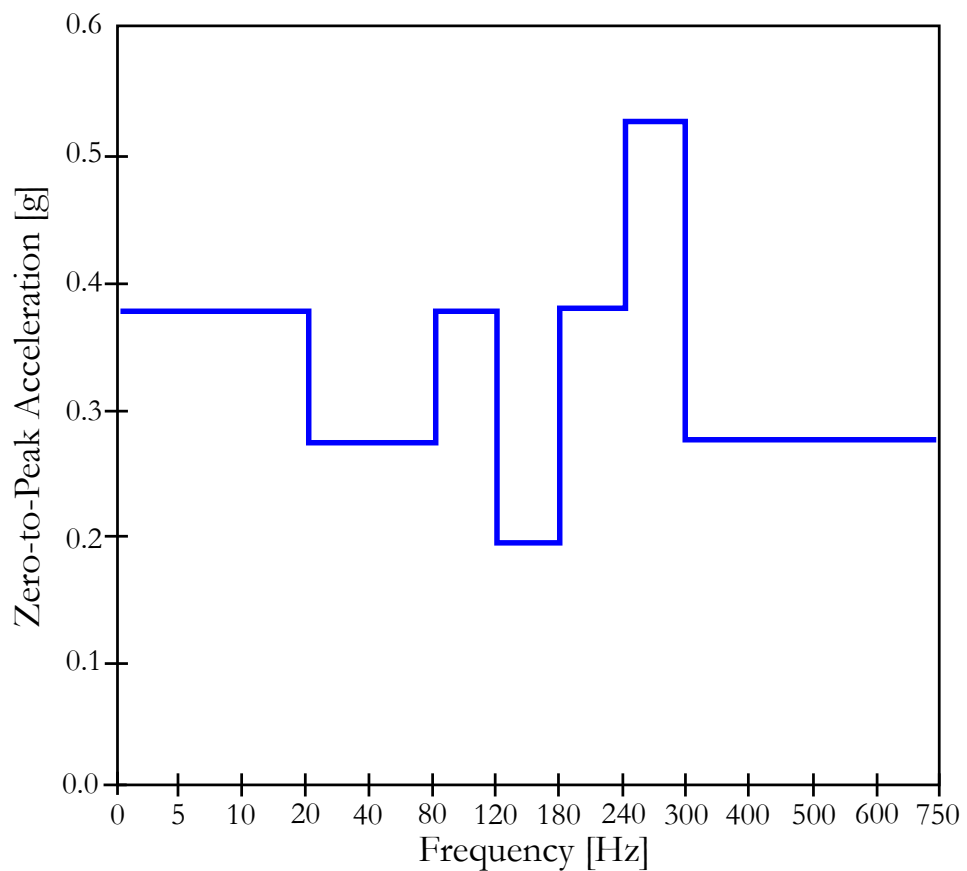


Figure 3.5: Bounding Envelope Zero-to-Peak Vibration Amplitudes for Multiaxial Testing (the Specification is applicable for each axis) *after* Sanders *et al* [16]

Although the consistency of data evaluation throughout the programme was very useful for relative comparisons, a potential drawback inherent in the zero-to-peak method is that random vibration tests are normally specified with a PSD [4]. In recent work on fuel assemblies McConnell [51] assumed that the 99% level zero-to-peak amplitudes were actually 3σ values and converted the zero-to-peak measurements to a PSD. Expressed mathematically the conversion is:-

$$A_{g^2/Hz} = \frac{\left(\frac{A_{0-Peak}}{3}\right)^2}{\Delta f} \quad (3.1)$$

A random vibration test uses a synthesized test signal from an average PSD coupled with a random, normally distributed phase array which are converted, usually by IFFT to time series data (Figure 3.6) [89, 90]. McConnell’s approximation clips the amplitude peaks slightly below the 3σ level, whereas some test standards suggest signal “drive clipping” at the 3σ level [91–93]. The implication is that the real transportation environment may have a significantly different distribution of peaks than that implied by a conventional random vibration shaker test.

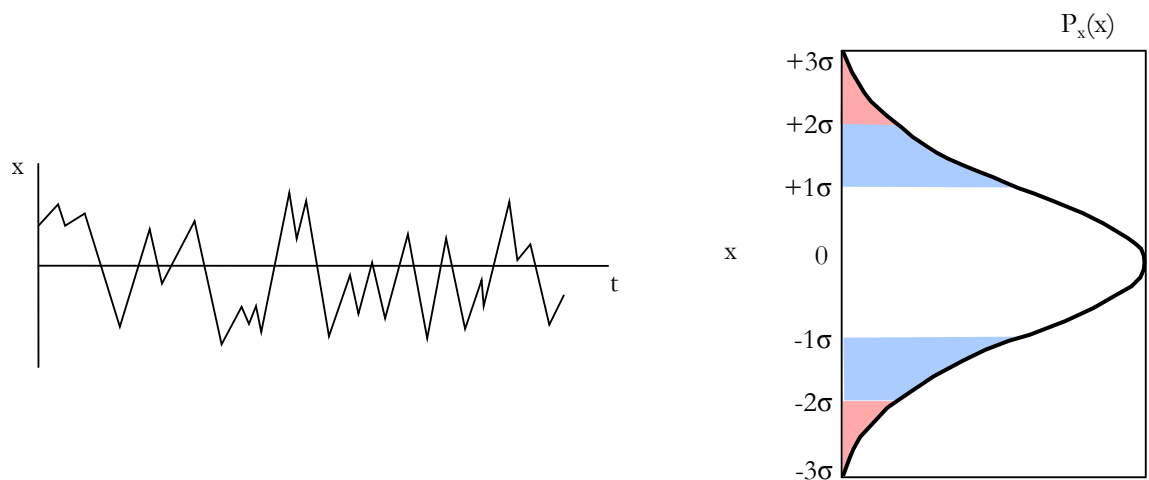
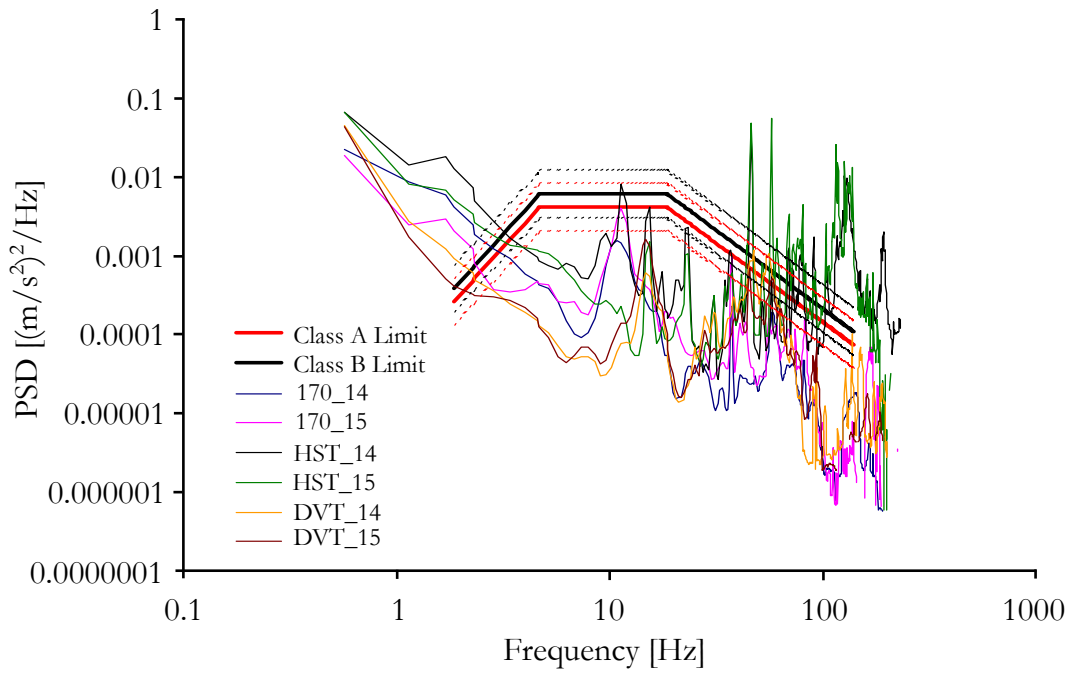
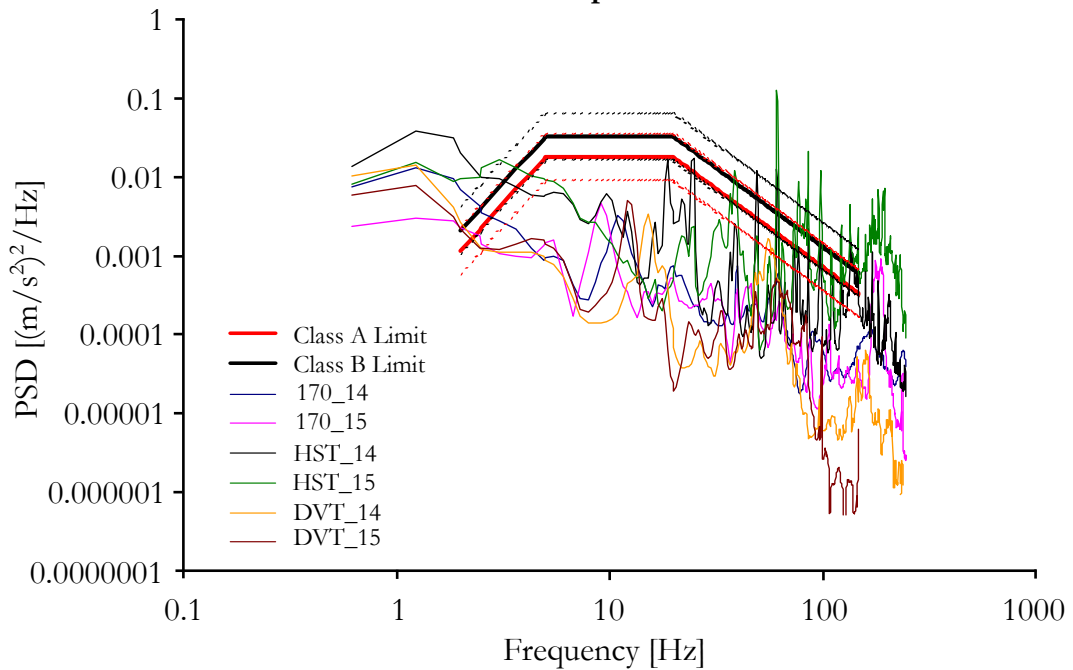


Figure 3.6: Gaussian Distribution

This effect has been investigated by collecting continuous time histories rather than using data loggers [14, 87, 89, 94, 95]. The present study is the only nuclear related study to have measured continuous time histories. The new data reported in the literature has prompted some developments in both data processing and test specification interpretation. For example Hampshire [14] carried out a study on body mounted equipment of passenger rail vehicles and compared vibration test specifications against continuous, acceleration measurements acquired over several thousand kilometres of typical rail journey usage.



(a) Lateral Acceleration Spectral Densities



(b) Vertical Acceleration Spectral Densities

Class A - equipment mounted directly to the rail car structure

Class B - equipment within a case that is mounted to the rail car

Dashed lines above and below the specifications represent allowable $\pm 3\text{dB}$ upper/lower bounds ($-0.5 \times \text{PSD}$ or $2 \times \text{PSD}$)

The time histories were divided into blocks of 4096 samples, a PSD was produced for each block and then each PSD was used to estimate an average PSD of the entire signal

Figure 3.7: Comparison of Measured Acceleration Spectral Densities with Test Specification provided in BS EN 61373 after Hampshire [14]

Hampshire's plotted the measured PSDs overlaid with those prescribed in the British Standard for shock and vibration tests of rail equipment (BS EN 61373) **Figure 3.7 [92]**. The measured PSDs represent *typical* or *average* vibratory spectra, the test envelope is for a functional test, therefore the two types of PSD should be comparable.

Hampshire noted that the specification is exceeded at low frequencies < 2 Hz and also above 40 Hz. The measured data indicated that the crest factor (ratio of peak to rms acceleration) was considerably larger than advised in BS EN 61373. This implies that the statistical distribution of peaks has much longer tails than a standard Gaussian distribution. His analysis highlighted mismatches in the characteristics of the rail vibration signal which affect its reproducibility on a shaker test. Hampshire concluded that tests performed using BS EN 61373 could be non-conservative.

These findings concur with several authors who have measured continuous vibration signals due to road transport and report that they are neither Gaussian nor stationary [94–96]. A signal is considered stationary if its statistical properties, such as its mean and rms, do not change over time. To achieve a more representative random vibration test, special methods for synthesizing input signals have been developed [87, 94, 95].

Rouillard [94] explains that a peak-hold¹ PSD partially addresses non-stationarity of signals and produces conservative input to shaker tests, however it is difficult to interpret in practice. As an alternative he created an algorithm that extracted blocks of data from continuous time histories that have a Gaussian distribution of amplitudes. By summing the distributions he was able to reproduce the *leptokurtic*² amplitude distribution of several measured signals.

In further work Rouillard [89] presents a method for implementing non-stationary random vibration signals on a test machine utilising a Random Vibration Controller (RVC) and Statistical Vibration Synthesizer (SVS), (**Figure 3.8**). Basing his approach on road vibrations, he assumes that measured signals are Gaussian in segments i.e. the underlying vibrations are from Gaussian distributions, but their rms values change throughout time making them non-stationary. By synthesizing standard random Gaussian signals for each segment and modulating them by statistically distributed rms and segment duration (obtained from field experiments), a non-stationary signal can be reproduced which satisfies both the average PSD and the amplitude distribution of transport vibrations.

¹The peak-hold method retains the maximum mean square values in each frequency band rather than averaging them

²A leptokurtic distribution describes a taller, more slender distribution with larger tails when compared with a standard normal, Gaussian distribution

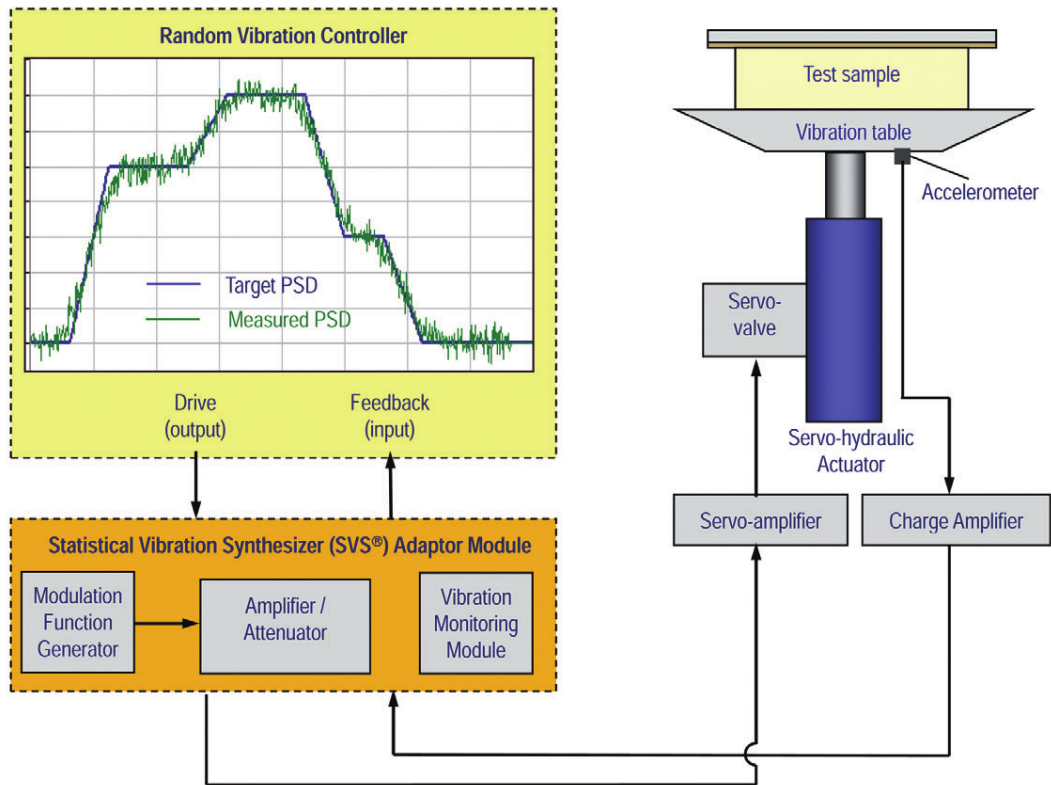


Figure 3.8: Experimental Configuration for Random Vibration Testing Non-Stationary Transportation Vibrations after Rouillard *et al* [89]

It is apparent that if accurate statistical properties of a non-Gaussian, non-stationary, random vibration environment are to be reproduced by shaker testing or computer simulation a significant amount of effort is required to define the driving signal. In assessments concerning the fatigue resistance of structures to random vibration loading, these factors would need to be addressed to ensure the test severity is acceptable.

On the other hand if the environment is well described by a Gaussian distribution and the vibrations are approximately stationary or the test is specified as a bounding, hypothetical case then derivation of loading conditions can be simplified.

3.1.3 Structural

In chapter 2 loading acting on nuclear packages was categorised into three types: quasi-static, shock and vibration. In the preceding sections it has been explained how transportation shock and vibration are treated experimentally for the purposes of characterising the loading environment to demonstrate fuel quality. It is also evident that shock loading, in particular shunting, has been studied to understand its influence on tie down systems. A common assumption made during the design of tie down systems is that their response during transportation remains linear, both with respect to material and geometry. A further assumption is that their response is quasi-static i.e. there are no inertial effects. Therefore in this section experimental studies relating to transportation loading of rail vehicles and tie down systems are reviewed.

Quasi-static loads are broadly defined as peak or cyclic for the design of tie down systems. Measured data is processed differently for dynamic (shock and vibration) and quasi-static loading. A number of different methods for processing data to derive peak and cyclic loading are considered; in particular counting algorithms. This is followed by an overview of quasi-static experimental studies carried out on nuclear tie downs and rail vehicles to establish loads.

3.1.3.1 Peak Loads

Following the measurement of dynamic data (typically accelerations or forces) to obtain peak loads a sequence of signals processing techniques are used to extract engineering information. For example a signal may be corrected for drift/spikes, filtered, processed with a peak/valley extraction algorithm and then subjected to a counting algorithm that reduces the data to a histogram format [79]. One such counting algorithm is called the Level Crossings Count, shown in **Figure 3.9** [97]. The results of this algorithm produce a histogram of acceleration levels versus number of exceedances [41, 56, 98–100]. This distribution can be used to analyse extreme values using statistical modelling methods i.e. extrapolation from curve/distribution fits [37, 41]

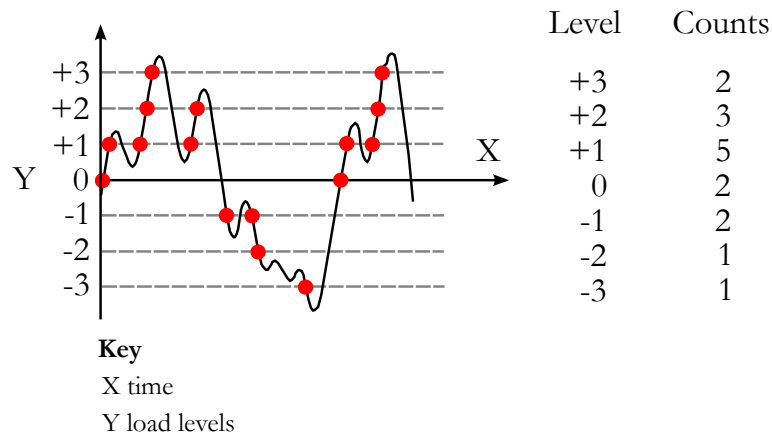
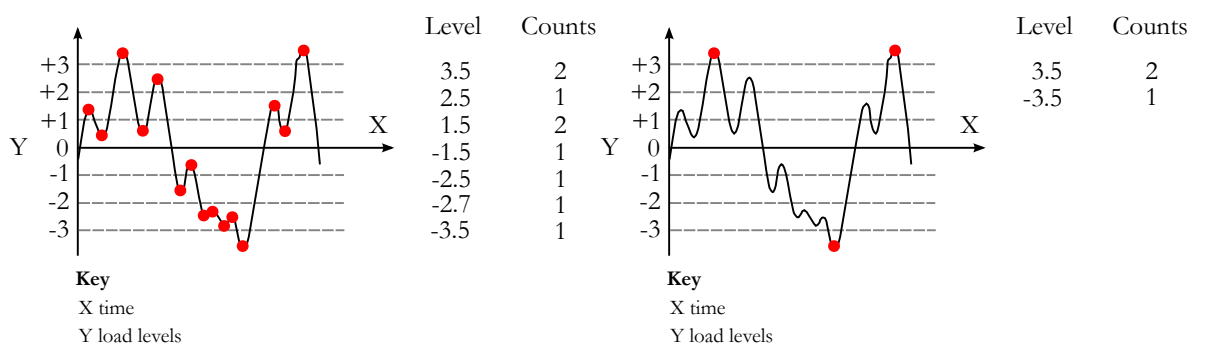


Figure 3.9: Level Crossings Counting Example [97]

Another procedure is the peak counting method which produces a histogram of acceleration amplitudes vs number of peaks [97]. By comparing **Figure 3.10a** with **Figure 3.10b** it should be apparent that there are two different peak counting techniques. The basic peak counting method counts every peak whereas the mean crossing (or *zero crossing*) technique only counts extrema that occur after the signal crosses either its mean or zero.



(a) Basic Peak Counting Example

(b) Peal Count Mean/Zero Crossings

Figure 3.10: Peak Counting Methods [97]

3.1.3.2 Cyclic Loads

For the purposes of fatigue analysis there are a number of cycle counting methods in existence, such as the range-pair, range-mean, level crossings and rainflow methods. For the purposes of fatigue analysis the rainflow method is generally regarded as the most accurate [97]. This is because the rainflow method counts cycles based on closed hysteresis loops which are known to cause fatigue damage to materials. **Figure 3.11** shows a diagram of a closed hysteresis loop, it is evident that the loop is closed on the reversal of load between 3-4.

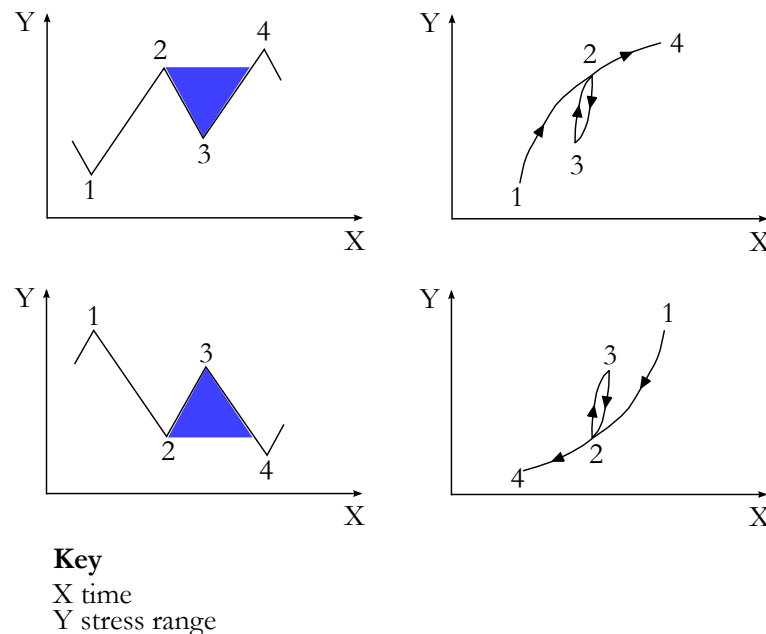


Figure 3.11: Rainflow Cycle Counting - Counts Closed Hysteresis Loops that Contribute to Fatigue Damage [97]

A rainflow cycle count produces a matrix of results; either a count of *binned* range and mean or a count of *binned* max and min. General guidance in the British Standards suggests either 32 or 64 bins should be used [97]. For comparative purposes between different load spectra this data output is quite cumbersome and therefore in many industries a level crossing count is carried out followed by a range pair count [37, 44, 79, 97, 101]. As an example **Figure 3.12** shows level crossings and range pair plots comparing two different wind turbine SLH's WISPER and WISPERX [37, 101]. Although this doesn't provide the accuracy of a rainflow matrix it does enable easier comparison between loading environments and is also used in the aerospace industry and for military and offshore applications.

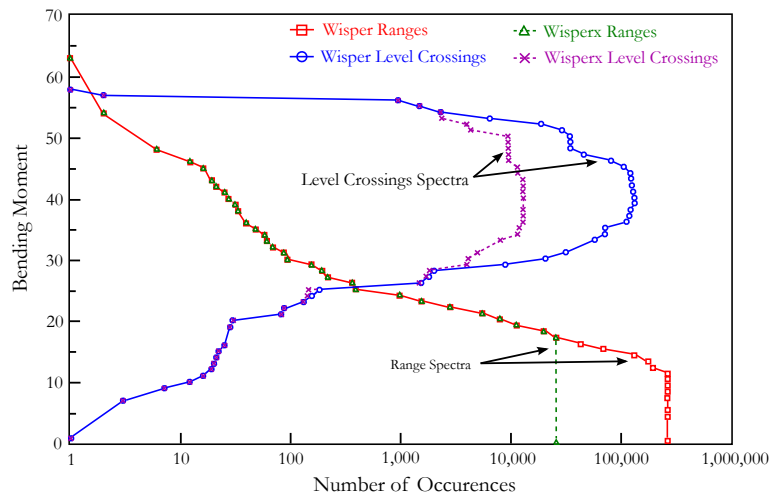


Figure 3.12: Comparison of Level Crossings and Range Pair Plots of the Wind Turbine SLH’s WISPER and WISPERX, derived from Rainflow Cycle Counting [101]

3.1.3.3 Experimental Studies on Quasi-Static Loads

In the UK an established methodology for the design of transport frames has successfully been applied for over forty years. It is based on the assessment of structural resistance to yielding, fracture and fatigue by applying conservative load factors adhering to the advisory material of the IAEA Regulations [2, 84, 85].

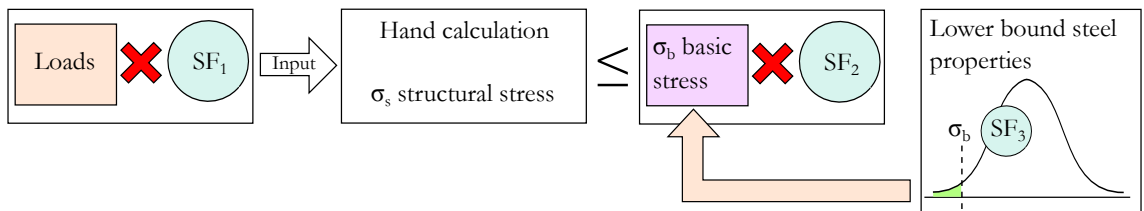


Figure 3.13: Basic Design Methodology for Tie Down Systems

Figure 3.13 shows a schematic of the basic design methodology. It should be apparent that there are three sets of multiplicative safety factors applied in the method. The first two are demarked SF_1 and SF_2 and are applied to the loading spectra and safe working stress limits respectively. SF_1 relates to assumed safety margins within the design load cases. SF_2 relates to safe working stress limits which are taken from BS 2573:1 1983, Rules for the Design of Cranes [102, 103]. The third safety factor, relates to the use of lower bound material properties for derivation of safe working stresses.

Fatigue assessment calculations are carried out using equivalent static loads prescribed in the modal standards and documented in TCSC 1006, see **Table 2.2** [12, 74, 75]. An additional safety factor in fatigue calculations is applied to the design life of

a structure. This is implied by the operational profile that the equivalent static load cases encompass. For example, Hampshire [14], whose methods for deriving fatigue load cases are covered in detail later in this section, suggests that an operational usage profile of a passenger rail vehicle might be 200,000 km per annum for 30 years. This kind of operational usage profile would grossly over estimate that of a tie down system for a nuclear package and is potentially very restrictive in design. Despite this the load cases proposed by Hampshire for rail vehicle bodies are actually the same as the current load cases in TCSC 1006 [74].

The current tie down system design methodology is therefore ultra conservative producing very safe tie downs with exceptional yielding, fracture and fatigue resistance. However it could be improved in three aspects:-

1. It is currently difficult to quantitatively establish safety margins due to uncertainty about real loading conditions.
2. It may be overly conservative for certain transport configurations (i.e. heavy packages) resulting in increased weight, material costs and design time [6, 7].
3. Without a thorough knowledge of the safety factors involved optimal transport solutions are limited.

The accurate definition of loading for structural assessment of tie down systems is possibly the most difficult aspect of characterising the transportation environment. Therefore different definitions of loads are required depending on the failure mode being assessed. For yielding and fracture assessments an estimate of the maximum loads experienced throughout service life is necessary. Because transportation loading is stochastic the required maximum is an extreme of a statistical distribution. These extremes cannot be established by experiment alone.

Similarly the definition of fatigue loading spectra requires the extraction and reduction of the number of fatigue inducing cycles and their associated ranges from measurements. These data need to be representative over the service life of a tie down system. Recently methods have been developed for rail vehicle fatigue assessments that may assist such definitions for tie downs systems [14, 77–79, 104].

During the 1980's Cory [84] measured tri-axial accelerations during a long haul journey of a 80 tonne package. The aim was to clarify design criteria for tie down systems. He reported results from road, rail and sea transportation modes from a package instrumented during a rail journey from France to Germany (2360 km). The unfiltered results from the rail journey were presented as peak count distributions of lateral, longitudinal and vertical accelerations (**Figure 3.14**). Unfortunately the tails of all the distributions were truncated which makes it impossible to assess the

rarity or magnitude of extremes. Cory argued that filtered measurements would be necessary to obtain quasi-static design criteria and higher peaks were due to short duration (high frequency) events. He concluded that future developments in acceleration monitoring would enhance the validity of experimental results and improve feedback to design.

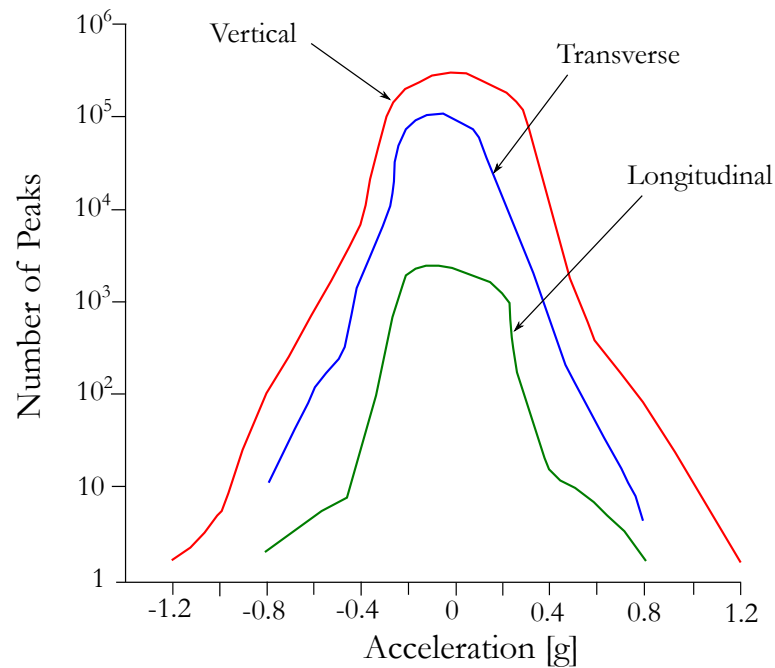


Figure 3.14: Triaxial Peak Acceleration Distributions Measured During a Long Haul Rail Journey *after Cory* [84]

In a study during road transportation Dixon [85] measured accelerations over approximately 1,000 miles on packages weighing < 20 tonnes. Dixon stated that the data acquisition system digitally sampled data at a frequency of 100 Hz. There are no details of the data acquisition system or filters used. The data processing system was programmed to automatically count the number of peaks in set acceleration bands throughout the journey.

Figure 3.15 shows acceleration amplitudes versus cycles normalised by 1000 hours of travel. Dixon opted to truncate the histograms at approximately $\pm 0.2g$ (only positive amplitudes shown in the figure) but states that 99% of vertical and lateral accelerations and 95% of longitudinal accelerations were below $\pm 0.2g$. If this is correct then most of the data collected is not shown in **Figure 3.15**.

No literature on filtering of small acceleration cycles for the purposes of establishing loads was found during this review, however truncation at $\pm 0.2g$ appears to be quite severe. In fatigue analysis the omission of small stress cycles has been the focus of some research studies [37, 47]. The outcome of these studies was to set filter levels

of measured stress time histories at a fraction of the structural materials' constant amplitude endurance limit.

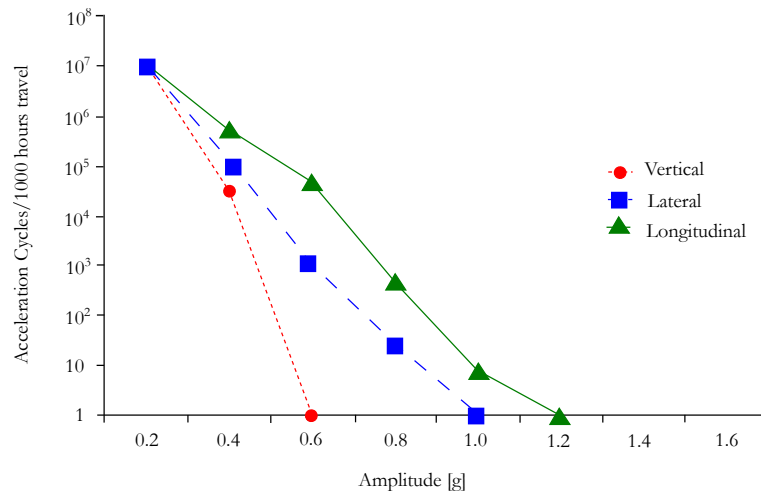


Figure 3.15: Normalised Acceleration Frequency During Road Transport after Dixon [85]

Dixon did not state which method he used to count acceleration cycles. Assuming the method used was similar to that described in [97] then Figure 3.15 accurately defines the extreme values and suggests that values greater than those presented are increasingly unlikely to occur. However without more precise description of the data processing interpretation is not possible.

Hampshire [14] conducted a research programme to establish design parameters for rail vehicle mounted equipment subjected to in-service loading on behalf of the Rail Safety Standards Board (RSSB). The study considered axlebox, bogie and body mounted equipment on passenger and non-passenger vehicles, but excluded freight vehicles. His methodology combined in-service measurements, computer modelling and statistical techniques to produce load cases to compare with the current Rail Group Standards [105]. The overarching methodology was:-

1. Nearly 2000 miles of in-service acceleration data was measured from the axle boxes, bogie frames and bodies of three different types of vehicle; HST Power Car, Class170 Turbostar and ICC225 DVT.
2. Displacements were also measured between the axle boxes and bogie frames and bogie frames and bodies to assist with the identification of different vehicle modes such as pitch, roll and yaw.
3. Validation of vehicle models was achieved using the measured data.
4. The performance of a variety of vehicles and degraded modes of transport likely to be encountered during service was predicted using the validated models.

- The results of the validated models were used to produce equivalent fatigue and proof load cases for the equipment mounted to axle boxes, bogie frames and bodies.

To validate the computer models each measured and computed channel of acceleration was processed to produce PSDs and the statistical quantities; root mean square (RMS) and extrema.

The measured body vertical and lateral acceleration PSD's indicated the energy distribution of the signals with respect to frequency. The PSDs at the vehicle bodies were also compared to those at the bogie frames. At frequencies < 25 Hz most of the energy at the bogie frames was attenuated at the bodies by two orders of magnitude. At frequencies >25 Hz the body responses were attenuated by more than two orders of magnitude.

After calibrating rigid body dynamic models of the vehicles, the calculated acceleration time histories, which incorporated degraded modes of transport, Hampshire used the data to obtain equivalent fatigue and proof loads. To estimate the proof loads firstly the data was low pass filtered at 150 Hz and then a peak count zero-crossing analysis was carried out.

To account for peaks that may occur in-service but were not calculated or measured an exponential curve was fitted to the histograms. The fitted curve was then used to extrapolate the data to obtain proof loads (**Figure 3.16**). The extrapolation was based on the postulate that a proof load would occur no more than 10 times per year. This technique is potentially very inaccurate due to the scatter and sparsity of the data in the tail of the distribution.

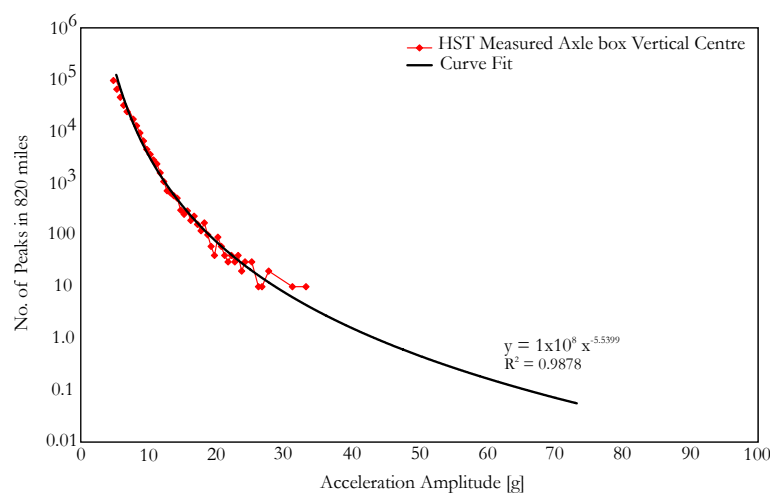


Figure 3.16: Vertical Acceleration Histogram from Axle box of Passenger Rail Vehicle. Extrapolation Method Proposed by Curve Fitting *after* Hampshire [14]

The derivation of fatigue load cases enabled a direct comparison with the current load cases specified in the Rail Group Standards. By applying a damage equivalence method to both the measured signal (variable amplitude) and the constant amplitude load case, the derivation of single value, multi-axial load cases was achieved [37, 43, 100, 106]. This was achieved by the following sequence of calculations:-

1. Low pass filter at 150 Hz.
2. Rainflow cycle count.
3. Multiply acceleration ranges by an arbitrary stress factor, X .
4. Multiply the number of cycles in each bin by the number of possible repetitions of the time history for the intended life of the vehicle/component.
5. Calculate fatigue damage from the result of (3) using any weld class, Q , from BS7608 for each acceleration bin and then use Miner's Law to obtain the total damage [107].

The typical design life used for constant amplitude fatigue assessment is 10^7 cycles. To equate the damage content of the signal to 10^7 cycles:

- 6 Iteratively adjusting the arbitrary stress factor, X , until the total damage was equal to 1.

The equivalent fatigue damage range was then obtained by:-

- 7 Dividing the allowable stress range from BS7608 [107] for the weld class, Q , at 10^7 cycles, by the adjusted arbitrary stress factor, X .

The procedure described assumes that a linear relationship exists between acceleration and stress. Hampshire [14] explained that the same answer was achieved regardless of which weld class was selected, because the contribution to the damage from each cycle is in linear proportion to the allowable stress for 10^7 cycles. Hampshire states that the use of an arbitrary stress factor in both forward and backward steps negates the effect of selecting different parameters for the material model. However Halfpenny [43] advises caution when deriving equivalent static loads for fatigue because the results are sensitive to the material parameters used in the calculations.

Hampshire [14] also suggested that for design purposes a histogram of acceleration ranges each applied for a fixed number of cycles was a more accurate method of simplifying signals to serve as fatigue design parameters. This method has been adopted in more recent studies on high speed trains in China for fatigue load derivation of rail bogies by Zhu and Zhang [44, 79].

Zhang [44] measured loads on rail bogies directly by manufacturing axle box springs and their supports into load transducers. Strains were also measured at critical locations on the bogie frame and fatigue damage calculated from the results. Using the measured loads as input he also predicted fatigue damage using a FEA model. In a final step referred to as a *damage consistency method*, he used a genetic optimisation procedure to adjust the measured loads to achieve equivalent measured and predicted fatigue damage. Zhang pointed out that the measured loads displayed dynamic characteristics and further work was required in this area.

In more recent work Zhu [79] manufactured a load transducer bogie frame and carried out a calibration of the bogie with a laboratory controlled experiment. The purpose of this calibration test was to obtain coefficients relating measured voltage to applied load on the bogie frames. Following this test, real time in-service measurements of load were carried out on a passenger rail vehicle running at 350km/h. In addition to the measured loads, strain time histories were measured at specifically identified points on the bogie frame.

Subsequently the measured loads were adjusted in an initial step using the calibration coefficients. Using the calibrated in-service loads and a static finite element modelling procedure, time histories were predicted at points on the bogie frame corresponding to the measured strain time histories locations. Zhu then performed a damage consistency calculation using a similar genetic optimisation procedure, as previously described in the study by Zhang [44] and obtained good agreement. **Figure 3.17** shows the load spectra resulting from this method that will form the basis for a larger study to standardise a load spectrum for rail bogies in China.

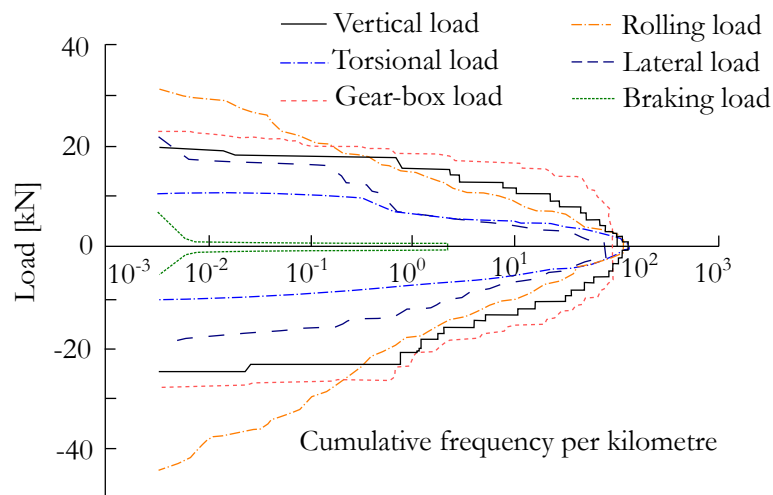


Figure 3.17: Quasi-Static Load Spectra after the Damage Consistency Calibration after Zhu et al [79]

3.2 Computer Simulation Techniques

For load identification purposes Finite Element Analysis (FEA) provides two main uses; to determine strain measurement positions for experimental methods and to inversely determine loading from measured strain responses. Additionally, used as a sensitivity analysis tool FEA can assess the structural response to variations in loading conditions [46, 62–64, 85, 108, 109]. The most simplistic analysis procedure, frequently used in industry is the linear, static analysis. With the addition of geometric or material non-linearities and suitable Newton-Raphson based solution procedures, this technique is also extended to solve non-linear, static problems.

There are a number of dynamic FEA methods, these can be broadly categorised into linear or non-linear dynamics. The techniques provide results in either the time or frequency domain. The three main frequency domain methods all involve the use of the modal superposition procedure:-

1. Harmonic.
2. Random vibration.
3. Shock response.

These methods rely upon accurate input load specifications obtained from measured data and processed as described in the previous section. There are also three main time domain analysis methods:-

1. Modal transient.
2. Implicit transient.
3. Explicit transient.

The modal transient analysis assumes a linear structural response and is the most computationally economical. The second two methods listed are most useful if non-linear structural response is expected.

Another valuable tool used to predict transportation loads of a vehicle is rigid body dynamics (RBD) analysis. Although some commercial FEA codes have (RBD) capability, traditionally these methods have evolved from computational, numerical integration techniques such as Runge-Kutta methods [55]. The main advantage to these methods over FEA is the speed in which they are solved. A disadvantage is the large number of unknown input parameters required to create a model of sufficient fidelity. Careful sensitivity analysis is required to verify the model and field testing is necessary for model validation [15, 71].

In the following section a review of the computational studies performed on tie downs and nuclear fuel assemblies during rail transportation is carried out. Other studies on various applications are also included to compare and contrast techniques.

3.2.1 Shunting and Coupling

In early work carried out by Sandia Laboratories, Magnuson [82] prepared a computer model of a rail wagon, package, tie down system and coupler to increase the understanding of longitudinal rail dynamics (Figure 3.18). A sensitivity study on shock attenuation couplers, tie down stiffness, impact velocity and package mass was undertaken and the results of the mathematical model were used to generate shock response spectra.

The main conclusion on tie down system design was that it should possess sufficiently high stiffness, to prevent relative motion of the package and the conveyance, thereby minimising the response of the package. Additionally when standard draft gear was used, the package response was attenuated by increasing package mass.

Conversely when shock attenuating couplers were used, the response of the package was not affected by changes in package mass if the tie down system was sufficiently stiff. Magnuson [82] noted that general studies of this type cannot treat all of the design dependant detail that will vary in every system but suggested that the method described may be used to investigate specific systems.

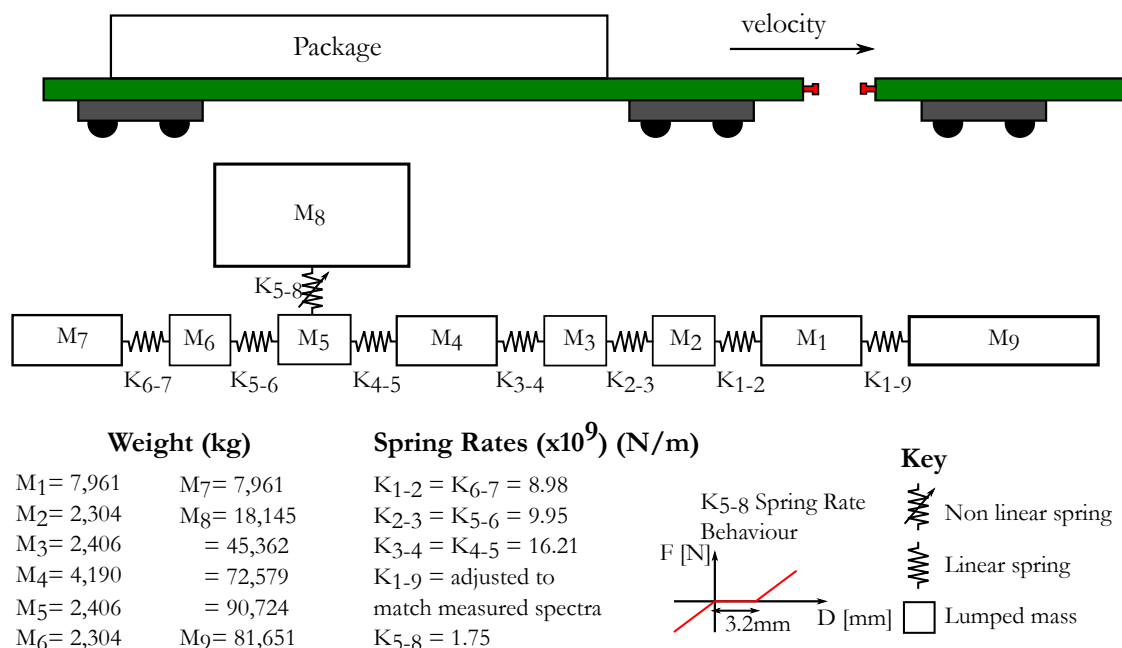


Figure 3.18: One Dimensional Dynamic Model of Rail Wagon for Assessing Low Velocity Impacts after Magnuson [82]

In a similar study Bartholomew [25] performed computer simulations of rail wagon impacts carrying large mass nuclear packages and the effects on tie down loads. Bartholomew's [25] approach extended the earlier work of Magnuson [82] by considering vertical dynamics. The model consisted of lumped masses and springs, three degrees of freedom assigned to each mass; two translational and one rotational. Masses 1 – 7 represented the rail wagon, masses 8 – 10 represented the package and mass 11 the stationary train (Figure 3.19).

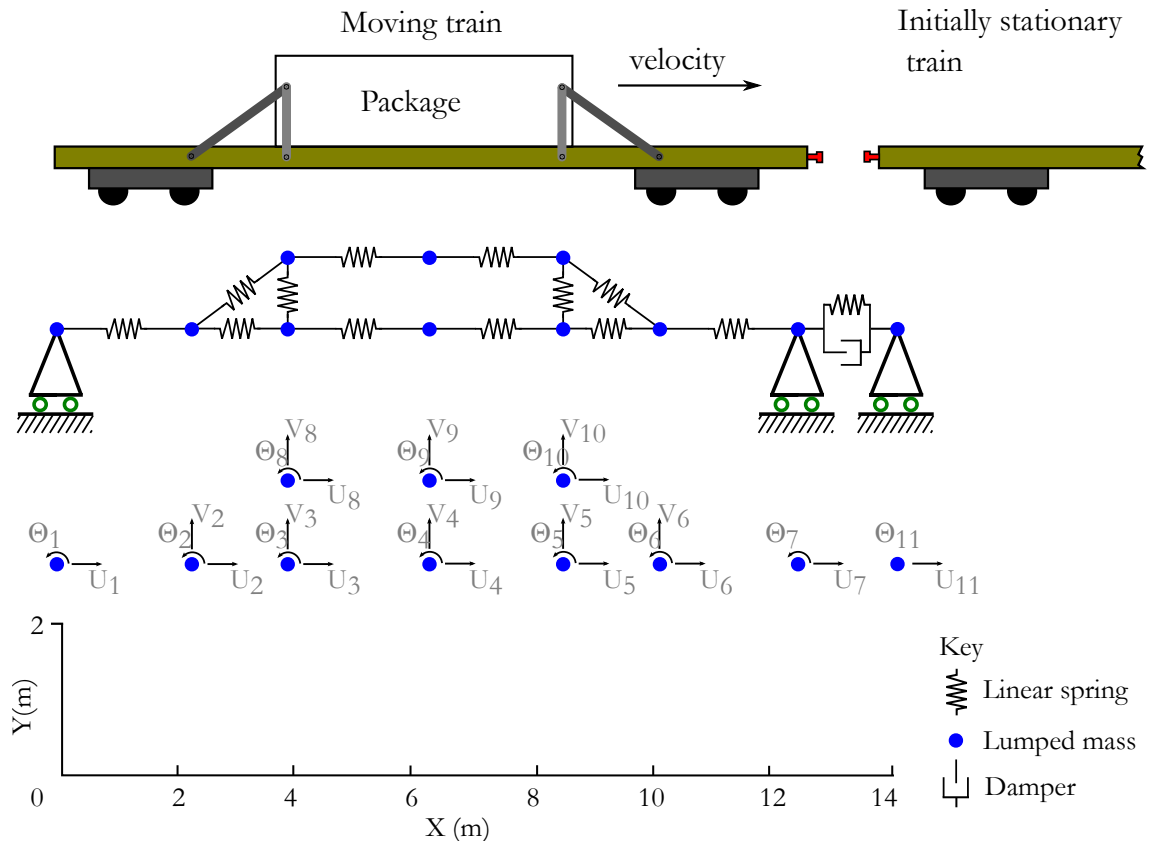


Figure 3.19: RICTL Rail Car Impact Cargo Tie Down Loads after Bartholomew [25]

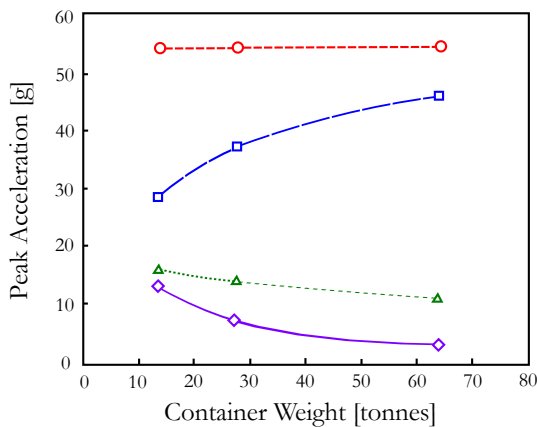
In a sensitivity analysis the package mass, impact velocity and tie down stiffness were varied to assess their effects on tie down loads. Bartholomew [25] claimed that by increasing package mass the package accelerations decreased (Figure 3.20a). However his results are only weakly related by three points. This is particularly evident in Figure 3.20b, where a local maxima is inferred by the fitted curve.

Despite the sparse data set, the results of the sensitivity study on package mass, shown in Figure 3.20a, exhibit logical trends. During a shock loading event it is reasonable to expect that if the package mass is increased, then the peak accelerations at the package will decrease. This is because the package inertia resists motion due to the rapid transient. It is therefore likely that the peak accelerations at the wagon bed would increase, since the energy remaining in the shock has to dissipate somewhere

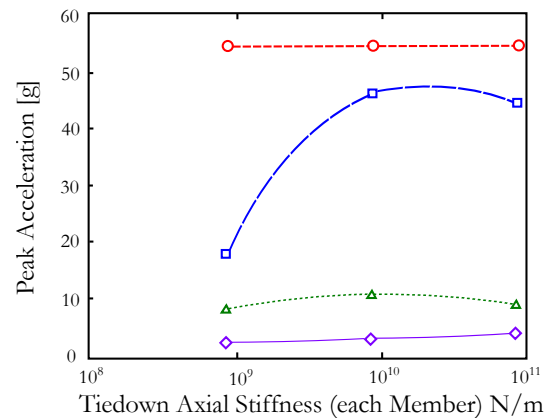
in the structure. However it is difficult to draw conclusions on tie down stiffness because the trend is not adequately described (Figure 3.20b).

Bartholomew’s [25] results also show that during an impact peak accelerations increase with increasing vehicle speed (Figure 3.20c). Again this is a logical result because increasing the vehicle speed increases the available kinetic energy in the system and a larger response is therefore expected.

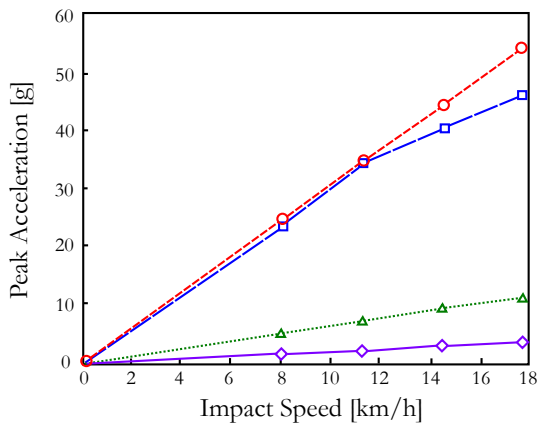
In conclusion he stated that the dynamic method of analysis provided significant advancement on static design methods and suggested that it should be validated by experimental methods.



(a) Peak Accelerations vs Package Mass during Train Impact at 11 mph



(b) Peak Accelerations vs Axial Tie Down Stiffness during Train Impact at 11 mph, 63.5 tonne Package



(c) Peak Accelerations vs Impact Speed during Train Impact, 63.5 tonne Package

- Horizontal deceleration of rail car at point of impact
- Vertical Acceration of Rail Car at Struck-End Container Attachment
- △ Horizontal Deceleration of Container c.g.
- ◇ Vertical Acceleration of Container c.g.

Figure 3.20: Key Results of Rail Wagon and Package Impact Model after Bartholomew [25]

Hanford Engineering Development Laboratory (HEDL) supported a rigorous analytical programme of work on the dynamic environment of nuclear packages during rail transportation from 1976 to 1984. Fields [20–22, 28, 28–32] published a total of 19 reports and papers on the subject. In 1978 Fields [30] published a first report on a dynamic model to predict vibratory motion within a spent fuel package during rail transportation [28]. The report described the possibility of mathematically modelling a two dimensional rail wagon and package system that would predict vibrations on spent fuel subjected to random excitations. A provisional model was also presented; a simple one dimensional, spring-mass system, excited with a rectangular pulse.

From 1978 onwards the emphasis of the work at HEDL shifted towards tie down structural assessments. From the test data acquired by Savannah River Laboratories (SRL), Fields [30] developed a more complex rail wagon, tie down and package model, called Cask Rail Car Dynamic Simulator (CARDS). Fields [20, 25, 82] improved upon previous analytical work carried out by Magnuson and Bartholomew through intensive model validation. CARDS was subsequently used for a comprehensive parametric and sensitivity analysis [22]. The validation method is discussed later in this chapter.

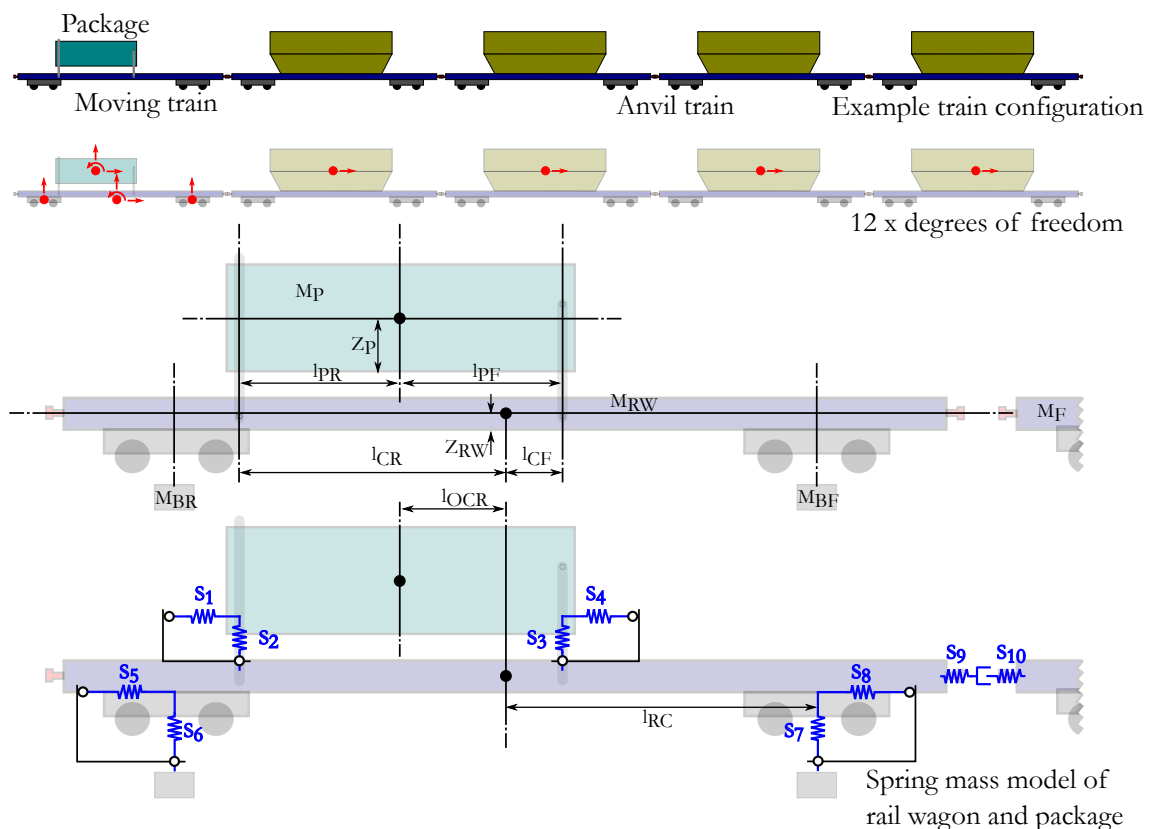


Figure 3.21: CARDS Computer Model after Fields [32]

The CARDS computer program considered the effects of longitudinal coupling of rail wagons due to shunting; considered the most onerous shock loading during rail transportation.

CARDS consists of 12 degrees of freedom which represent the rail wagon, tie down system and package, impacting a series of stationary wagons (anvil cars) (**Figure 3.21**). The package and rail wagon each have three degrees of freedom (DOFs); longitudinal, vertical and rotational (pitch). Each bogie on the moving train has 1 vertical DOF and each anvil wagon has 1 longitudinal DOF.

Fields used a sub-modelling approach to break the system into manageable portions for validation and programming purposes. A bending sub-model of the wagon body was developed and incorporated into CARDS, but it was never validated.

Both the suspension and rail wagon coupler mechanisms were treated as sub-models. By treating these complex sub-assemblies separately, Fields was able to supplement the equations of motion with auxiliary equations that represented the coupler mechanism and suspension as equivalent stiffness terms. For example an auxiliary equation for the suspension was written as:-

$$k_{56} = k_6[1 - \mu_{D6}\beta_6|\dot{Y}_{RW56}|^{\alpha_6}\text{sgn}(\dot{Y}_{RW56})] \quad (3.2)$$

where:-

k_{S6} = Equivalent spring constant for rear suspension

μ_{D6} = Coefficient of friction in damper (rear)

β_6 = Fraction of load on suspension applied perpendicular to sliding surface damper

\dot{Y}_{RW56} = Vertical velocity of the rail wagon (rear)

α_6 = Factor that allows the damping term to vary as a function of the absolute value of the velocity raised to the power

The non-linear equations also included terms for vertical motion, longitudinal load on the suspension dampers and a damping force due to friction in the suspension damper. Similarly the coupler mechanism accounts for a “solid” state under severe compression, loss of energy due to package sliding, non-linear compaction and rebound behaviour and friction between the two coupler surfaces which opposes ro-

tational motion.

Due to the parametric nature of the program it was possible to isolate components of the system, analyse different configurations of anvil train and/or “hammer” train or assess the influence of design parameters of the system [31]. It was also possible to use calculated or measured coupler forces to produce a dynamic response from the rail wagon and package.

The calculation of a time history representative of real loading conditions, suitable for use in a testing facility, is not straightforward. A post processor called Cask Rail Car Response Spectrum Generator (CARRS) was developed to derive equivalent single degree of freedom representations of the relative longitudinal, vertical and rotational motion between the package and wagon [32]. The derivation and application of the equations is carefully explained in [22].

The results from CARDS indicate that both the vertical and longitudinal motion of the package significantly influence the motion of the support (wagon). This was confirmed by comparing the contributions of the package inertial forces to the total summation of the vertical and longitudinal forces acting on the rail wagon. For some, non nuclear transport applications, special techniques have been developed to account for this effect [57].

Dynamic coupling terms in the equations of motion introduce two moments to account for an offset centre of gravity of the package and rail wagon, when $l_{CR} \neq l_{CF}$, and the rail wagon and coupler, when $Z_{RW} \neq Z_P$ (Figure 3.21). Fields showed that this rotational motion needs to be accounted for in a SRS calculation.

CARRS uses the support accelerations calculated by CARDS and the equivalent single degree of freedom equations to generate absolute maximum longitudinal, vertical and rotational SRS. The equations for the support accelerations contain a mixture of rotational terms and longitudinal or vertical accelerations. This means that they are not just the vertical or longitudinal acceleration of the rail wagon but are representative of the motion of the wagon.

The support accelerations are therefore forcing functions that may be used as input to a shaker table for any 1-DOF device. The key assumptions are that the shaker table is prescribed motion equivalent to the forcing functions and that the shaker is not influenced by the device attached to it.

Fields [22] selected two groups of parameters for sensitivity analysis; the first was a set of single parameters and the second a set of composite parameters (on the request of the US NRC). The parameters were ranked according to how sensitive the response variables were to changes. Forces and accelerations at various points of the

system were selected as response variables.

The struck end and base end vertical and horizontal tie down loads were selected as tie down response variables. The results showed that the tie down loads were moderately sensitive to changes in package mass, longitudinal tie down stiffness and vertical distance between the package centre of gravity and its external surface. The most influential parameter was package mass.

Ontario Hydro Research Division undertook a large programme of work to assess the effects of the shock and vibration transport environment on irradiated CANDU (Canadian Deuterium Uranium) fuel bundles. A total of 13 papers and reports were published between 1975 and 1986, however only a limited number are currently available for review.

Elbestawi *et al* [23] assessed the effects of rail wagon coupling on CANDU fuel bundles. The fuel bundles were loaded in fuel modules, stacked two high inside a transportation package (**Figure 3.22**) [24]. The package was seated in a transport frame bolted to the rail wagon with four bolts.

It was not stated how the package was constrained to the transport frame, but appeared to be either a gravity system or fixed to the transport frame by the package trunnions and bolted keep plates. The total mass of the loaded package and tie down was 38 tonnes and the rail wagon was 27 tonnes.

The Finite Element Method (FEM) was used for analytical modelling. A planar 2-D model consisting of 1-D spring and beam elements and lumped masses was created. The rail wagon, tie down system, package and coupler were all included, however there is no suspension or running gear model. Vertical dynamic behaviour is therefore limited to the flexible modes of the tie down system and wagon bed; this approach would not excite the vehicle bounce or pitching modes.

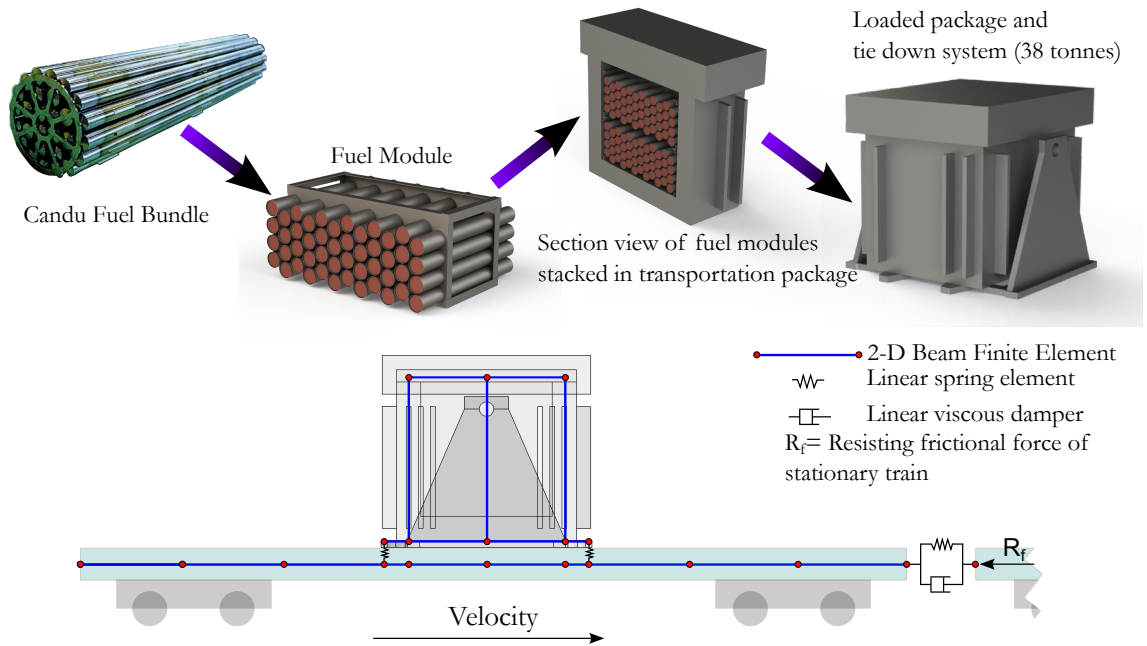


Figure 3.22: Finite Element Model of Rail Wagon, Tie Down System, Package and Coupler after Elbestawi *et al* [23]

An initial velocity of 10 mph was applied to the model and a response was induced by a resisting force applied to the coupler. This force was equivalent to the frictional force of a stationary train of mass 226.8 tonnes assuming a static coefficient of friction of 0.2. A linear viscous damping model was used in parallel with a linear spring to model the coupler. Rayleigh damping was also applied to the tie down, package and wagon by assuming that the factors α and β equal 0.2. These factors are related to the fraction of critical damping by the following equation:-

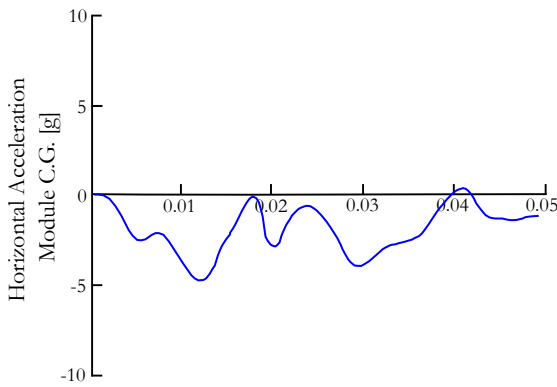
$$\zeta = \frac{\alpha}{2\omega_i} + \frac{\beta\omega_i}{2} \quad (3.3)$$

Since ω_i refers to the *ith* natural frequency the equation implies that the lower frequency modes are damped by β , mass proportional damping and the higher frequency modes are damped by α , stiffness proportional damping.

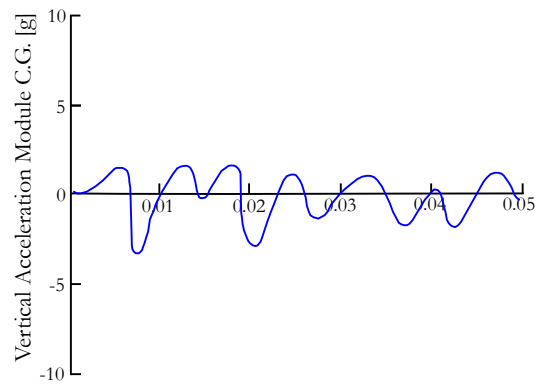
The model was solved using a transient, explicit, dynamics algorithm. Elbestawi points out that a time step was selected that was less than the lowest period of free oscillation in the structure, critical to ensuring the transient dynamic solution remained stable.

Figure 3.23 shows the resulting acceleration time histories generated by the model. These time histories were converted in to SRS and used as an excitation input to a

model of the fuel module.



Acceleration Time Profile for Rail Wagon Carrying 38 tonne Package Striking 226.8 tonne Stationary Train at 10mph



Acceleration Time Profile for Rail Wagon Carrying 38 tonne Package Striking 226.8 tonne Stationary Train at 10mph

(a) Predicted Longitudinal Acceleration Time History due to Rail Shunting

(b) Predicted Vertical Acceleration Time History due to Rail Shunting

Figure 3.23: FEA Predictions of Fuel Bundles due to Rail Wagon Shock after Elbestawi [23]

Dixon [85] carried out a programme of research on tie down systems involving both experimental and analytical work. Although mainly focused on road transport Dixon reported that a FEA model was developed of a rail wagon, package and tie down system. The model was used to assess low velocity impacts (minor incidents) of a rail wagon, package and tie down system running into a stationary train at 5 mph and 7 mph.

Package mass, speed and buffer characteristics were varied to understand the highest maximum longitudinal acceleration that could be achieved. The study concluded that a package and its conveyance with a gross laden weight (GLW) of 185 tonnes could experience a maximum longitudinal acceleration of 5 g at the centre of mass of the package. Dixon pointed out that this may cause the derailment of the train prior to the maximum peak acceleration.

Read *et al* [46] provided an approach to satisfying the competent authorities for tie down assessments. Their methodology included an assessment of a minor mishap during normal conditions of transport. A rail wagon, tie down system and package were modelled using the Explicit FEM technique (Figure 3.24). The buffers were modelled with springs and their stiffness tuned until the regulatory acceleration levels were obtained.

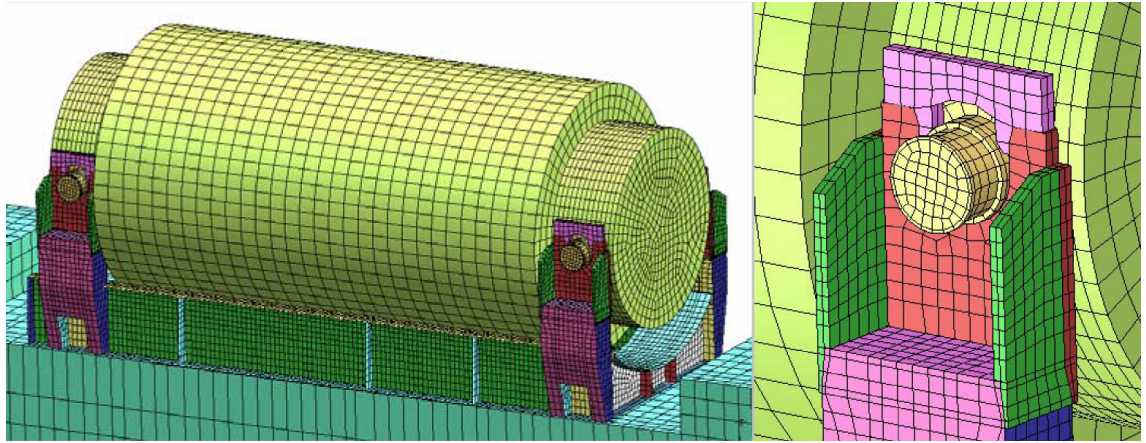
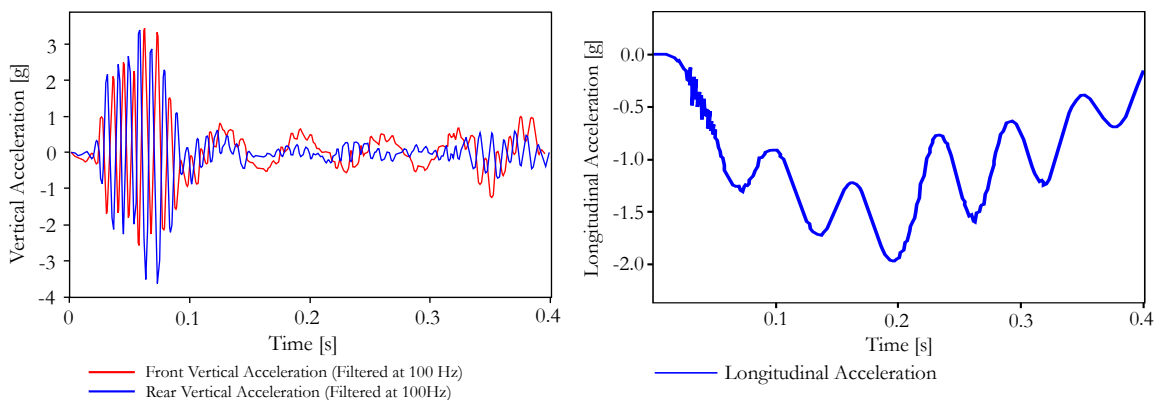


Figure 3.24: FEA Model of Rail Wagon, Package and Tie Down System *after Read et al [46]*

After low pass filtering at 100 Hz the vertical accelerations were found to be higher than the longitudinal accelerations for the first 100 ms (**Figure 3.25a**). At the maximum vertical acceleration of 3.5 g the longitudinal deceleration was approximately half its maximum at 1 g (**Figure 3.25b**).

Significantly the coexisting lateral and vertical accelerations, at the peak longitudinal deceleration, were much lower than the acceleration factors commonly applied in tie down system design to assess normal conditions of transport [2]. On this basis it was concluded the current assumptions made during tie down system design were conservative.



(a) Front and Rear Vertical Accelerations (b) Longitudinal Acceleration Time History

Figure 3.25: Finite Element Prediction of Accelerations acting on a Heavy Package during Rail Impact under Regulatory Conditions *after Read et al [46]*

3.2.2 Vibration

Tartary [60] designed anti vibration mounts for a medium sized (13 tonne) nuclear package. **Figure 3.26** shows a drawing of a 3 degree of freedom vehicle model representing a trailer and suspension and a nuclear package suspended from the trailer on anti vibration mountings. Tartary [60] reduced the design and calculation procedure by applying notching of the road excitation input spectra, **Figure 3.27**. This method is similar to that described by Soucy [59] on force limited vibration for the Canadian Space Agency. **Figure 3.27** provides a diagrammatic explanation of how notching the input loading was implemented to successfully design anti vibration mounts.

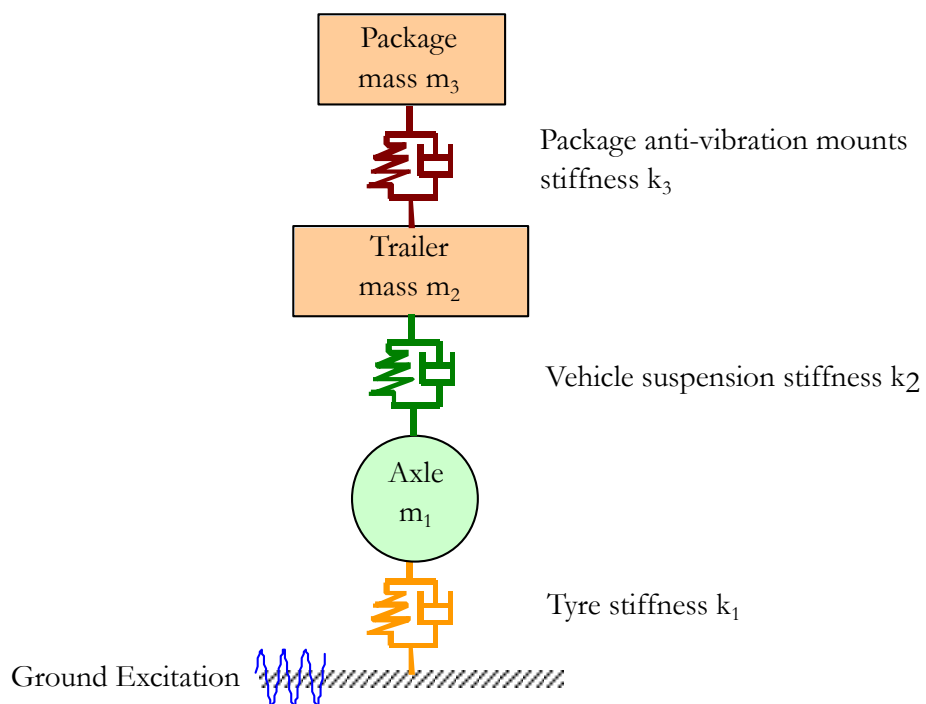
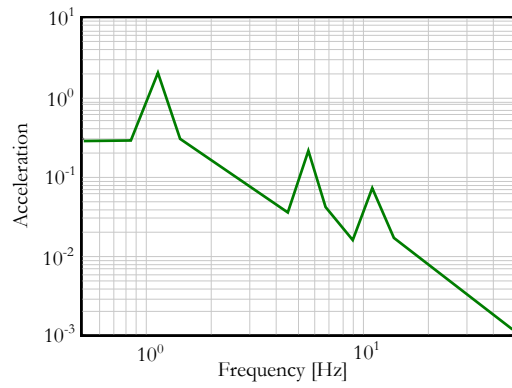
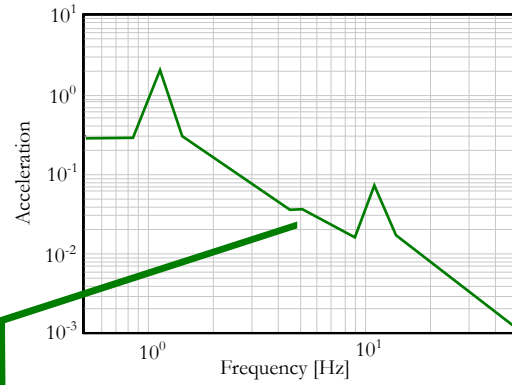


Figure 3.26: A 3 Degree of Freedom Road Vehicle, Package and Anti Vibration Mounts Model after Tartary [60]

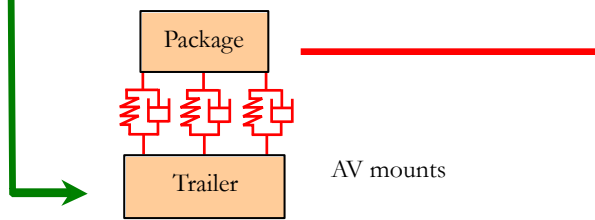
Notching the excitation input was necessary to remove the resonance due to dynamic coupling of the original package and trailer. This is an important effect when considering transport systems with conveyance and package masses that are similar [57–59]. Ignoring these effects would potentially make design very difficult or even impossible because of the sensitivity of accelerations predicted at the fuel assemblies due to the large variation in input loading.



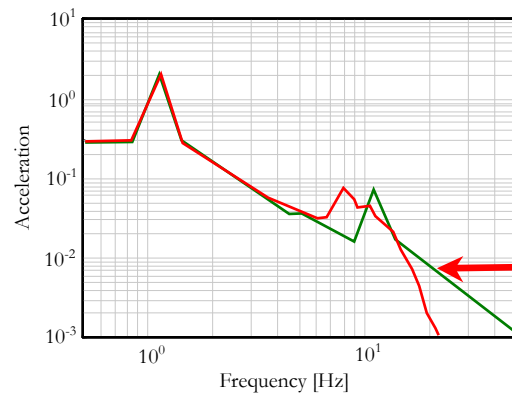
Envelope of spectra coming from measurements or standards for configurations close to M4/12 package transport configuration



Resonance due to coupling with original package removed. This spectrum is selected as input for the model



Simplified vehicle and suspended package model consisting only in trailer mass, AV mounts and package. This takes into account the trailer and package coupling leading to an upward shift in suspension resonance



Computation of Package Response

Figure 3.27: Notching Method to Simulate Road Transportation of Package and assess effect of Anti-Vibration Mounts *after* Tartary [60]

3.2.3 Crashworthiness

In the rail industry during the last decade several authors have developed models for accident events that would not typically be assessed by experiment. In particular the analysis of high speed train collisions with deformable objects has been studied in detail. A noteworthy contribution has been made by Xue [62–65, 108–111] with several papers to improve the understanding of passenger rail vehicle design and response in such scenarios.

The methods described in this area of the literature feed in to the current work in two ways. Firstly there is a need to understand accident conditions during tie down system design. This is to achieve a weak link which fails during an accident, preventing damage to its package. Secondly the methods may be adapted to model normal conditions of transport, in particular for shunting [2]. For this purpose the opportunity to validate a model by comparison with experiment is also more plausible.

Xue [62] developed explicit FEA crash models of a leading rail cab vehicle and three deformable targets including a 40t object (Figure 3.28). For comparison the rail cab was also assessed in a crash into a rigid target. The steel was modelled as elastic-plastic, with a kinematic hardening material model. The stress-strain curves were simplified using a bilinear relationship with an elastic and plastic region of the material response.

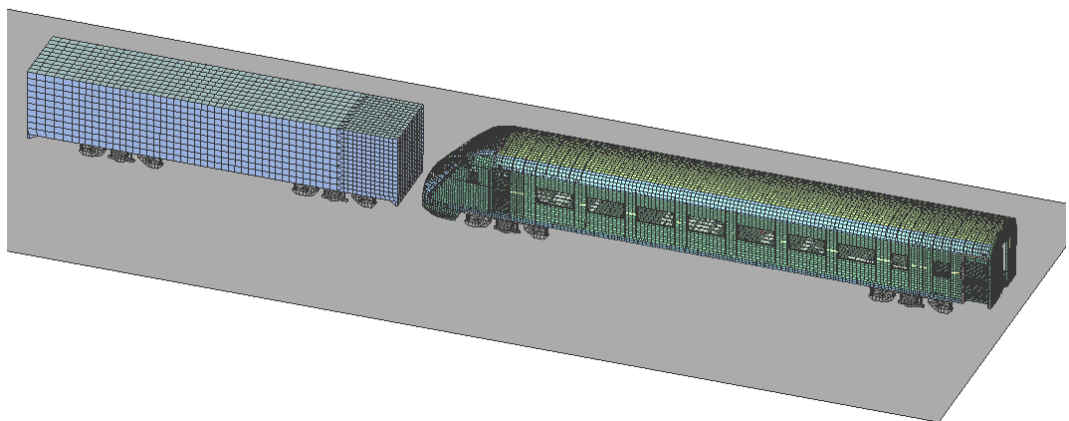


Figure 3.28: FEA Model of a Leading Rail Cab Vehicle and a 40 tonne Deformable Object after Xue *et al* [63]

The modelling of the wheel track interface was simplified by assuming the wheels were under full braking and do not rotate. The tread of the wheels was assumed to be flat and the track was modelled as a rigid surface. This aspect of the modelling was critical to assessing the potential for derailment, and the conclusions were that the detail omitted is necessary. In future work it was proposed that the wheel track interface should be included with a rigid body dynamics tool coupled with FEA.

Xue *et al* [62] also carried out a comparative study of the modelling approaches to rail vehicle crashes. As an introduction to the work they criticise the current design approach utilising proof loads for the purposes of crashworthiness, as the resulting structures become too stiff and perform badly during impacts. They are also critical of some of the current methodologies used in crashworthiness assessments, in particular the use of symmetry models and the use of rigid wall impact targets [64].

A sensitivity study on the effects of using deformable and rigid targets showed that in some circumstances the use of a rigid wall can mask design weaknesses and that rigid wall impacts can provide resisting moments that correct irregular deformation behaviour (**Figure 3.29**). Xue *et al* [62] explains that his modelling research has led to the conclusions that half symmetry vehicle models may not be a safe assumption due to asymmetric load redistribution during the impact event [109–111].

In a more recent study by Sun *et al* [65] a RBD approach has been used to develop a model based on Xue's [108] previous publication. Their validated model was then used for sensitivity analysis of vehicle speed and number of vehicles in the train. In a final step the model was used to parametrically vary the crush zone parameters to reduce decelerations in frontal impacts. Despite different methodologies Xue and Sun independently reached similar conclusions. The research highlights that current design of crush zones in passenger rail vehicles are too short and stiff. Furthermore static design methods currently recommended in the Rail Group Standards do not allow for satisfactory design of crush zones in an impact scenario. As an example Sun showed that by increasing the crush zone length from 1 m to 2 m during a crash at 70km/h the peak decelerations experienced by the first car can be reduced from 40 g to 15 g.

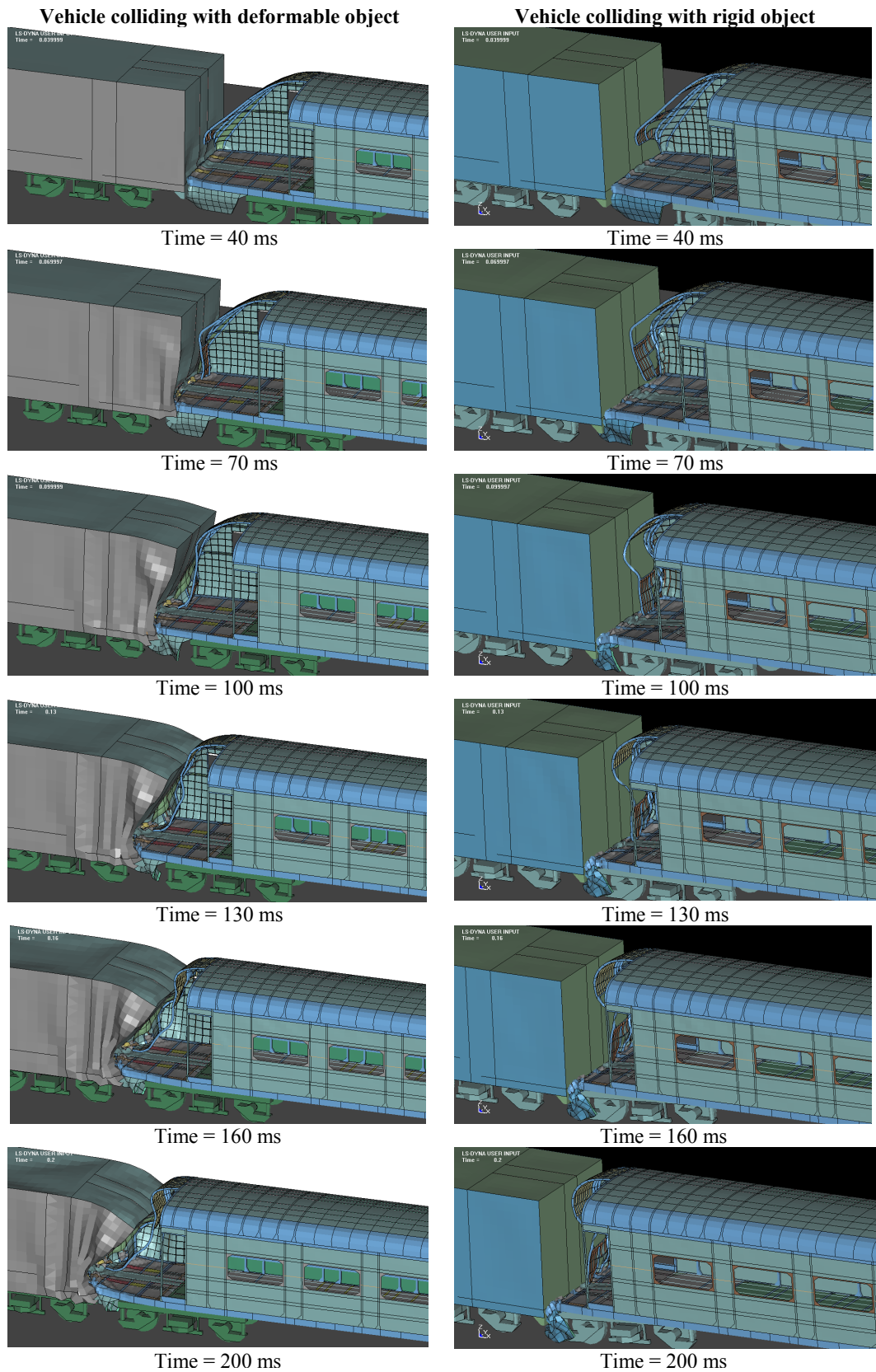


Figure 3.29: Crash Progress of a Vehicle Colliding with a 40t Object of Deformable and Rigid Structure after Xue *et al* [108]

3.2.4 Fatigue

The guidance documents for the design of tie down systems require that the possibility of fatigue failure is addressed during development [2]. However design justification can be difficult for particularly heavy packages because the standards do not reduce design loads on the basis of increased package mass. This problem is compounded due to the low operational usage of many tie down systems which are incompatible with the standard design loads that are based on much more arduous service life histories, such as 100,000 km/year over 30 years [45] or 200,000km/year over 30 years [14].

There are two alternative methods of assessment that are based on measured or calculated loads. In the first approach measured loads are applied as inputs to a FEA model. The second method uses loads calculated with RBD as input loads for FEA. Heyes [112] outlines the three main steps in a fatigue assessment as:-

1. Define the loading spectra.
2. Establish a load-strain relationship.
3. Define a strain (or stress) life relationship.

He identifies the definition of suitable loading spectra as the most challenging aspect of accurate fatigue assessments. Central to this kind of assessment is the assumption of linearity between the measured loading and the stress/strain responses. If this assumption is valid then fatigue assessments are greatly simplified because it allows the stress results at any point on a structure to be recovered from a linear static, unit load model and response histories to be constructed. This is achieved by scaling and superposition of the unit load stresses with measured input loads [113, 114].

Peng *et al* [77] developed a method for constructing response time histories when the expected structural response is non-linear due to elastic-plastic material behaviour. Essentially the method involved calculating the strain response to several non-linear analyses and then using regression analysis on the responses to derive a series of multivariate, quadratic functions. Finally the functions are applied to measured loads to obtain strain time histories that include the effects of non-linear material behaviour. In a similar paper the scaling and superposition procedure has also been extended by Speckert [115] to account for geometric non-linearities such as contact.

Baek *et al* [78] have developed and applied a fatigue assessment approach for rail bogie frames. They stated that a standardised load history must be developed for more accurate development work. In contrast Wannenburg argues that some of the

computational approaches that use transient FEA, multi parameter strain-life fatigue assessments and standardised load-histories (established from extensive field measurements) are difficult to implement for "special" purpose applications [42]. In his paper he suggests that an equivalent static fatigue load can be derived for non-standard transport requirements that will suffice for fatigue design.

In their paper on damage tolerant approaches to rolling-stock life management, Peng *et al* [116] calculated large non-conservative differences between life predictions using measured Australian rail-road inputs and the North American SLH used for design. As an alternative to using measured data as loading some research has been carried out to develop methods for calculating fatigue life on a purely theoretical basis [15, 78, 104, 117].

It is apparent that many approaches have been used to apply measured loads for fatigue assessments, some with good success. There is also evidence in the literature of methods for calculating these loads using RBD [14, 15, 78, 117]. To develop a SLH for nuclear transport applications would invariably require that measurements be obtained to validate computer models. These computer models may then attempt to fill the missing gaps in knowledge [10, 14].

3.2.5 Validation

In this final section of the chapter an overview of validation techniques associated with the various modelling methods reviewed in the preceding sections is presented.

The rail vehicle dynamic modelling work of Fields [20] provides the earliest example of detailed validation work in the nuclear transportation industry. Fields based validation of CARDS on two techniques:-

1. Theil's Inequality Coefficients – A statistical technique for comparing, in the time domain, the differences between predicted and measured values of a time varying response variable.
2. Visual comparison between the calculated and measured time responses.

Theil's Inequality Coefficient will vary between 0 and 1, where a value of 0 is a case of perfect equality (or agreement) and 1 is a case of maximum inequality. It is calculated using the following formulae:

$$U = \frac{\sqrt{\left[\frac{1}{n} \sum_i^n (Y_{Pi} - Y_{Ai})^2 \right]}}{\sqrt{\left[\frac{1}{n} \sum_i^n Y_{Pi}^2 \right]} + \sqrt{\left[\frac{1}{n} \sum_i^n Y_{Ai}^2 \right]}} \quad (3.4)$$

where:-

Y_P = time history of predicted accelerations

Y_A = time history of actual accelerations

i = index

n = number of point in time history

Validation studies for six of the SRL tests were undertaken. An example of one particular comparison made between the SRL tests and CARDS is described here. In the example the CARDS program was run for two cases; the method of excitation of the rail wagon was applied by either calculated or measured coupler forces. Theil's Inequality Coefficients were calculated for six response variables (Table 3.5).

The individual values for the vertical accelerations of the package were poor in both case 1 and 2, despite good Theil's Multiple Inequality Coefficients,. This was at-

tributed to phase differences between measured and calculated values. Fields pointed out that both the magnitude and frequency of the measured and calculated signals were in good agreement (**Figure 3.30a** & **Figure 3.30b**).

During testing the maximum frequency of interest was estimated by specialists at Sandia Laboratories as 1100 Hz. The original signals from SRL were sampled at 5.12 kHz and to reduce the data for analysis purposes every second data point was considered; this effectively adjusted the sampling frequency to 2.56 kHz.

Based on the Nyquist’s sampling theorem this would retain frequency content up to 1.28 kHz, however to capture peak content up to 1100 Hz the sampling frequency should have been at least 10 times that (11 kHz). As a consequence many of the peaks presented within the measured (and calculated) time histories were jagged in appearance (**Figure 3.30**).

Response Variable	Theil’s Two Variable Inequality Coefficients ¹	
	Case 1 - Measured Coupler Forces	Case 2 - Calculated Coupler Forces
Coupler force (if applicable)	0.000	0.223
Longitudinal tie down force	0.158	0.194
Longitudinal acceleration of package	0.205	0.254
Longitudinal acceleration of rail wagon	0.211	0.445
Vertical acceleration of package far end	0.600	0.776
Vertical acceleration of package struck end	0.656	0.470
Theil’s Multiple Inequality Coefficient	0.059	0.214

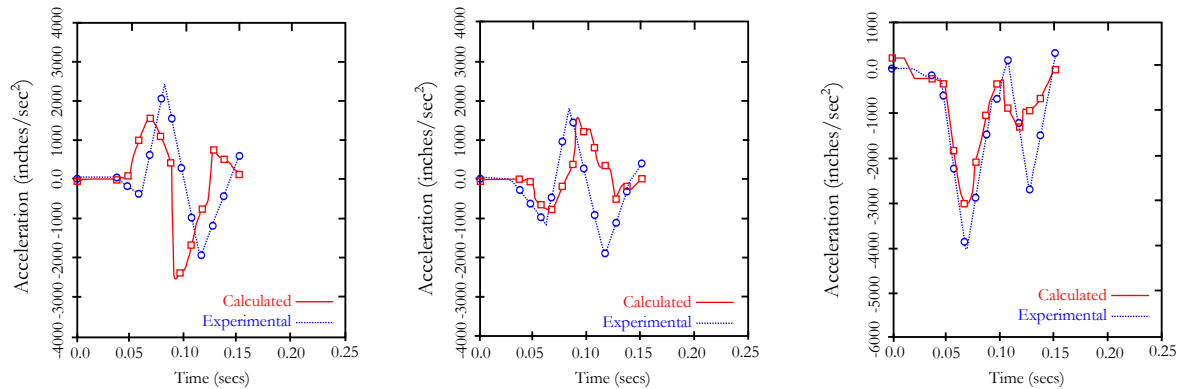
¹ A value of 0 indicates best agreement and a value of 1 indicates poorest agreement

Table 3.5: Theil’s Inequality Coefficients for Response Variables Determined using Calculated and Measured Coupler Forces *after* Fields [22]

Fields filtered the measured data by removing spectral lines of magnitude of a Fast Fourier Transform (FFT) and then taking the inverse FFT (IFFT) of the remaining spectrum. The measured longitudinal accelerations were low pass filtered with a cut-off frequency of 100 Hz and the vertical accelerations at 50 Hz. The reason for using the filter was to remove high frequency noise within the system; he stated that no attempt to characterise the noise was made (**Figure 3.30**).

Validation could have been improved by additional care in the selection of measurement sampling frequency and filter design. However the aims of the project,

to provide a validated analytical model for parametric and sensitivity studies on tie down loads, were achieved.



(a) Vertical Acceleration Time History of Package Far End (Frequency Domain Low Pass Filter 50 Hz)

(b) Vertical Acceleration Time History of Package Struck End (Frequency Domain Low Pass Filter 50 Hz)

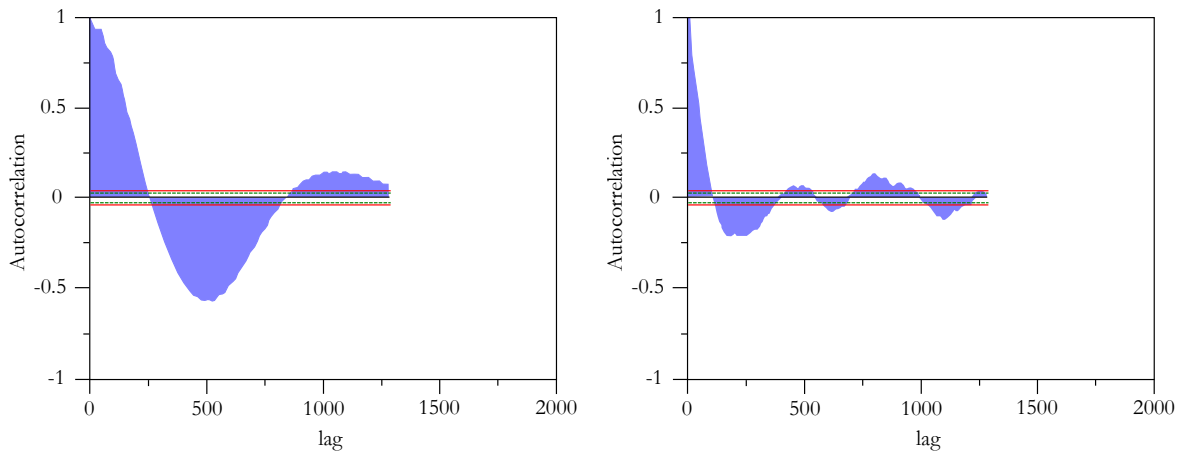
(c) Longitudinal Acceleration Time History of Package (Frequency Domain Low Pass Filter 100 Hz)

Figure 3.30: Comparison of Calculated and Experimental Acceleration Time Histories from a Rail Wagon and Package Impact *after* Fields [22]

A useful validation procedure was demonstrated by Chaika *et al* [118] who carried out an experimental and numerical study to determine the loads acting on a moving military vehicle. They used a specifically written RBD computer program called DADS (Dynamic Analysis Design System) to model a tank running over different size speed bumps at varying speeds. In conjunction with the modelling a series of experiments to provide measured loads were also performed.

To validate the model Chaika [118] proceeded with a detailed analysis of the residuals between measured and calculated force time histories. As an initial step he examined the residuals for evidence of any trends or frequency content that would suggest a mathematical or physical difference between the model and test. He then carried out a more rigorous evaluation of the residuals firstly by calculating the autocorrelation function (Figure 3.31). If the model and experiment are in good agreement then the character of the residuals would be white noise. Pure white noise is evident in an autocorrelation function when its value is one at a lag of zero and zero at all non zero lag values [119].

Figure 3.31a indicates that at low speeds the two signals have certain correlation patterns that are not white noise. At higher speeds the residuals tend towards a white noise process (Figure 3.31b). The red and green lines in Figure 3.31 represent the 90% and 95% confidence intervals respectively.



(a) Autocorrelation of the residuals between simulation and experiment of moving vehicle over speed bump at 7.7 mph

(b) Autocorrelation of residuals between simulation and experiment of moving vehicle over speed bump at 25.5 mph

Figure 3.31: Autocorrelation function of the residuals between DADS Simulation and Experimental Data after Chaika *et al* [118]

Analysis of the residuals in the frequency domain indicated low frequency components were present; a further indication that their structure was not white noise and that the simulations and experiments were not in agreement.

Sarin *et al* [120] reviewed several methods and techniques used to compare short, transient, measured acceleration time histories to those generated by simulations of automotive crash tests. He points out that some commonly used techniques such as the correlation coefficient and cross correlation function can produce low values which are misleading. This is explained because these methods do not take account of phase differences in measured signals. More advanced techniques based on dynamic time warping (DTW) were explored [121]. DTW systematically distorts one signals to match the other and provides a distance measure of how much distortion is required to obtain the match. Sarin concluded that DTW can provide phase, magnitude and slope error which will assist in developing a consistent validation metric to assess agreement between computer simulations and experiments of transient events.

3.3 Summary

- There are a large variety of packages in existence, however this variation is not reflected in the load cases available to tie down system designers. Although historical records indicate there is no safety issue with tie down systems there is evidence in the literature of disagreement over which load cases should be applied in design.
- Previous measurement campaigns have provided enough detail to characterise some aspects of the transportation environment, however several authors have highlighted the need for more measured data during rail transportation of heavy packages.
- No analytical work on routine conditions of transport has been carried out to supplement previous measurement campaigns of real journeys. The focus of previous simulation work has been shunting and coupling of rail wagons laden with a package.
- All of the literature reviewed on long haul journey measurements used on-board data processing techniques to reduce the data as it was acquired. Therefore no continuous measurements of acceleration or strain have ever been obtained. This would provide information on the characteristics of the signals, particularly for vibration and fatigue analysis, two areas that are not as well established as the static strength design loads.

4. A Method for Measuring Acceleration and Strain during a Routine Rail Journey of a Heavy Nuclear Package

4.1 Introduction

A lack of data on heavy packages was highlighted throughout the previous chapters as an area that required additional experimental work. This chapter describes a method for measuring accelerations and strains during a routine journey by rail of an unloaded 99.7 tonne nuclear package.

The heavy package was transported between Barrow-in-Furness and Sellafield with a transport frame used as the tie down system to the rail wagon. This experiment provided data on mechanical loading and additionally measured strain response of the tie down system.

Continuous time histories were digitally oversampled providing unclipped peak data up to 100 Hz. This is a different approach to previous studies, where onboard data reduction has been relied upon to efficiently handle storage requirements [11, 84, 85]. Using onboard data reduction is common practice but it does require some pre-existing knowledge of the environment to reduce the data successfully.

Conversely the measurement of continuous time histories provides a complete data set, minimising the potential of missing an event of interest during the test. Because strain gauges have been used the data presents a new opportunity to validate a computer model with measurements from a real journey.

4.2 Aims and Objectives

- To measure dynamic acceleration and strain data from a tie down system during a rail journey.
- Present scientific rationale for selection of measurement points on the structures.
- To assist in characterising the routine conditions of transport.
- To provide an experimental basis for comparison of design parameters with the Rail Authorities and the IAEA Regulations.
- To provide data for computer modelling and validation.

4.3 Method

The measurements were taken during a routine journey by rail from Barrow-in-Furness to Sellafield [122]. The rail vehicle consisted of two locomotives and three rail wagons. Two of the wagons acted as spacer wagons between the locomotives and the central wagon which transported the package and its tie down system. The central wagon, called a KXA-C, having previously been used for only 611 miles, was in excellent running condition and therefore a favourable environment for the tie down system was expected.

The first part of the test was the loading of the package onto the tie down system. The strain gauges were fitted to the frame prior to lifting but during this operation no measurements were taken. The package was lifted off the frame and the strain gauges and accelerometers were calibrated. Strain and acceleration were measured during the reloading of the package onto the frame.

The second part of the test was the continuous measurement on all data channels. Due to unforeseen circumstances several minutes of data were not collected in the central section of the journey (**Figure 4.1**).



Figure 4.1: Map of Rail Journey from Barrow-in-Furness to Sellafield Site, Cumbria

Figure 4.2 shows a CAD model of the rail wagon and package. **Figures 4.3 & 4.4** show the positions and labels of each transducer denoted by yellow (wagon) and red (frame) stars. A total of 8 triaxial accelerometers were used, four accelerometers were mounted to the stanchions of the frame, one on each stanchion. Two more accelerometers were mounted at the centre of each of the saddles, another on the wagon bed near the frame to wagon interface. The final accelerometer was mounted on the bogie of the rail vehicle.

Twelve strain gauge rosettes were mounted to various locations on the frame (**Figure 4.8**). During the loading test one of the strain gauge rosette legs was found to be faulty, on channel 34, rosette number 6. A new rosette was fitted for the journey measurements.

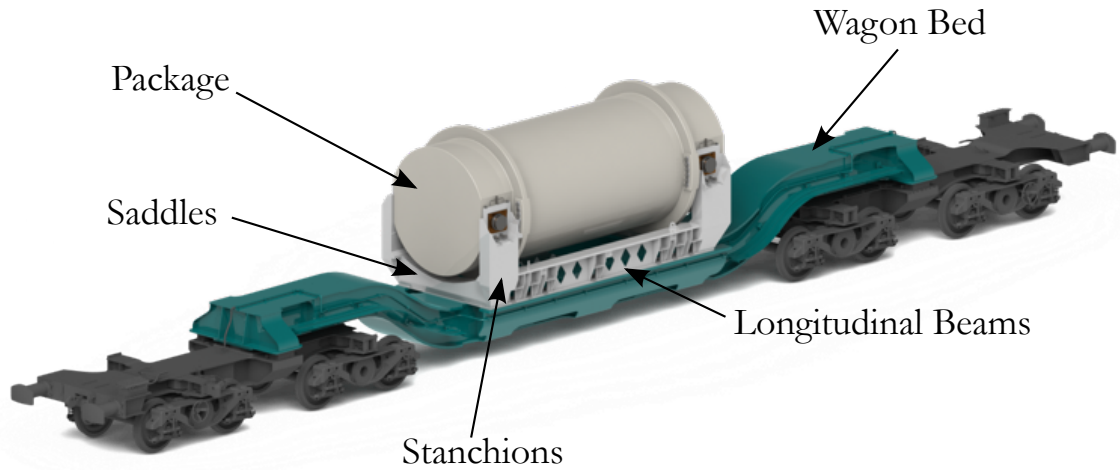


Figure 4.2: CAD Model of Rail Wagon, Package and Tie Down System

4.3.1 Selection and Positioning of the Accelerometers

Endevco 7920A-10 variable capacitance accelerometers were chosen for the test to enable measurements at low frequencies < 0.5 Hz. This was important to identify quasi-static loading. The maximum anticipated frequency range for the environment was DC - 100 Hz [14]. The frequency range of the selected accelerometers, DC - 500 Hz, was therefore more than sufficient for the experiment.

Redundancy was built in to the test by using more accelerometers than necessary. This ensured that if an instrument failed or suffered malfunction, the test would still produce some data from the other channels. For example all four of the transport frame stanchions were instrumented.

The accelerometers were mounted on suitably stiff members of the transport frame with an adhesive. This enabled the accelerometers to be mounted and removed without permanent damage to the structure.

One ideal location to position the accelerometer was at the centre of mass of the package, however at the exact position of the centre of mass there was no physical structure to mount an accelerometer. To identify loading on the transport frame two alternative positions were suggested; the four stanchions and the wagon bed.

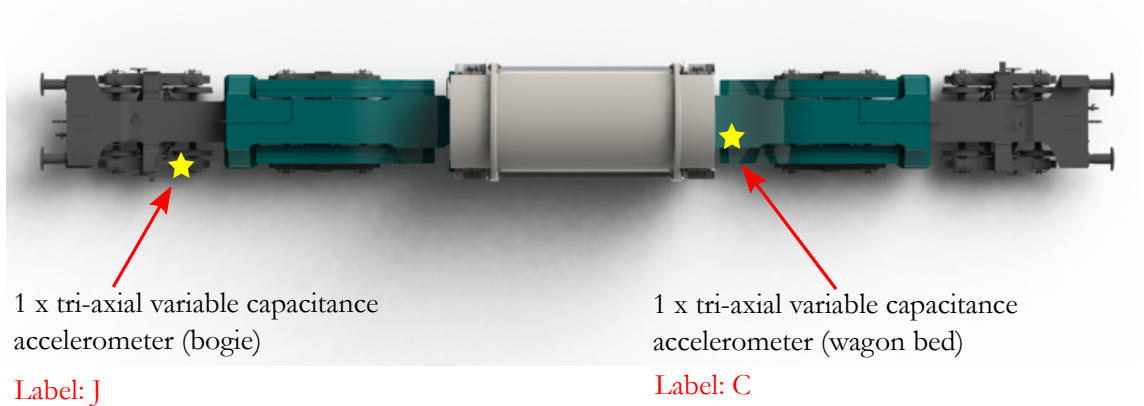


Figure 4.3: Accelerometer Positions

Mounting the accelerometers to the stanchions meant that they were as close to the centre of mass of the package as practically possible. The wagon bed measurement was included to provide an insight into the vibrational energy transmitted through the wagon bed into the frame and package. By selecting accelerometer positions in various locations on the conveyance, tie down and package it is possible to 'map' out the source of accelerations that arise during transport and also compare relative motion between positions.

It is noteworthy that most previous studies on transportation of nuclear packages have positioned accelerometers on the bed of the conveyance so this measurement location enables comparison with those studies [11, 82, 84].

Two further accelerometers were mounted to the centre of the saddle sections between the lid stanchions and the base stanchions. These positions were selected to study the transmission of vibration through the frame.

The final accelerometer was positioned on a bogie of the rail wagon, which was used to understand how much vibration was present from the wheel-track interface and how much energy contained in the signal was filtered out by the suspension. This was used as a point of reference to understand the source of the accelerations.

CHAPTER 4. A METHOD FOR MEASURING ACCELERATION AND STRAIN DURING A ROUTINE RAIL JOURNEY OF A HEAVY NUCLEAR PACKAGE

6 x tri-axial variable capacitance accelerometers on frame
DC - 100 Hz

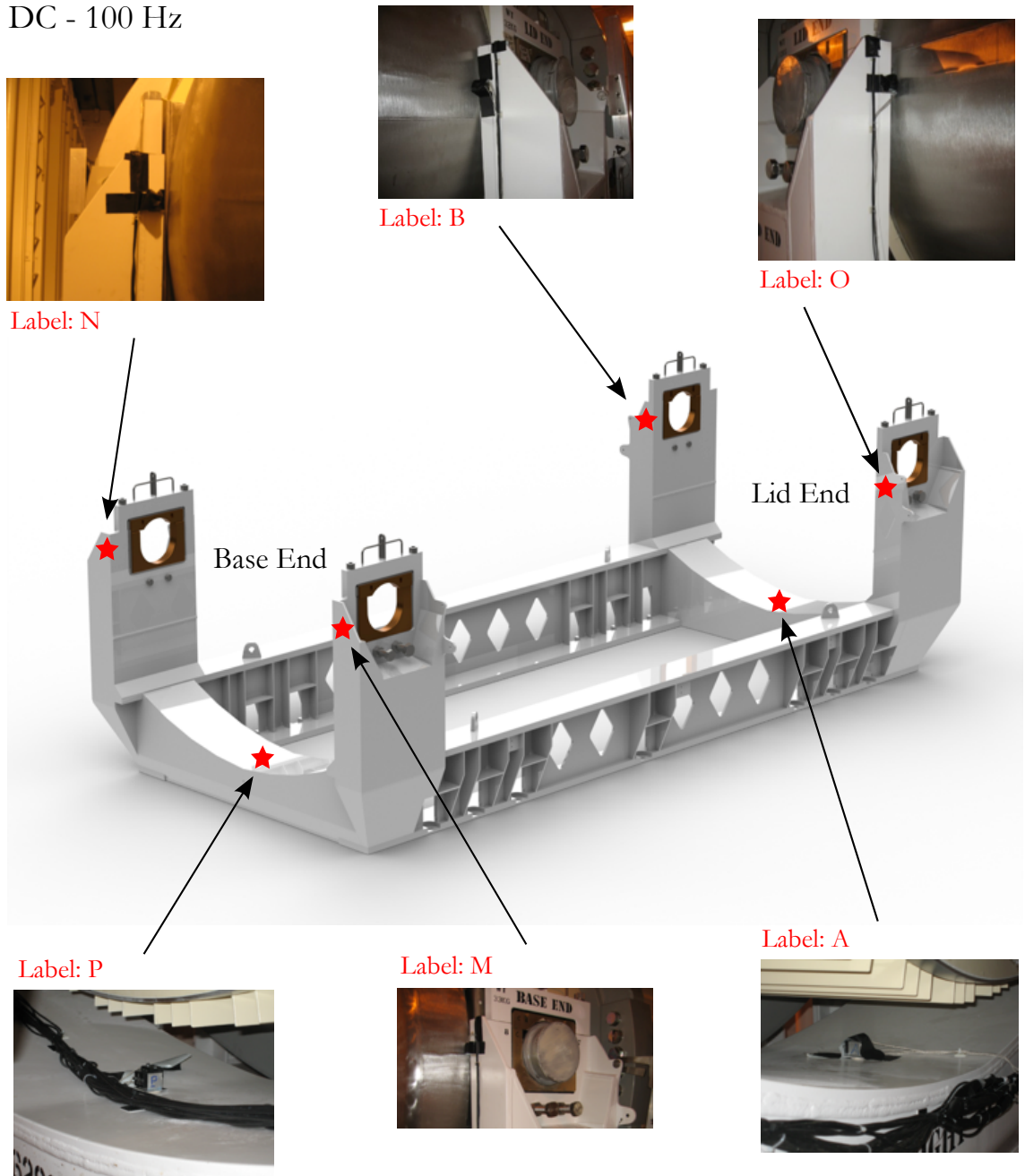


Figure 4.4: Accelerometer Positions on Transport Frame

4.3.2 Selection and Positioning of the Strain Gauges

A Finite Element Analysis was carried out to predict regions of highest strain. During transport the loading is multi-axial, random and dynamic therefore it was anticipated that the principle axes of strain will rotate throughout the journey. It was decided that FEA could predict the positions of highest strain but strain gauge rosettes should be chosen to eliminate any concerns over orientation of uniaxial strain gauges.

This ensures that if strains occurred in unexpected directions, or where slightly off-axis due to test set-up, the measurements would still be successful. Peak local stresses were identified from the results of the FEA model and the rosettes were positioned based on those locations.

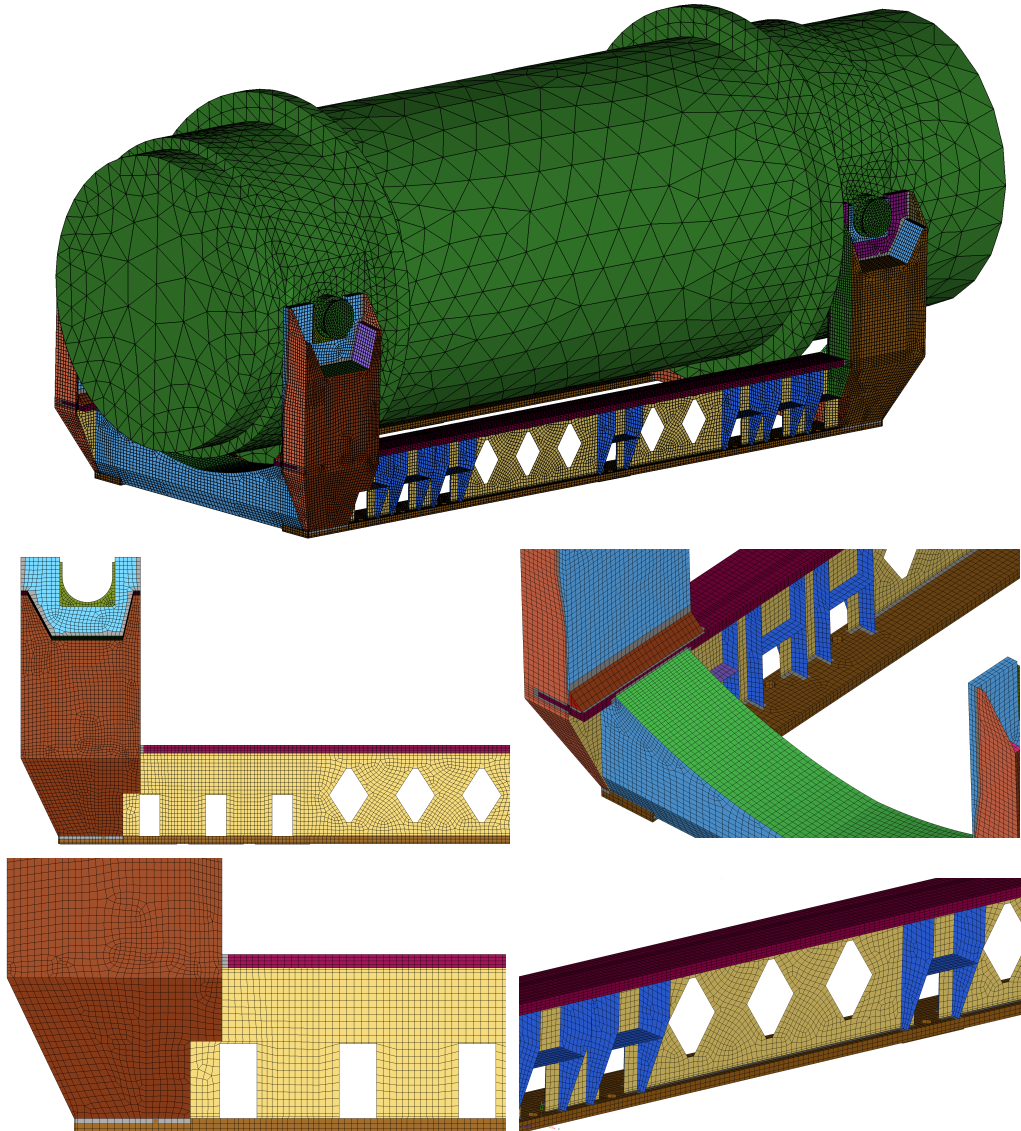


Figure 4.5: Finite Element Model of the Transport Frame and Package

The pre and post processing was done using Altair Hyperworks [123] and the model was solved with ANSYS [124]. The geometry was constructed using manufacturing drawings and a hybrid shell and brick mesh was created. The mixture of bricks and shells was enforced by the construction of the transport frame which is fabricated with thick plates ($\approx 15\text{mm}$) butt-welded to very thick supporting members ($\approx 50\text{mm}$). The model is shown in Figure 4.5.

To improve stress resolution and avoid hourglassing of elements in bending SOLID185 elements with KEYOPT(2) set to 0 were chosen. This element formulation is called the B-Bar method in the ANSYS documentation or selectively reduced integration. The formulation improves bending behaviour of full integration elements alleviating pressure locking but not shear locking. In practical terms these elements bend more realistically than single point or full integration solid elements but are slightly too stiff. The shell element formulation used was SHELL181 with KEYOPT(3) set to 2, a full integration shell element.

A linear elastic stainless steel material model based on British Standards material data was assigned to the mesh with a Young's modulus of 200,000 MPa, Poisson's ratio of 0.3 and density of $7,800 \text{ kg/m}^3$ [125].

Load Cases	Longitudinal [g]	Lateral [g]	Vertical [g]
1	1		
2		1	
3			1
4	0.25	0.25	-1.3
5	0.25		
6		0.25	
7			0.3

Table 4.1: Load Cases for Finite Element Analysis of the Tie Down System and Package used to Select the Position of Strain Gauges

The package was modelled as a lumped mass equivalent to the 99.7 tonne package in the test. The nodes at the base of the longitudinal beams of the frame were fixed in all directions, preventing rigid body motion and a linear static analysis was performed. A variety of load cases were considered, based on estimates of what the loading may be during the journey and acceleration factors quoted in the regulatory guidance and codes of practice [2, 74]. Table 4.1 lists the load cases considered.

The loads were applied simultaneously in some load cases and independently in

others. This was to minimise the chance of missing a strain hot-spot due to the superposition of simultaneously occurring multi-axial loads. Zhang [44] and more recently Zhu [79] carried out similar studies for the purposes of identifying loads on rail vehicle bogies and their preference was to apply unit loads independently.

During post-processing stress contour plots were used to detect regions of high stress. The areas that indicate the highest stress gradients were considered to be locations where a high signal to noise ratio would be expected during the test and therefore selected for strain gauging.

An example of the results due to load case 4 are shown in **Figures 4.6 & 4.7**. The contours of principal stress in **Figure 4.6** indicate that the stanchions and their trunnion bushes are the most highly stressed areas. The predominant loading is due to gravity which acts through the centre of mass of the package and causes compressive stresses at the interface between the package trunnions and the transport frame trunnion bushes.

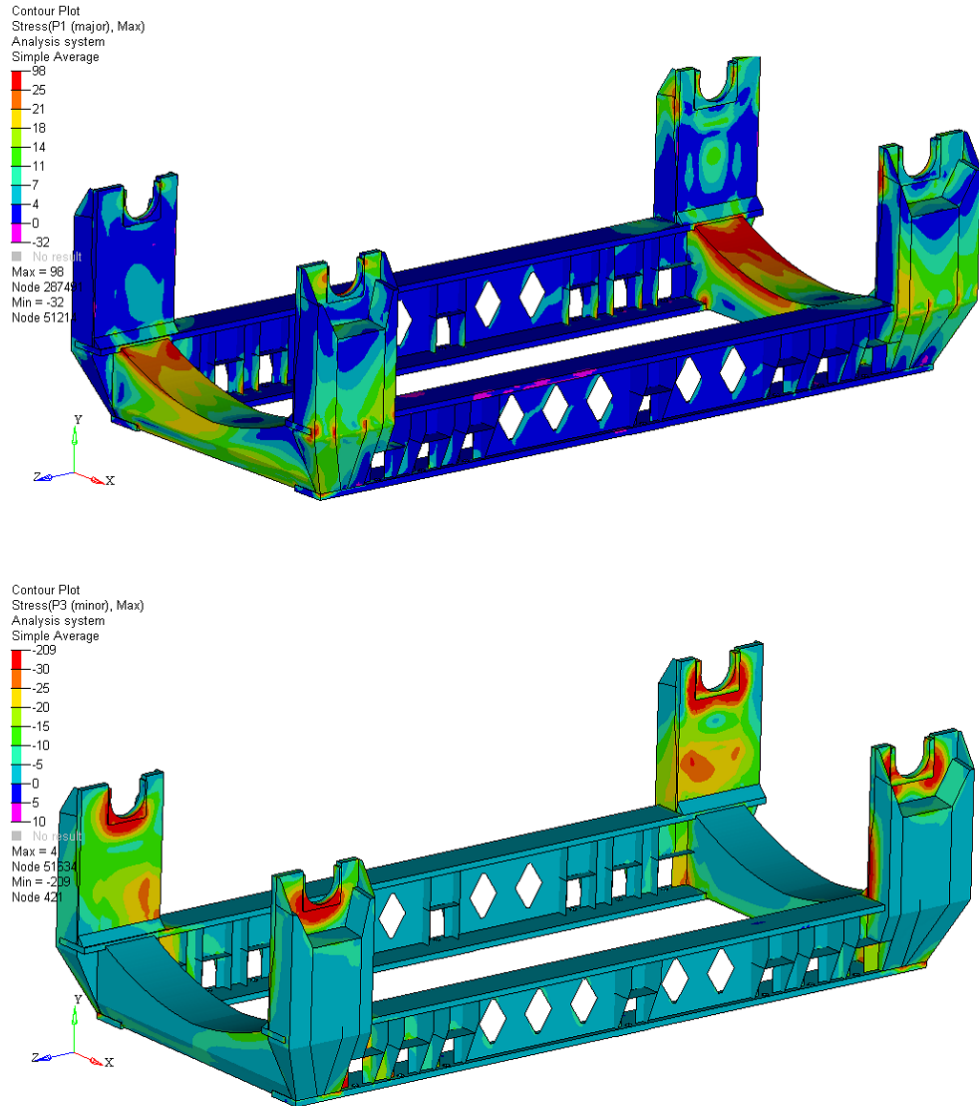


Figure 4.6: Principal Stress Contour Plots of Transport Frame (in units of MPa)

This maximum tensile stresses that occur are on the top plates of the saddle sections. These stresses occur due to lateral loading. There is marginally more stress at the base end of the tie down due to longitudinal positioning of the centre of gravity of the package, which causes a slight twisting to occur when loaded laterally.

Figure 4.6 also indicates that the longitudinal beams are not highly stressed and therefore no strain gauges were fitted to these areas. This is potentially surprising because the beams have many cut out holes with sharp corners that are typical stress raisers, however the load paths into the cut outs are prevented by the rigidity of the saddles and stanchions.

CHAPTER 4. A METHOD FOR MEASURING ACCELERATION AND STRAIN DURING A ROUTINE RAIL JOURNEY OF A HEAVY NUCLEAR PACKAGE

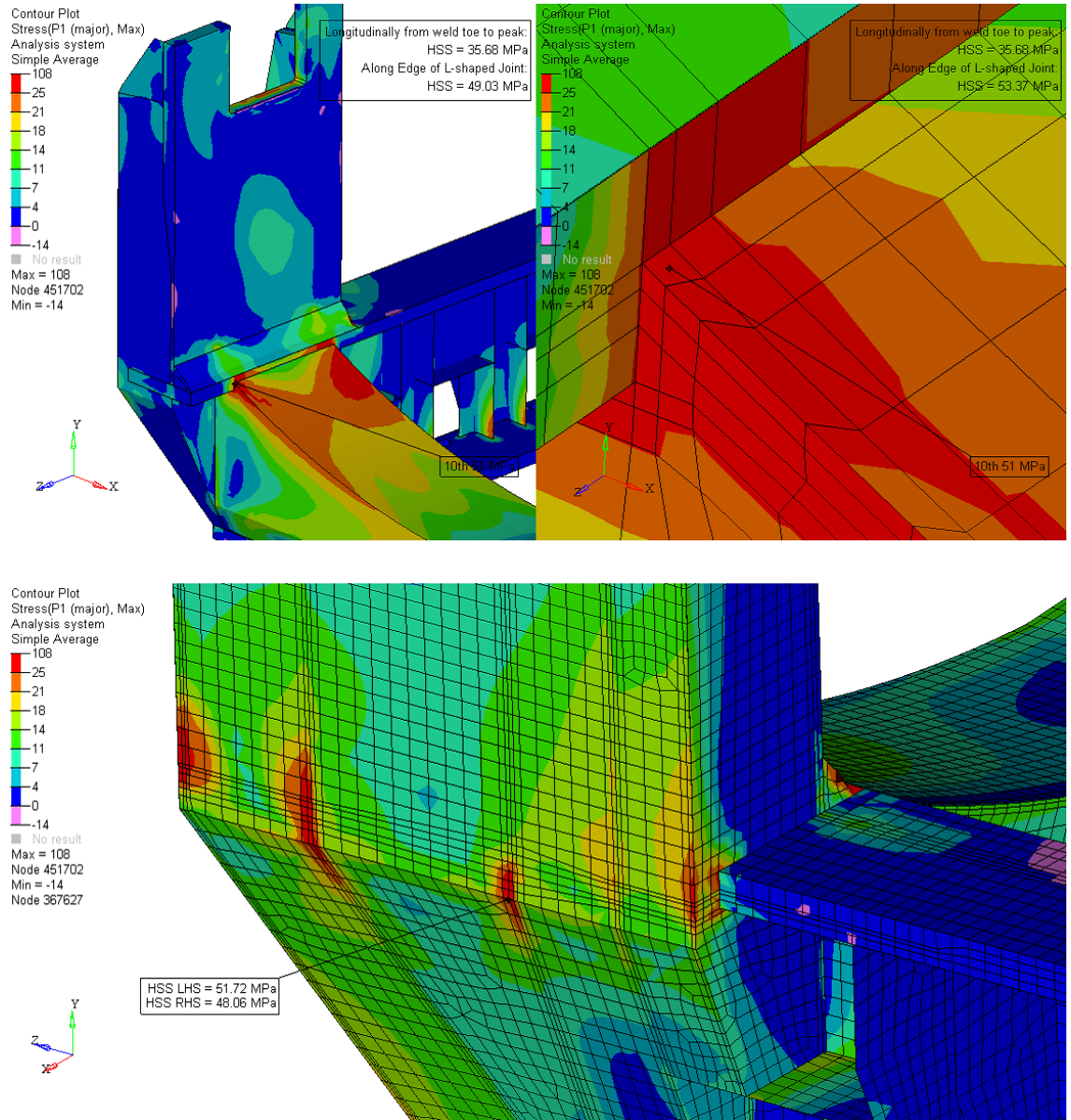


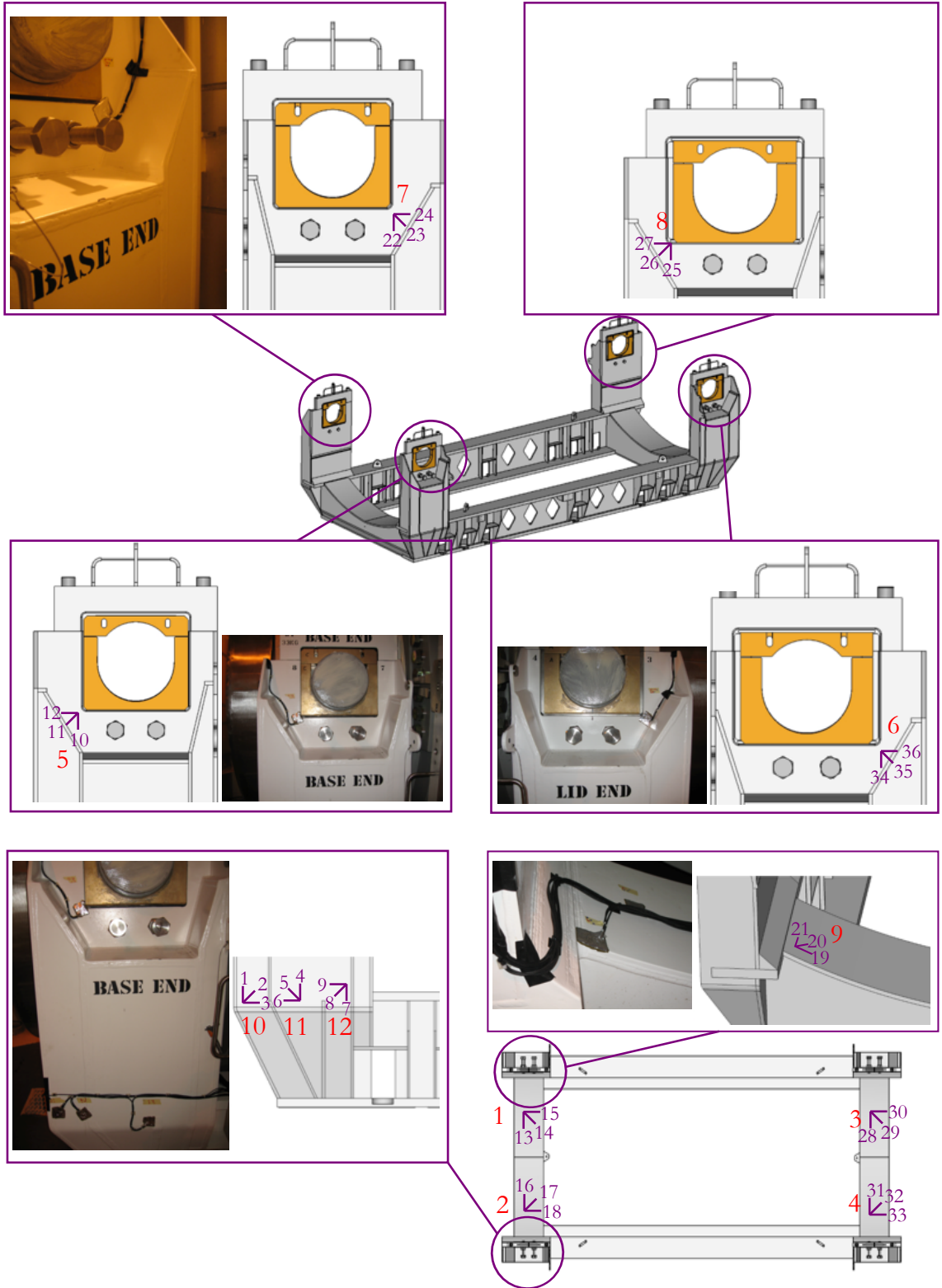
Figure 4.7: Principal Stress Hot Spot Locations (in units of MPa)

Figure 4.7 shows several welded joints that the FEA model indicates as local areas of high stress gradient. Most of these areas are near 90° corners where shell elements are merged with either shell or brick elements to replicate T-joints or L-joints. If stresses in these areas occur at single nodes they are due to numerical singularities and are considered a spurious artefact of the mesh.

The hot-spots in this model occur over small areas (and several nodes) that would promote stress raisers due to sharp changes in geometry or their position within a load path. Therefore they were considered as plausible stress concentrations. Using guidance from the Welding Institute these hot-spot stresses can be interpreted for structural (fatigue) assessments based on specific mesh discretisation criteria, weld geometry and plate thickness [126].

To gain a better understanding of their significance on this study, four of these areas were strain gauged $\approx 15\text{mm}$ away from each weld toe. Three strain gauge rosettes were positioned on the stanchion front plate at the welded joints to its internal stiffeners. The other strain gauge rosette was positioned at the corner weld between the saddle top plate, side plate and stanchion. **Figure 4.8** shows all of the positions selected for strain gauging.

CHAPTER 4. A METHOD FOR MEASURING ACCELERATION AND STRAIN DURING A ROUTINE RAIL JOURNEY OF A HEAVY NUCLEAR PACKAGE



Numbers in red refer to strain gauge numbering
 Individual legs of rosettes are numbered in purple

Figure 4.8: Strain Gauge Labels and Positions

4.3.3 Data Acquisition System and Transducers

4.3.3.1 Accelerometers

The transportation environment was expected to produce quasi-static, vibration and shock type loading. The selection of accelerometers was therefore critical to ensure that each type of loading was measured correctly. It was evident from the literature review that large accelerations (100's of g's) were not anticipated, so specialist shock instrumentation, such as low sensitivity charge mode piezoelectric or piezo-resistive accelerometers were excluded [127].

These devices require a carefully designed signal conditioner with a band-pass filter to reduce zero shift and accelerometer resonance. Charge mode accelerometers also require high cost, low noise coaxial cables.

This simplified the instrumentation choice to either internal electric piezoelectric (IEPE) or variable capacitance accelerometers. IEPE accelerometers include onboard electronics that mitigate the need for an amplifier and require only standard cables. They have a wideband frequency response from a few Hz to several thousand Hz and high sensitivity, making them a good choice for low level, wideband vibration typical of a transportation environment. The major drawback of IEPE accelerometers for this experiment was their poor response to very low frequencies which would not detect quasi-static motion.

For this reason variable capacitance (VC) accelerometers were selected. These transducers are sometimes referred to as "DC responding", which means that they detect constant acceleration i.e. they respond to gravity or centrifugal acceleration. This makes them ideal to detect cornering and other vehicle manoeuvres but they also have a wide enough frequency response to measure transportation vibration and shock.

Two Endevco VC accelerometer models, the 7920A-2 and the 7920A-10, were considered for use. The designation -2 and -10 relates to their magnitude range of ± 2 g or ± 10 g respectively. The -2 variant has a high static sensitivity of 1000 mV/g and a narrow frequency response $\pm 5\%$ in the range DC - 15 Hz. The -10 variant has a lower sensitivity of 200 mV/g and a wider frequency response $\pm 5\%$ in the range DC - 500 Hz.

The 7920A-10 model was selected because it offered a larger acceleration range of ± 10 g and a sufficiently wideband frequency response from DC - 500 Hz [128]. These attributes were at the expense of a lower static sensitivity. This was not considered to cause any limitation to the test because the lowest measurable acceleration is bound

by either the accelerometer resolution or the noise level of the amplifier. The Endevco 7920A-10 has a minimum discernible signal or resolution of 0.0025 g (within the frequency range DC - 100 Hz). The amplifier noise level is quoted as 50 μV which means based on its static sensitivity of 200 mV/g the minimum detectable signal above the noise level of the amplifier is 0.00025 g. So the accelerometer resolution of 0.0025 g was determined as the lower bound measurable acceleration, which is considerably below the level of interest in this study.

The variable capacitance accelerometers are also low impedance devices and therefore suitable for use with standard cables. Cable noise and length were therefore not considered a major issue.

4.3.3.2 Strain Gauges

CEA-06-250UR-120 strain gauge rosettes, supplied by Vishay Micro-Measurements were selected for the strain measurements. Rectangular rosettes were chosen instead of tee or delta rosettes because the direction of principal strains were unknown.

The strain sensing material in this type of strain gauge is a Constantan alloy which is extensively used due to its high strain sensitivity (gauge factor), good resistivity, fatigue resistance and large elongation. One possible drawback with Constantan alloy is its tendency to drift, although this is most noticeable above 65°C. For this reason temperature compensated strain gauges have been selected by matching their coefficient of thermal expansion with the steel used for the transport frame.

The gauges were mounted with a adhesive directly applied to their polyimide backing material. The backing material was suitable for elongations of up to 20%, much larger than the expected strains in this experiment. The Datasheet states that the gauges have a maximum elongation of 50,000 $\mu\text{m}/\text{m}$ (5%) and a fatigue life of 10^6 cycles due to constant amplitude loading of $\pm 1500 \mu\text{m}/\text{m}$.

The recommendations from Vishay Micro-Measurements [129] when choosing gauge length is that it should be no more than 1/10 of the stress concentration of interest. This type of strain gauge is only supplied in one length, 6mm, therefore the rosette is capable of detecting a stress concentration area $> 60\text{mm}^2$. For the nominal measurements positions this was considered to be sufficient. However the FEA mesh of the welded joints may not be sufficiently refined to accurately determine the strain concentration size and position. Due to commercial time constraints this was not addressed but left outstanding as a minor technical risk that the strain gauges at the welded joints may not be optimally positioned or of appropriate size.

The final part of the strain gauge selection was choice of resistance. These strain gauge rosettes are normally available in 120 Ω and 350 Ω , however at the time of the experiment the suppliers only had 120 Ω gauges. The benefit of a 350 Ω gauge would be an increased signal-to-noise ratio. **Figure 4.9** summarises this section with a detailed breakdown of the strain gauge identification number selected for the test.

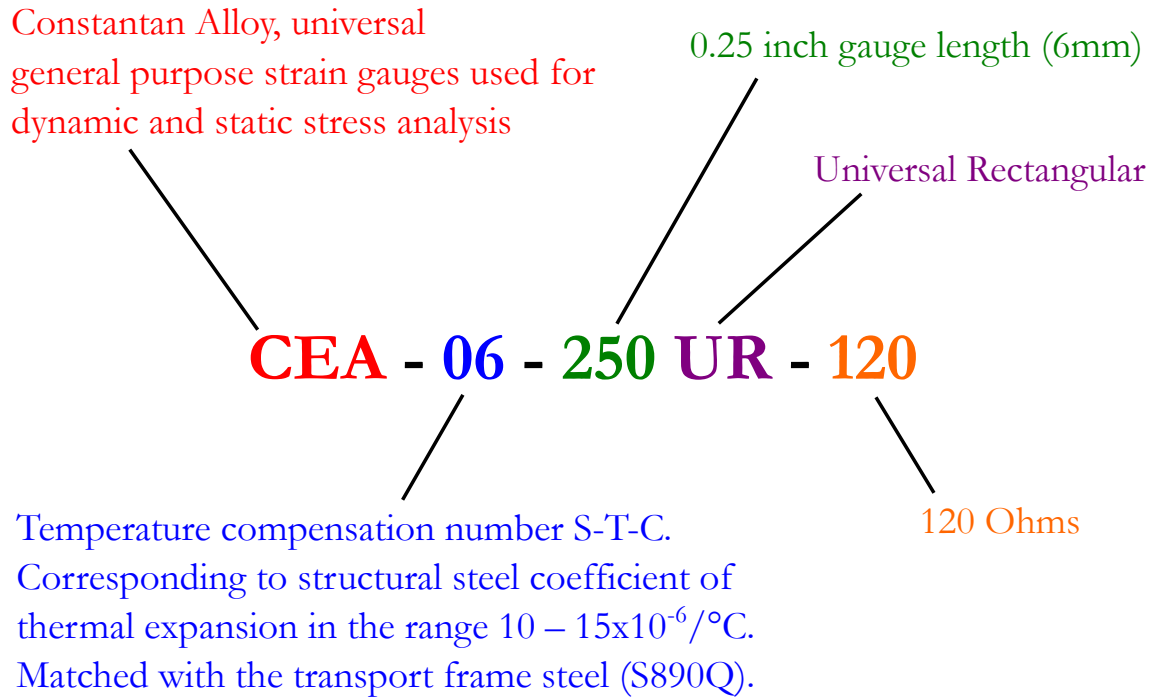


Figure 4.9: Breakdown of the Strain Gauge Rosette Identification Number used to Measure Strain in this Experiment [130]

4.3.3.3 Signal Conditioner and Amplifier

A HBM MGCplus ML801b signal conditioner and amplifier DAQ was used. It is a modular system which enabled the accelerometers, strain gauges and GPS instrumentation to be processed simultaneously by the same equipment.

The accelerometers were connected to a 10V DC module with a bridge circuit similar to that used for piezo-resistive accelerometers. The strain gauges were connected to the AP814 full bridge module.

The DAQ was set to a sample rate of 1200 Hz. A digital anti-alias Butterworth low pass filter, with a filter cut-off frequency of 100 Hz was used. This frequency range of interest was selected based on Hampshire's work on vibrations on passenger rail vehicles [14].

4.4 Results

4.4.1 Loading Test

An example of the measured strains is shown in **Figure 4.10** the measurements have been converted into minimum and maximum principal stresses, using the commercial signals processing package Glyphworks [131]. The software uses standard equations for the conversion and adjusts the measurements using transverse sensitivity correction factors supplied on the strain gauge packaging and mechanical material properties. British Standards materials data was applied because material test certificates were not available [125]. This introduces a small error into the conversion but not enough to change the results significantly.

Rosette	Minimum Principal Stress [MPa]	Maximum Principal Stress [MPa]
1	-3.79	-1.28
2	-4.70	1.99
3	-2.81	-1.43
4	-2.16	1.91
5	-2.16	0.52
6	N/A	N/A
7	-1.29	0.49
8	-1.73	1.85
9	-10.26	-0.87
10	-1.77	2.45
11	3.71	4.46
12	1.92	3.27

Table 4.2: Maximum Principal Stresses Converted from Measured Strains during Loading Test

The peak values of minimum and maximum principal stresses are shown in **Table 4.2**. It is evident that the values of measured strain during the loading of the package on to the frame are very low. This was attributed to a very well designed and built transport frame but also to the wagon suspension which provided a cushion for the frame reducing the stress within its members. This condition is evidently not the

worst case for loading the package on to frame, **Figure 4.8**. The maximum stress of 10.26 MPa was a compressive stress found in rosette 9, a welded joint on the base end saddle section of the frame. The stresses in the other welded joints were also marginally higher than the nominal locations.

Accelerometer Label	Lateral Acceleration [g]	Vertical Acceleration [g]	Longitudinal Acceleration [g]
A	0.06	0.08	0.04
P	0.12	0.04	0.04
B	0.08	0.12	0.07
M	0.15	0.16	0.07
N	0.07	0.18	0.18
O	0.14	0.14	0.16
C	0.03	0.02	0.02
J	0.32	0.21	0.10

Table 4.3: Absolute Maximum Accelerations Measured during Loading Test

The measured accelerations are shown in **Figure 4.11** and the absolute maximum values of acceleration are shown in **Table 4.3**. As expected the accelerations were low, the largest acceleration of 0.32g occurring in the lateral direction on the bogie **Figure 4.3**. It is possible that this occurs due to the running gear settling after displacing under the weight of the package. The most likely reason for the maximum acceleration being lateral and not vertical was because the package was loaded one trunnion at a time and the momentary asymmetry of the weight caused the bogie frame to roll slightly.

Both **Figures 4.10 and 4.11** indicate three events occurred during the loading operation. The accelerations and strain corroborate one another; as each trunnion interfaces with the frame the strains increase and there is a burst of energy in the acceleration measurements. The first burst produced the maximum acceleration, evident visually from the time histories. The second burst is of slightly longer duration and likely to be due to two trunnions impacting the trunnion bushes simultaneously. The noisy response of the accelerometers during this measurement is due to the contact interactions between the trunnion bushing arrangement and the package trunnions.

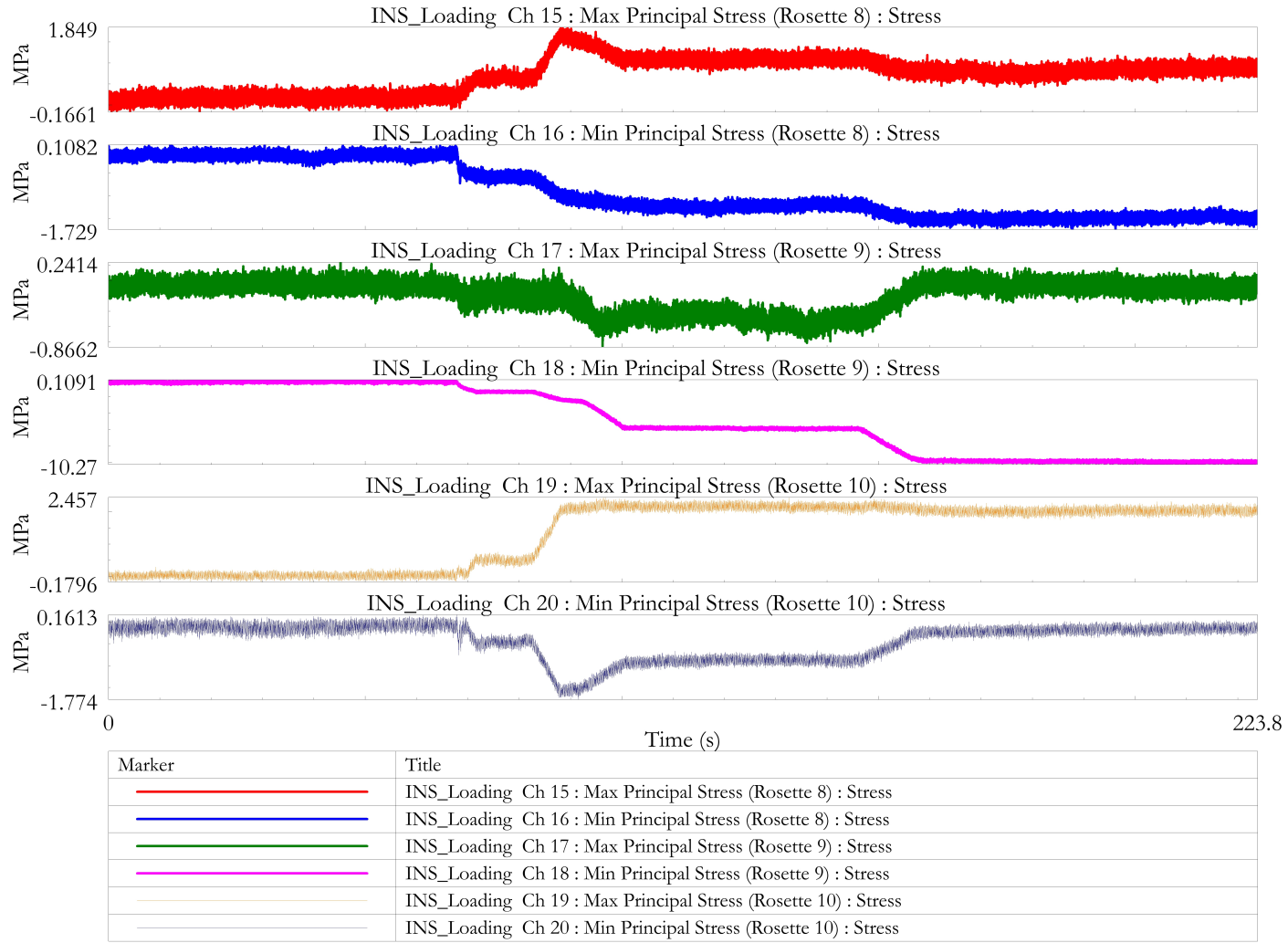


Figure 4.10: Example of Strains Measured during Loading of Package onto Tie Down System

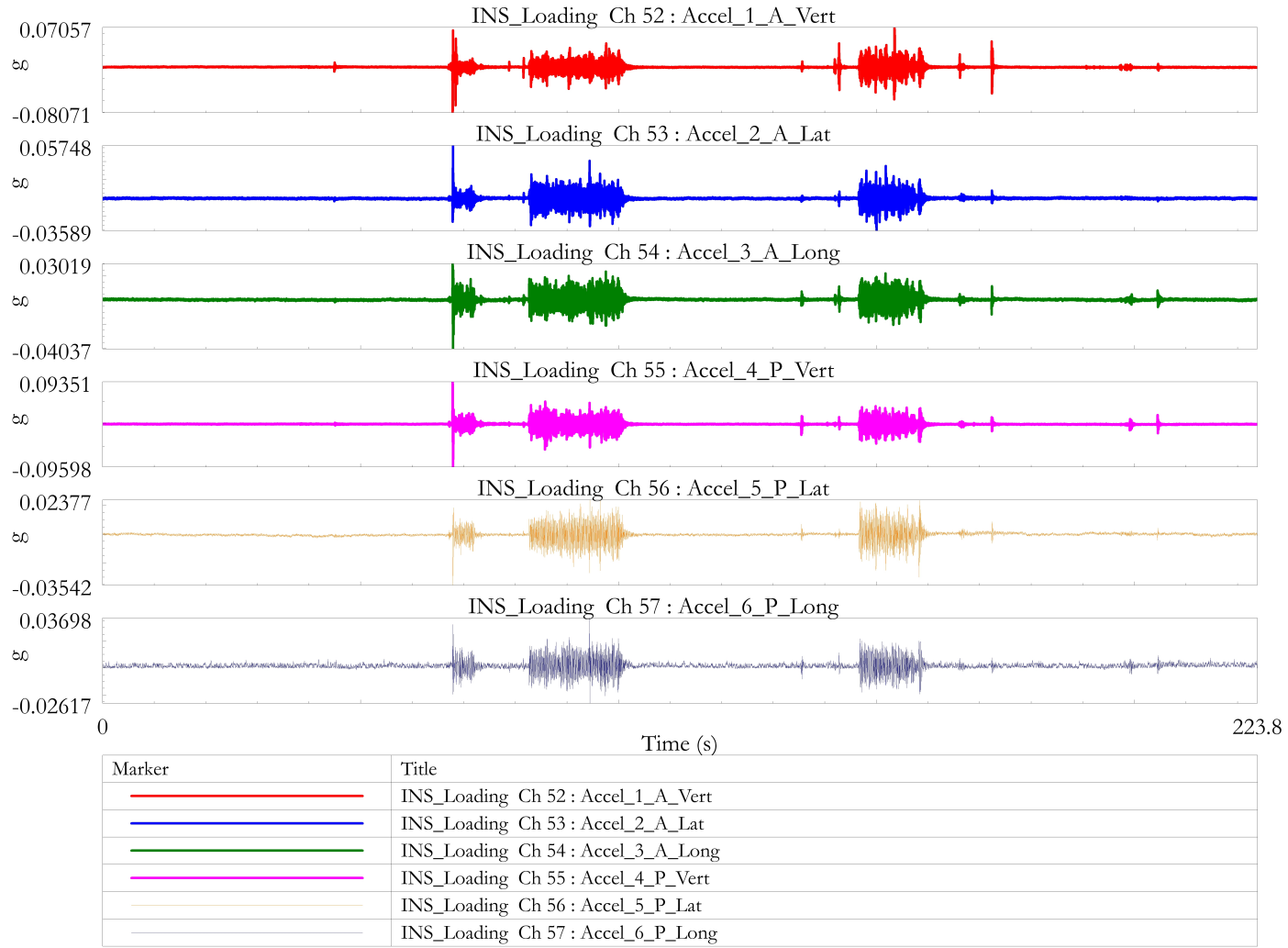


Figure 4.11: Example of the Accelerations Measured during Loading of Package onto Tie Down System

4.4.2 Journey Test

Typical results of the journey measurements are shown in **Figures 4.12 – 4.15**. An example of the measured strain time histories are shown in **Figure 4.12**, again the strains have been converted into maximum and minimum principal stresses. The peak values of minimum and maximum principal stress recorded are shown in **Table 4.4**.

Rosette	Minimum Principal Stress [MPa]	Maximum Principal Stress [MPa]
1	11.79	12.81
2	7.54	13.52
3	-13.41	9.69
4	-8.89	9.69
5	-6.04	6.21
6	-5.14	8.46
7	-6.41	4.57
8	-6.36	8.88
9	-10.88	15.27
10	-5.57	6.05
11	-12.04	9.45
12	-12.66	10.04

Table 4.4: Maximum Principal Stresses Converted from Measured Strains during Journey Test

The strains measured during the journey were lower than expected. This was partially explained by a maximum speed restriction of 40 mph in place for the train, which was imposed by Network Rail due to the large mass of the package. A mass of this size had not be previously transported by rail along this route.

Again the strain gauges at the welded joints produced marginally higher results, the maximum stress of 15.27 MPa throughout the journey was measured on rosette 9 positioned at the weld between the saddle section and stanchions.

The time histories exhibited some apparent drift which was small but noticeable due to the the low magnitude of the signals. Visual examination of the time histories also indicated that both quasi-static and vibrational strains were measured.

Accelerometer Label	Lateral Acceleration [g]	Vertical Acceleration [g]	Longitudinal Acceleration [g]
A	0.48	0.62	0.38
P	0.61	0.65	0.43
B	0.48	0.29	0.16
M	0.42	0.32	0.14
N	0.46	0.33	0.55
O	0.66	0.33	0.22
C	0.58	0.87	0.43
J	4.76	8.03	6.73

Table 4.5: Absolute Maximum Accelerations Measured during Journey Test

Figure 4.13 & 4.14 show the time histories of accelerations at two of the stanchions and the wagon bed and bogie. The absolute maximum values of acceleration are shown in **Table 4.5**. In keeping with the strain results the accelerations were low.

However the accelerations were also in keeping with previous measurement campaigns and expectations. For example Cory [84] indicated that the maximum accelerations during rail transport of the 80 tonne Excellox package occurred in the vertical direction and that the lowest accelerations occurred in the longitudinal direction. By comparing the wagon bed measurements from accelerometer C during this journey and the results from Cory's [84] study during which the accelerometers were also positioned on the wagon bed, the same trend is evident.

The time histories exhibited long drop out sections which were explained by the GPS vehicle running speed measurements shown in **Figure 4.15**. The vehicle running speed indicated that when the vehicle came to rest the acceleration signals tended to zero. This was also present in the strain time histories, however the drift made it less detectable. For this reason simultaneous processing of the signals was considered very important.

GPS measurements also enable identification of events in the acceleration and strain time histories to be compared to vehicle running speed and location i.e. additional information on extreme or rarely occurring events can be extracted.

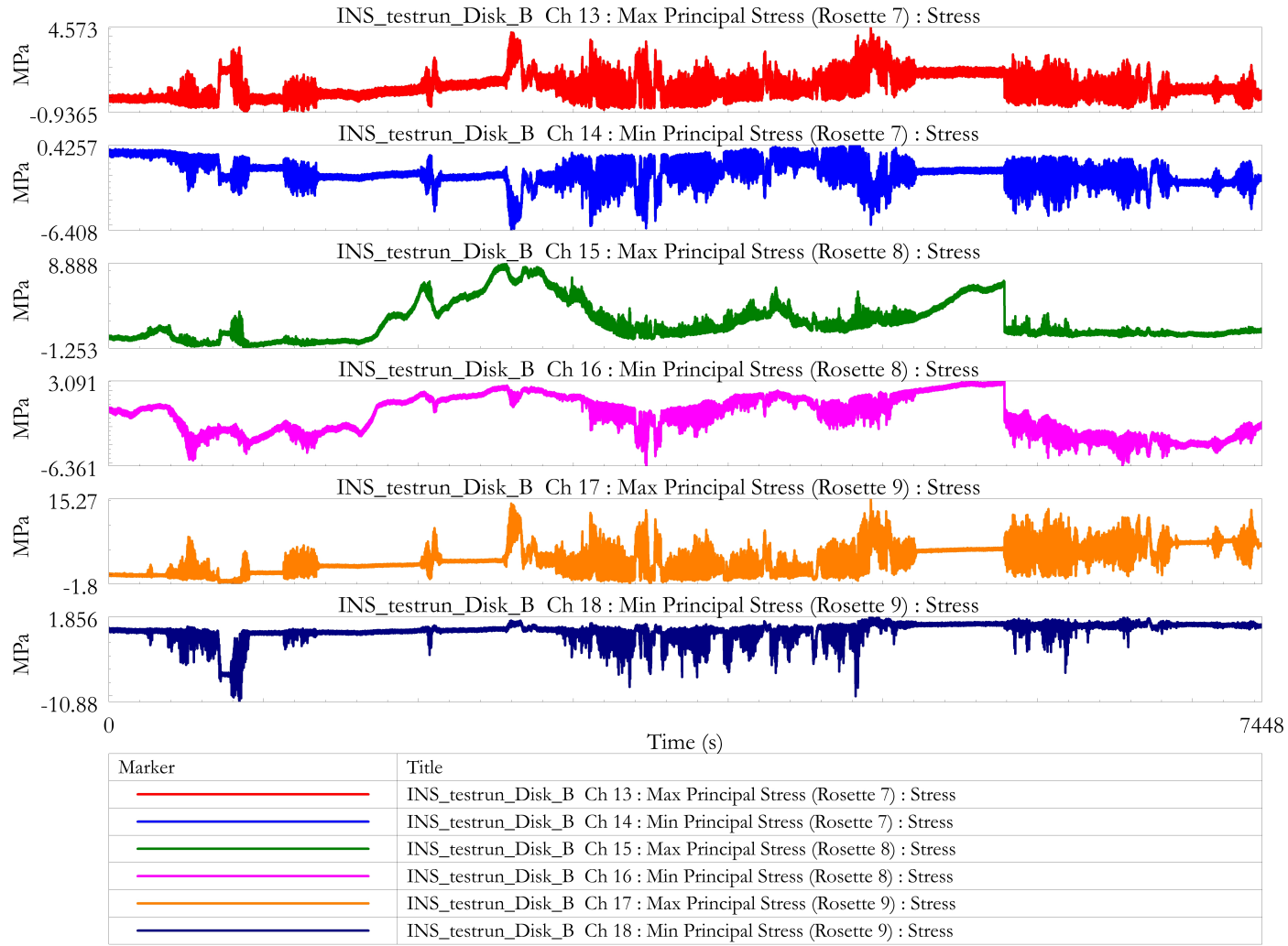


Figure 4.12: Example of Strain Time Histories Collected during the Rail Journey

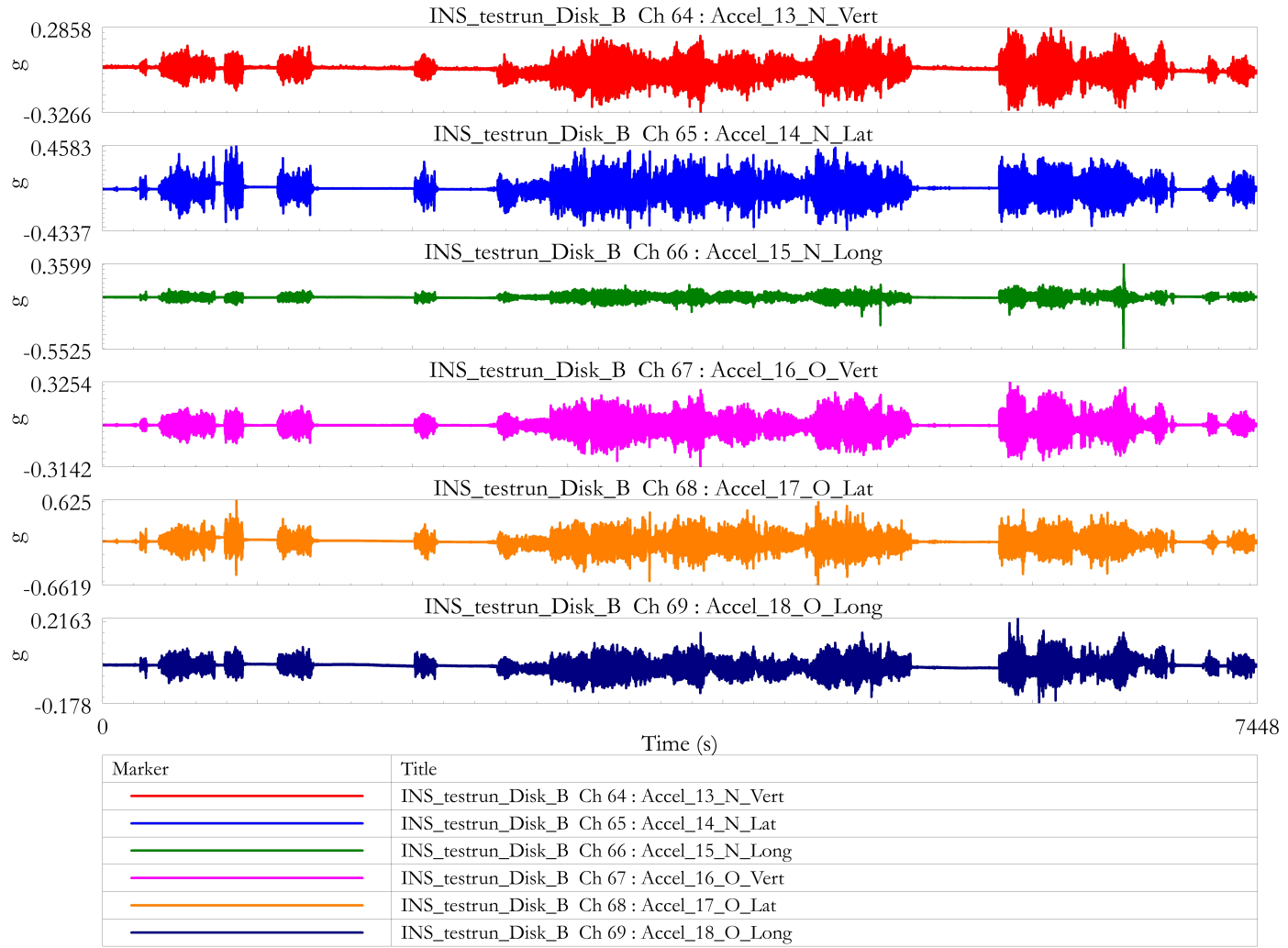


Figure 4.13: Example of the Acceleration Time Histories Collected from the Tie Down System during the Journey

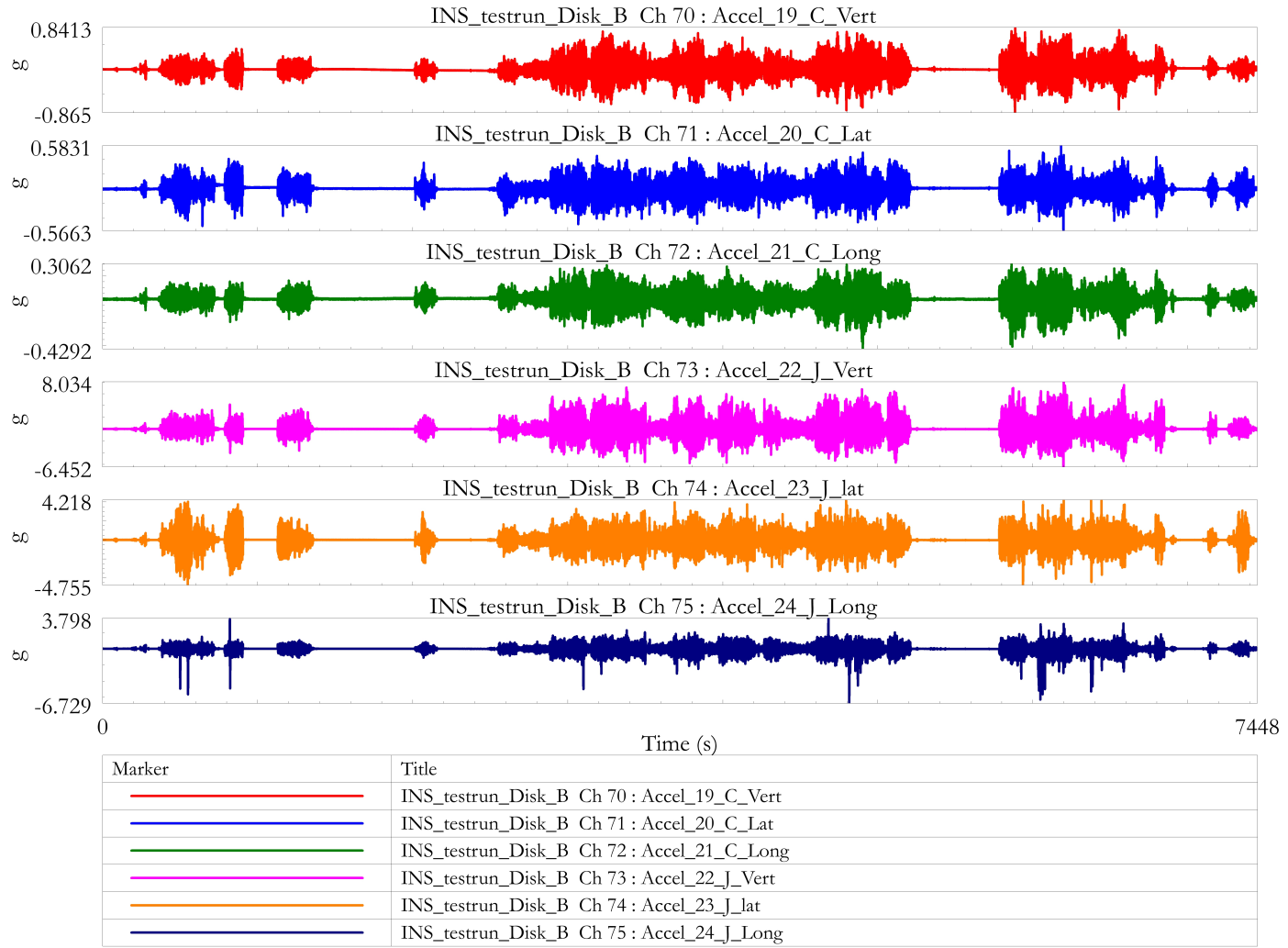


Figure 4.14: Example of Acceleration Time Histories Collected from the Wagon Bed (Accel. C) and Bogie Frame of the Wagon (Accel. J) during the Rail Journey

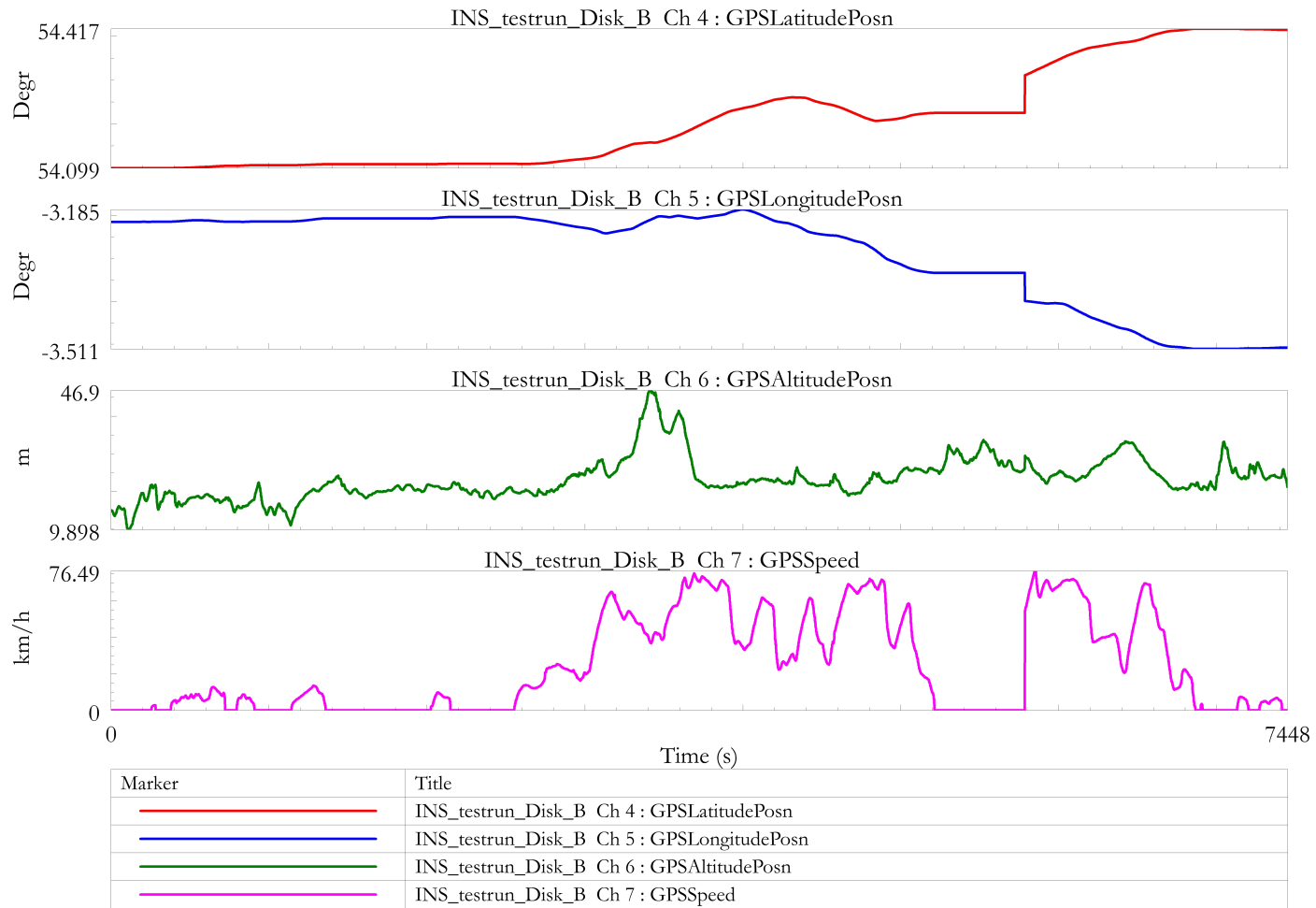


Figure 4.15: Latitude, Longitude, Altitude and Vehicle Speed Time Histories

4.5 Discussion

4.5.1 Comparison of Results with Important Studies and Designer’s Guidance Documents

Due to the many differences between previous measurement campaigns and this study an order of magnitude comparison has been carried out in this section. No direct comparison is possible because the entire test set-up, journey, running speed, conveyance, package and tie down are all different between the studies.

The largest amplitude accelerations in all three axes were measured on the bogie (Label J); vertical 8g, lateral 4.8g and longitudinal 6.7g. These are typical values of acceleration for a rail bogie and in good agreement with Hampshire’s experimental work [14].

On the tie down system the lateral and vertical accelerations were generally of a similar order of magnitude to those found in the Codes of Practice and Regulations, see Table 4.6. As previously mentioned the raw, peak acceleration data was a similar magnitude to the results of Cory [84] however the accelerations were considerably lower than the research of Singh [11]. This is important because Singh’s [11] work was used as evidence and cited by Fourgeaud [8] in an article that proposed revising the IAEA Regulations [2] advisory design parameters for tie downs. The present work suggests that this is not necessary.

	SSG-26 Table IV.2 [g]	Stanchion (Accel. N) [g]	Saddle (Accel. P) [g]	Wagon Bed (Accel. C) [g]
Lateral	0.5	0.46	0.61	0.58
Longitudinal	4.0 (1.0) ¹	0.55	0.43	0.43
Vertical	1.0 ±0.3	0.33	0.65	0.87

¹ Lower acceleration factors are allowed if dedicated movements with special rail wagons are made. Additionally, higher acceleration factors are required if snatch lifting on the attachment points is likely to occur, or if the rail wagons are to be carried on certain roll-on/roll-off ferries

Table 4.6: Comparison of Raw Measured Acceleration Peaks vs Advisory Acceleration Factors

The measured longitudinal accelerations were found to be an order of magnitude lower than those recommended in the advisory material for the Regulations, TCSC 1006 and the Rail Group Standards [2, 74, 105]. This is likely to be attributed to the documented accelerations accounting for shunting operations, which were not permitted during this transportation.

The measurements show that large magnitude accelerations arise as a consequence of the wheel-track interface and are filtered by the suspension system. This is evident by the magnitude of the acceleration levels that are highest at the bogie and attenuate upwards through the structure (Figure 4.16). It is also evident that the nature of the accelerations and stresses are highly cyclic. Therefore an under designed tie down system may fail due to two possible failure modes; yielding or fatigue. However in this experiment the stresses at the measured locations were very low and the results indicate that the tie down system will not fail in this environment.

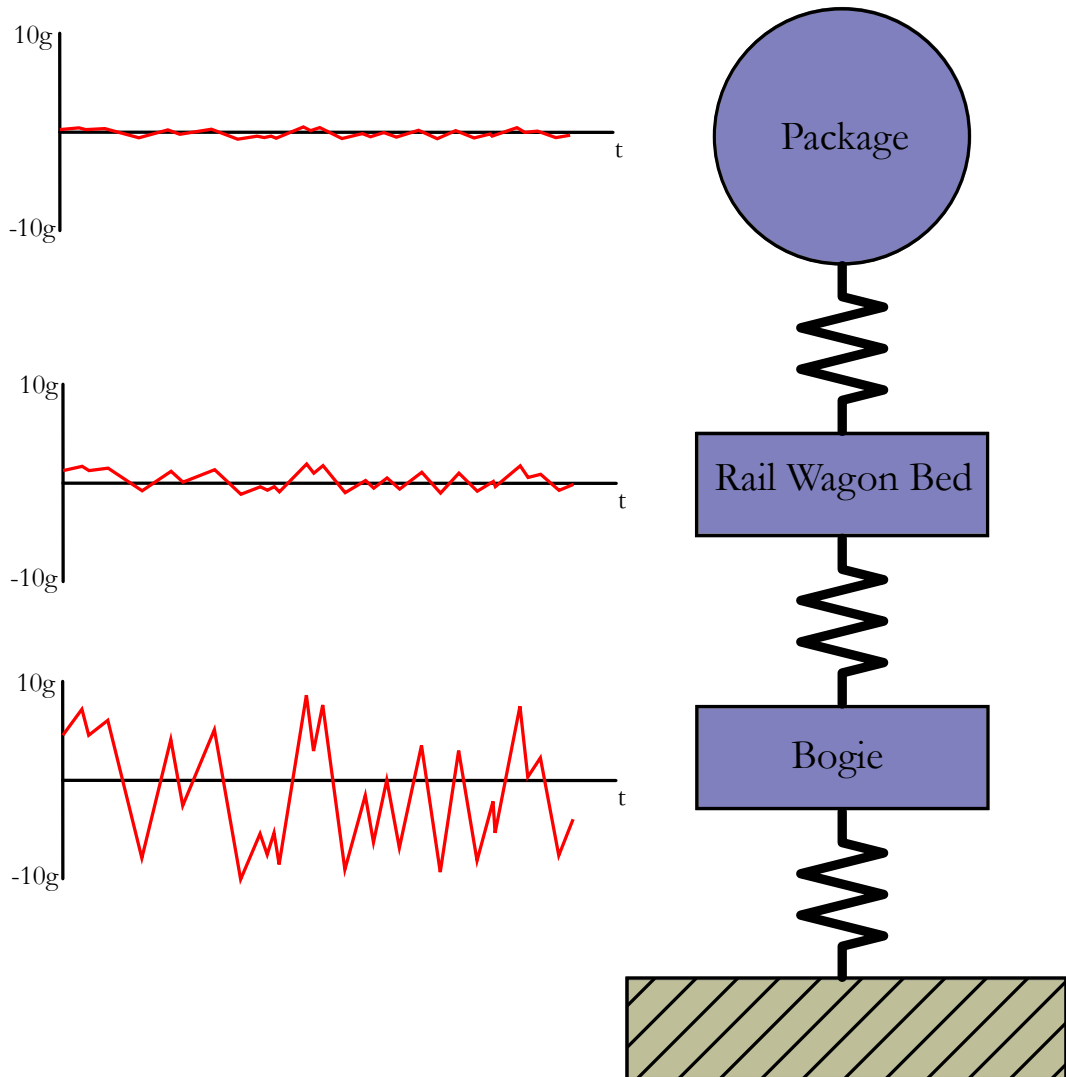


Figure 4.16: Schematic of Vertical Load Transmission and Attenuation

4.5.2 Benefits from the Measured Data

Because of the high sampling rate and careful selection of the instrumentation used for measuring the accelerations and strains good estimates of the random vibration environment can be made using Fourier techniques. This is carried out in the next chapter.

Ensuring new fuel quality is very important to energy companies utilising nuclear power. This data provides the ability to test surrogate fuel assemblies in a laboratory representing real, routine transport conditions or to benchmark existing test specifications. The major benefit to this is the ability to understand if any adverse effects on the fuel are caused by transportation loading prior to its use in a reactor.

Similarly the transport of high burn-up fuel may pose challenges in the future with respect to its integrity due to transportation loads. When irradiated spent fuel cladding undergoes embrittlement and concerns arise due to the potential for leaking fuel pins. Measured data from experiments such as this one, if correctly processed, provide the best possible characterisation of the transport environment to assess the response of surrogate fuel safely in a laboratory prior to transport.

For strength and fatigue analysis of tie down structures the acceleration data can be reduced to turning points and rainflow cycle counted producing measured fatigue loading [43]. This methodology is suitable provided the correct frequency content is included in the signal and the relationship between measured acceleration and strain is demonstrated to linearly proportional [38]. Similarly for strength assessment based on prevention of yielding the nature of the measured accelerations and strains offer the ability to carry out model validation, verification of existing design methodologies and demonstration of safety margins in current designs.

Due to the variety of potential uses for this data it is important to confirm the nature of the peaks by further analysis. In particular frequency analysis is essential to underpin any digital filtering used to remove content in the signal that is not appropriate for design use.

4.5.3 Limitations of the Data

In addition to understanding the potential uses for the data it is important to also understand its limitations. The journey was relatively benign, so the measurements, for the reasons discussed throughout this chapter are not representative of a worst case.

In particular no longitudinal shunting operations were measured during the operations, therefore the longitudinal acceleration measurements are only representative of journey loads. This is an important result because any longitudinal coupling of vehicles that occurred did not result in a detectable response from the package or tie down. However the train was very short and therefore the overall coupling mass between vehicles was not potentially as large as it could be, therefore the condition tested is best described as a typical case.

Another example is the loading of the package on to the tie down which was carried out when the tie down was already mounted to the wagon. This reduces the stresses experienced by the tie down and whilst this is important for establishing safety margins does not constitute a worst case.

4.6 Summary

- An experimental procedure has been created that will provide data sufficient for computational methods of design.
- The data can be used to customise tie down system design for particular applications, extend fatigue life, verify existing designs and benchmark FEA.
- The results show that strains in the tie down system are very low. Strain occurs as a consequence of the relative motion between the conveyance and package.
- The highest accelerations were measured at the bogie and are due to the harsh wheel-track interface. It is therefore overly conservative to apply the entire content of the acceleration signal to the package centre of mass.
- The data should be filtered prior to deriving load cases for design of tie downs to remove signal content that is not quasi-static.
- The nature of the signals is highly cyclic therefore there are two important failure modes to consider during tie down system design; yielding and fatigue.
- A data set useful for vibration analysis of the ride quality of the vehicle has been generated. This is particularly useful for characterising the vibration environ-

CHAPTER 4. A METHOD FOR MEASURING ACCELERATION AND STRAIN
DURING A ROUTINE RAIL JOURNEY OF A HEAVY NUCLEAR PACKAGE

ment of fuel assemblies transported within heavy packages by rail. It may also be used as the basis for a shaker test specification.

5. Signals Analysis of the Measured Accelerations and Strains

5.1 Introduction

The experiment described in the previous chapter produced 36 strain and 24 acceleration time histories each consisting of nearly 9 million data points per channel. In this chapter signals processing techniques have been used to reduce the data for the purposes of characterising the loading environment of the tie down system and package.

Analysis has been carried out to understand the frequency content of the loading experienced by the tie down system and also the extent of vibration transmission into the package. A method for deriving PSDs of the data has been explicated which should provide an industry standard for interpreting and processing vibration signals.

A standardised method for deriving PSDs assists in the transport of fuel between different countries because numerous approaches to vibration analysis are currently used resulting in inconsistent interpretations [14, 16, 51, 60]. This also provides a more informed starting point for digital filtering of the signals to estimate quasi-static peak accelerations for tie down design purposes. A method for designing digital filters and understanding their characteristics when applied to the signals in this experiment is presented.

The raw acceleration data has been filtered with several different filter designs to study their effects on the resulting peaks. Furthermore to demonstrate what constitutes a good or bad filter design, sensitivity studies have been conducted to show how the distributions of peaks and their statistics are altered significantly by selection of certain filter parameters.

The filter design methodology described in this chapter also forms the basis for validating an FEA model described in **Chapter 6**.

5.2 Aims and Objectives

- Derive PSDs useful for validating computer models, to guide the specification of vibration tests and for understanding the frequency content of the measured signals.
- Compare the PSDs at various measured points on the conveyance and tie down to identify which frequencies are transmitted into the package.
- Present a method for designing filters to estimate quasi-static accelerations acting on tie down systems.
- Assess the sensitivity of filtered accelerations to different filter designs.
- Compare the quasi-static accelerations with those quoted during other experimental work and in the IAEA Regulations Advisory Material [2].

5.3 Initial Visual Interpretation and Error Detection of the Measured Signals

All of the signals were visually examined prior to any processing for obvious signs of errors such as spikes, drift or clipped peaks. The strain time history from rosette 9 (at the end of the weld between the base end saddle and stanchion) has been selected as an example that highlights many of the key attributes of each signal (**Figure 5.1**).

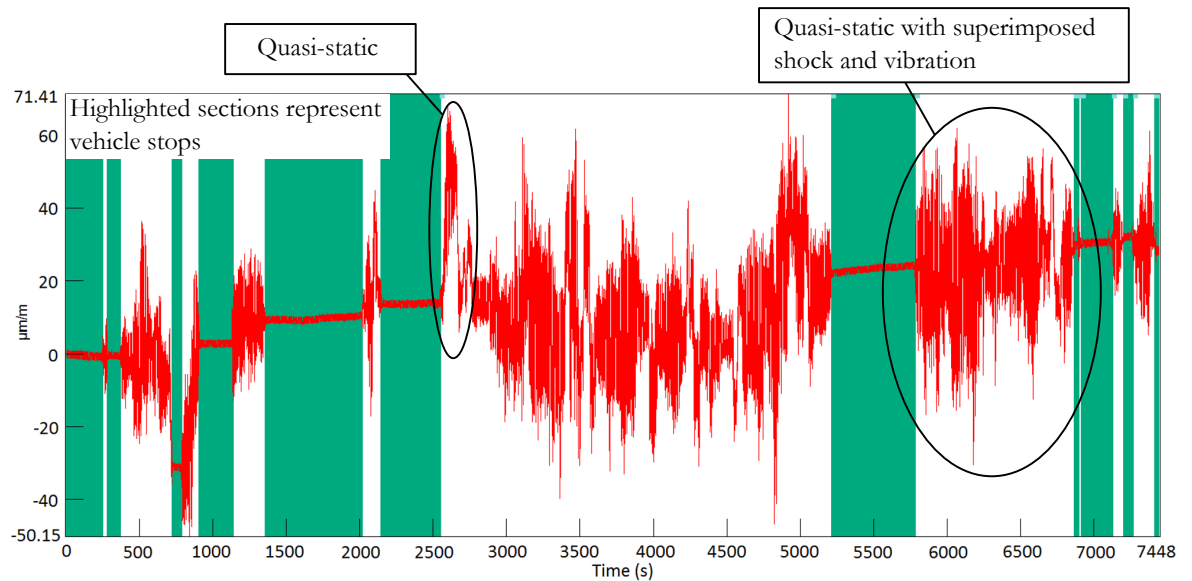


Figure 5.1: Typical Strain Time History Characteristics

The time history consists of a number of sections where the measurements reduced to the noise floor of the instrumentation. These sections are called signal dropouts [132]. In the figure several signal dropouts exist and are highlighted in green, these sections all correspond to time periods where the vehicle came to rest.

The strain signal commences with a $0 \mu\text{m}/\text{m}$ mean but at the end of the journey, over 2 hours later, the mean value of the measurements drifted to $\approx 25 \mu\text{m}/\text{m}$. Although temperature compensated strain gauges were used during the experiment the measurements indicate that apparent drift was not eliminated. Some drift may be attributed to real temperature variations e.g. small amounts of thermal expansion on one side of the tie down system exposed to solar insolation. However, in all of the time histories drift was considered a small error and therefore acceptable. It is possible that it was only detected by visual examination due to the low overall values of strain and relatively high signal to noise ratio.

A spike detection algorithm was used on each signal. This works by assessing large changes in signal gradient, on a point-by-point basis. In regions where potential spikes may have occurred the data was also visually examined close-up with the data points displayed. No spikes were found with either the spike detection algorithm or by visual examination.

The data were plotted as probability density functions (PDF) to check for clipped peaks. This was considered highly unlikely due to the low magnitudes of acceleration and strain measured. If the signals were clipped, the PDF distribution would display a spike in each tail. As expected there was no evidence of signal clipping in any of the time histories.

5.4 Frequency Analysis

5.4.1 Power Spectral Density

The Power Spectral Density (PSD) enables the study of random time histories in the frequency domain. Here the PSD is used predominantly to understand the frequency content in the signal and as a guide for selecting a filter cut-off frequency. The measured time histories have been transformed to PSDs using Welch's [133] calculation method that provides the mean square amplitude of the signal in discrete frequency intervals [134]:-

1. To refine the DAQ anti-alias filter each time history has been low pass filtered at 100 Hz with an 8th order Butterworth digital filter. This filter provides a good roll-off rate and good stop band attenuation for these signals. For a detailed explanation of the filters used in this chapter and their characteristics see **Section 5.5 [135–137]**.
2. The time histories were then subdivided into segments of 4096 points, resulting in 2182 segments. This produced a high frequency resolution, $\delta f \approx 0.3$ Hz, whilst still achieving excellent statistical properties of the PSD due to the large number of segments being averaged.
3. Next a linear trend was removed from each segment. This limits the definition of very low frequency (quasi-static) signal content in the PSD. As an estimate of the bounding lower frequency, f_{low} , consider that the peak/trough at the end of each segment represents a quarter cycle. The segment duration is known, $T_f = Ndt = 3.41$ seconds, resulting in $f_{low} = 0.07$ Hz. Therefore the slowest occurring peak that will be represented in the PSD will last for no more than 3.41 seconds. It is noteworthy that if no trend is removed there is a spurious spike at DC present in all of the PSDs which results from apparent drift and small zero baseline errors.
4. To improve the estimate, each segment was passed through a Hanning window function and overlapped by 50%. Carrying out a fast Fourier transform without a window function may result in, smaller, erroneous peaks (side lobes) adjacent to larger spectral peaks. However the use of a window function also increases the width of the central lobe so there is a trade-off. By overlapping the data many more segments can be included in the estimate improving its statistical properties and minimising error [41].
5. The final step was to apply a fast Fourier transform per segment and then av-

erage all segment PSDs [41, 56, 138].

5.4.2 Strain PSDs

The strain PSDs did not contain any spectral information of significance above 40 Hz, so only the frequency range 0 - 40 Hz was plotted. The resulting PSDs were all very similar so here an example is provided from each leg of the strain gauge rosettes from two of the welded joints (Figure 5.2). Each channel exhibited a similar spectral signature; the energy is distributed in three distinct frequency bands, 0 - 4 Hz, 4 - 16 Hz, 19 - 29 Hz.

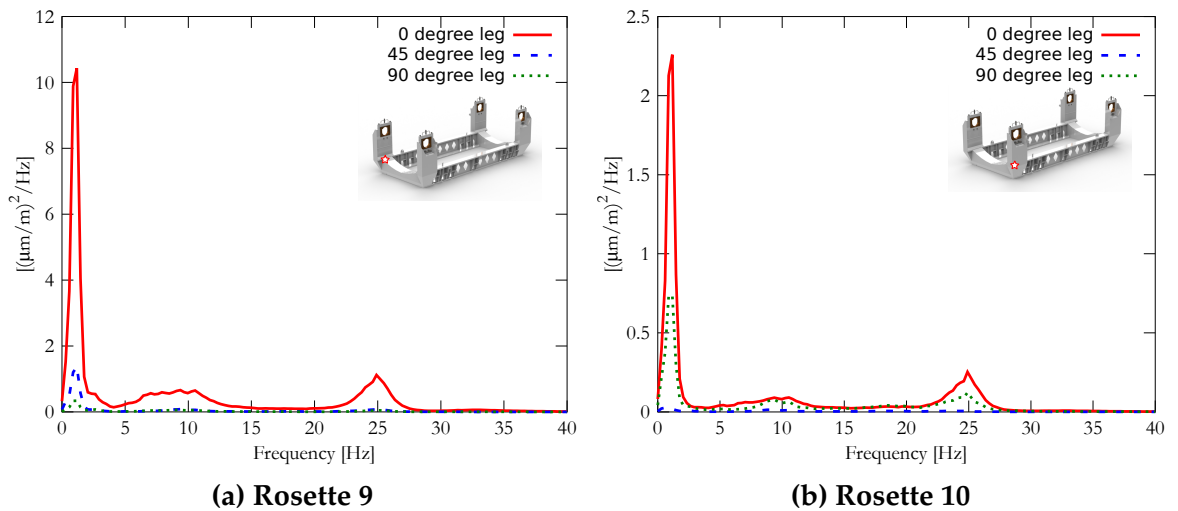


Figure 5.2: Example Strain PSDs for Strain Gauge Rosettes 9 and 10

5.4.3 Acceleration PSDs

At every measurement position the vertical, lateral and longitudinal accelerations were notably different. This was in keeping with expectations, as the vehicle manoeuvring would result in significant differences in accelerations depending on the axis. For example the major contribution to the vertical axis is vibrational energy from the track, whereas the lateral axis consists of a mixture of quasi-static and vibrational loading. The longitudinal axis measures decelerations and accelerations of the vehicle and interaction between adjacent vehicles.

Overlaying each of the vertical, lateral and longitudinal PSDs from the six measurement points on the tie down system revealed that they were identical. However a similar comparison between the acceleration PSDs from the tie down, the wagon bed and bogie showed differences. Scrutinising those differences helps develop a better understanding of the package and tie down behaviour during the journey.

The acceleration levels from the wagon bed were higher than those measured on the tie down system. The highest overall accelerations were measured at the bogie which has a broadband spectrum that is dominated by vertical vibration energy. The difference between the overall magnitude and area under the PSD curves at the bogie and wagon bed shows how much of the vibration energy is attenuated by the rail vehicle suspension system acting as a mechanical filter (**Figure 5.3**).

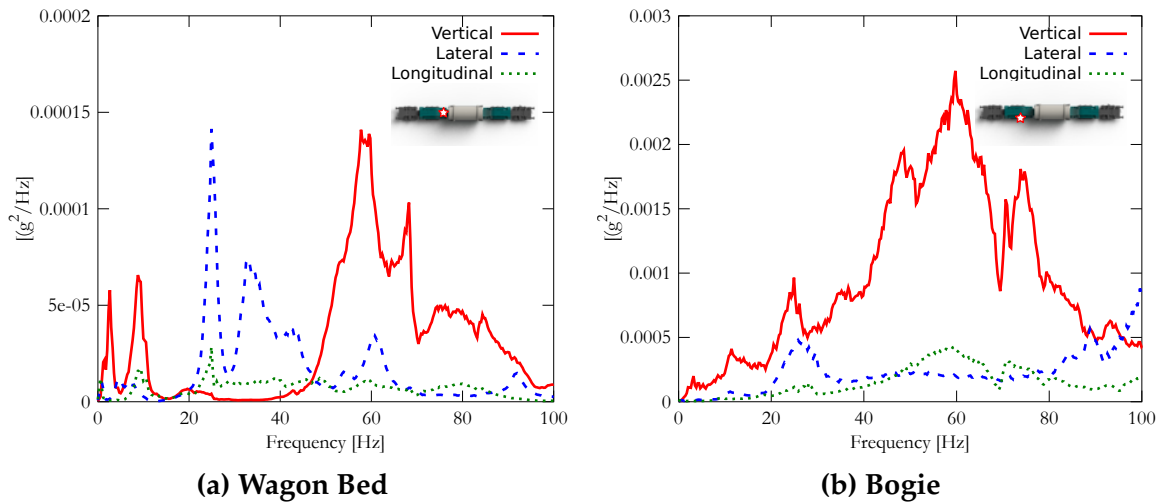


Figure 5.3: Acceleration PSDs at Wagon Bed and Bogie

The equivalence or similarity of the acceleration PSDs at the tie down allowed for data reduction. The lid end accelerations were excluded from this analysis to concentrate on the slightly higher base end data. Only one of the stanchions is considered because the spectra at the base end stanchions were identical.

Accelerometers from the wagon bed, the stanchion and the saddle, have been selected for comparison (**Figure 5.4**). The wagon bed accelerometer has been included in the selection since this provides the best location to determine what relative motion occurs between the base of the tie down system and its stanchions.

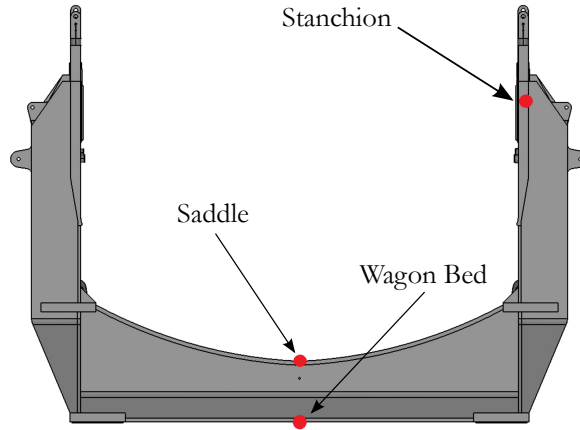


Figure 5.4: Accelerometers Selected for Detailed Analysis

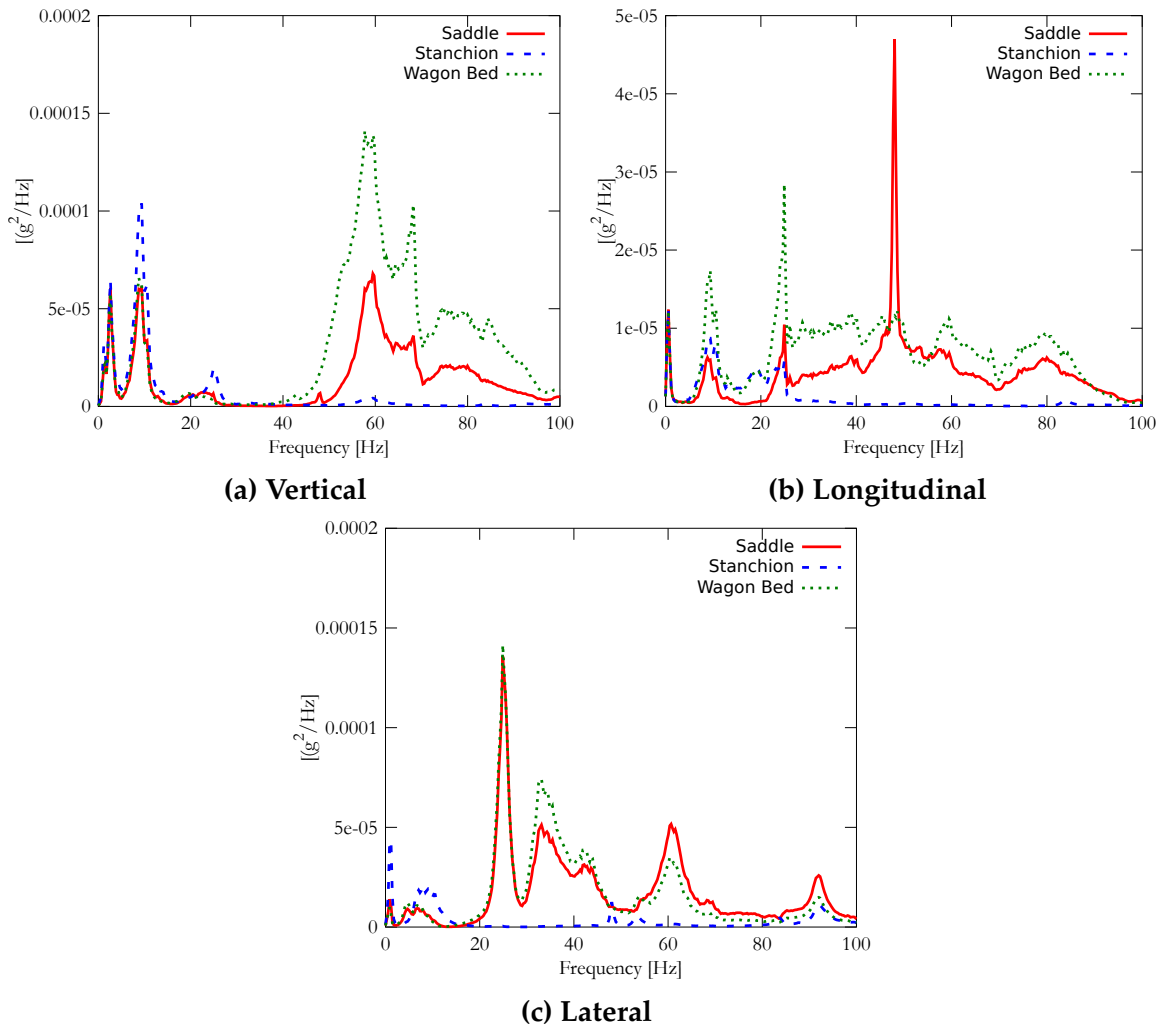


Figure 5.5: PSDs from Measured Accelerations at Wagon Bed, Saddle and Stanchion

5.4.3.1 Vertical Acceleration PSDs at the Wagon Bed and Tie Down

The vertical acceleration PSDs for the three accelerometers are shown in **Figure 5.5a**. At frequencies below 40 Hz three peaks are present between 0 - 4 Hz, 4 - 16 Hz and 19 - 29 Hz, these frequency bands match those in the strain PSDs. At frequencies below 29 Hz the energy is marginally higher at the stanchion than at the wagon bed or saddle. Above 29 Hz the vibration intensity is much higher at the wagon bed and saddle than it is at the stanchion.

This is due to the effects of the large package inertia, which at frequencies >29 Hz, attenuates any input from the moving vehicle i.e. the large mass doesn't have time to respond. Conversely, at frequencies <29 Hz the opposite occurs and the vertical acceleration at the package is amplified and slightly higher than at the wagon bed or saddles. This is particularly clear in the frequency range 4 - 16 Hz. The first peak <4 Hz is likely to be due to quasi-static loading. However, there is little relative vertical motion between any of the measurement points at these low frequencies.

5.4.3.2 Longitudinal Acceleration PSDs at the Wagon Bed and Tie Down

The longitudinal acceleration PSDs for the three accelerometers are shown in **Figure 5.5b**. Their overall vibration level is lower than in the vertical and lateral directions. Three small peaks are evident at 9.5 Hz, 25 Hz and 48 Hz. The energy level is very low at the stanchion across the whole frequency range with marginally higher levels of vibration existing at the wagon bed and saddle.

5.4.3.3 Lateral Acceleration PSDs at the Wagon Bed and Tie Down

The lateral acceleration PSDs for the three accelerometers are shown in **Figure 5.5c**. Below 30 Hz the peaks occur in the frequency bands 0 - 4 Hz, 4 - 16 Hz and 19 - 29 Hz which correspond to the strain and vertical accelerations PSDs. There are, however, some subtle changes in the vibration signatures. Below 20 Hz the stanchion vibration intensity is marginally higher than the wagon bed and saddle. Above 20 Hz the energy levels at the stanchion are significantly reduced whereas at the wagon bed and saddle they increase.

Again the large mass and inertia of the package causes track induced vibrations to be attenuated, in this instance at frequencies >20 Hz. The first peak <4 Hz is due to quasi-static loading and low frequency vibration. However, unlike the vertical accelerations, there are larger peaks at the stanchion than the wagon bed which indicates lateral motion of the package is occurring relative to the conveyance. Similar relative

lateral motion is evident in the second frequency range 4 - 16 Hz. This is the most obvious reason for these frequencies ranges to also appear in the strain PSDs.

Conversely there is a significant peak at 25 Hz at the wagon bed and saddle that is not present in the stanchion PSD. This is indicative of motion of the wagon bed relative to the package and is the most likely cause of the third frequency band in the strain PSDs between 19 - 29 Hz. It can be concluded from this analysis that the lateral accelerations are the dominant source of structural loading on the tie down system.

5.5 Digital Filtering

In this section digital filtering is explored for the purposes of separating the loads acting on the tie down system from the higher frequency loads that are attenuated by the package mass. Initially an overview of the filter requirements is presented and the complexities of designing an appropriate filter introduced.

The filter design is ultimately an optimisation problem but has not been treated as one here. Instead the approach adopted was to select three commonly used filter types and then design different filters using their frequency response, step response and poles and zeroes in the z-domain to assess their suitability.

Following this process a sensitivity study of the effects of different filters with good and bad characteristics have been applied to the acceleration time histories at the base end stanchion and wagon bed assuming a filter cut-off frequency $f_c = 17.5$ Hz; a first estimate based on the acceleration PSDs.

In **Chapter 6** a FEA model is used in combination with successive filtering of both the acceleration and strains at various cut-off frequencies to determine when a linear model agrees best with the experimental data. This section provides the foundation to that study by assessing the effects of low pass filtering between 1 - 20 Hz and ensuring a stable and robust filter design for all f_c values.

To conclude, a quick method for estimating a filter cut-off frequency is presented. Based on this method some time domain trends have been observed that are informative when interpreting tie down loads from measurements. The findings are also indicative of the margins of safety present in current vibration test specifications for fuel assessments involving similar transport configurations i.e. similar package, wagon and tie down.

5.5.1 Filter Requirements

The design of a filter to extract low frequency content for structural analysis involves careful consideration of both its frequency and time domain characteristics [139]. In the frequency domain the filter behaviour in the pass band, transition band and stop band can be crucial. The filter roll-off rate dictates at what frequency the minimum stop band attenuation is achieved. Since the preservation of peaks in the pass band is of utmost importance to the structural engineer, pass band ripple should be minimised or eliminated during filter design. In addition filtering causes a phase distortion, here this has been corrected by the use of a forward-backward filtering algorithm.

Butterworth and Chebyshev Type 1 filters continue to attenuate in the stop band i.e. beyond the cut-off frequency signal attenuation continues indefinitely. Elliptic and Chebyshev Type 2 filters behave differently as they enable control over the permissible stop band attenuation. A minimum acceptable stop band attenuation was set to 1% of the signal amplitude or -40 dB using the formula [136]:-

$$Gain/Loss_{dB} = 20 \log_{10} \left(\frac{A_{stopband}}{A_{passband}} \right) \quad (5.1)$$

Filter Order	Frequency [Hz]
1	517
2	164
4	55
8	31

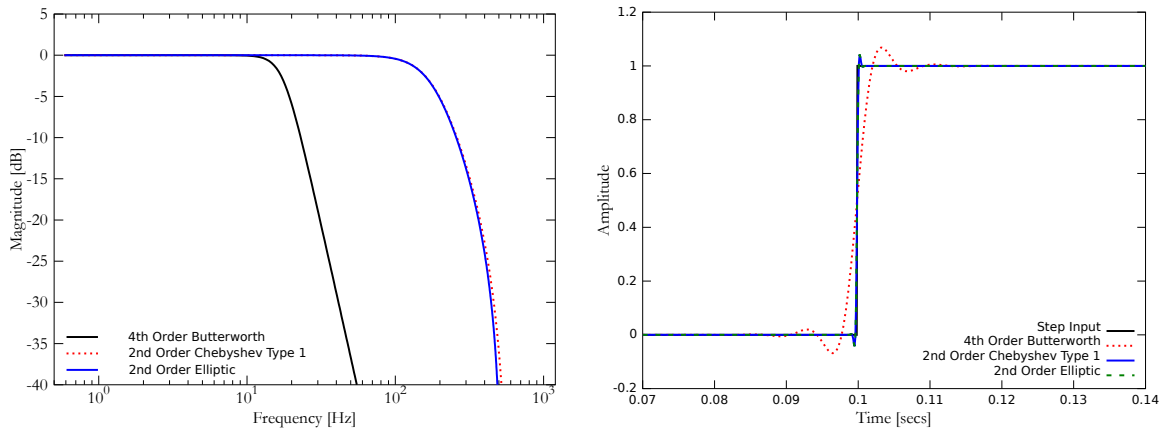
Table 5.1: Frequencies at which Various Butterworth Filters Attenuate to -40dB

As an example the frequency at which the minimum stop band attenuation of 1st, 2nd, 4th and 8th order, low pass, Butterworth filters with a cut-off frequency of 17.5 Hz is shown in **Table 5.1**. Higher order filters provide better roll-off rates and therefore achieve the desired stop band characteristics at lower frequencies. In this example the transition band occurs in the frequency range between the filter cut-off frequency and the frequencies listed in **Table 5.1**. The higher the roll-off rate the narrower this band becomes and the more accurately the filter removes content above the cut-off frequency.

Higher roll-off rates are achieved at the expense of poorer filter performance in the time domain. Increasing filter orders, decreases stability and the filter exhibits over-

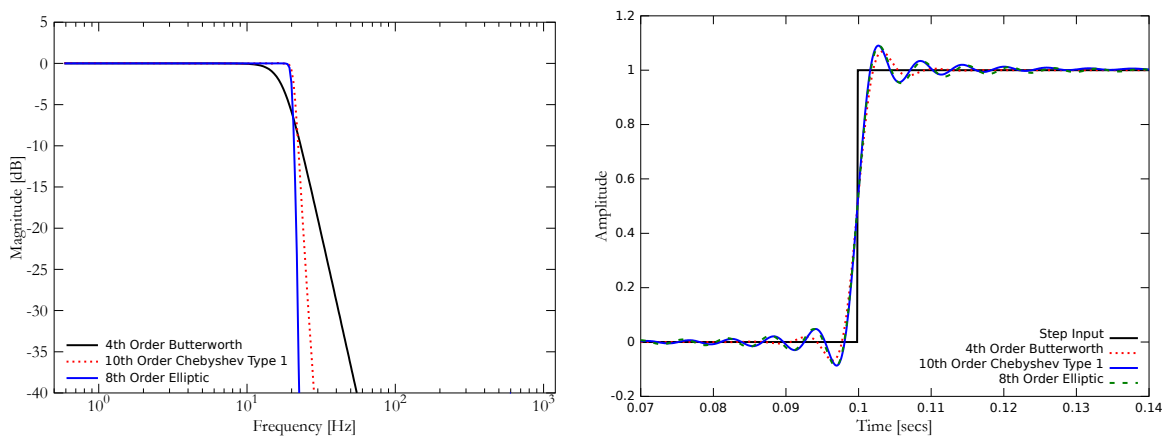
shoot and ringing in the time domain, which can degrade its performance. This is the area of most uncertainty in this filter design; firstly because the exact filter cut-off frequency is not known and secondly it is difficult to quantify the level of error that can be attributed to a filter that leaks in the transition band and a filter that overshoots and rings in the time domain.

Sensitivity studies of these filter characteristics have been carried out. Three types of Infinite Impulse Response (IIR) filters were considered for the structural analysis; the Butterworth, Elliptic and Chebyshev Type 1 filters. A 4th order Butterworth filter was chosen initially due to the compromise between overshoot and ringing in the time domain and roll-off rate and stop band attenuation in the frequency domain. For comparison the Bode magnitude and step response plots of the various filters used in the sensitivity study are provided (Figures 5.6 & 5.7).



(a) Example of a Bode Magnitude Plot for Lower Order Filters (b) Example of the Step Response for Lower Order Filters

Figure 5.6: Filters Designed to Minimise Time Domain Ringing



(a) Example of a Bode Magnitude Plot for Higher Order Filters (b) Example of the Step Response for Higher Order Filters

Figure 5.7: Filters Designed to Maximise Roll-off Rate

The final step in the filter design is to analyse their stability. This was done by analysing the poles in a pole-zero plot in the z-domain, **Figure 5.8**. The filter is stable if the poles, denoted as X, are inside of the unit circle. As the poles get closer to the edge of the unit circle then the filter stability becomes marginal. If the filter is unstable it will have poles outside of the unit circle.

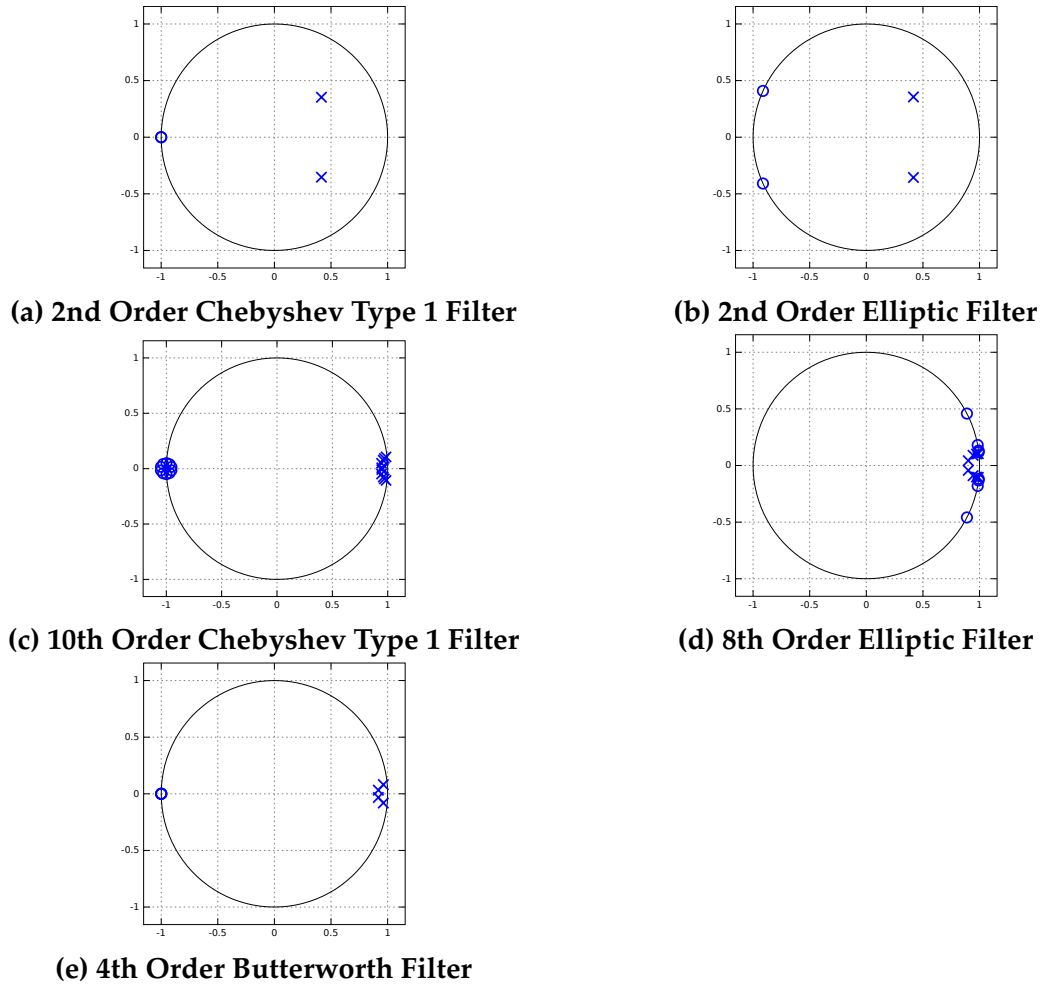


Figure 5.8: Pole-Zero Plot in Z-Domain of Five Low Pass Filter Designs, $f_c = 17.5$ Hz and $f_s = 1200$ Hz (O = Zeroes and X = Poles)

Figures 5.8a & 5.8b indicate that the lower order Chebyshev Type 1 and Elliptic filters are inherently more stable than their higher order counterparts shown in **Figures 5.8c & 5.8d**. The obvious trade-off is that their roll-off rate is poor and to achieve a good (or excellent) roll-off rate a higher order filter must be used which increases instability.

Figure 5.8e indicates that a 4th order Butterworth filter with $f_c = 17.5$ Hz is stable with a small margin. Its roll off rate is not as good as the 8th or 10th order filters assessed, but it is comparable. Crucially, for the ability to select a very low f_c , such as 1 Hz, this filter remains stable whereas higher order filters do not. Furthermore those filters that are stable with $f_c = 1$ Hz, no longer have better frequency domain

characteristics than the 4th order Butterworth filter.

5.6 Sensitivity of Acceleration Extrema due to Filter Design

In this section the triaxial accelerations measured by accelerometer N, at the base end stanchion have been used. A base end accelerometer was chosen because the base end accelerometers detected marginally higher raw peaks than the lid end. Accelerometer N was also positioned on a stanchion, so it was closer to the centre of mass of the package than the wagon bed accelerometer.

To assess the sensitivity of the acceleration extrema to different filter designs, the filter cut-off frequency was again set to 17.5 Hz. The signals were first filtered with a 4th order, forward-backward, low-pass Butterworth filter (**Figure 5.6 & 5.7**). Four other forward-backward, low pass filter designs were used to compare the effects of filter roll-off rates and time domain ringing on the extrema.

To minimise time domain ringing a 2nd order Chebyshev Type 1 and a 2nd order Elliptic filter were selected (**Figure 5.6**). To maximise roll-off rate a 10th order Chebyshev Type 1 and an 8th order Elliptic filter were selected (**Figure 5.7**). The allowable passband ripple of all the Chebyshev and Elliptic filters was set to -0.0001 dB which tends towards a flat passband response at the expense of roll-off rate. The poorer roll-off rate is particularly prominent in the lower order Chebyshev and Elliptic filters. The Elliptic filters stopband attenuation was set to a minimum of -40 dB.

The results of the two studies using Chebyshev Type 1 and Elliptic filters are provided for comparison with those from the 4th order Butterworth filter (**Table 5.2 – 5.4**). The statistics provide some clues about the distributions that the data sets produce. They also show some discrepancy between the lower order filters designed to minimise time domain ringing and the higher order filters designed to maximise roll-off rate.

Filter Designed to Maximise Roll-Off Rate				
Filter Type	Mean	SD	Min	Max
	[g]	[g]	[g]	[g]
4th Order Butterworth	0.0065	0.0213	0.1590	0.1590
8th Order Elliptic	0.0065	0.0214	-0.1595	0.1612
10th Order Chebyshev Type 1	0.0064	0.0214	-0.1604	0.1609

Filter Designed to Minimise Time Domain Ringing				
Filter Type	Mean	SD	Min	Max
	[g]	[g]	[g]	[g]
4th Order Butterworth	0.0065	0.0213	-0.1590	0.1590
2nd Order Elliptic	0.0065	0.0283	-0.2692	0.2713
2nd Order Chebyshev Type 1	0.0065	0.0289	-0.2817	0.2840

Table 5.2: Statistics of Filtered Lateral Accelerations

Filter Designed to Maximise Roll-Off Rate				
Filter Type	Mean	SD	Min	Max
	[g]	[g]	[g]	[g]
4th Order Butterworth	-0.0195	0.0259	-0.2434	0.2086
8th Order Elliptic	-0.0195	0.0262	-0.2540	0.2189
10th Order Chebyshev Type 1	-0.0194	0.0264	-0.2605	0.2190

Filter Designed to Minimise Time Domain Ringing				
Filter Type	Mean	SD	Min	Max
	[g]	[g]	[g]	[g]
4th Order Butterworth	-0.0195	0.0259	-0.2434	0.2086
2nd Order Elliptic	-0.0195	0.0295	-0.3239	0.2702
2nd Order Chebyshev Type 1	-0.0195	0.0295	-0.3242	0.2715

Table 5.3: Statistics of Filtered Vertical Accelerations

Filter Designed to Maximise Roll-Off Rate				
Filter Type	Mean	SD	Min	Max
	[g]	[g]	[g]	[g]
4th Order Butterworth	-0.0010	0.0106	-0.0932	0.0804
8th Order Elliptic	-0.0010	0.0111	-0.0951	0.0816
10th Order Chebyshev Type 1	-0.0010	0.0114	-0.1051	0.0825
Filter Designed to Minimise Time Domain Ringing				
Filter Type	Mean	SD	Min	Max
	[g]	[g]	[g]	[g]
4th Order Butterworth	-0.0010	0.0106	-0.0932	0.0804
2nd Order Elliptic	-0.0010	0.0132	-0.4091	0.2130
2nd Order Chebyshev Type 1	-0.0010	0.0132	-0.4134	0.2247

Table 5.4: Statistics of Filtered Longitudinal Accelerations

To understand the likelihood of seeing larger peaks, histograms were constructed from the various filtered signals by carrying out a level crossing analysis. As described in chapter 3 a level crossing analysis is used to count the number of occasions a signal exceeds a given level [41, 97, 98]. By setting intervals and counting the number of crossings within each interval a histogram of the results is obtained. The level crossing histogram is often a precursor for probabilistic analysis on extreme values [41, 56, 138, 140].

The number of intervals was set to 150 and accelerations $\leq 1\%$ of the maximum acceleration in the signal, about the mean of the signal, were omitted from the count. The algorithm was set to count only the accelerations above the interval level and not on it.

An example of all the lateral acceleration histograms is shown in Figure 5.9. The abscissa of the histograms shows the range of acceleration levels exceeded and the ordinate shows the number of crossings. It is evident that the shape and size of the histograms due to the higher order filtered signals are all similar but those due to the lower order filtered signals are significantly different. In particular the number of crossings increases dramatically for the lower order filters because these filters allow far more of the signal content through the transition band. This results in many more low amplitude occurrences and higher amplitude exceedances in those signals filtered with 2nd order filters i.e. the entire distribution shrinks with increasing filter order.

The statistical properties of the higher order filtered signals were very similar and

comparable to the results from the 4th order Butterworth filter. The lower order filters produced vastly different histograms due to the leaky nature of the filters in the frequency domain. This demonstrates the importance of a high roll-off rate and shows that some overshoot and ringing in the time domain is permissible.

In all cases the distributions indicate clearly that peak accelerations occur rarely and the larger the peaks the less likely they are to occur. This is because the tails of the distributions are exponentially decreasing therefore the likelihood of larger accelerations gets smaller as the peaks get larger.

Despite the approximately bell-shaped appearance of the data attempts to fit the data to normal, log-normal and Weibull distributions indicated a poor fit.

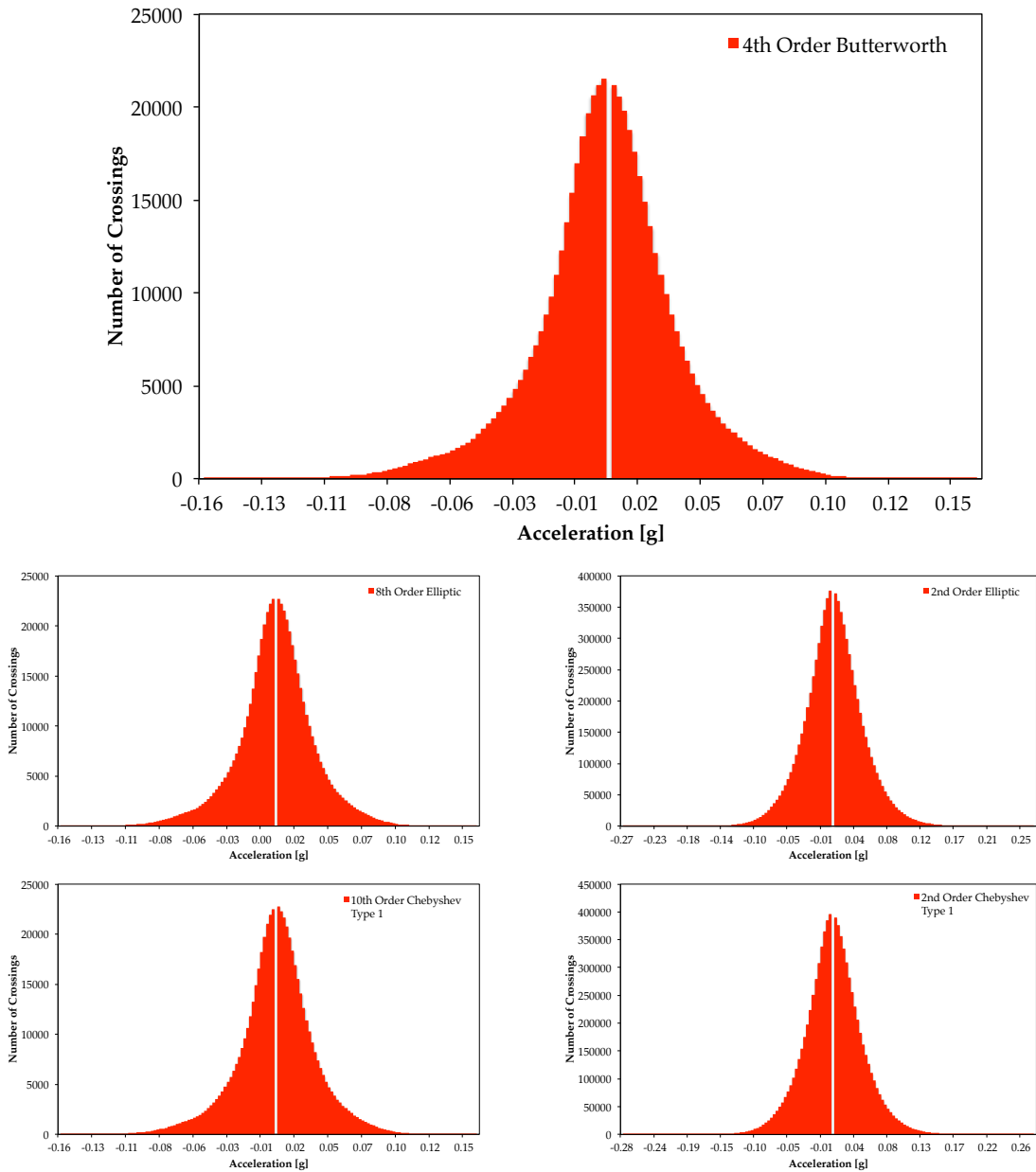


Figure 5.9: Level Crossing Histograms of Low Pass Filtered Lateral Accelerations at 17.5 Hz. Resulting Distributions from Various Filter Designs

5.7 Effect of Filter Cut-Off Frequency on Acceleration Extrema

Using the same time history from accelerometer N at the base end stanchion a further study was carried out to assess the sensitivity of peaks due to changing the filter cut-off frequency.

A low pass, forward-backward, 4th order Butterworth filter was designed and proved to be sufficient for the task of varying filter cut-off frequencies between 1 - 100 Hz. For f_c values < 4 Hz the 4th order Butterworth filter was marginally stable but possessed a superior roll-off rate than a 4th order Chebyshev Type 1 or Elliptic filter (at least when they are designed with negligible allowable pass band ripple of -0.0001 dB).

The cut-off frequency was varied in increments of 1 Hz from 1 - 20 Hz and then in increments of 10 Hz from 20 - 100 Hz. The resulting acceleration extrema showed an increasing trend as the filter cut-off frequency increased (**Table 5.5**).

The trend in the extrema is not linear and no simple mathematical relation exists between cut-off frequency and acceleration peaks. In general the difference between extrema of the low pass filtered signals between 10 - 20 Hz is small, the largest changes observed are in the vertical minima (**Figure 5.10**).

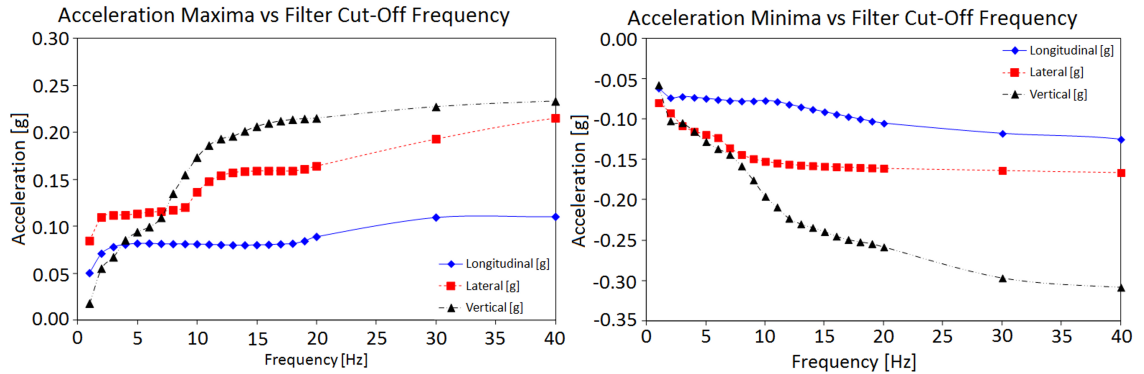


Figure 5.10: Acceleration Extrema vs Filter Cutoff Frequency

Stanchion	Vertical [g]		Lateral [g]		Longitudinal [g]	
	Max	Min	Max	Min	Max	Min
Filter Cutoff Frequency [Hz]						
1	0.018	-0.058	0.085	-0.080	0.050	-0.062
2	0.055	-0.102	0.110	-0.093	0.071	-0.074
3	0.067	-0.105	0.112	-0.108	0.078	-0.072
4	0.085	-0.115	0.112	-0.115	0.081	-0.073
5	0.094	-0.128	0.113	-0.119	0.082	-0.075
6	0.099	-0.137	0.115	-0.123	0.082	-0.076
7	0.109	-0.144	0.116	-0.136	0.081	-0.077
8	0.135	-0.158	0.117	-0.144	0.081	-0.078
9	0.155	-0.176	0.120	-0.149	0.081	-0.078
10	0.173	-0.196	0.136	-0.152	0.081	-0.077
11	0.186	-0.209	0.148	-0.155	0.081	-0.079
12	0.193	-0.223	0.154	-0.156	0.080	-0.082
13	0.196	-0.230	0.157	-0.157	0.080	-0.085
14	0.201	-0.234	0.158	-0.158	0.080	-0.088
15	0.206	-0.239	0.159	-0.159	0.080	-0.091
16	0.210	-0.245	0.159	-0.159	0.081	-0.094
17	0.212	-0.249	0.159	-0.160	0.081	-0.097
18	0.213	-0.252	0.159	-0.160	0.082	-0.100
19	0.214	-0.254	0.161	-0.161	0.084	-0.103
20	0.215	-0.258	0.164	-0.161	0.089	-0.105
30	0.227	-0.297	0.193	-0.164	0.110	-0.118
40	0.233	-0.308	0.215	-0.166	0.110	-0.125
50	0.237	-0.312	0.225	-0.168	0.112	-0.149
60	0.248	-0.315	0.223	-0.172	0.114	-0.181
70	0.254	-0.317	0.217	-0.175	0.115	-0.217
80	0.256	-0.318	0.214	-0.178	0.117	-0.253
90	0.257	-0.319	0.217	-0.181	0.121	-0.287
100	0.258	-0.320	0.225	-0.184	0.123	-0.316

The IAEA Advisory Material [2] states a frequency range of 10 - 20 Hz to use as a cut-off frequency relative to defining quasi-static loads

Table 5.5: Acceleration Extrema due to different Filter Cutoff Frequencies

5.8 A Quick Estimate of the Filter Cut-Off Frequency based on Displacement PSDs

A method for obtaining a suitable filter cut-off frequency has been devised by comparing PSDs at the stanchion and wagon bed. The acceleration PSDs were integrated twice in the frequency domain to produce displacement PSDs. As the purpose of the filter is to obtain quasi static loads for structural design, displacements PSDs were considered to be more closely related to structural stress and strain than accelerations. Since the standard approach used in tie down system design is to apply the loading to the centre of mass of the package, it is postulated that the cut-off frequency can be determined as the frequency at which the PSDs become lower at the stanchion, than those at the wagon bed. As a first approximation, three potential cut-off frequencies have been identified from the PSDs (Figures 5.11 - 5.13). The proposed cut-off frequencies are listed in Table 5.6.

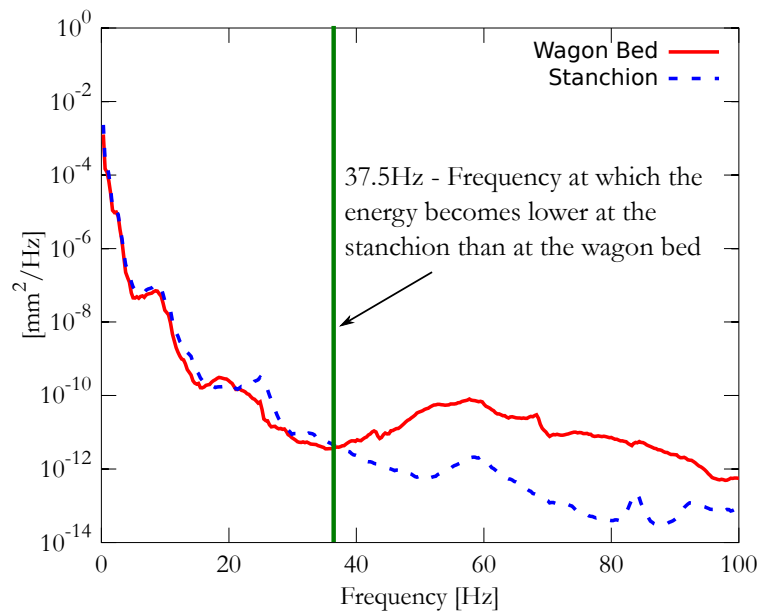


Figure 5.11: Vertical Displacement PSD from Wagon Bed and Stanchion

In the longitudinal and lateral axis the f_c 's fall in the 10 - 20 Hz range. However in the vertical axis the f_c is 37.5 Hz. Figure 5.11 indicates that the curves also cross at ≈ 15 Hz but they clearly diverge at 37.5 Hz. At all frequencies < 37.5 Hz they are virtually identical, indicating that there is very little relative movement vertically between the package and wagon bed.

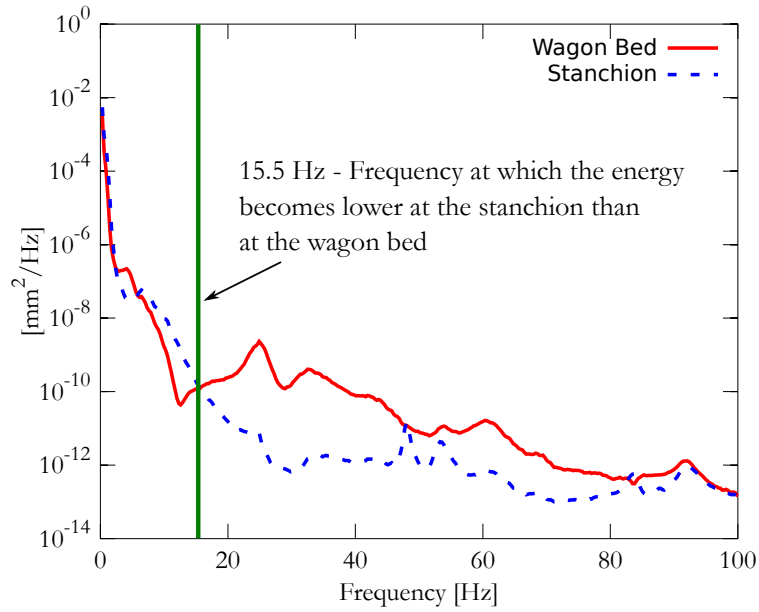


Figure 5.12: Lateral Displacement PSD from Wagon Bed and Stanchion

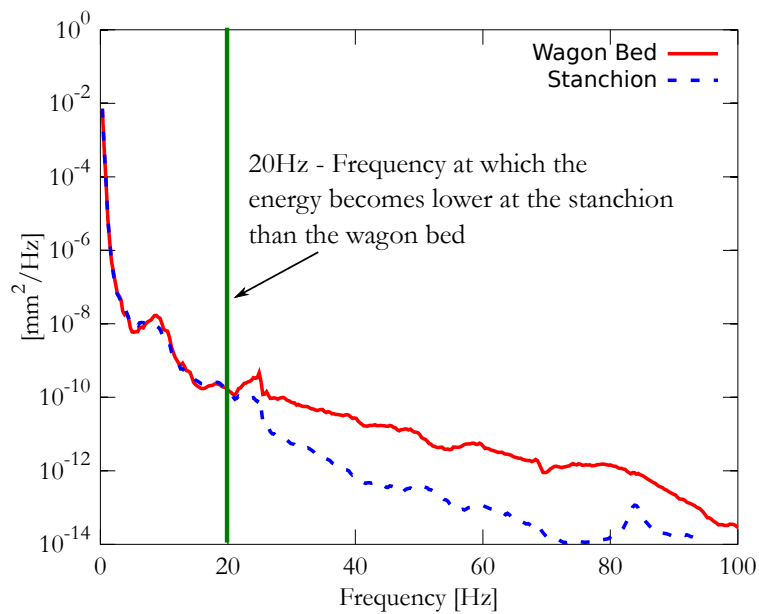


Figure 5.13: Longitudinal Displacement PSD from Wagon Bed and Stanchion

	Longitudinal	Lateral	Vertical
Frequency [Hz]	20	15.5	37.5

Table 5.6: Possible Filter Cutoff Frequencies

5.9 Trends Observed in the Statistics of the Filtered Accelerations

Using the filter cut-off frequencies from **Table 5.6** and selecting a 4th order, forward-backward, Butterworth filter the wagon bed and stanchion time history records have been filtered and the resulting signals have been compared. Three comparative filtering studies have been conducted on the signals by:-

1. Low pass filtering with a cut-off frequency of 100 Hz.
2. Low pass filtering with the cut-off frequencies from **Table 5.6**.
3. Band pass filtering, where the lower cut-off frequencies have been taken from **Table 5.6** and the upper cut-off frequency set to 100 Hz.

Some statistics from the resulting time histories are presented (**Tables 5.7 - 5.9**).

	Wagon Bed [g]			Stanchion [g]		
	RMS	Max	Min	RMS	Max	Min
Longitudinal	0.03	0.31	-0.43	0.02	0.12	-0.32
Vertical	0.07	0.78	-0.85	0.04	0.26	-0.22
Lateral	0.05	0.57	-0.56	0.03	0.22	-0.18

Table 5.7: Statistics of Acceleration Signals Low Pass Filtered at 100 Hz

	Wagon Bed [g]			Stanchion [g]		
	RMS	Max	Min	RMS	Max	Min
Longitudinal	0.02	0.12	-0.12	0.01	0.09	-0.11
Vertical	0.03	0.22	-0.18	0.04	0.23	-0.19
Lateral	0.02	0.11	-0.15	0.02	0.16	-0.16

Table 5.8: Statistics of Acceleration Signals Low Pass Filtered at Cutoff Frequencies from Table 5.6

	Wagon Bed [g]			Stanchion [g]		
	RMS	Max	Min	RMS	Max	Min
Longitudinal	0.03	0.33	-0.37	0.01	0.17	-0.25
Vertical	0.06	0.78	-0.79	0.01	0.09	-0.07
Lateral	0.04	0.54	-0.56	0.01	0.14	-0.16

Table 5.9: Statistics of Acceleration Signals Band Pass Filtered, Lower Cutoff Frequencies from Table 5.6 and Upper Cutoff Frequencies at 100 Hz

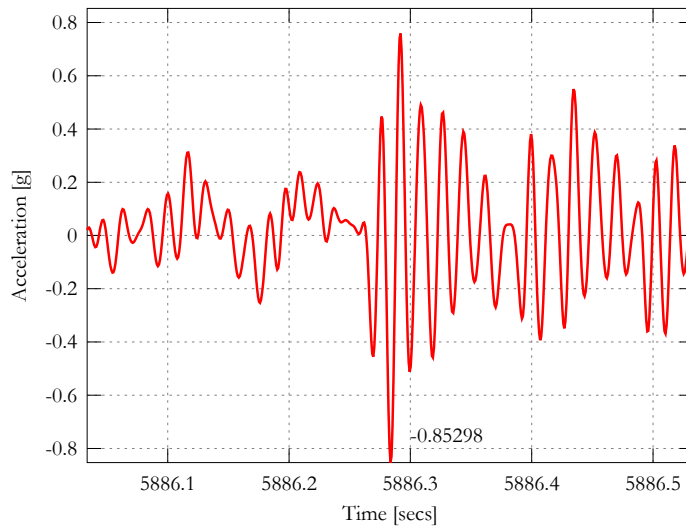
At the wagon bed the largest peak acceleration of -0.85 g was measured in the vertical direction (Table 5.7). The signal is shown in a close up of this peak and the low pass and band pass filtered signals are also shown for comparison (Figure 5.14). It is evident that the peak is a high frequency oscillation. To understand how this peak transmits through to the package, a similar figure has been created for the stanchion time history during the corresponding time period (Figure 5.15). Following the trend identified in chapter 4 the overall level of acceleration is lower at the stanchions than the wagon bed (Figure 5.14a & Figure 5.15a) and the low frequency content is similar at the wagon bed and stanchions (Figure 5.14b & Figure 5.15b). The peaks in Figures 5.14 & 5.15 are summarised in Table 5.10.

	Low Pass 100Hz	Low Pass 37.5Hz	Band Pass 37.5 Hz - 100Hz
Wagon Bed [g]	-0.85	-0.18	-0.79
Stanchion [g]	-0.21	-0.19	-0.07

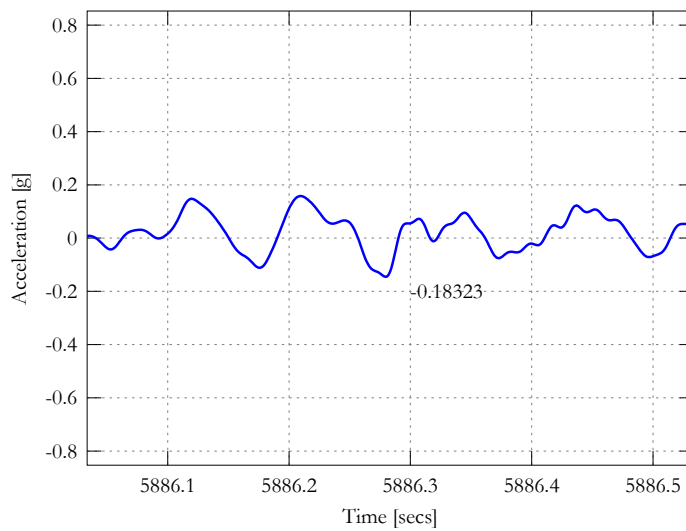
Table 5.10: Transmission of Peak Vertical Acceleration from Wagon Bed into Package

The high frequency peaks measured at the wagon bed have been attenuated by an order of magnitude at the stanchions, from -0.79 g to -0.07 g (Figure 5.14c & Figure 5.15c). These results are emphasised in overlaid time history plots of the peak at both the stanchion and wagon bed (Figure 5.16a & 5.16b). Figure 5.16a is low pass filtered at 37.5 Hz and Figure 5.16b is band pass filtered between 37.5 Hz – 100 Hz. It is evident that the signals are in-phase and hence at low frequency a state of near rigid body motion exists.

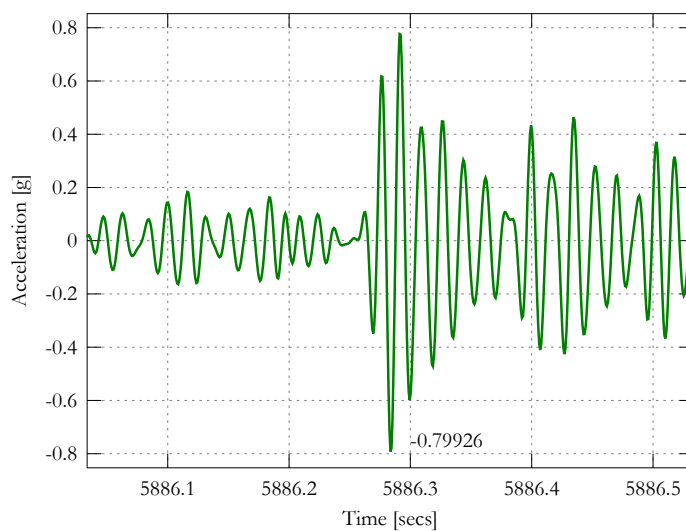
This is an important result that has implications both for the interpretation of tie down loads and for vibration transmission in to fuel assemblies during transport. In the case of tie down loads, many previous studies have positioned instrumentation at the wagon bed [11, 26, 27, 84, 85]. Depending on the signal conditioning during these measurements there is the possibility that the tie down loads have been over-estimated due to their measurement position. This would occur if they have been digitised at a high enough sampling rate to capture the high frequency content which is attenuated at the package but present at the wagon bed. The same principle applies to vibration of fuel assemblies, in particular for many of the studies carried out in the US, these findings are a good indication of margins of safety in test specifications based on similar transport configurations [16–18, 26, 27, 82].



(a) Low Pass Filtered at 100 Hz

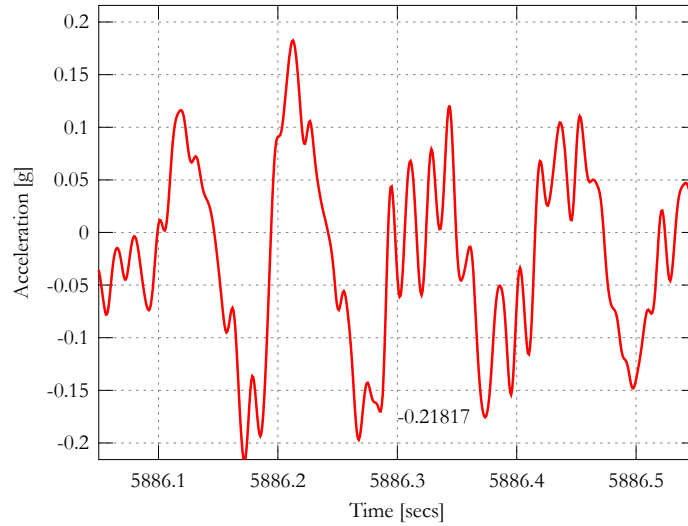


(b) Low Pass Filtered at 37.5 Hz

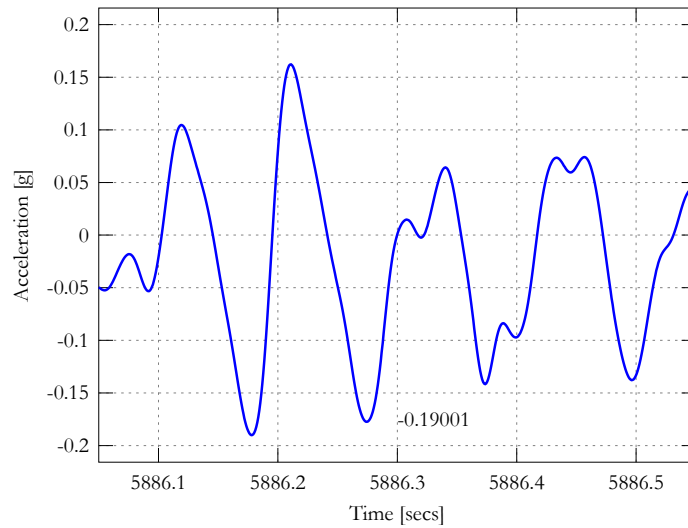


(c) Band Pass Filtered at 37.5 - 100 Hz

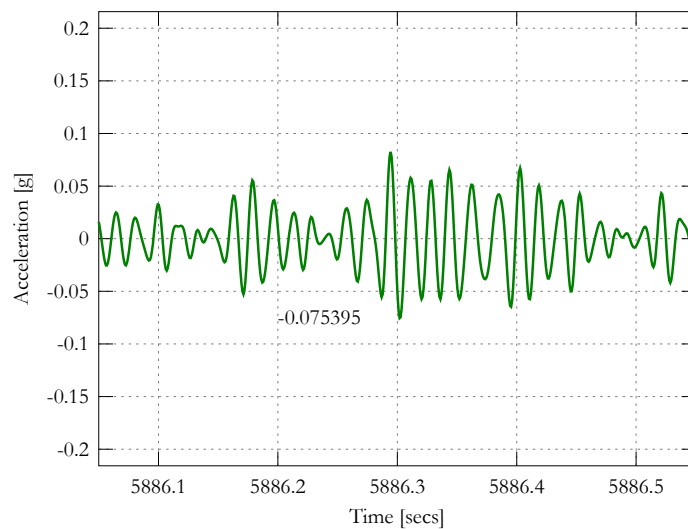
Figure 5.14: Peak Vertical Acceleration Measured at Wagon Bed



(a) Low Pass Filtered at 100 Hz

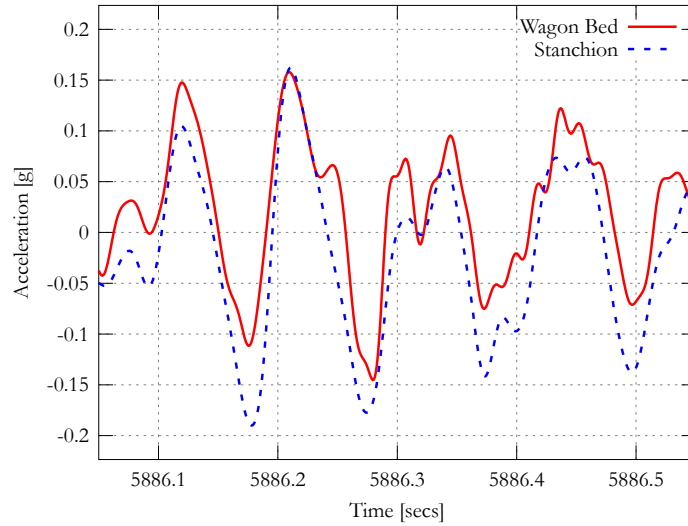


(b) Low Pass Filtered at 37.5 Hz

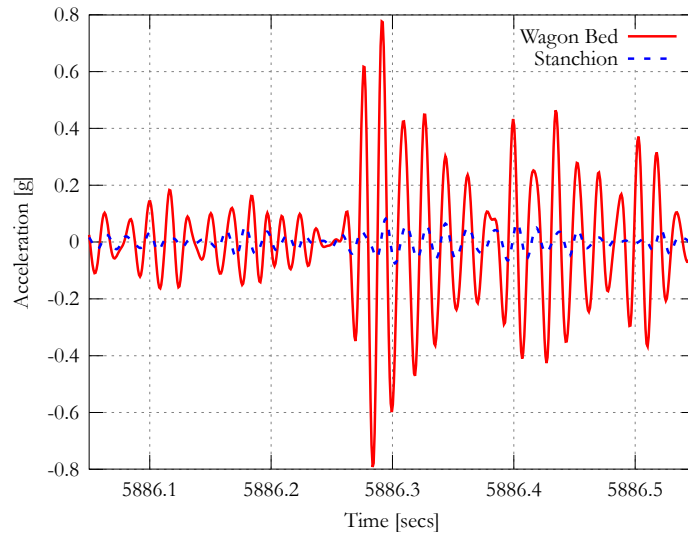


(c) Band Pass Filtered at 37.5 - 100 Hz

Figure 5.15: Peak Vertical Acceleration Measured at Stanchion



(a) Low Pass Filtered at 37.5 Hz



(b) Band Pass Filtered 37.5 Hz - 100 Hz

Figure 5.16: Filtered Peak Vertical Acceleration Measured at Stanchion and Wagon Bed

5.10 Discussion

5.10.1 Frequency Analysis

The high frequency oscillations (> 25 Hz) of the wagon bed are attenuated at the stanchions by the large package mass that doesn't have time to respond to the motion due to inertia. The energy at the wagon bed in the lateral and vertical acceleration PSDs appears to be the cause of the peak at 25 Hz in the strain PSDs. If a tie down design was produced using reduced acceleration factors compared with guidance material, this could influence fatigue life due to the larger number of cycles that occur at high frequencies. It should be noted that fatigue calculations were carried out and no fatigue damage was found in any of the measured strain time histories.

In general the loading expected to affect tie down system design is low frequency i.e. < 25 Hz. Two main frequency ranges of interest were identified, between 0 - 4 Hz and 4 - 16 Hz. In the range 0 - 4 Hz the strain peak was quite pronounced and corresponded with both lateral and vertical accelerations. In the range 4 - 16 Hz there was no distinct peak in the strain PSD just marginally higher spectral content. The acceleration PSDs differed; the vertical PSD exhibited a distinct peak whilst the lateral PSD displayed a band of increased energy, similar to the strains.

5.10.2 Filter Design

Different filters and their characteristics have been assessed to ensure the robustness of the analysis. When designing a filter to obtain quasi-static accelerations where the main concern is preserving the acceleration extrema, the results showed that the roll-off rate of the filter was the most influential characteristic. For this reason when applying higher order, forward-backward filters the resulting signals all possessed similar statistical properties but for 2nd order filters the statistical properties differed.

An estimate of the filter cut-off frequency was based on the postulate that the frequency at which the energy levels at the stanchion fall below those at the wagon bed is the most suitable to use as a cut-off frequency. This is logical since current design practice of tie down systems is to apply loads at the centre of mass of the package. The results also suggested that the cut-off frequencies were, in general, close to those suggested in the advisory material [2]. As this method is not directly based on the natural frequencies of the tie down system and package it is not necessarily the most accurate way of separating quasi-static content from the signals.

5.10.3 Peak Analysis

Comparing the quasi-static acceleration factors quoted in the advisory material to the results of this study from the stanchion accelerometer highlights two main differences. The measured accelerations are quoted as approximate as their actual value depends on which filter is used:-

1. The advisory longitudinal acceleration factor of 1 g for dedicated movements with special rail wagons is an order of magnitude higher than those measured (≈ 0.1 g) [2].
2. The advisory lateral acceleration factor of 0.5 g is also considerably larger than the measured, filtered, accelerations (≈ 0.16 g) [2].

The vertical acceleration factor of 1 ± 0.3 g, where 1 g is assumed to be the force of gravity, appears to agree with the measured accelerations (downwards ≈ 0.26 g and upwards ≈ 0.22 g). A summary of this comparison is shown in **Table 5.11**.

	SSG-26 Table IV.2	Measured [g]
Lateral	0.5	0.16
Longitudinal	1.0	0.1
Vertical	1.0 ± 0.3	0.22(U) 0.26(D)

Table 5.11: Comparison of Filtered Measured Accelerations Peaks vs Advisory Acceleration Factors

5.11 Summary

- Welch's [133] method for calculating PSDs has been presented and its implementation has led to successful corroboration of the strain signals with their source in the multiaxial accelerations. The results indicate that the lateral accelerations are the dominant axis of tie down loading and that the strains incurred by the tie down system are most sensitive to lateral loading.
- Spectral analysis indicated that frequency content of the wagon bed accelerations > 25 Hz is attenuated by the package mass and is not present at the tie down stanchions. This was later confirmed by filtering and time domain analysis.
- It is possible that accelerations acting on tie downs for heavy packages determined in previous studies may be over-estimated. This is because most previous studies have been carried out by measuring at the wagon bed. If the measurements were acquired at a high sampling frequency and not filtered appropriately, then track induced vibrations may have been measured and not tie down loads. There is no adverse safety consequence of this because over-estimated loads result in conservative design.
- Vibration test specifications developed from measurements that have been obtained at the wagon bed of a rail wagon transporting a heavy package may also be over-estimated as the results from this study indicate that the package inertia attenuates the high frequency oscillations.
- A filter design methodology has been established and implemented on the time histories. The study indicates that the peak accelerations are most sensitive to the selection of filter roll-off rate. For this reason the highest order filter that can be designed and remains stable will provide the most accurate filtered signal.
- For filter cut-off frequencies between 1 - 100 Hz a 4th order, forward-backward Butterworth filter provided acceptable frequency domain characteristics and remained marginally stable at very low cut-off frequencies.
- A quick method for selecting a quasi-static filter cut-off frequency f_c has been devised based on displacements obtained using frequency domain integration of acceleration PSDs. This is a first approximation which provided some useful insight into the behaviour of the package during transportation.

6. Comparison of Strains Predicted with Finite Element Analysis and Measurements

6.1 Introduction

This chapter uses the results obtained from the experiment described in **Chapter 4** and the signals processing techniques implemented in **Chapter 5** to validate a more detailed Finite Element model of the tie down system. From the outset it was decided that the primary requirement of the comparison was to determine how well a linear static FEA model can predict the measured strains. This was done because industrial time constraints and regulatory guidance do not always allow for complex non-linear or dynamic models of tie down systems and rail vehicles.

To compare the predicted strain results with measured strains a number of methods have been used. A correlation coefficient has been used to judge the linear dependence of the data sets. The predicted and measured PSDs have been compared. The residual time history between the predicted and measured time histories has also been converted into a PSD to identify any frequencies that the model does not predict. The measured strains and residuals have also been analysed using an auto-correlation function which provides an indication of what trends are present in the measured strains and whether those trends have been modelled successfully.

To understand the significance of contact non-linearities that are present in reality, two non-linear FEA models have also been developed. Several load cases have been considered to determine whether the strain response remains linear at elements in the model corresponding to strain gauged locations during the test.

The measured accelerations and strains have been filtered with varying f_c to establish which f_c achieves best agreement. This serves two purposes; the first is that it validates the model within a certain frequency range and the second is that it improves on the methods suggested in the previous chapter for selecting a f_c . This demonstrates effective use of the experimental results with FEA and highlights how the techniques compliment each other.

6.2 Aims and Objectives

- Create an improved FEA model of the tie down system used during the rail journey measurements.
- Use the model to assess the effects of contact non-linearities in the tie down system on the predicted strains at strain gauge locations.
- Establish a basis for using a linear, small displacement analysis to reconstruct strain time histories using measured accelerations as input signals.
- Validate the model using spectral, linear correlation and statistical techniques.
- Draw conclusions on the suitability and predictive capabilities of the model.

6.3 Overview

The thorough design of tie down systems presents a broad set of load cases due to the transportation environment. Designs are required to withstand everyday operational usage including package loading/unloading, lifting, tilting and quasi-static loads that arise during transportation. These requirements are satisfied by designing the system for strength.

The cyclic nature of these loads and the residual dynamic transportation loads require that the system is also designed to provide sufficient fatigue resistance. Additionally, in the event of an accident the tie down system must not damage the package in such a way that impairs its safety. This requirement has led to the design of weak links in some tie downs, ensuring that under a given accident condition the package safety is not compromised.

In **Chapter 5** methods for filtering the measured accelerations during a rail journey of a 99.7 tonne nuclear package were described. Quasi-static accelerations for comparison with the current design parameters were estimated. In this chapter the dynamic acceleration and strain data is systematically passed through a low pass filter, whilst varying its cutoff frequency between 1 Hz – 100 Hz. The filtered tri-axial acceleration time histories are used to scale the results of a linear static Finite Element Model (FEM) at specific elements in the model corresponding to strain gauge locations. The scaled vertical, lateral and longitudinal accelerations are then summed to calculate

strain time histories. The calculated strain time histories are compared with actual measurements.

For the method to be applicable a linear mathematical model must be used to predict the response of the tie down to the transportation loading. A successfully validated computer model has several key benefits:-

1. Safety margins based on experimental results can be quantified.
2. Provides an opportunity to assess other areas of the structure where no measurements were taken.
3. Improves interpretation of experimental results i.e. provides a justification for choice of filter cutoff frequency (f_c) to obtain loads for design.
4. Presents the possibility of reconstructing acceleration time histories from the measured strains i.e. inversely determine tie down loading based on material response not structural motion.

The improved FEM of the tie down system has been constructed and its idealisation explained. Methods for simplifying the complex frame to package interface are emphasised. Linearisation of the interaction between contacting parts enables the scaling and superposition method used to calculate strain time histories. This requires careful analysis to determine the validity or error caused by omitting non-linear effects.

6.4 Correlation between Measured Accelerations and Strains

For linear static analysis to be applicable a linear dependency between the measured accelerations and strains must exist. If the strains are linearly dependent on the accelerations then, in theory, they can be predicted using a suitable mathematical model which relates them.

The Pearson correlation coefficient (ρ) is calculated as follows:-

$$\rho = \frac{C_{xy}}{\sigma_x \sigma_y} \quad (6.1)$$

where:-

C_{xy} = Covariance between two random
variables x and y

σ_x = Standard deviation of x

σ_y = Standard deviation of y

This correlation coefficient provides a measure of linear dependency between two sets of random data [41]. When comparing acceleration and strain signals $\rho = \pm 1$ for perfect linear dependency and $\rho = 0$ when the strains and accelerations are independent of each other.

6.4.1 Assessing the Strength of the Correlation

Wirsching *et al* [41] provide guidance on interpreting intermediate values of ρ however it is useful to first highlight some of the sources of random error or noise that weaken correlation. In signals analysis the terminology "strength" or "weakness" indicate the degree of dependence between one signal and another. Three main sources of error are proposed in Figure 6.1.

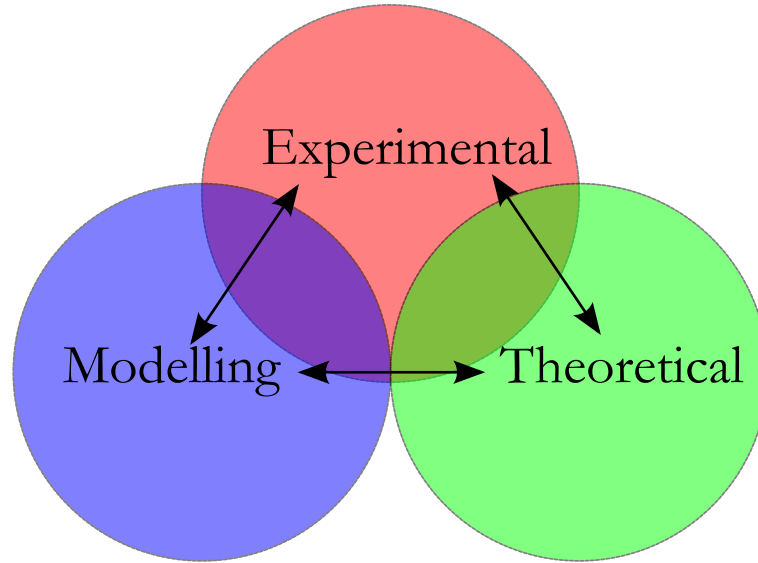


Figure 6.1: Sources of Error

When ρ deviates from ± 1 at least one or more of these sources are the cause of the weakened correlation. The total error can be described as follows:-

$$\epsilon_{total} = \epsilon_{experimental} + \epsilon_{modelling} + \epsilon_{theoretical} \quad (6.2)$$

Breaking down these sources of error further, to pinpoint root causes of weak correlation:-

$$\epsilon_{experimental} = \epsilon_{electrical} + \epsilon_{temperature} + \epsilon_{procedural} \quad (6.3)$$

$$\epsilon_{modelling} = \epsilon_{modelling\ assumptions} + \epsilon_{numerical\ (rounding)} \quad (6.4)$$

$$\epsilon_{theoretical} = \epsilon_{non-linearities} + \epsilon_{dynamic\ effects} \quad (6.5)$$

Each of these error sources consist of a number of different variables that degrade the strength of the correlation. Wirsching [41] suggests that if the total random error is $1/2$ the strength of the signal then $\rho \approx 0.9$ and the dependency between the signals is considered strong.

If the error is about the same strength as the signal then $\rho \approx 0.7$ and the dependency between the signals is considered moderate. When $\rho < 0.7$ this is an indication of weak dependence of strains on accelerations.

The Coherence function calculates the correlation coefficient across a range of frequencies for a given input and output time history or “channel”. Based on an examination of the magnitude and direction of each strain channel it was evident that the

strain response was dominated by lateral loading which concurs with the findings from the previous chapter. Therefore the coherence function for each strain channel was calculated using the lateral acceleration measurements from the tie down system base end stanchion as the input channel. **Figure 6.2a** shows an example of a coherence function with the frequency axis set to 0 – 100 Hz.

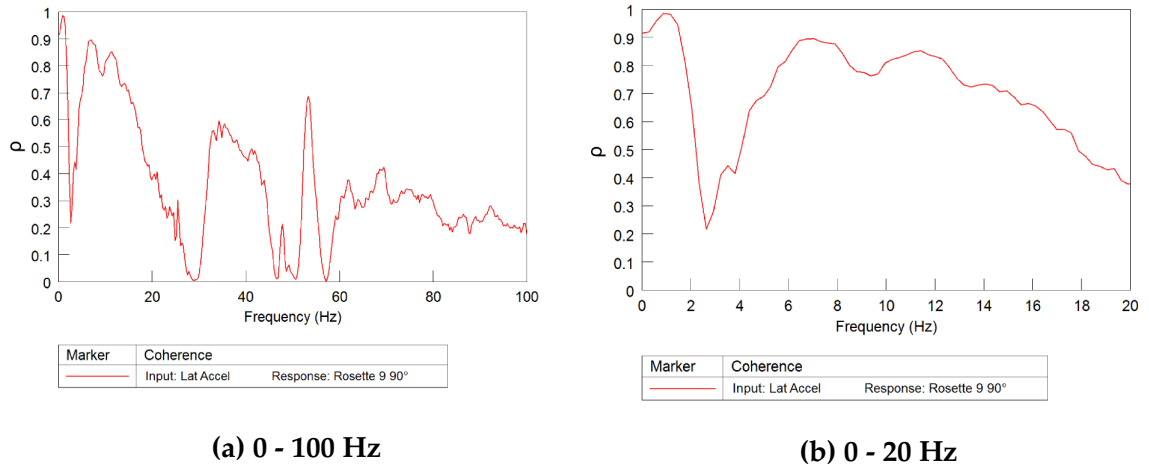


Figure 6.2: Example of Coherence between Measured Acceleration and Strain

Figure 6.2b shows the same coherence plot between 0 – 20 Hz. This frequency range has been chosen because the anticipated quasi-static content of the signal is < 20 Hz. The coherence function shows that all the signals are at least moderately correlated between 0 – 2 Hz and 5 Hz – 15 Hz. This suggests that a linear model is appropriate, at least for this frequency range. The combination of vertical and longitudinal acceleration influences, although small, is expected to increase Coherence in the 2 - 5 Hz range.

6.4.2 Data Cleansing

Data cleansing is a necessary process to make a comparison between calculated and measured peak strains. It is common practice to carry out some basic data cleansing normally to remove any DC offset and very low frequency content (drift) [132, 138].

The acceleration data was visually examined and not corrected further. However it was observed that the strains were very low, close to the noise floor of the instrumentation in some cases. Because of this any small amount of drift and offset that is present is evident visually.

The drift present may be due to real physical loading such as thermal expansion. It may also be attributed to thermal errors, however this was minimised by the use of temperature compensated strain gauges [138]. Where necessary an attempt to remove drift was made using 1st or 2nd order polynomial curves (Figure 6.3). The removal of drift does not affect correlation, it just allows better comparison of peaks.

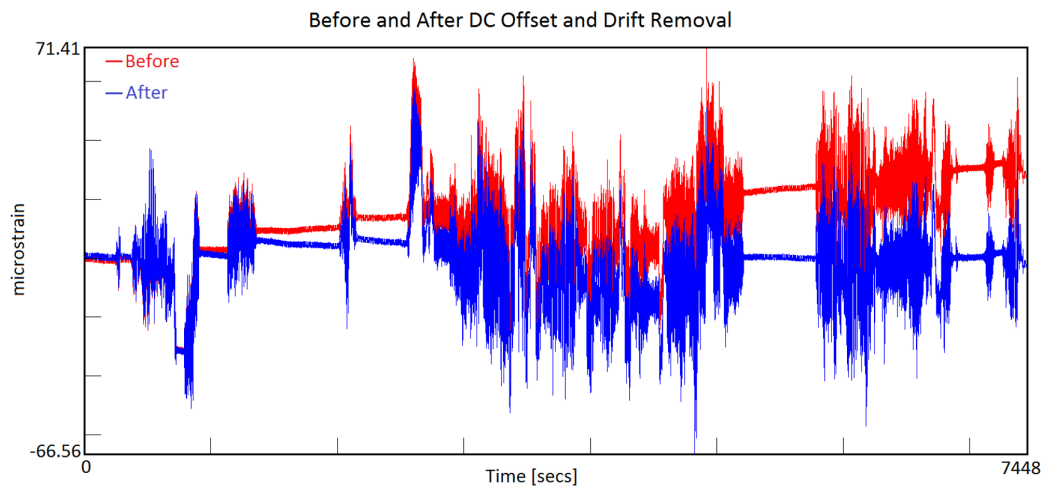


Figure 6.3: An Example of Data Cleansing used on some of the Measured Strain Time Histories

6.5 Tie Down System - General Arrangement

Figure 6.4 shows an exploded 3-D CAD model of the tie down system (inset is the assembled structure). The main structural members are the saddles, longitudinal beams and stanchions, all manufactured from high strength stainless steel plates joined by welding. The trunnion bushes are made of a phosphur bronze.

Overall Dimensions

Height = 1903.5mm

Width = 2670.0mm

Length = 5977.5mm

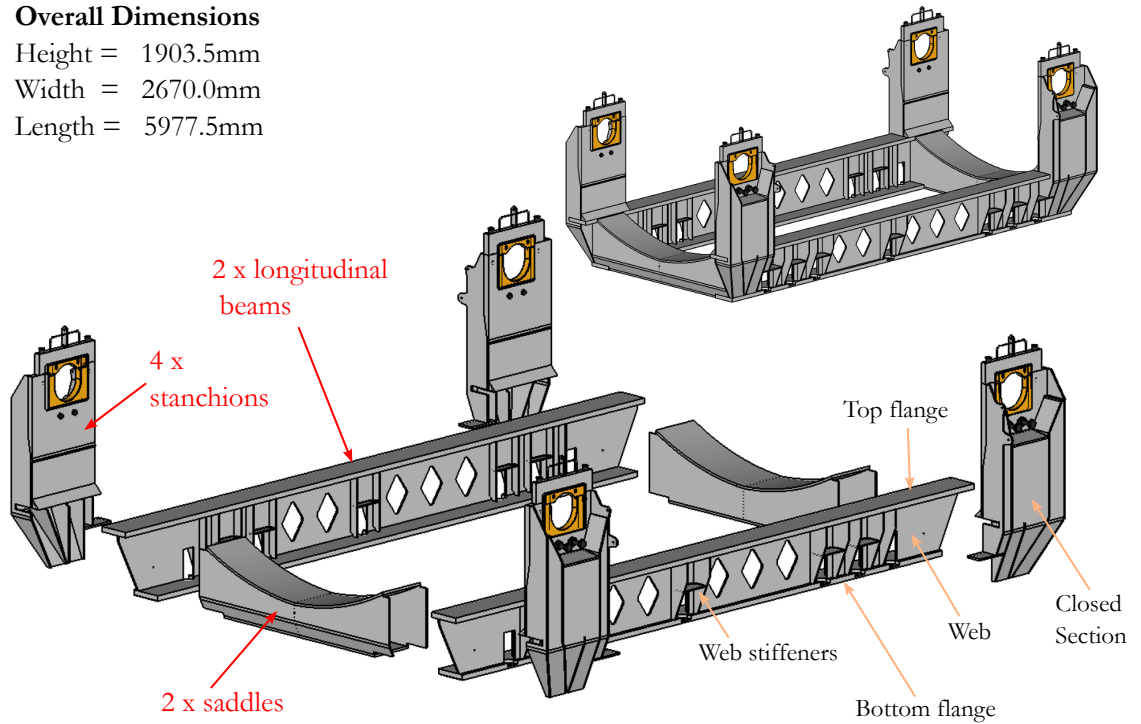


Figure 6.4: Details of the Tie Down System Construction

A mixture of partial and full penetration butt welds are used for joining the plates. Where possible the welds are double sided, however many closed sections exist and the welds are often, by necessity, single sided. Additionally due to its large size the welds are all manual and therefore stop/start sections are expected.

Figure 6.5 shows a close up of the package trunnion interface at the lid end stanchion of the tie down system. The trunnion bush is designed to allow ± 20 mm of longitudinal sliding due to package thermal expansion/contraction. This is an area of analytical complexity for two reasons. The first is that this area consists of many contacting parts (some omitted here for clarity). The second is the geometrical configuration of the stanchion which enforces modelling simplifications, often in areas that warrant detail.

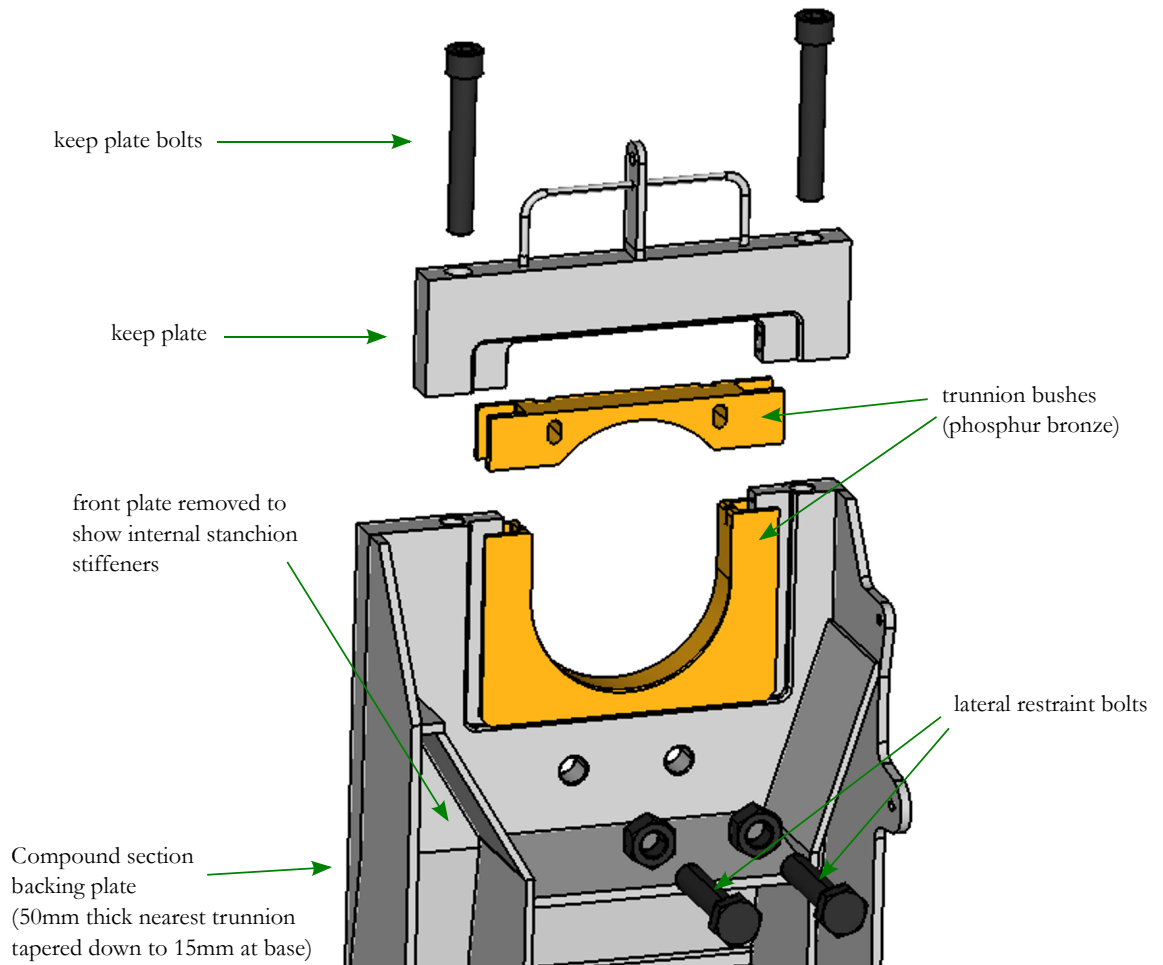


Figure 6.5: Detail of Lid End Trunnion Bushes and Upper Stanchion

For example the backing plate is a compound section, consisting of a 50 mm thick section at the trunnion bushes, a tapered section and 15 mm thick section at its base **Figure 6.5**. The lateral restraint bolts combined with the irregular welded structure on the backing plate outward facing surface and the keep plates and their bolts are difficult to mesh with brick elements, but not suitable for shell element idealisation, therefore some modelling compromises are necessary.

The overarching compromise arises when connecting a hybrid shell and brick element mesh together. There is a disparity in nodal degrees of freedom between the two element types and the usual method of eliminating unwanted mechanisms due to this is by adding an extra row of shell elements "painted" over the surface of the connecting bricks. This method approximates load transfer across the joints but predicted stresses and strains at this type of interface are often in doubt.

6.6 Finite Element Model

The model was pre-processed using Hyperworks 12.0 [123]. All solutions were obtained using the sparse, direct, linear solver in Abaqus 6.13 [141]. **Figure 6.6** shows a wireframe view of the entire tie down system and a “dummy” package. As only limited information on the package was available it was modelled, excluding shock absorbers, with 4-noded tetrahedral elements and the density of the linear elastic material model was adjusted to obtain a mass of 99.7 tonnes.

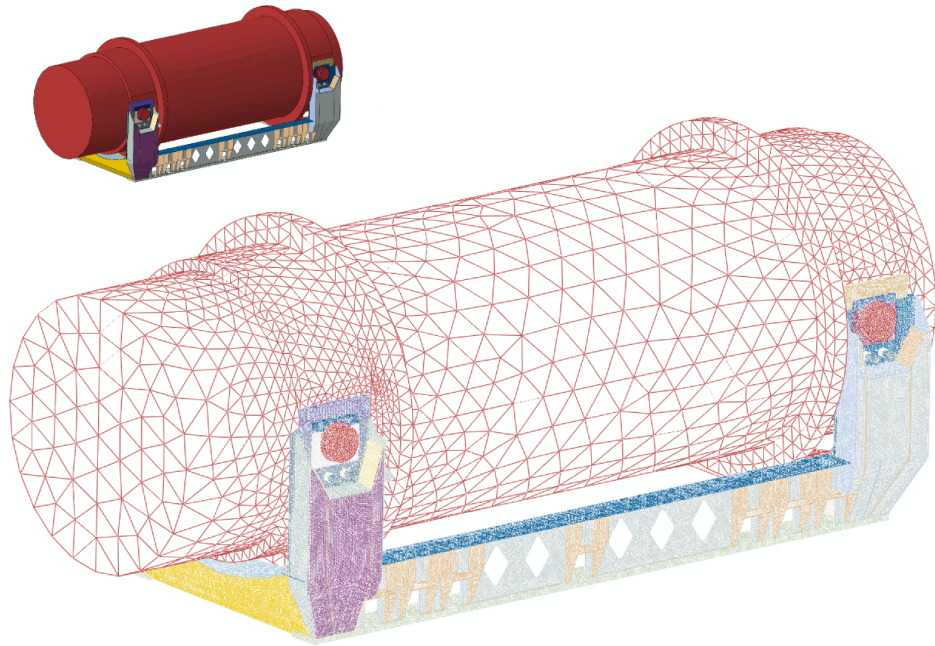


Figure 6.6: Finite Element Model of Tie Down System and Dummy Package

Details of the finite element mesh of the tie down are shown in **Figure 6.7**. The mesh consists of a mixture of 8-node brick elements and 4-node shell elements (C3D8 and S4). To maintain good element shape a small number of wedge and triangular elements have been used. A total of 568,416 elements: 135,696 quadrilaterals, 108 triangles, 394,340 bricks and 258 wedges were used in the model. A global element size of 15 mm was selected, although smaller elements were used in some areas to resolve intricate details properly.

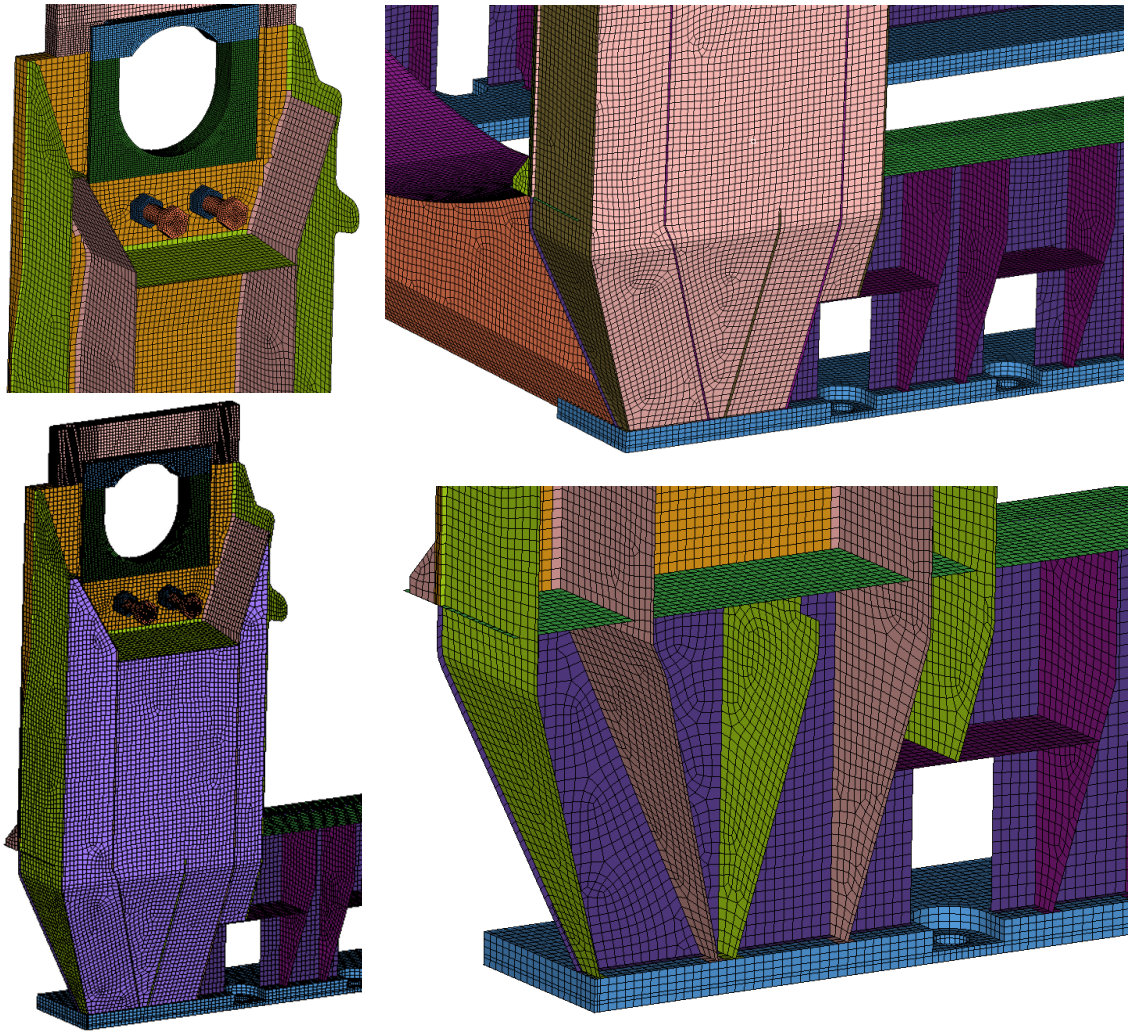


Figure 6.7: Details of Finite Element Mesh of Tie Down System

The mesh of the trunnion interface retained most of the original design detail however the keep plate bolts and wear plates beneath the sliding, lid end trunnion bush have been omitted. The interacting parts have been meshed with a finer, solid element mesh (≈ 5 mm) this allows obvious definition of master and slave surfaces in non-linear sensitivity studies. Included in the model are the lateral restraint bolts represented with solid elements; their threaded portions are modelled by merging the nodes at the interface between the bolts, nuts and the stanchion back plates. **Figure 6.8** shows the mesh of the lid end trunnion attachments and lateral restraint bolts.

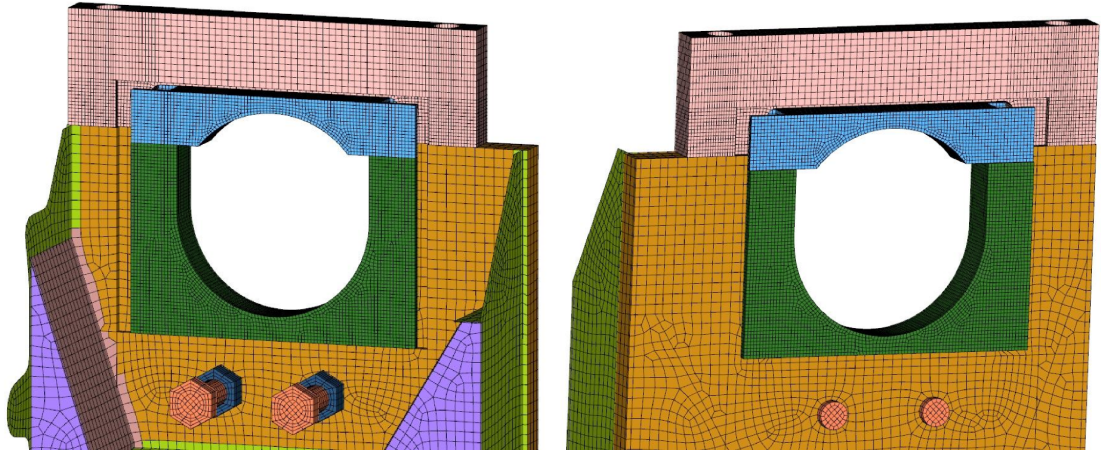


Figure 6.8: Finite Element Mesh of Lid End Trunnion Attachments and Restraint Bolts

6.6.1 Materials Modelling

During the rail journey the tie down system was not subjected to loads sufficient to cause non-linear material behaviour. Therefore in this model all the materials have been modelled with a linear elastic material model, the properties used are listed in **Table 6.1** and the 0.2% yield stress is provided for reference.

Material	Grade	ρ [kg/m^3]	E [GPa]	ν	$\sigma_{0.2\%}$ [MPa]	References
High Strength Stainless Steel	S890Q	7,800	200	0.3	960	[125]
Phosphur Bronze		7,600	121	0.3	123	[142]
Carbon Bolt Steel	BS898 12.9	7,800	192	0.3	1100	[143]

Table 6.1: Material Properties applied to Finite Element Model

6.6.2 Boundary Conditions and Loads

The tie down system is connected to the swan neck wagon bed with 14 x M45 bolts. To isolate the tie down from the wagon it is necessary to constrain the model to eliminate any rigid body motion. In this analysis the tie down bolts are omitted and the entire lower surface of the bottom flange of the longitudinal beams is constrained (**Figure 6.9**). This overconstrains the structure slightly but sensitivity analysis showed that alternative methods, such as constraining only the nodes at the bolt holes, produced minor differences in structural response at the elements corresponding to the strain gauged positions.

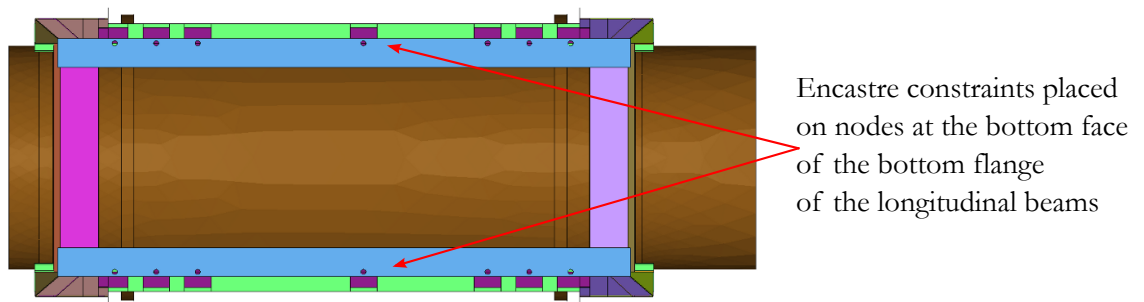


Figure 6.9: Boundary Conditions Applied to the Model

The unit load model was run in three uncoupled, linear perturbation steps, with a different load cases for each step (**Figure 6.10**). Distributed loads were used to apply an acceleration of 1 g to the whole model in the lateral, longitudinal and vertical directions. A comparison of the total computation time for the model is shown for 1, 2, 4, 6 and 8 CPUs (**Table 6.2**).

6.6.3 Quality Checks

The model was checked for warnings and the summation of the reaction forces in X, Y and Z at the constrained nodes were written to the .dat file. The forces balanced with those calculated using Newton's 2nd law based on the mass of the model and the applied load.

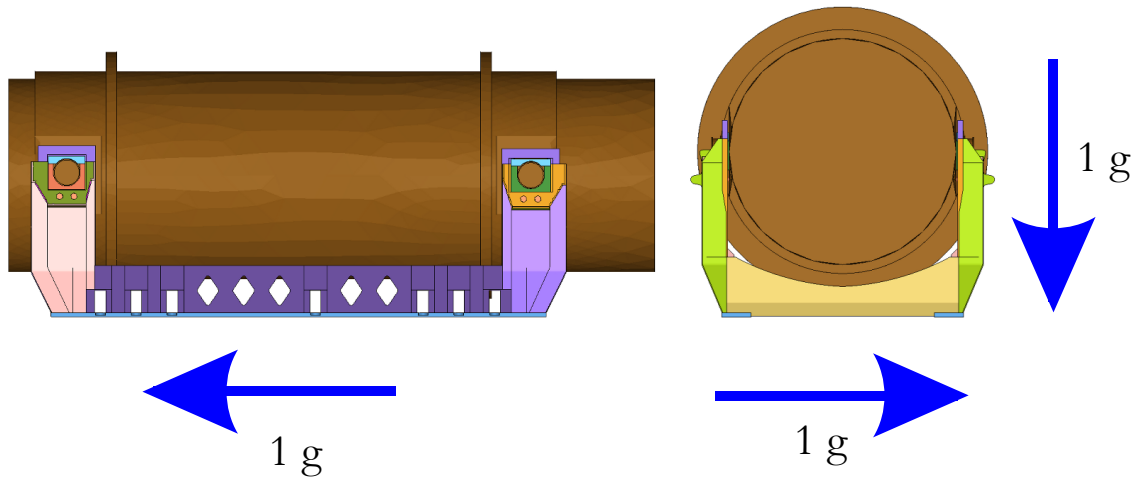


Figure 6.10: 3 x 1g Load Cases (Unit Loads)

CPU	Wall Clock Time [min:secs]	RAM [Gbytes]
1	11:30	13
2	10:05	13
4	9:28	13
6	8:47	13
8	8:48	13

Table 6.2: Run Times to Completion for Linear Model

6.6.4 Calculating Strain Time Histories

To obtain strain time histories a combination of scaling and superposition of the FEA results was used with the measured acceleration time histories as follows [112, 113]:-

$$\varepsilon_{ij}(t) = \sum_{k=1}^N \varepsilon_{(ij,k)} L_k(t)$$

$\varepsilon_{ij}(t)$ = the strain tensor at a time t

$\varepsilon_{ij,k}$ = the strain tensor due to unit load

$L_k(t)$ = the acceleration time history

where

k = lateral, vertical or longitudinal loading

Elements were selected that correspond to the measured strain locations and their strain tensors used in the scaling and superposition algorithm (Figure 6.11). This method accounts for multi-axial loading of the structure. A 30-minute section of the measurements during the journey were low pass filtered with a 4th order, forward-backward, Butterworth filter. Strain time histories were calculated using the filtered accelerations measured at the base end stanchion (accelerometer N). This process was repeated for 28 different filter cut-off frequencies 1 Hz – 20 Hz in 1 Hz increments and 20 Hz – 100 Hz in 10 Hz increments. These calculations were carried out in nCode DesignLife [131].

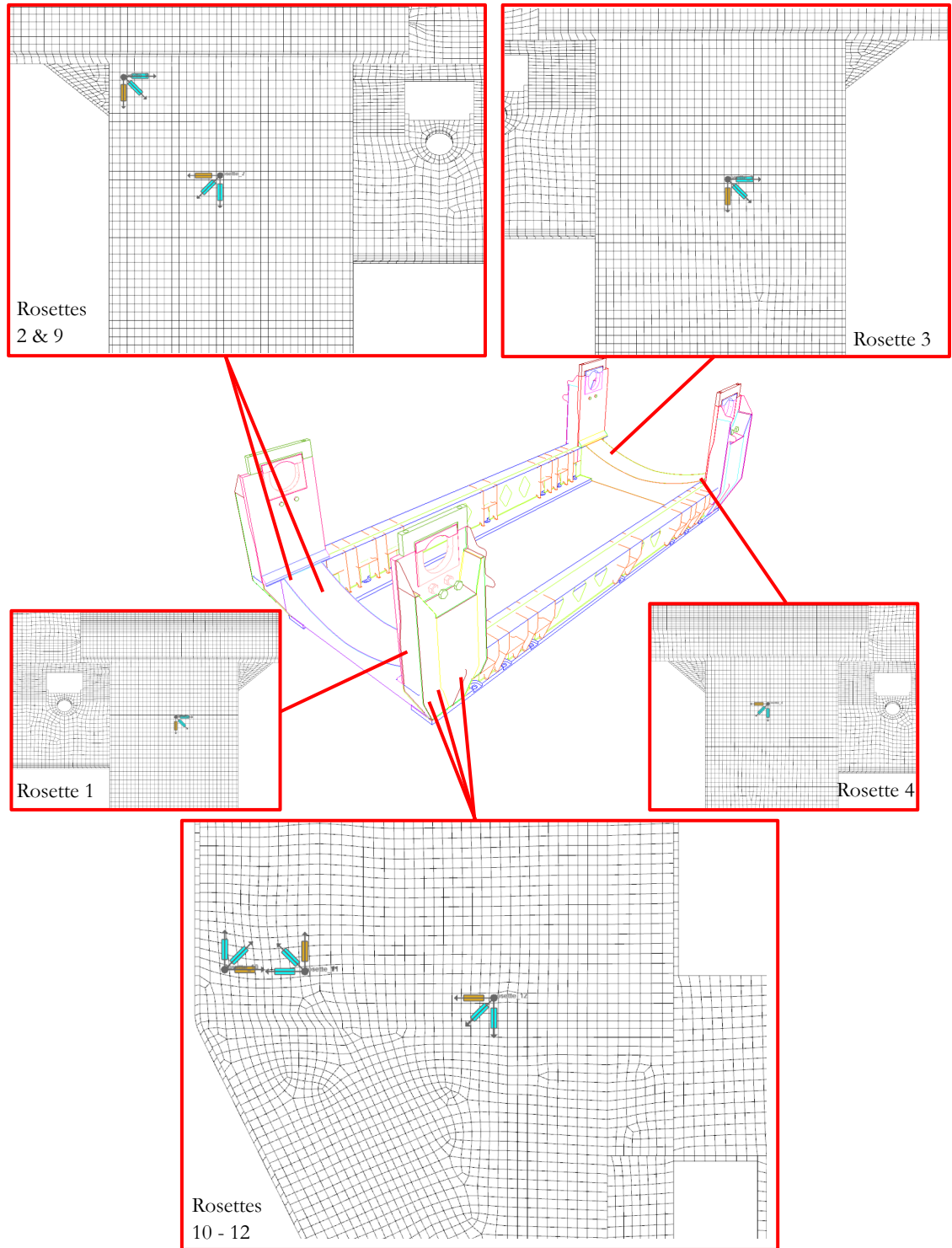


Figure 6.11: Locations and Orientations of the Virtual Strain Gauges

6.6.5 Contact Modelling

Modelling the contacting parts has been achieved by either, meshing parts congruently and merging the nodes at the mating interfaces or by modelling with a contact pair, which is then “tied”, effectively bonding the parts together and achieving the desired linearisation.

Both methods require several important assumptions to hold or they will produce inaccurate results due to load path variations caused by sliding between contacting surfaces. Sensitivity analysis has been carried out to confirm the validity and effect of the major assumptions. There is a lot of contact present between different parts of the tie down system, rail wagon and package; the two most important contact interactions for this study are now identified and discussed.

6.6.6 Contact at the Trunnion Attachments

There are several contacting parts in the trunnion attachments of the tie down system (**Figure 6.5**). The floating lid end trunnion bush could cause sliding and non-linear geometric effects which may affect the strain results in the stanchions. A hand calculation, assuming a coefficient of friction $\mu = 0.35$ which is typical of steel to phosphur bronze contact, shows that an acceleration of 0.1 g would be enough to overcome friction, resulting in sliding of the trunnion bush. This could arise due to heavy braking or cornering at speed. Lateral sliding of the trunnion bush is prevented due to the lateral restraint bolts, however only frictional forces prevent the floating trunnion bush from sliding due to longitudinal loading.

6.6.7 Lateral Restraint Bolts

The lateral restraint bolts are fitted to the tie down system through threaded holes in the stanchion back plates (**Figure 6.5**). They are adjusted to make contact with the package prior to transportation and held in place with a locking nut. This will produce a small bearing stress between the package side wall and the end of the bolt shank. Under lateral loading a change in the load paths may occur, as one stanchion will bend away from the restraint bolts, causing them to experience a compressive force exerted by the package and transmitted through to the stanchion. The opposite stanchion will bend towards the package, therefore any bearing stress between the end of the restraint bolt and the package side wall will decrease or in the limiting

case, contact will be lost, resulting in differences in stanchion stresses and strains under reversed loading.

6.7 Sensitivity Analysis

A preliminary review of the modelling assumptions and loading was carried out to assess the validity of the scaling and superposition approach. In **Chapter 5** low pass filtering of measured accelerations with a cutoff frequency of 20 Hz produced the following load ranges:-

$$\begin{aligned}\text{Lateral} &= [-0.16g, 0.16g] \\ \text{Longitudinal} &= [-0.11g, 0.09g] \\ \text{Vertical} &= [-0.26g, 0.22g] \text{ (excluding gravity)}\end{aligned}$$

Accelerations in the frequency range 0 – 100Hz, produced larger load ranges:-

$$\begin{aligned}\text{Lateral} &= [-0.18g, 0.23g] \\ \text{Longitudinal} &= [-0.32g, 0.12g] \\ \text{Vertical} &= [-0.32g, 0.26g] \text{ (excluding gravity)}\end{aligned}$$

In the frequency range 0 – 100 Hz the longitudinal accelerations are large enough to cause sliding of the trunnion bushes. Since they occur rapidly (> 20 Hz) their significance on this study is minimal. The lateral and vertical load ranges do not vary significantly with f_c , however, the lateral loading may be enough to cause contact loss between the package and restraint bolts.

In the following section FEA results are compared by reviewing stresses at elements corresponding to the strain gauge positions. These elements are called the virtual strain gauge rosettes (**Figure 6.11**).

6.7.1 Non-Linear Effects during Longitudinal Loading

To assess the effects of using a tied contact at the "floating" lid end trunnion bushes, a half symmetry model was created for non-linear analysis. The symmetry model retained five of the virtual strain gauge rosettes. The package was remodelled in brick elements with a refined mesh at the lateral restraint bolt contact areas and the trunnions (Figure 6.12).

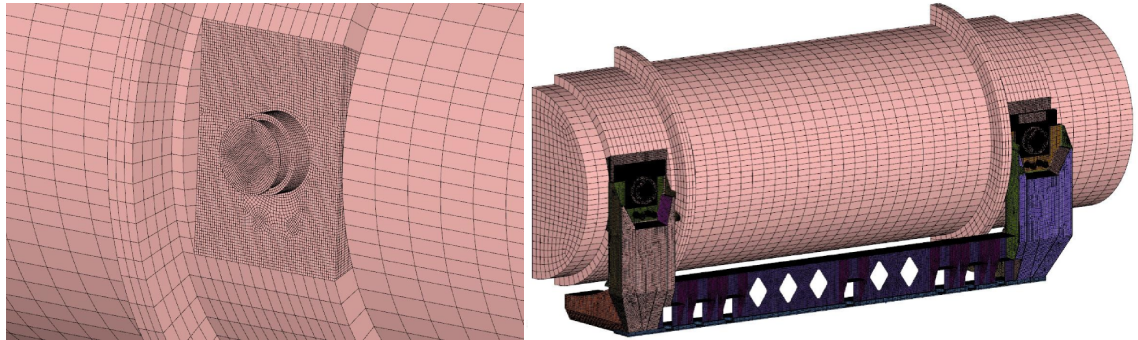


Figure 6.12: Detailed Mesh of Package Required for Non-Linear Studies

Speckert published a method for calculating time histories on a rail vehicle ball joint based on a set of non-linear analyses that represent various combinations of load direction and magnitude [115]. Here a non-linear analysis has been carried out to assess the contact effects of the trunnion bushes and lateral restraint bolts on the FEA results.

The analysis is run in two sequential load steps; the first to calculate a vertical preload due to gravity and also include the range of vertical loading. In the second step, a range of longitudinal loads have been prescribed, a matrix of runs is provided in Table 6.3. Consideration of the combined vertical and longitudinal load cases is necessary to obtain contact forces between the trunnion bushes, tie down and package that resist longitudinal motion.

Vertical	Load Cases - Longitudinal Acceleration [g]										
	Longitudinal										
-1.32	-	-	-	-	-	-	-	-	0.03	0.07	0.12
	0.32	0.27	0.22	0.17	0.12	0.07	0.03				
-1.0	-	-	-	-	-	-	-	-	0.03	0.07	0.12
	0.32	0.27	0.22	0.17	0.12	0.07	0.03				
-0.74	-	-	-	-	-	-	-	-	0.03	0.07	0.12
	0.32	0.27	0.22	0.17	0.12	0.07	0.03				

Table 6.3: Combination of Loading in Non-Linear Analysis

The half symmetry model consisted of 414,535 elements and produced 1.7×10^6 degrees of freedom. A single model ran in approximately 1.5 hours on 8 CPUs and used 23 gigabytes of RAM. The 30 non-linear runs were solved on a Linux server.

To reduce the overall solution time the first step was run only once per vertical load and a restarted analysis was then used to vary the longitudinal load cases. The line search method was used which provided additional computational efficiency. These techniques reduced the overall computation time from (an estimated) two days to approximately 5 hours. Both the pre and post processing were automated with a combination of shell scripts and HyperMath programming detailed in the Appendix of this thesis [123].

Figure 6.13 shows that the von Mises stress response is non-linear in the load space analysed (i.e. lateral acceleration set to zero). The predicted stresses are very low for all five of the virtual rosettes, which is in agreement with the strain measurements that did not appear to be influenced by longitudinal loading. The Finite Element results do demonstrate that non-linearity is present and significant in this tie down system, however it will have a diminishingly small effect on this study because of the negligible influence of longitudinal loading during the experiment.

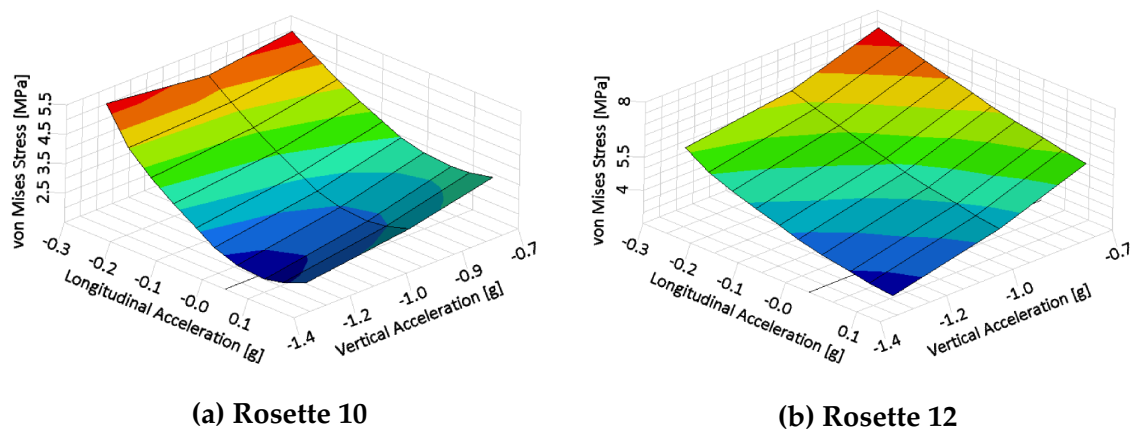


Figure 6.13: Example of von Mises Stress Results from Virtual Strain Gauges during Combined Longitudinal and Vertical Loading

6.7.2 Non-Linear Effects during Lateral Loading

The half symmetry tie down model and remodelled package were reflected and combined by merging the nodes on the symmetry plane to produce a complete FEA model for non-linear analysis of lateral loading. The potential for non-linear effects arising during lateral loading was considered to be independent of the other loading directions. This is because the contact pressure that develops between the lateral restraint bolts and the package side wall is not due to gravitational effects. This analysis was also carried out in two steps. Gravity was applied in the first step, to make the stresses comparable to the non-linear longitudinal study and the results of this step were restarted for 10 lateral load cases in the range -0.18 g to 0.23 g.

Figure 6.14 provides a schematic to show the effects of the lateral restraint bolts contacting the package side wall during lateral loading. It is clear that the effective bending moment arm changes during load reversals, something that the linearised unit load model cannot account for.

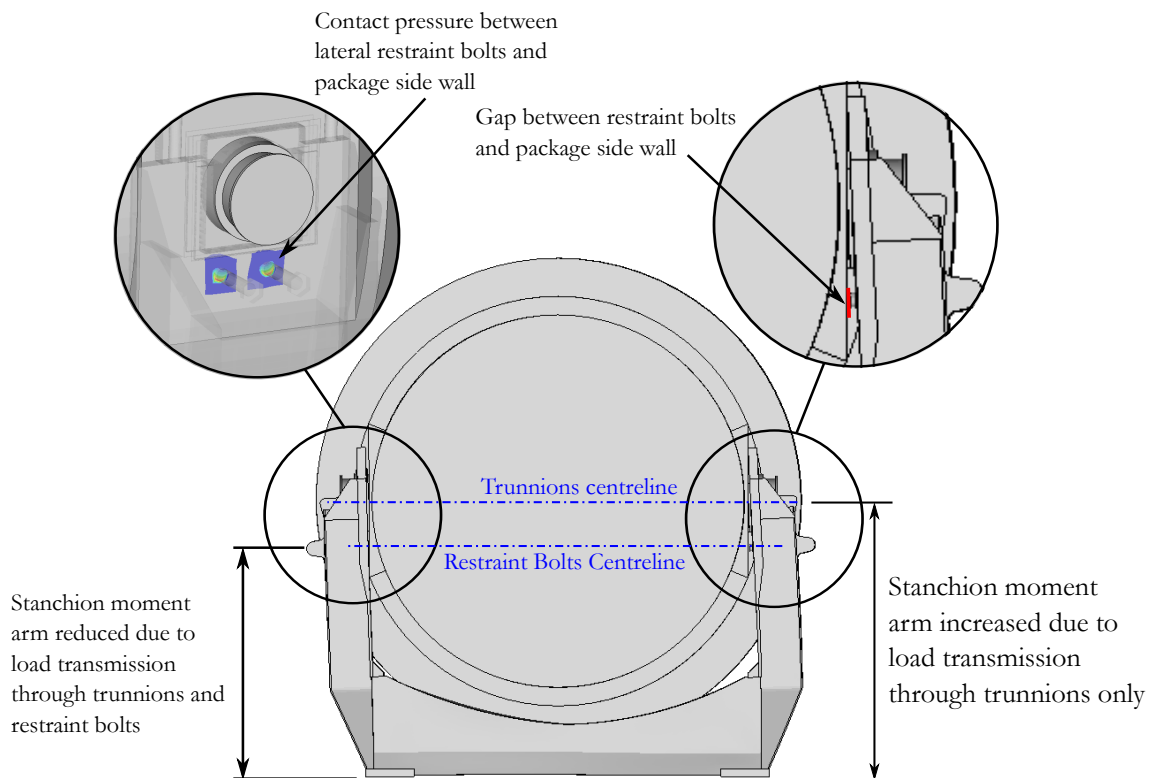


Figure 6.14: FEA Sensitivity Analysis, Non-Linear Lateral Load Case to Assess the Effects of Discontinuous Contact Behaviour between the Package Side Walls and Tie Down Lateral Restraint Bolts

At all the virtual strain gauges the von Mises stresses due to lateral loading are much larger than those predicted due to longitudinal loading.

The virtual strain gauges 10 - 12 are most likely to be effected by the bending response of the stanchion due to the presence of contact non-linearity. (Figure 6.15) presents the results from rosette 10 and 12 for both the non-linear and unit load analyses.

The stress results called "Nonlinear contact opened" are due to positive lateral loads which cause the contact between the trunnion restraint bolts and package to open. Those called "Nonlinear contact closed" are due to negative lateral loads (or a reversal) that causes the gap between the trunnion restraint bolts and the package to close and contact pressure to develop. The unit load model results are called "Linear bonded", the lateral restraint bolts are effectively glued to the side wall of the package.

The results are fitted with trend lines and their coefficient of determination is annotated. This provides a measure of how linear the stress response is to increased loading.

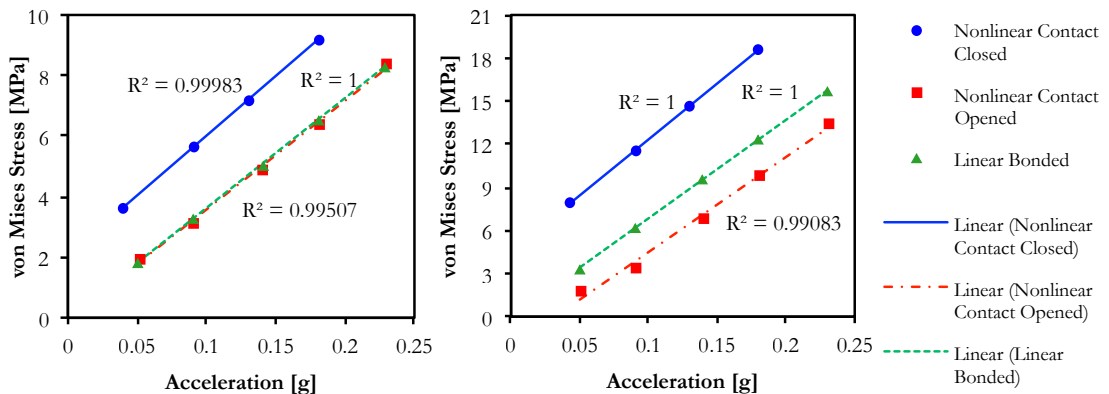


Figure 6.15: Sensitivity Analysis, Example of Non-linear and Linear Load Case Stress Results

6.7.3 Vertical Load Application

The presence of gravity causes the load range to be offset by -1 g. When applying the unit load this has been neglected because during the experimental procedure the strains and accelerations were measured during the loading of the package onto the tie down system and then zeroed prior to the journey. Therefore both positive and negative, measured vertical accelerations and tensile and compressive measured strains result from vertical loading.

The tensile strains due to vertical loading are offset by the compressive preload on the structure due to gravity. In reality the strains resulting from vertical loading will remain compressive unless a vertical acceleration > 1 g is experienced. If this does occur then the package is essentially weightless and the load path changes significantly. In this case the unit load model will not predict the load reversal correctly, however in the experiment the largest upwards, vertical acceleration was 0.26 g.

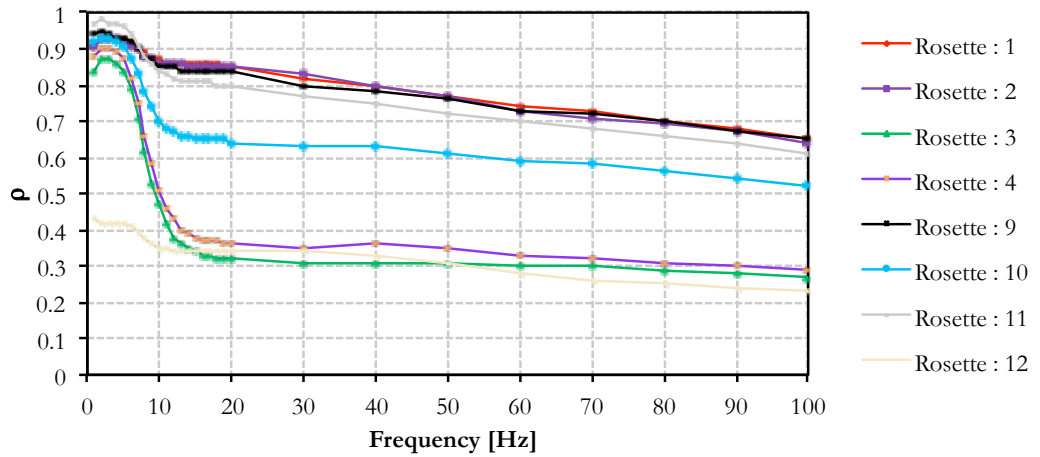
The direction of load applied to the model is also important as it changes the sign of the predicted stresses. It was necessary to account for this in the superposition procedure by pre-multiplying the acceleration time history by -1.0.

6.8 Correlation between Predicted and Measured Strains

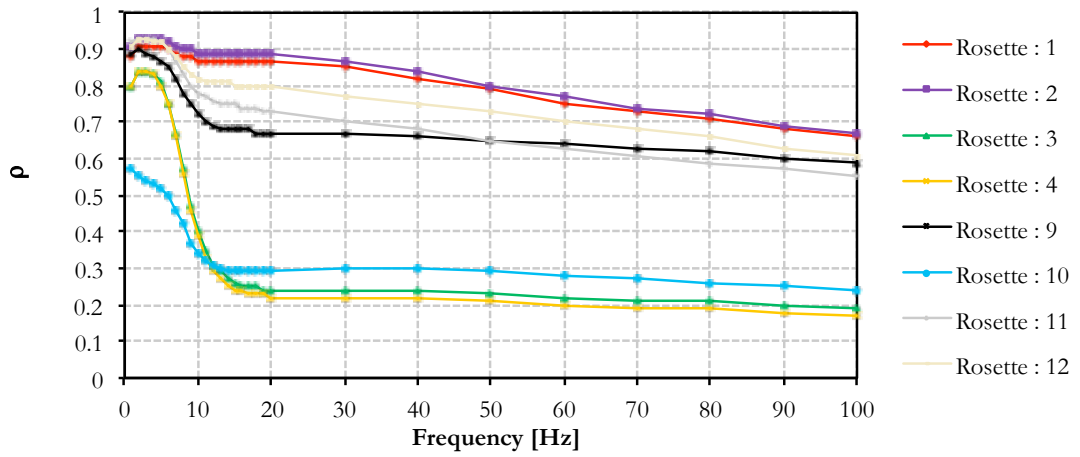
For a quantitative assessment of the correlation between the measured and calculated strain time histories a script was written to calculate the correlation coefficient for each of the signals generated at different filter cutoff frequencies in HyperMath, see Appendix. The results are plotted as correlation coefficient vs filter cutoff frequency for each of the strain gauge rosettes (**Figure 6.16**).

It is evident that a number of the channels produced poor agreement particularly at frequencies > 5 Hz. Visual examination of the signals with weak correlation indicated that some of the channels contained strain content $< |10| \mu\text{m}/\text{m}$. These channels were discarded from any further processing because they were considered small enough to be structurally insignificant and also too small to be accurately represented by the finite element model. The remaining results were collated and are shown in **Figure 6.17**.

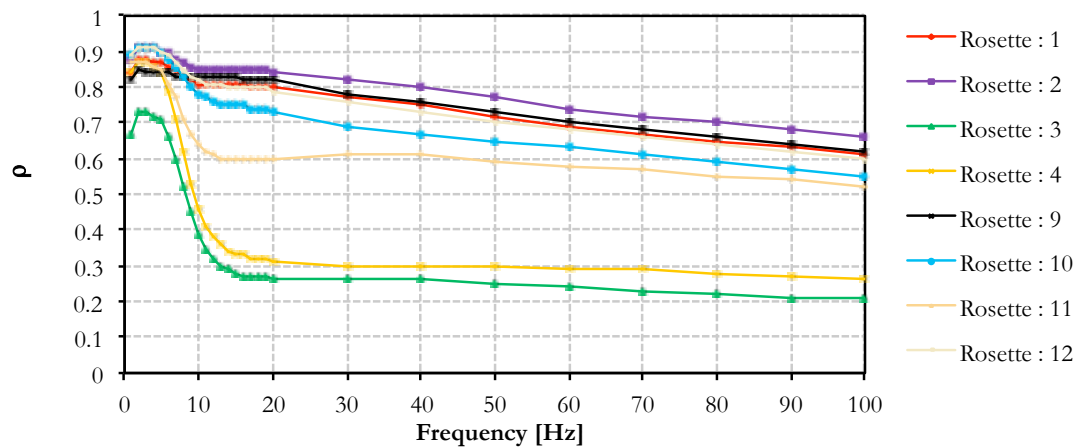
At filter cutoff frequencies < 5 Hz all the channels achieve at least moderate correlation ($\rho > 0.7$) and in many cases strong correlation ($\rho > 0.9$). **Figure 6.17** shows that there are 2 channels that still produce very weak correlation > 5 Hz. The anomalous results were found on two legs of rosette 3 (the third leg was previously discarded due to low strains levels). This was the only rosette, in the collated results, that was situated at the lid end of the structure. Therefore rosette 3 was re-run using the acceleration time histories from a lid end accelerometer. This was the subject of further investigation discussed later in this chapter. The final correlation results are shown in **Figure 6.18**.



(a) Strain Gauge Correlation (0°)



(b) Strain Gauge Correlation (45°)



(c) Strain Gauge Correlation (90°)

Figure 6.16: Preliminary Correlation Results

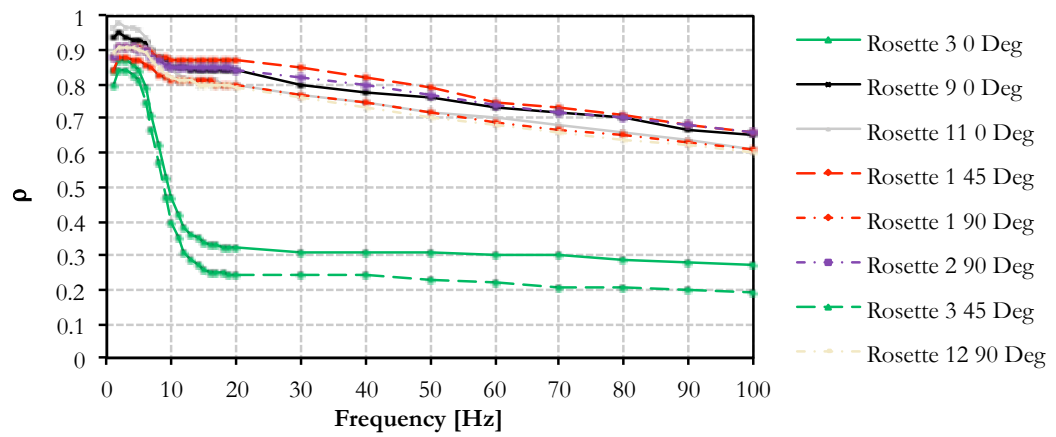


Figure 6.17: Correlation Results with Channels $< |10| \mu\text{m/m}$ Removed

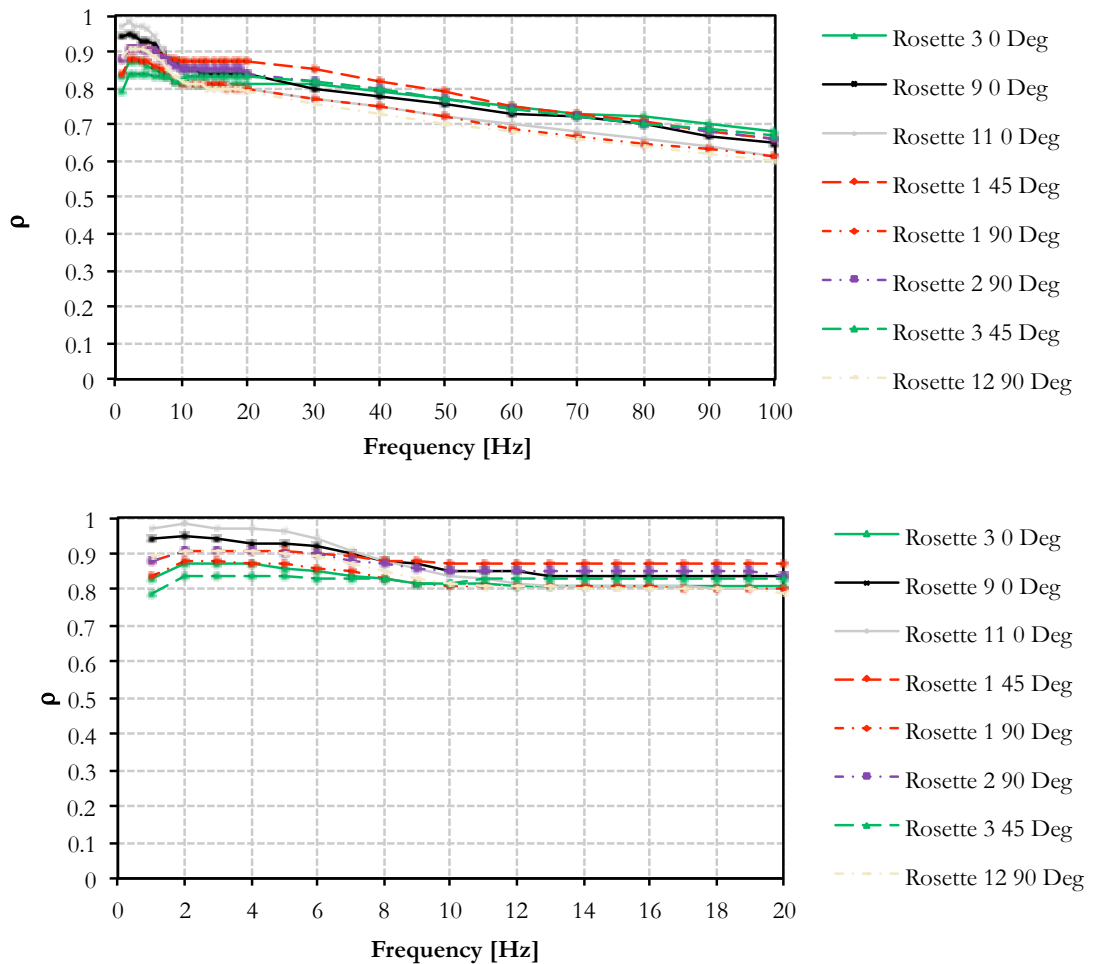


Figure 6.18: Final Correlation Results

Five of the eight channels display strong correlation between 2 Hz – 5 Hz. At frequencies above 5 Hz the correlation is moderate and constant between 10 – 20 Hz, $\rho \approx 0.8$. As the f_c increases above 20 Hz the correlation becomes weaker.

Due to the large size of each time history, which contained 2×10^6 points, smooth scatter cross plots and time history slices have been used to provide a visual indication of the correlation (**Figure 6.19**) [144]. The most extreme outliers in the data are shown in the cross plots as small black points and a smoothing contour kernel used to blend the colours to distinguish densely populated areas of the cross plot from sparsely populated areas. The colour blue indicates the highest density of points and as the density decreases blue changes to red and then from red to white. The results indicate that as the f_c is reduced the outliers become more clustered and the scatter reduces.

The time history slices were produced by setting a time window that displayed approximately 10 cycles based on the f_c . Several different starting points were analysed, here an example is shown at 280 seconds that illustrates the effects of the filters in the time domain. The weak correlation obtained with $f_c = 100$ Hz is characterised by small high frequency oscillations in the FEA strains which arise due to the noisy acceleration measurements at high frequency.

The weakest correlation was found on rosette 12, filtered at 100 Hz, $\rho = 0.6$ (**Figures 6.19a & 6.19b**). Moderate correlation was achieved on rosette 12, filtered at 20 Hz, $\rho = 0.79$ (**Figures 6.19c & 6.19d**). Very strong correlation was achieved on rosette 12, filtered at 2 Hz, $\rho = 0.91$ (**Figures 6.19e & 6.19f**). The strongest correlation achieved was $\rho = 0.98$ on Rosette 11.

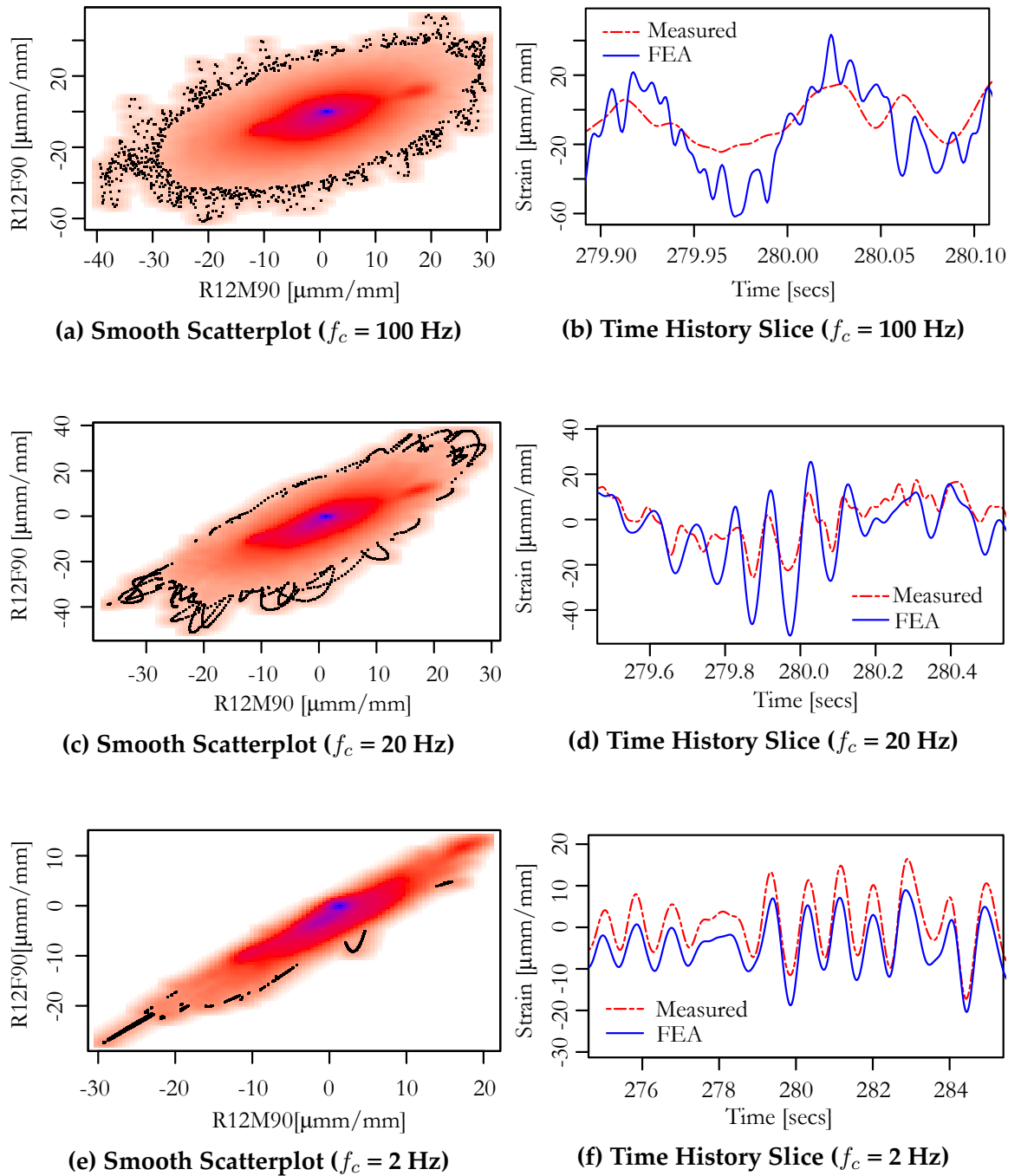


Figure 6.19: Effects of (f_c) on Correlation of Strain Gauge Rosette 12

6.9 Cause of Lid End Anomaly

Preliminary assessments indicated that correlation of rosettes 3 and 4 at the lid end was moderate at very low frequencies < 2 Hz and becomes weaker with increased f_c . The strains measured on rosette 4 were too low and no further correlation assessments on this rosette were attempted. Two legs of rosette 3 did have strains $> |10| \mu\text{m}/\text{m}$ and much better correlation was achieved across the 0 – 100 Hz range using accelerometer measurements from a lid end stanchion as input. This prompted further investigation into the differences in the accelerations at each of the stanchions. Some important observations were made from the lateral accelerations.

The left and right stanchion acceleration time histories were compared at either end of the tie down. Four filters were used; two low pass filters with cutoff frequencies of 100 Hz and 2 Hz and two band pass filters with cutoff frequencies of 2 Hz – 20 Hz and 20 Hz – 100 Hz. The results showed that below 2 Hz the only differences between the signals were due to DC offset. Between 2 Hz – 20 Hz the signals agreed very well, however above 20 Hz the signals possessed their own signature. Therefore it was concluded that high frequency oscillations were different between left and right stanchions and that low frequency oscillations were similar.

The same process was then carried out between the lid and base end accelerations (**Figure 6.20**). It is evident from the 2 Hz low pass filter that the motion of the stanchions is in-phase and very similar, this is likely to be due to gross vehicle movement such as cornering, **Figure 6.20d**. Between 2 Hz – 20 Hz the signals are 180° out of phase which indicates a yawing motion of the package superimposed on vehicle manoeuvring, **Figure 6.20c**.

This explains why the predicted strains at the lid end saddles correlated better at frequencies between 2 Hz – 20 Hz when the lid end accelerometer was used as input. It also indicates that the modelling assumptions of using measured loads from the stanchions of the tie down system and applying them to the centre of gravity of the package and tie down system can cause correlation error. The implications for design are that a tie down system must be able to withstand asymmetric loading between lid and base end stanchions.

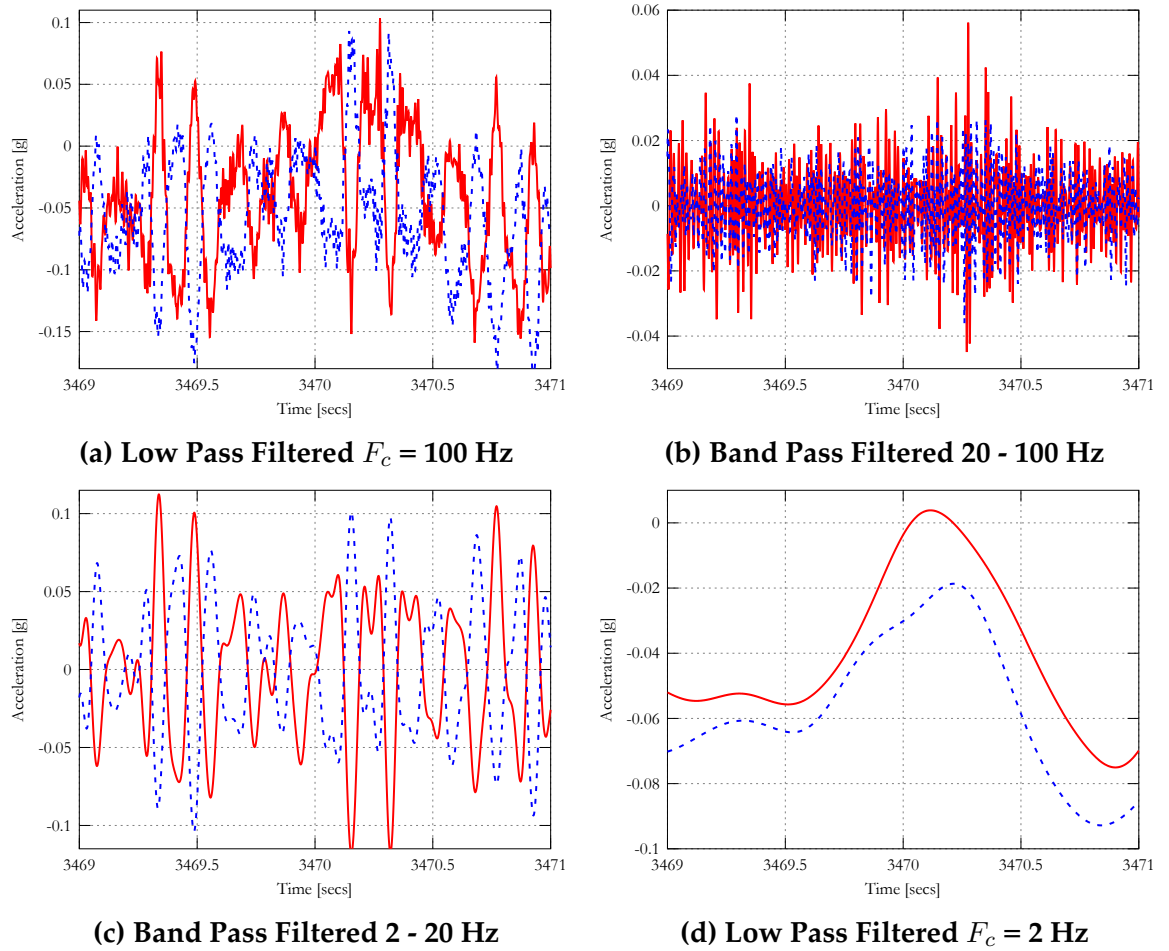


Figure 6.20: Time History Slice Comparison of Filtered Base and Lid End Lateral Accelerations at the Tie Down Stanchions

6.10 Analysis of Residuals

In this section the correlated time histories have been compared using spectral analysis and autocorrelation functions. All computations were carried out using the open source, high level interpreted language GNU Octave and verified with the commercial software nCode Glyphworks [131, 145].

Initially the PSDs of the measured and predicted signals where overlaid. This pinpoints which frequencies match between experiment and analysis. To quantify the level of agreement the residuals were calculated by subtracting corresponding measured time histories from those predicted. The residual PSDs were included as a third overlaid plot. An example is shown in log-log axes over the full frequency range for the 90° leg of rosette 12, **Figure 6.21**. The same PSD is also plotted on linear axes over the narrower frequency range of 0 - 30 Hz (**Figure 6.22**).

The results indicate that the predicted and measured strain PSDs are similar at frequencies < 40 Hz. At frequencies > 40 Hz the predicted strains are significantly over predicted.

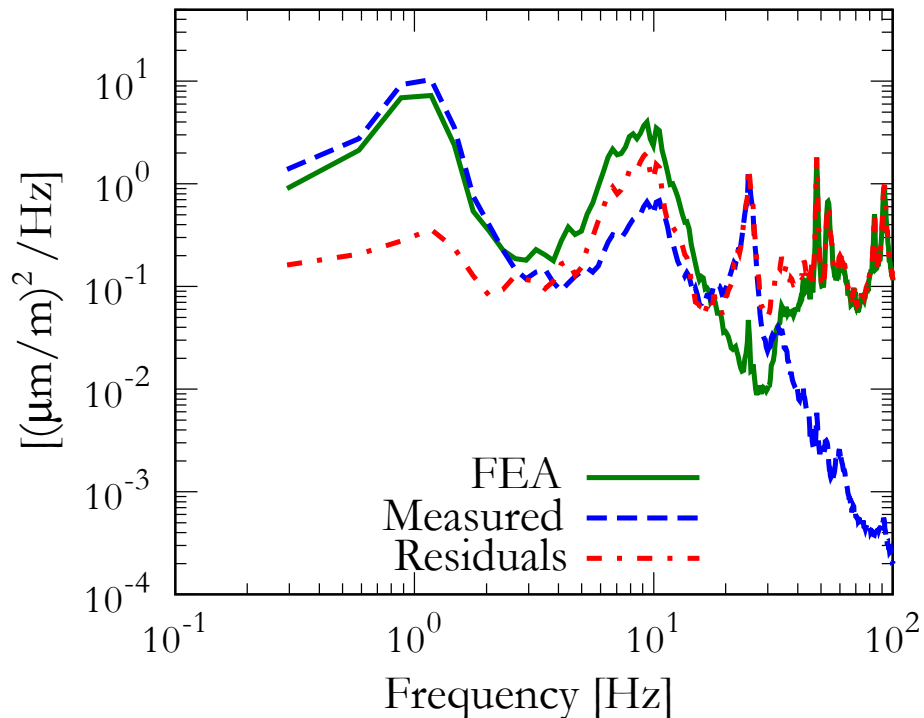


Figure 6.21: Comparison between Predicted and Measured Strain Time Histories, Converted into PSDs, Log-Log Scale, Full Bandwidth

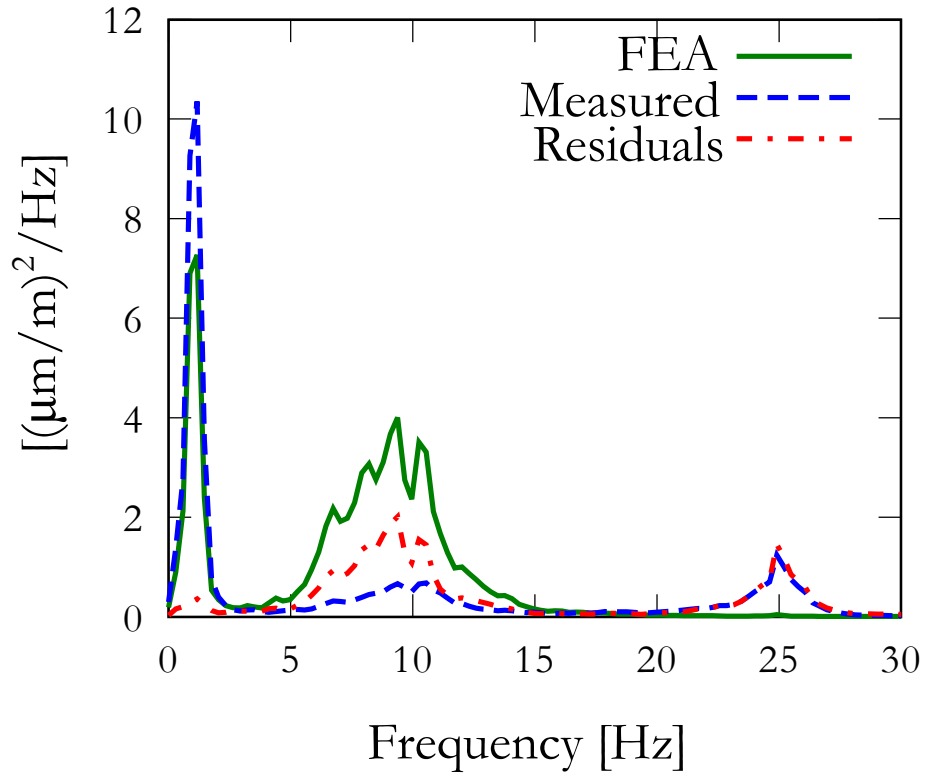


Figure 6.22: Comparison between Predicted and Measured Strain Time Histories, Converted into PSDs, 0 - 25 Hz

To verify these results autocorrelation functions have been used. The autocorrelation function (ACF) calculates the correlation coefficient, ρ , of the signal by continuously shifting the signal relative to itself to build a plot of ρ vs lag, called the correlogram. An ACF has been calculated for each correlated, measured strain signal and also for each residual time history. Results of each correlogram for different values of lag (number of points) are found in the appendix.

Figures 6.23 & 6.24 show correlograms from the measured strains of the 90° leg of rosette 12 and the residuals. The correlogram of the measurements possesses a narrow band signature, which is due to the peak between 0 - 3.5 Hz. The residuals on the other hand tend towards a white noise signature, demonstrating that the model successfully predicts the dominant trend in the measured strains.

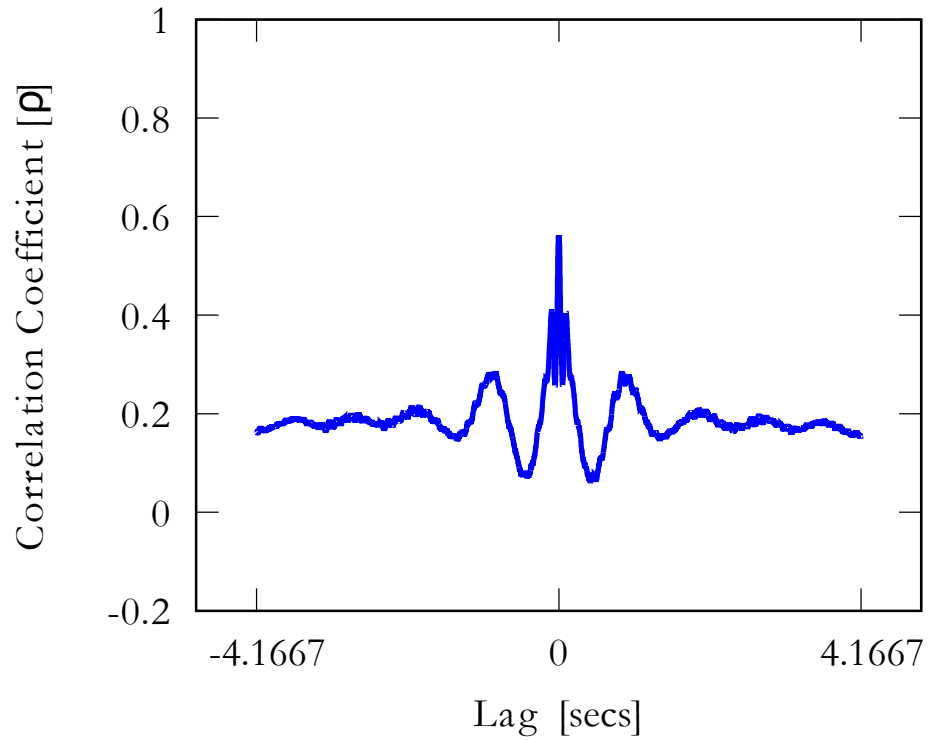


Figure 6.23: Correlogram of the Measured Strain Signal from the 90° Leg of Rosette 12

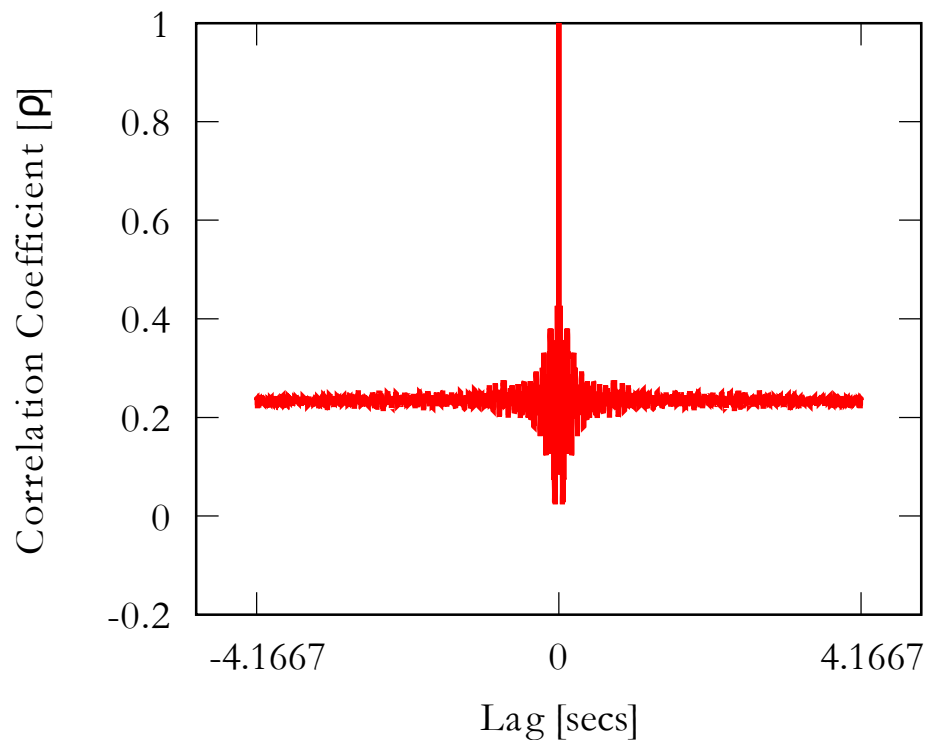


Figure 6.24: Correlogram of the Residuals between the Measured and Predicted Strain Signal from the 90° Leg of Rosette 12

6.11 Discussion

Data for fatigue load cases are currently in shortage for tie down design. This is due to the wide variation of packages and transport systems, difficulties in collecting experimental data and limited usage schedules. The nature of the data collected here is ideal for fatigue assessments, but larger measured strains would be necessary to calculate fatigue life and perform comparative fatigue analysis. A rainflow cycle count of the acceleration signals would produce conservative data for fatigue load cases by selecting a low pass filter cutoff frequency > 3.5 Hz.

A dynamic model would be more suitable for predicting response > 3.5 Hz. However this would come at considerable time and effort to prepare, solve and validate. The results of this study have shown that the small strains at higher frequencies are unlikely to cause fatigue damage and therefore no attempt to produce a dynamic model has been made.

Examining the lower frequency range more closely it is clear that the agreement between 0 - 3.5 Hz is very good. In the range 3.5 Hz - 15 Hz the predicted energy content in the strain signals is higher than in the measured signals. This concurs with expectations; a linear static model is only really suited to predicting very low frequencies.

To improve agreement the scaling and superposition procedure could be adapted to handle contact non-linearities. One method to achieve this is to fit polynomial response functions of finite element stresses at each rosette location, based on a set of non-linear analysis results that consider the measured load ranges and various combinations of loading. The scaling can then proceed by calculation of the strain time histories based on the fitted polynomials.

The analysis showed that the mean square of the signals were often under predicted at very low frequencies, possibly as a result of the chosen finite element discretization size. However at frequencies greater than 3.5 Hz treating measured accelerations as quasi-static tends to over predict the spectral content and therefore the fatigue damage and peaks. This is attributed to the large inertia of the package which attenuates any high frequency strain response.

At higher frequencies the acceleration response measured nearest the package is also attenuated, this model demonstrates that a linear relationship between measured accelerations and strains does not exist at higher frequencies, i.e. the linear model tends to overpredict higher frequencies strains because it does not include inertial dynamic effects.

6.12 Summary

- A linear static FEA of the tie down system has been successfully validated using strain and acceleration measurements with weak signal content.
- It was demonstrated that at least moderate correlation can be achieved with a properly prepared model.
- Spectral and residual analysis highlighted that the dominant source of loading occurred as a narrow band process between 0 - 3.5 Hz and the FEA correlation was strong at these frequencies.
- This level of agreement between FEA and a field experiment, which is highly uncontrollable, is very satisfactory.

7. Conclusions

The overall aim of this thesis was to improve current understanding of the mechanical loading acting on nuclear packages during routine conditions of rail transport. To focus the thesis a transport frame for a heavy nuclear package has been used as a case study. The work is also relevant to the loading acting on nuclear fuel during transport.

The literature review highlighted a paucity of experimental data for heavy nuclear packages during transportation. Several previous studies related to the transport of nuclear packages have used onboard data processing, resulting in condensed data sets that provide only limited information on the mechanical loading environment.

For instance, some studies used data acquisition systems that logged peak accelerations [84, 85]. This produces a very condensed data set that can be used to build up a statistical distribution of the peaks but discards important information in the raw analogue signals such as cycle sequence and frequency.

Other studies have used trigger levels to measure "bursts" of transient data [11]. Although this is useful to reduce data by measuring the most severe events, it does not provide a data set that describes every aspect of the loading environment. It can be difficult to separate quasi-static, shock or vibration loading with very short bursts of data. For example to separate shock from vibration the measurement needs to be long enough to identify non-stationary bursts of energy (shock) from steady-state vibrations.

Triggered measurements are typically carried out with piezo-electric accelerometers that have poor frequency response < 0.5 Hz. Therefore quasi-static loading may not be accurately measured. Additionally, the use of triggers requires a detailed knowledge of the environment to set appropriate trigger levels. This technique is most useful for monitoring the vibration environment to determine if set acceleration limits have been exceeded during a transport. However, it is insufficient to fully characterise the loads.

It was evident in the literature that some form of filtering was required to interpret measured data correctly [84, 85]. In some studies filters have been applied with limited or no justification for their design [5, 46]. This has been treated in some detail in this work; focus was directed at correctly filtering measurements and understanding the effects of poorer filter design choices.

The experiment carried out was developed to measure strain and acceleration at multiple locations of a tie down system and rail wagon throughout an entire journey. The measurement of acceleration and strain simultaneously provides both input and output data for computer simulations. It has been demonstrated throughout the previous chapters that measuring strains assists the interpretation of accelerations and guides filter design.

Measuring accelerations at the tie down system, rail wagon bed and bogie enabled the loading to be "mapped" throughout the transport system. The results indicated that the vibration source was due to the wheel-track interface and this was attenuated vertically throughout the wagon and tie down by the large package mass. Quasi-static vertical motion of the package and wagon was in-phase and similar in magnitude. It was concluded that the tie down was most sensitive to lateral quasi-static accelerations.

The data acquisition system was setup with a sampling rate of 1200 Hz to accurately recover peaks up to 100 Hz. Variable capacitance accelerometers were selected as they are capable of measuring low frequencies down to DC. Due to the nature of the instrumentation selected it was possible to simultaneously measure quasi-static, shock and vibration data. Therefore a very comprehensive description of the loading acting on packages, tie downs and fuel was achieved.

Vehicle speed and GPS position were also measured to allow time synchronous identification of events. For example a peak strain can be matched to a peak acceleration and the location and vehicle running speed at which they occurred during a journey can be identified. This proved very useful for confirming that signal drop-outs corresponded to vehicle stops and were not due to measurement error.

A standard method for calculating PSDs has been presented that enables relative comparison between any continuous time history measurement from any environment (i.e. this method is also suitable for interpreting road or sea measurements). Here PSDs were used to compare signals measured at different points on the conveyance, tie down and package. The results from the bogie measurements were broadband acceleration signals with high amplitude and RMS values. The wagon bed acceleration signals were also broadband but contained lower amplitudes and a lower RMS.

The PSDs revealed that the higher frequency acceleration signal content (> 25 Hz) resulted from the wheel-track interface and reduced the nearer the measurement position to the package. At the package itself low amplitude, low frequency accelerations were measured. The higher frequencies and amplitudes present at the wagon bed were attenuated by the large package mass.

A number of digital filters were designed for the purposes of assessing the sensitivity of the resulting signals to each filter design. Butterworth, Elliptic and Chebyshev Type I filters have been used with various filter orders and f_c to demonstrate their effects on resulting signal statistics and distributions. The main conclusions were that the lower order digital filters had the largest adverse affect on the results whereas higher order filters produced more consistent results. The important parameter in the filter design for separating quasi-static signal content from shock and vibration was the f_c . This study showed that selection of a f_c in the range 10 - 20 Hz and use of a properly designed higher order Butterworth/Elliptic/Chebyshev Type I filter produced acceleration signals with similar peak distributions.

Analysis of the measured strains indicated that they were very low at all times during the journey, demonstrating the excellent safety inherent in the tie down system. Using the British Standard BS 7608 [107] for fatigue assessments of welded steel joints it was not possible to calculate a fatigue life from any of the measured strain signals because the magnitude of the strains were so low. However the analysis did indicate that lots of small, non-damaging cycles occurred during the two hour experiment.

The low level of strains created some difficulties for the purposes of validating a FEA model. The main question that arose during validation with weak measured strain signal content was; what strength of signal was required to obtain a valid comparison? This question was answered in **Chapter 6** where it was demonstrated that at least moderate correlation could be achieved with several strain signals that contained a minimum peak amplitude of $|10| \mu\text{m}/\text{m}$.

To challenge the commonly used assumption in industrial design that tie down system response to acceleration loading is linear static, a linear static model was compared against the measured strains. This ultimately led to a more informed understanding of the measured accelerations. The model provided a means for inversely determining a f_c to extract accurate quasi-static loading from the accelerations.

To thoroughly evaluate the linear static assumption detailed non-linear analysis was carried out. Initially attention was dedicated to understanding the differences in results between a linear static and geometrically non-linear FEA model. The non-linear model considered frictional contacting surfaces between mating parts and the

linear model assumed that the sliding interfaces were perfectly bonded.

It was evident from the longitudinal load cases considered that stress response in the model corresponding to the strain gauged locations from the test, varies non-linearly due to increasing longitudinal loading. This did not affect this study significantly for two reasons:-

1. Measured longitudinal loading was very low.
2. The tie down response was less sensitive to longitudinal loading at the measured strain locations.

In the lateral load case the stress response was linearly related to applied load but discontinuous due to load reversals caused by the open/shut contact condition between the lateral restraint bolts and the package side walls. This resulted in small differences in magnitude between predicted strain signals and measurements but did not affect correlation because the response throughout the load range remained linear.

The conclusions from the non-linear FEA studies indicated that, any non-linearity would not detrimentally affect comparison with the experimental results. Therefore a linear static model was used to reconstruct strain time histories for the purpose of model validation.

During the process, smooth scatterplots were used to cross-plot the measured and predicted strains containing millions of data points. These plots provide a means of identifying the density of points with colour, highlighting outliers and the ability to gain a qualitative overview of how many outliers are present between data sets. By successive filtering of the signals and then cross-plotting, it was identified that low pass filtering the signals at smaller f_c removed outliers and at these low frequencies the model converged to a strong linear correlation. The Pearson's Correlation Coefficient confirmed this, a maximum value of $\rho = 0.98$ was achieved on one particular strain gauge channel after low pass filtering at 2 Hz.

To assess the full bandwidth of results in the frequency domain spectral analysis was used. In the first instance measured and predicted PSDs were overlaid. This analysis indicated that the general trend between the data sets were similar at frequencies < 40 Hz.

A PSD of the residuals between the measured and predicted strains was also produced for each correlated signal. It was evident from the residual PSDs that the measurements and predictions were a good match at frequencies < 5 Hz.

An autocorrelation function (ACF) was then used to assess the underlying trend

present in the measured strains. The correlogram of the measured strains exhibited a classical narrow band signature. The ACF was then used to assess the residuals between the FEA and measurements. The correlogram of the residuals indicated a white noise process demonstrating that the model successfully predicted the *real* measured strains in the frequency band 0 - 3.5 Hz.

The analysis results serve as evidence that a linear static FEA model was sufficiently accurate to predict the response of a tie down system to the rail transportation loads measured during this test. The analysis of residuals between the measured and predicted strains, indicate that the predominant frequency range in this study was 0 - 3.5 Hz.

At frequencies > 3.5 Hz, the linear static model over predicted the magnitude of measured strains. This was due to the linear scaling of higher frequency accelerations which would be attenuated by dynamic inertial effects of the package. A dynamic model would more accurately predict time histories for fatigue calculations. The loading history of the tie down system is short with infrequent return periods and the evidence from this study indicates there are no concerns about fatigue resistance. Therefore there was no motive to develop a dynamic model.

Importantly this study indicates that the quasi-static advisory acceleration factors quoted in the regulations are higher than the raw acceleration data measured in this experiment. The regulations suggest low pass filtering of accelerations to obtain quasi-static loads for design purposes and suggest a f_c between 10 - 20 Hz for a 100 tonne package.

In **Chapter 5** filtering within the guidance of the regulations indicated a further reduction of the quasi-static loads was possible. In **Chapter 6** it was demonstrated that the spectral content of the strain signals was narrow banded between 0 - 3.5 Hz. Low pass filtering with an $f_c = 3.5$ Hz results in even further reduction to estimated loads.

It is noteworthy that this experiment represents a typical case not a worst case scenario and is limited to only one data set. Therefore some caution is advised before drawing generalised conclusions on the magnitude of advisory acceleration factors. Notwithstanding this statement, the present work is supporting evidence that the real world loading is significantly less onerous than advised and FEA can successfully predict measured tie down strain response.

8. Recommendations for Further Work

Further work on rail shunting during train formation of a wagon loaded with a package, would provide valuable engineering data. Shunting has been studied in detail by engineers in the U.S. and Canada where the requirements for handling vehicles loaded with heavy dangerous goods rely on marshalling yard operations.

In the UK there are currently no marshalling yards used for handling wagons laden with nuclear transport packages. As a consequence the formation shunting operations carried out in the UK constitute much lower loading than the marshalling yard operations carried out routinely in North America and elsewhere in Europe.

Experimental and analytical assessment of this area would assist in weak link design and provide further supporting evidence of the safety inherent in current tie down designs. An experiment designed to output results of the typical magnitude of longitudinal accelerations experienced by tie downs during train formation would be invaluable. The data could also be used to validate a dynamic model for sensitivity analysis to assess the effects of changing various design parameters.

It is recommended that sensible guidelines for fatigue assessments of tie down systems are proposed based on usage. New designs should be screened based on operational specification. For existing designs there is occasionally the requirement for re-assessment. In these circumstances a detailed operational history would be required.

The routine conditions during road and sea transportation should be studied applying some of the techniques used in this thesis. Sea transport is the anticipated worst case mode of transport for loading acting on packages. Measurements at sea should be carried out over several days during the most likely period of the year for storm conditions to occur. For sea loading the experimental design is crucial to ensure that the environment is fully characterised and central to this is a strategy to collect and condense sufficient data over a much longer time period than the rail journey studied here.

9. References

- [1] IAEA. "SSR-6 Regulations for the Safe Transport of Radioactive Material". International Atomic Energy Agency, Vienna, 2012.
- [2] IAEA. "SSG-26 Advisory Material for the IAEA Regulations for the Safe Transport of Radioactive Material: Specific Safety Guide". International Atomic Energy Agency, Vienna, Austria, 2014.
- [3] P. McConnell, D. Ammerman, and K. Sorenson. "Loading on Fuel Rods in a Surrogate PWR Assembly Subjected to Simulated Normal Conditions of Truck Transport". In *17th International Symposium on the Packaging and Transportation of Radioactive Material*, San Francisco, 2013.
- [4] B. E. Hempy. "Type A Shipping Package Harmonic Assessment Methodologies". *Packaging, Transport, Storage & Security of Radioactive Material*, 25(1):30–37, March 2014.
- [5] N. Baumet and S. Chais. "Measuring the Acceleration of a Nuclear Transport Cask during Routine and Normal Transport Conditions". In *17th International Symposium on the Packaging and Transportation of Radioactive Material*, San Francisco, 2013.
- [6] T. Glead-Owen. "Design Loading Factors in Road Transport of Very Heavy Packages". In *17th International Symposium on the Packaging and Transportation of Radioactive Material*, San Francisco, 2013.
- [7] P. Purcell. "Designing Tie-Down Systems For Heavy RAM Packages – Should Revised Design Criteria Apply?". In *16th International Symposium on the Packaging and Transportation of Radioactive Material*, London, 2010.
- [8] S. Fourgeaud, G. Sert, K. Ben Ouaghrem, and I. Le Bars. "External Loads Applied to Packages during Routine Transport". *Packaging, Transport, Storage & Security of Radioactive Material*, 22(2):99–103, June 2011.
- [9] B. Desnoyers. "Stowage and Retention of Radioactive Packages during Trans-

- port: Which Rules should be Acceptable?”. *Packaging, Transport, Storage & Security of Radioactive Material*, 23(3/4):191–197, December 2012.
- [10] A. Apel, V. Ballheimer, C. Kuschke, S. Schubert, and F. Wille. “Approach for use of Acceleration Values for Packages of Radioactive Material under Routine Conditions of Transport”. *Packaging, Transport, Storage & Security of Radioactive Material*, 24(2):55–59, December 2013.
- [11] S. P. Singh, G. J. Burgess, and P. Rojnuckarin. “Test Protocol for Simulating Truck and Rail Vibration and Rail Impacts in Shipments of Automotive Engine Racks”. *Packaging Technology and Science*, 8(1):33–41, 1995.
- [12] *BS EN 61373-2010 Railway Applications: Rolling Stock Equipment - Shock and Vibration Tests*. BSI Standards Limited, 2010.
- [13] CR WAG TSI. “Technical Specification for Interoperability Relating to the Subsystem Rolling Stock - Freight Wagons”. Technical report.
- [14] M. Hampshire. “Engineering Vibration Environment for Rail Vehicle Mounted Equipment”. Technical report, Rail Safety Standards Board, 2004.
- [15] S. Dietz, H. Netter, and D. Sachua. “Fatigue Life Prediction of a Railway Bogie under Dynamic Loads through Simulation”. *Vehicle System Dynamics*, 29(6):385–402, June 1998.
- [16] T. L. Sanders, K. D. Seager, Y. R. Rashid, P. R. Barrett, A. P. Malinauskas, R. E. Einziger, H. Jordan, T. A. Duffey, S. H. Sutherland, and P. C. Reardon. “A Method for Determining the Spent-Fuel Contribution to Transport Cask Containment Requirements”. Technical report, Sandia National Labs., Albuquerque, New Mexico (United States), 1992.
- [17] C. Magnuson. “Shock Environments for Large Shipping Containers During Rail Coupling Operations”. Technical report, Sandia National Labs., Albuquerque, New Mexico (United States), 1980.
- [18] C. Magnuson. “Shock and Vibration Environment During Normal Rail Transportation of Heavy Cargo”. Technical report, Sandia National Labs., Albuquerque, New Mexico (United States), 1982.
- [19] J. W. Forest. “Irradiated Fuel Transportation Shock and Vibration Program”. Technical report, Ontario Hydro, Toronto, ON (Canada). Research Center, 1985.
- [20] S. R. Fields. “Dynamic Analysis to Establish Normal Shock and Vibration Environments Experienced by Radioactive Shipping Packages, Vol. 2”. Technical

- Report HEDL-TME 83-8, Hanford Engineering Development Lab., Richland, Wash. (USA), 1983.
- [21] S. R. Fields. "Dynamic Analysis to Establish Normal Shock and Vibration of Radioactive Material Shipping Packages, Quarterly Report". Quarterly Progress Report NUREG/CR-2146, Hanford Engineering Development Laboratory, United States, 1981.
- [22] S. R. Fields. "Dynamic Analysis to Establish Normal Shock and Vibration of Radioactive Material Shipping Packages, Final Summary Report, Vol. 3". Final Report NUREG/CR-2146, Hanford Engineering Development Laboratory, United States, 1983.
- [23] M. A. Elbestawi and D. F. Lau. "Irradiated Fuel Shock and Vibration Environment During Off-Site Transportation". Technical report, Ontario Hydro Research Lab., Toronto (Canada), 1983.
- [24] B. P. Dalziel, M. A. Elbestawi, and J. W. Forest. "CANDU Irradiated Fuel Transportation: The Shock and Vibration Program". Technical report, Ontario Hydro, Toronto, Canada, Toronto, Canada, 1986.
- [25] R. J. Bartholomew. "Cargo Response to Railcar Impact and Tiedown Load Analysis". Technical report, Los Alamos Scientific Lab., N.Mex. (USA), 1978.
- [26] S. Petry. "Rail Tiedown Tests with Heavy Casks for Radioactive Shipments". Technical report, Savannah River Laboratory, 1980.
- [27] G. Lamoreaux, A. Trujillo, and C. Magnuson. "Truck and Vibration Environment During Normal Conditions". Technical report, Sandia National Labs., Albuquerque, New Mexico (United States), 1981.
- [28] S. R. Fields. "SAVIT: A Dynamic Model to Predict Vibratory Motion within a Spent Fuel Shipping Cask; Rail Car System". Technical report, Hanford Engineering Development Lab., Richland, Wash. (USA), 1978.
- [29] S. R. Fields. "Dynamic Analysis to Establish Normal Shock and Vibration Environments Experienced by Radioactive Shipping Packages, Vol. 1". Technical Report HEDL TME 81-15, Hanford Engineering Development Lab., Richland, Wash. (USA), 1978.
- [30] S. R. Fields and S. J. Mech. "Dynamic Analysis to Establish Normal Shock and Vibration Environments Experienced by Radioactive Material Shipping Packages". Technical report, 1978.
- [31] S. R. Fields. "Dynamic Analysis to Establish Normal Shock and Vibration of

- Radioactive Material Shipping Packages". In *Proceedings of the 6th International Symposium on Packaging and Transportation of Radioactive Materials*, Berlin, Germany, 1980.
- [32] S. R. Fields. "Simulation of the Dynamic Response of Radioactive Material Shipping Package - Railcar Systems During Coupling Operations". In *Proceedings of the 17th Annual Symposium on Simulation*, ANSS '84, pages 95–117, Piscataway, NJ, USA, 1984. IEEE Press.
- [33] K.-T. Kim. "A Study on the Grid-to-Rod Fretting Wear-Induced Fuel Failure Observed in the 16×16 KOFA Fuel". *Nuclear Engineering and Design*, 240(4):756–762, April 2010.
- [34] S. Li and W. Cui. "Generation and Application of a Standardised Load-Time History to Critical Ship Structural Details". *Ships and Offshore Structures*, 9(4):365–379, July 2014.
- [35] J. A. Epaarachchi and P. D. Clausen. "The Development of a Fatigue Loading Spectrum for Small Wind Turbine Blades". *Journal of Wind Engineering and Industrial Aerodynamics*, 94(4):207–223, April 2006.
- [36] B. Oelmann. "Determination of Load Spectra for Durability Approval of Car Drive Lines". *Fatigue and Fracture of Engineering Materials and Structures*, 25(12):1121–1125, 2002. 1121.
- [37] P. Heuler and H. Klätschke. "Generation and Use of Standardised Load Spectra and Load-Time Histories". *International Journal of Fatigue*, 27(8):974–990, August 2005.
- [38] A. Halfpenny. "Accelerated Vibration Testing based on Fatigue Damage Spectra".
- [39] L. P. Pook. "Spectral Density Functions and the Development of Wave Action Standard History (WASH) Load Histories". *International Journal of Fatigue*, 11(4):221–232, July 1989.
- [40] T. Irvine. "Equivalent Static Loads for Random Vibration", 2009.
- [41] P. H. Wirsching, T. L. Paez, and K. Ortiz. *Random Vibrations: Theory and Practice*. Dover Publications Inc., Mineola, NY, June 2006.
- [42] J. Wannenburg, P. S. Heyns, and A. D. Raath. "Application of a Fatigue Equivalent Static Load Methodology for the Numerical Durability Assessment of Heavy Vehicle Structures". *International Journal of Fatigue*, 31(10):1541–1549, October 2009.

-
- [43] A. Halfpenny. "Methods for Accelerating Dynamic Durability Tests". In *Proceedings of the 9th International Conference On Recent Advances in Structural Engineering*, Southampton, 2006. nCode International Ltd, Sheffield.
- [44] S. Zhang. "Study on Testing and Establishment Method for the Load Spectrum of Bogie Frame for High-Speed Trains". *Science in China Series E: Technological Sciences*, 51(12):2142–2151, December 2008.
- [45] J. L. San Román, C. Álvarez Caldas, and A. Quesada. "Structural Validation of Railway Bogies and Wagons Using Finite Elements Tools". *Proceedings of the Institution of Mechanical Engineers, Part F: Journal of Rail and Rapid Transit*, 219(3):139–150, June 2005.
- [46] J. Read, S. Owen, and C.-F. Tso. "Tie-Down Assessment of Radioactive Material Packages on Conveyances: Approach to Competent Authority Approval Applications in Accordance with TS-R-1 (July 2004) and TS-G-1.1 (June 2002)". *Packaging, Transport, Storage & Security of Radioactive Material*, 16(2):109–124, 2005.
- [47] P. Heuler and T. Seeger. "A Criterion for Omission of Variable Amplitude Loading Histories". *International Journal of Fatigue*, 8(4):225–230, October 1986.
- [48] J. C. P. Kam. "Wave Action Standard History (wash) for Fatigue Testing Off-shore Structures. *Applied Ocean Research*, 14(1):1–10, 1992.
- [49] W. Fricke and H. Paetzold. "Full-Scale Fatigue Tests of Ship Structures to Validate the S–N Approaches for Fatigue Strength Assessment". *Marine Structures*, 23(1):115–130, January 2010.
- [50] W. Fricke, A. von Lilienfeld-Toal, and H. Paetzold. "Fatigue Strength Investigations of Welded Details of Stiffened Plate Structures in Steel Ships". *International Journal of Fatigue*, 34(1):17–26, January 2012.
- [51] P. McConnell. "Fuel Assembly Test Shaker Plan - Tests for Determining Loads on Used Nuclear Fuel under Normal Conditions of Transport". Technical report, Sandia National Labs., Albuquerque, New Mexico (United States), 2012.
- [52] M. Biot. "Theory of Elastic Systems Vibrating Under Transient Impulse with an Application to Earthquake-Proof Buildings". *Proceedings of the National Academy of Sciences of the United States of America*, 19(2):262, 1933.
- [53] T. Irvine. "An Introduction to the Shock Response Spectrum", 2012.
- [54] C. Lalanne. "Mechanical Vibration and Shock Analysis: Second Edition", volume 2. ISTE, 2010. 1.
-

- [55] W. T. Thomson and M. D. Dahleh. *"Theory of Vibration with Applications"*. Prentice Hall, Upper Saddle River, N.J, 5th edition, August 1997.
- [56] D. E. Newland. *"An Introduction to Random Vibrations, Spectral & Wavelet Analysis"*. Dover Publications Inc., 3rd edition edition, July 2005.
- [57] R. J. Scavuzzo. *"Naval Shock Analysis and Design"*. The Shock and Vibration Information Analysis Center, Booz-Allen and Hamilton, Inc, Falls Church, Va., 2000.
- [58] T. Scharton. "Force Limited Vibration Testing Monograph". Technical Report RP-1403, NASA Reference Publication, 1997.
- [59] Y. Soucy, V. Dharanipathi, and R. Sedaghati. "Comparison of Methods for Force Limited Vibration Testing". In *Proceedings of the IMAC XXIII Conference*, volume 31. 31 January–3 February 2005, Orlando Fla. Society for Experimental Mechanics, Bethel, Connecticut, Paper No. 295, 2005.
- [60] J. P. Tartary. "BNFL M4-12 Anti-Vibration Mountings Preliminary Design". Technical report, BNFL, 2001.
- [61] K. B. Smith, E. S. Parker, and D. J. Iler. "Railcar Service Spectra Generation for Full-Scale Accelerated Fatigue Testing". In *ASTM Special Technical Publication*, pages 62–84, 2002. 62.
- [62] X. Xue. "Modelling Collisions of Rail Vehicles with Deformable Objects". Technical report, Rail Safety Standards Board, 2005.
- [63] X. Xue, F. Schmid, and R.A. Smith. "A Study of Modelling Approaches for Rail Vehicle Collision Behaviour". *International Journal of Crashworthiness*, 9(5):515–525, September 2004.
- [64] X. Xue, M. Robinson, F. Schmid, and R. Smith. "Rail Vehicle Impact Analysis: A Critique of the Suitability of the Rigid Wall Model and the Assumption of Symmetrical Behaviour". *Proceedings of the Institution of Mechanical Engineers, Part F: Journal of Rail and Rapid Transit*, 229(2):173–185, February 2015.
- [65] Y. Q. Sun, C. Cole, M. Dhanasekar, and D. P. Thambiratnam. "Modelling and Analysis of the Crush Zone of a Typical Australian Passenger Train". *Vehicle System Dynamics*, 50(7):1137–1155, July 2012.
- [66] D. Thomas, M. Berg, and S. Stichel. "Measurements and Simulations of Rail Vehicle Dynamics with Respect to Overturning Risk". *Vehicle System Dynamics*, 48(1):97–112, January 2010.
- [67] K. B. Smith and W. C. Shust. "Bounding Natural Frequencies in Structures

- I: Gross Geometry, Material, and Boundary Conditions". In *Proceedings of the XXII International Modal Analysis Conference, Society of Experimental Mechanics*, 2004.
- [68] R. D. Cook, D. S. Malkus, M. E. Plesha, and R. J. Witt. *Concepts and Applications of Finite Element Analysis*. John Wiley & Sons, New York, NY, 4th edition, October 2001.
- [69] D. Hitchings. *A Finite Element Dynamics Primer*. NAFEMS, January 1992.
- [70] S. Iwnicki, editor. *Handbook of Railway Vehicle Dynamics*. CRC Press, May 2006.
- [71] T. Butz, B. Simeon, and M. Stadler. "Optimal Design of Experiments for Estimating Parameters of a Vehicle Dynamics Simulation Model". *Journal of Computational and Nonlinear Dynamics*, 5(3):031011, 2010.
- [72] N. Jones. *Structural Impact*. Cambridge University Press, 2nd edition, December 2011.
- [73] COTIF. "Convention Concerning International Carriage by Rail, Appendix C - Regulations Concerning the International Carriage of Dangerous Goods by Rail (RID)", 2013.
- [74] "TCSC 1006 Guide to the Securing/Retention of Radioactive Material Payloads and Packages During Transport".
- [75] RSSB. *GM/GN2688 Guidance on the Structural Design of Rail Freight Wagons including Rail Tank Wagons*, Issue 4. RSSB, 2010.
- [76] S.J. Maheras and S.B. Ross. "Transportation Shock and Vibration", 2013.
- [77] J. C. Peng, Y. X. Zhao, L. Y. Yu, and A. G. Yang. "Finite Element Analysis on Fatigue Stress History of a Railway Bogie Bolster". *Advanced Materials Research*, 44-46:195–200, 2008.
- [78] S. H. Baek, S. S. Cho, and W. S. Joo. "Fatigue Life Prediction based on the Rainflow Cycle Counting Method for the End Beam of a Freight Car Bogie". *International Journal of Automotive Technology*, 9(1):95–101, February 2008.
- [79] N. Zhu, S.-G. Sun, Q. Li, and H. Zou. "Theoretical Research and Experimental Validation of Quasi-Static Load Spectra on Bogie Frame Structures of High-Speed Trains". *Acta Mechanica Sinica*, 30(6):901–909, February 2015.
- [80] P. Belforte, F. Cheli, G. Diana, and S. Melzi. "Numerical and Experimental Approach for the Evaluation of Severe Longitudinal Dynamics of Heavy Freight Trains". *Vehicle System Dynamics*, 46(sup1):937–955, September 2008.

-
- [81] F. Cheli and S. Melzi. "Experimental Characterization and Modelling of a Side Buffer for Freight Trains". *Proceedings of the Institution of Mechanical Engineers, Part F: Journal of Rail and Rapid Transit*, 224(6):535–546, November 2010.
- [82] C. Magnuson. "Shock and Vibration Environments for Large Shipping Containers on Rail Cars and Trucks". Technical report, Sandia National Labs., Albuquerque, New Mexico (United States), 1977.
- [83] J. Wang, H. Wang, B. Bevard, and R. Howard. "Reversal Bending Fatigue Test System for Investigating Vibration Integrity of Spent Nuclear Fuel during Transportation". In *17th International Symposium on the Packaging and Transportation of Radioactive Material*, San Francisco, 2013.
- [84] A. R. Cory. "Flask Tiedown Design and Experience of Monitoring Forces". *International Journal of Radioactive Materials Transport*, 2(1-3):15–22, January 1991.
- [85] P. Dixon. "Package Tiedowns - A Programme of Measurement and Assessment". *International Journal of Radioactive Materials Transport*, 8(3-4):339–344, 1997.
- [86] ASTM. D4003 Test Methods for Programmable Horizontal Impact Test for Shipping Containers and Systems, 2003.
- [87] V. Rouillard and R. Richmond. "A Novel Approach to Analysing and Simulating Railcar Shock and Vibrations". *Packaging Technology and Science*, 20(1):17–26, January 2007.
- [88] N. Klymyshyn, S. Sanborn, H. Adkins, and B. Hanson. "Fuel Assembly Shaker Test Simulation". Technical Report FCRD-UFD-2013-000168, Pacific Northwest National Laboratory, 2013.
- [89] V. Rouillard and M. A. Sek. "Synthesizing Nonstationary, Non-Gaussian Random Vibrations". *Packaging Technology and Science*, 23(8):423–439, December 2010.
- [90] G. Rill. *Road Vehicle Dynamics: Fundamentals and Modeling*. CRC Press, Boca Raton, FL, October 2011.
- [91] ASTM. D4728-01 Standard Test Method for Random Vibration Testing of Shipping Containers, 2001.
- [92] BS EN 12663-2:2010 "Rail Applications - Structural Requirements of Railway Vehicle Bodies. Part 2 Freight Wagons". BSI Standards Limited, 2010.
- [93] MIL-STD-810G *Vibration*.

-
- [94] V. Rouillard. "Statistical Models for Nonstationary and Non-Gaussian Road Vehicle Vibrations". *Engineering Letters*, 17(4):227–237, December 2009.
- [95] S. Otari, S. Odof, J. B. Nolot, P. Vasseur, J. Pellet, N. Krajka, and D. Erre. "Statistical Characterization of Acceleration Levels of Random Vibrations during Transport". *Packaging Technology and Science*, 24(3):177–188, April 2011.
- [96] D. Smallwood. "Generating Non-Gaussian Vibration for Testing Purposes". *Sound and Vibration*, 39(10):18–24, October 2005.
- [97] BS EN ISO 898-1:2013 "Mechanical Properties of Fasteners made of Carbon Steel". BSI Standards Limited, 2013.
- [98] S.O. Rice. "Mathematical Analysis of Random Noise". *The Bell System Technical Journal*, 23(3):282–332, July 1944.
- [99] M. Karlsson. "Load Modelling for Fatigue Assessment of Vehicles: A Statistical Approach". Ph.D., Chalmers Univ. of Technology, Göteborg, 2007.
- [100] G. Genet. "A Statistical Approach to Multi-Input Equivalent Fatigue Loads for the Durability of Automotive Structures". Ph.D., Department of Mathematical Sciences, Division of Mathematical Statistics, Chalmers University of Technology and Göteborg University, Göteborg, 2006.
- [101] A. A. ten Have. WISPER and WISPERX.
- [102] "BS 2573-2-1980 Rules for the Design of Cranes, Part 1: Specification for Classification, Stress Calculations and Design Criteria for Structures". BSI, 1980.
- [103] "BS 2573-1:1983 Rules for the Design of Cranes, Part 1: Specification for Classification, Stress Calculations and Design Criteria for Structures". BSI, 1983.
- [104] B. Miao, W. Zhang, J. Zhang, and D. Jin. "Evaluation of Railway Vehicle Car Body Fatigue Life and Durability using a Multi-Disciplinary Analysis Method". *International Journal of Vehicle Structures and Systems*, 1(4), November 2009.
- [105] Rail Group Standards. "Guidance on the Structural Design of Rail Freight Wagons Including Rail Tank Wagons". Technical Report GMGN 2688, Rail Safety Standards Board, 2010.
- [106] H. B. Hendriks and B. H. Bulder. "Fatigue Equivalent Load Cycle Method". Technical Report ECN-C-95-074, The Netherlands, 1995.
- [107] BS 7608:2014 "Guide to fatigue design and assessment of steel products". BSI Standards Limited, 2014.
-

- [108] X. Xue, R. A. Smith, and F. Schmid. "Analysis of Crush Behaviours of a Rail Cab Car and Structural Modifications for Improved Crashworthiness". *International Journal of Crashworthiness*, 10(2):125–136, March 2005.
- [109] X. Xue and F. Schmid. "Crashworthiness of Conventionally Designed Railway Coaching Stock and Structural Modifications for Enhanced Performance". In *Proceedings from the 5th European LS DYNA Users Conference*, 2005.
- [110] X. Xue. "*Passive Safety in Train Design : A Statistical Analysis of Railway Accidents and a Study of Crashworthiness of Rail Vehicles with Recommendations for Enhancement*". Ph.D., University of Sheffield, 2004.
- [111] X. Xue, R. Smith, F. Schmid, and M. Robinson. "Rail Vehicle Impact Analysis: The Instable Propensity of Structural Responses and the Critical Scenarios of Structural Failure". *Proceedings of the Institution of Mechanical Engineers, Part F: Journal of Rail and Rapid Transit*, December 2014.
- [112] P. Heyes, J. Dakin, and C. St.John. "The Assessment and Use of Linear Static FE Stress Analyses for Durability Calculations". In *9th International Conference on Vehicle Structural Mechanics and CAE*, Warrendale, PA, April 1995. SAE International.
- [113] Y.-L. Lee. "*Metal Fatigue Analysis Handbook: Practical Problem-solving Techniques for Computer-aided Engineering*". Butterworth-Heinemann, August 2011.
- [114] N. A. Al-Asady, S. Abdullah, A. K. Ariffin, S. M. Beden, and M. M. Rahman. "Comparison Between Experimental Road Data and Finite Element Analysis Data for the Automotive Lower Suspension Arm". *European Journal of Scientific Research*, 29(4):557–571, 2009.
- [115] M. Speckert. "Calculation of Stress Time Signals of Multi Bolted Joints Located at a Ball Joint of a Railway Vehicle". Technical report, Idealisation of Bolted Joints, NAFEMS, 2010.
- [116] D. Peng, R. Jones, and T. Constable. "Tools and Methods for Addressing the Durability of Rolling Stock. *Engineering Failure Analysis*, 34:278–289, December 2013.
- [117] H. S. Kim and H. J. Yim. "Computational Durability Prediction of Body Structures in Prototype Vehicles". *International Journal of Automotive Technology*, 3(4):129–135, December 2002.
- [118] M. Chaika, C. Riedel, C. A. Tan, H. Jiang, and T.-C. Sun. "Correlation Between Simulations and Experimental Data for Military Vehicle Applications". Warrendale, PA, April 1995. SAE International.

-
- [119] C. Chatfield. *"The Analysis of Time Series: An Introduction"*. Chapman and Hall/CRC, Boca Raton, FL, 6th edition, July 2003.
- [120] H. Sarin, M. Kokkolaras, G. Hulbert, P. Papalambros, S. Barbat, and R. Yang. "Comparing Time Histories for Validation of Simulation Models: Error Measures and Metrics". *Journal of Dynamic Systems, Measurement, and Control*, 132(6):061401, 2010.
- [121] T. Giorgino. "Computing and Visualizing Dynamic Time Warping Alignments in R: The dtw Package". *Journal of Statistical Software*, 31(7):1–24, 2009.
- [122] A D Cummings, J Krywonos, P Purcell, G Rothwell, and R English. An Experimental Procedure for Measuring Accelerations and Strains from a Tie Down System of a Heavy Nuclear Transport Package during a Rail Journey. *Packaging, Transport, Storage & Security of Radioactive Material*, 23(3-4):167–177, 2012, <http://dx.doi.org/10.1179/1746510913Y.0000000014>.
- [123] Altair. Hyperworks 12.0, www.altairhyperworks.co.uk.
- [124] ANSYS Mechanical Release 13.0, www.ansys.com/products.
- [125] BS EN 10025-6:2004 *"Hot rolled products of structural steels – Technical Delivery Conditions for Flat Products of High Strength Structural Steels in Quenched and Tempered Condition"*. BSI Standards Limited, 2004.
- [126] A. Hobbacher. "Recommendations for the Fatigue Design of Welded Joints and Components". Technical report, International Institute of Welding, 2008.
- [127] A. S. Morris and R. Langari. *"Measurement and Instrumentation: Theory and Application"*. Academic Press, Boston, MA, 2nd revised edition, September 2015.
- [128] Meggit. Endevco Accelerometer 7920a, Datasheet.
- [129] Vishay Micro-Measurements. "Strain Gauge Selection: Criteria, Procedures, Recommendations". *Online document*, 2007.
- [130] Vishay Semiconductors. "Vishay, Micro-Measurements General Purpose Strain Gauge, Rectangular Rosette, Datasheet". 2012.
- [131] HBM nCode. Design Life 9.1, www.ncode.com/en/products/.
- [132] BS EN 15433-3:2007 *"Transportation Loads - Measurements and Evaluation of Dynamic Mechanical Loads - Part 3: Data Validity Check and Data Editing for Evaluation"*. BSI Standards Limited, 2007.
-

-
- [133] P. Welch. The Use of Fast Fourier Transform for the Estimation of Power Spectra: A Method based on Time Averaging over Short, Modified Periodograms. *IEEE Transactions on Audio and Electroacoustics*, 15(2):70–73, June 1967.
- [134] A. Brandt. *Noise and Vibration Analysis: Signal Analysis and Experimental Procedures*. Wiley-Blackwell, 1st edition, February 2011.
- [135] R. Allred. *Digital Filters for Everyone*. CreateSpace Independent Publishing Platform, Florida, 2nd edition, June 2013.
- [136] S. Smith. *Digital Signal Processing: A Practical Guide for Engineers and Scientists*. Newnes, Amsterdam ; Boston, 3rd revised edition, November 2002.
- [137] F. Kihm. "How to Choose between Butterworth and Fast Fourier Filters". Technical report, nCode International, 2005.
- [138] J. S. Bendat and A. G. Piersol. *Random Data: Analysis and Measurement Procedures*. Wiley-Blackwell, 4th edition, March 2010.
- [139] A. D. Cummings, J. Krywonos, P. Purcell, G. Rothwell, and C. Matthews. Filtering and Analysis of Accelerations and Strains Measured on a Tie Down System of a Heavy Nuclear Transport Package during a Routine Rail Journey. *Packaging, Transport, Storage & Security of Radioactive Material*, 24(1):23–35, 2013, <http://dx.doi.org/10.1179/1746510913Y.00000000027>.
- [140] H. O. Madsen, S. Krenk, and N. C. Lind. *Methods of Structural Safety*. Dover Publications Inc., Mineola, NY, March 2006.
- [141] Dessault Systemes. Abaqus/Standard (version 6.13-1). www.3ds.com/products-services/simulia/portfolio/abaqus/latest-release/.
- [142] J. Carvill. *Mechanical Engineers Data Handbook*. Butterworth-Heinemann, December 2012.
- [143] "BS ISO 12110-2:2013 Metallic Materials - Fatigue Testing - Variable Amplitude Fatigue Testing". BSI Standards Limited, 2013.
- [144] R Core Team. "R: A Language and Environment for Statistical Computing. R Foundation for Statistical Computing", 2014.
- [145] J. W. Eaton, D. Bateman, and S. Hauberg. *GNU Octave Version 3.0.1 Manual: A High-Level Interactive Language for Numerical Computations*. CreateSpace Independent Publishing Platform, 2009. ISBN 1441413006.

Appendices

A. HyperMath Scripts

Script to Check Stability of Butterworth, Elliptic and Chebyshev Filters

```
1  Clc()
2  ClearAll()
3  DeleteAllPlots()
4
5  /*
6  Flo and Fhi are the normalized corner frequencies in Hz of a
7  digital filter.
8  For a low pass filter, Flo = 0.
9  For a high pass filter, Fhi = 0 or 1.
10 For a band pass filter, Fc1 < Fc2.
11 For a band stop filter, Fc1 > Fc2.
12 Num, Den = Butter (Order,Fc1,Fc2)
13 */
14 flo = 2           // Low Cut Off Freq
15 fhi = 15         // High Cut off Freq
16 fs = 1200        // Sampling Frequency
17 nsamples = 10000 // Number of frequency points to generate
18 fnyq = fs/2      // Nyquist Frequency
19 n = 4            // Filter Order
20
21 ///////////////          Step Response          ///////////////
22
23 x = Zeros([10000;1])
24 x([1000:10000]) = 1
25 z = [0:1e-4:(1-1e-4)];
26
27 // Filter Coefficients
28
29 b, a = Butter(n,flo/fnyq,fhi/fnyq)
30 y = Filtfilt(b,a,x);
31
32 // Plot Unit Step Input
33
34 PlotLine(z,x)
35 SetLineColor([0,0,255])
36 SetLegend("Input")
37
38 // Plot Butterworth Filter Step Response
39
40 PlotLine(z,y)
41 SetLineColor([255,0,0])
42 SetLegend("4th Order Forwards-Backwards Butterworth")
43 SetTitle("Step Response")
44 SetXRange([0,0.2])
45 SetYRange([-0.5,1.5])
46 SetXLabel("Time (secs)")
47 GridOn()
48
49 ///////////////          Bode Plots          ///////////////
50
51 fr = Freq(nsamples,fs/2)
52
53 // Butterworth filter
54
```

```

55  b, a = Butter(n,flo/fnyq,fhi/fnyq)
56  Response = MagRes(b,a,fr,fs)
57
58  PlotLine(fr,Response,'new')
59  SetLineColor([255,0,0])
60  SetLegend("4th Order Butterworth")
61  SetYLabel("Magnitude of filter char. [dB]")
62  SetYScale('db20')
63  SetXScale('log')
64  SetXRange([0.01,500])
65  SetYRange([0.1,1.414])
66  SetXLabel("Frequency")
68  SetTitle("Bode Magnitude Plot")
69  LegendOn()
70  GridOn()
71
72
73  //// Pole-Zero Plot in Z-Domain ////
74
75  // Filter Coefficients
76
77  b, a = Butter(n,flo/fnyq,fhi/fnyq)
78
79  RPoles = Real(PolyRoots(a))
80  IPoles = Imag(PolyRoots(a))
81
82  // Unit Circle
83
84  RAxis =[-1.0:0.01:1.0]
85  l = Length(RAxis)
86  IAxis = []
87  IAxisN = []
88
89  for i = 1,l do
90
91      IAxis(i) = Sqrt(1-(RAxis(i)^2))
92      IAxisN(i) = -Sqrt(1-(RAxis(i)^2))
93
94  End
95
96  PlotLine(RAxis,IAxis,'new')
97  SetLineColor([0,0,255])
98  SetYLabel("Imaginary")
99  PlotLine(RAxis,IAxisN)
100 SetLineColor([0,0,255])
101 SetXLabel("Real")
102 SetTitle("Pole-Zero Plot in Z-Domain")
103 PlotScatter(RPoles,IPoles)
104 SetMarkerColor([255,0,0])
105 LegendOff()
106 GridOn()

```

Script that Generates Correlation Coefficient at each Selected Filter Cutoff Frequencies

```

1  Clc()
2  ClearAll()
3
4  function correlation(meas,calc,l)
5  {
6
7      c,s,f = PolyCurveFit(meas,calc,l)
8
9      Rxy = s[2]
10
11     return Rxy
12 }
13
14 ///////////////          M A I N          \\\\\\\\\\\
15 //
16 //
17 //
18 // Read in time histories
19
20 cutoff = [1,2,3,4,5,6,7,8,9,10,11,12,13,14,15,
           16,17,18,19,20,30,40,50,60,70,80,90,100] //Hz
21
22 rosnum = 1
23 path = "C:/CURRENT_RESULTS/FEA_CALIBRATION/
24 TIE_DOWN_SYSTEM_FEA_MODEL/
25 Correlation_Study/Rosette_" + rosnum + "/"
26 // Open a text file in write mode
27
28 fid = Open(path + "Rosette" + rosnum + ".txt","w+")
29
30 looplength = Length(cutoff)
31
32 for i = 1, looplength do
33
34     filename          = "Rosette" + rosnum + "_" + cutoff(i) +
35                         "HzLP_Accel_N"
36     Processed_Sigs   = path + filename + ".rsp"
37
38     TIME              = ReadVector(Processed_Sigs,"Time")
39     Meas_0deg         = ReadVector(Processed_Sigs,"TIME_HISTORY",
40                                     "Strain Gauge_AC_13_Vert","Values")
41     Meas_45deg        = ReadVector(Processed_Sigs,"TIME_HISTORY",
42                                     "Strain Gauge_AD_14_45Deg","Values")
43     Meas_90deg        = ReadVector(Processed_Sigs,"TIME_HISTORY",
44                                     "Strain Gauge_AE_15_Long","Values")
45     Calc_0deg         = ReadVector(Processed_Sigs,"TIME_HISTORY",
46                                     "Gauge:rosette_1 (Rectangular) Top Strain at
47                                     angle 0","Values")
48     Calc_45deg        = ReadVector(Processed_Sigs,"TIME_HISTORY",
49                                     "Gauge:rosette_1 (Rectangular) Top Strain at
50                                     angle 45","Values")
51     Calc_90deg        = ReadVector(Processed_Sigs,"TIME_HISTORY",

```

```

                                "Gauge:rosette_1 (Rectangular) Top Strain at
                                angle 90","Values")
42
43     l = Length(TIME)
44
45     if cutoff(i) == 1 then {
46
47         print(fid::write("\n Rosette : ", rosnum))
48         print(fid::write("\n 4th order Butterworth low pass filter "))
49         print(fid::write("\n Cutoff  0deg  45deg  90deg  "))
50         print(fid::write("\n Freq [Hz] "))
51         Rxy0 = correlation(Meas_0deg,Calc_0deg,l)
52         Rxy45 = correlation(Meas_45deg,Calc_45deg,l)
53         Rxy90 = correlation(Meas_90deg,Calc_90deg,l)
54         print(fid::write(string.format("\n %9i ", cutoff(i), "\t")))
55         print(fid::write(string.format("%8.2f %8.2f %8.2f", Rxy0,
56                                     Rxy45, Rxy90)))
57     } else {
58
59         Rxy0 = correlation(Meas_0deg,Calc_0deg,l)
60         Rxy45 = correlation(Meas_45deg,Calc_45deg,l)
61         Rxy90 = correlation(Meas_90deg,Calc_90deg,l)
62         print(fid::write(string.format("\n %9i ", cutoff(i), "\t")))
63         print(fid::write(string.format("%8.2f %8.2f %8.2f", Rxy0,
64                                     Rxy45, Rxy90)))
65     } end
66
67     print("Percentage Complete", (i/looplevelength)*100, "%")
68
69 end
70
71 fid::close()
```

B. Reduced Abaqus Input Files

Unit load model

```
** ABAQUS Input Deck
** Generated using HyperMesh-Abaqus Template Version : 12.0
**
** ABAQUS/STANDARD 3D
**
** UNITS: tonnes, mm, s
**
** Example Node input (reduced)
*NODE
    1, 1100.0, 335.0, -1250.0
    .. .. .. ..
    .. .. .. ..
**
** Example element input (reduced)
*ELEMENT, S4, ELSET = STANCHION
    1, 1, 2, 3, 4
    .. .. .. ..
    .. .. .. ..
*ELEMENT, C3D8, ELSET = STANCHION_BACKPLATE
    1000, 1, 2, 3, 4, 5, 6, 7, 8
    .. .. .. ..
    .. .. .. ..
**
** Example section input (reduced)
*SOLID SECTION, ELSET= STANCHION_BACKPLATE, MATERIAL=S890Q
*SHELL SECTION, ELSET=STANCHION, MATERIAL=S890Q
15.0, 5
** Node set used to apply boundary conditions
*NSET, NSET=BASE
    84749, 84750, 84751, 84752, 84753, 84754,
*MATERIAL, NAME=PACKAGE
*DENSITY
3.3420E-09,0.0
*ELASTIC, TYPE = ISOTROPIC
200000.0, 0.3, 0.0
*MATERIAL, NAME=PHOSPHUR_BRONZE
*DENSITY
7.6000E-09,0.0
*ELASTIC, TYPE = ISOTROPIC
121000.0, 0.3, 0.0
*MATERIAL, NAME=S890Q
*DENSITY
7.8000E-09,0.0
*ELASTIC, TYPE = ISOTROPIC
200000.0, 0.3, 0.0
*SURFACE INTERACTION, NAME = CONTACT
** Example Contact Pair definition (reduced)
*CONTACT PAIR, INTERACTION=CONTACT, ADJUST=0.5, TIED, TYPE=SURFACE TO SURFACE, SMALL
SLIDING
package_side_wall, mech_stops
*SURFACE, NAME=package_side_wall
package_side_wall,
*SURFACE, NAME=mech_stops
mech_stops,
**
**Boundary Conditions
*BOUNDARY
BASE,1,3,
** Lateral load case
*STEP, PERTURBATION
LATERAL 1g
*STATIC
*LOAD CASE, NAME = LAT LOAD
** Apply g-load to whole model
*DLOAD
,GRAV,9810.0,1,,
*END LOAD CASE
*OUTPUT, FIELD, NAME = STRESS_STRAIN
*NODE OUTPUT
U
*ELEMENT OUTPUT
S,E
*END STEP
```

```
** Longitudinal Load Case
*STEP, PERTURBATION
LONGITUDINAL 1g
*STATIC
*LOAD CASE, NAME = LONG_LOAD
** Apply g-load to whole model
*DLOAD
,GRAV,9810.0 ,,,1
*END LOAD CASE
*OUTPUT, FIELD, NAME = STRESS_STRAIN
*NODE OUTPUT
U
*ELEMENT OUTPUT
S,E
*END STEP
** Vertical Load Case
*STEP, PERTURBATION
VERTICAL 1g
*STATIC
*LOAD CASE, NAME = VERT_LOAD
** Apply g-load to whole model
*DLOAD
,GRAV,9810.0 ,,,1
*END LOAD CASE
*OUTPUT, FIELD, NAME = STRESS_STRAIN
*NODE OUTPUT
U
*ELEMENT OUTPUT
S,E
*END STEP
```

Reduced Nonlinear Models

Gravity Preload Model

```

** ABAQUS Input Deck
** Generated using HyperMesh-Abaqus Template Version : 12.0
**
** ABAQUS/STANDARD 3D
**
** UNITS: tonnes, mm, s
**
** Example Node input (reduced)
*NODE
    1,      1100.0,      335.0,      -1250.0
    ..     ..         ..         ..
    ..     ..         ..         ..
**
** Example element input (reduced)
*ELEMENT, S4, ELSET = STANCHION
    1,      1,      2,      3,      4
    ..     ..         ..         ..
    ..     ..         ..         ..
*ELEMENT, C3D8, ELSET = STANCHION_BACKPLATE
    1000,   1,      2,      3,      4,      5,      6,      7,      8
    ..     ..         ..         ..         ..         ..         ..         ..
    ..     ..         ..         ..         ..         ..         ..         ..
**
** Example section input (reduced)
*SOLID SECTION, ELSET= STANCHION_BACKPLATE, MATERIAL=S890Q
*SHELL SECTION, ELSET=STANCHION, MATERIAL=S890Q
15.0
,      5
** Node set used to apply boundary conditions
*NSET, NSET=BASE
    84749,   84750,   84751,   84752,   84753,   84754,
**
*MATERIAL, NAME=PACKAGE
*DENSITY
3.3420E-09,0.0
*ELASTIC, TYPE = ISOTROPIC
200000.0 ,0.3 ,0.0
**
*MATERIAL, NAME=PHOSPHUR_BRONZE
*DENSITY
7.6000E-09,0.0
*ELASTIC, TYPE = ISOTROPIC
121000.0 ,0.3 ,0.0
**
*MATERIAL, NAME=S890Q
*DENSITY
7.8000E-09,0.0
*ELASTIC, TYPE = ISOTROPIC
200000.0 ,0.3 ,0.0
**
*SURFACE INTERACTION, NAME = CONTACT
*FRICTION
0.35,
** Example Contact Pair definition (reduced)
*CONTACT PAIR, INTERACTION=CONTACT, ADJUST=0.0, TYPE=SURFACE TO SURFACE
package_side_wall, mech_stops
*SURFACE, NAME=package_side_wall
package_side_wall,
*SURFACE, NAME=mech_stops
mech_stops,
**
**Boundary Conditions
*BOUNDARY
BASE,1,3,
** Lateral load case
*STEP, NAME= GRAVITY, NLGEOM = YES
Gravity Preload
*STATIC
0.1 ,1.0 ,0.01 ,0.2
** Apply g-load to whole model
*DLOAD
, GRAV, 9810.0 ,1,
**
*OUTPUT, FIELD, NAME = STRESS_STRAIN
**
*NODE OUTPUT
U
**
*ELEMENT OUTPUT

```

```
S, E
*CONTACT OUTPUT
CSTRESS,
CDISP
*RESTART, WRITE, OVERLAY
*END STEP
```

Parameterised Restart Input File

Filename: LATRES_MIN_0_18.inp

```

** ABAQUS Input Deck
** Generated using HyperMesh-Abaqus Template Version : 12.0
**
** UNITS: tonnes, mm, s
**
** ABAQUS/STANDARD 3D
**
*RESTART, READ
*PARAMETER
gload = -0.18
gravity = 9810.0
load = gload * gravity
** Lateral Load Case
*STEP, NAME = Lateral Load, NLGEOM = YES
*STATIC
0.1 ,1.0 ,0.01 ,0.2
** Apply lateral loading and maintain gravity load
*DLOAD, OP=MOD
,GRAV,-9810.0 ,,1,
,GRAV,<load> ,1,,
*OUTPUT, FIELD, NAME = STRESS_STRAIN, FREQUENCY = 10
*NODE OUTPUT
U
*ELEMENT OUTPUT, ELSET = STRESSES
S,
*CONTACT OUTPUT
CSTRESS,
CDISP,
*END STEP

```

Shell Program that Automatically Generates Multiple Input Files for Sensitivity Studies

```

#!/bin/bash

appendfname=(MIN_0_18 MIN_0_13 MIN_0_09 MIN_0_04 0_05 0_09 0_14 0_18
0_23)
appendgload=(-0.18 -0.13 -0.09 -0.04 0.05 0.09 0.14 0.18 0.23)

for (( i = 0 ; i < ${#appendfname[@]} - 1 ; i ++ )) do

    cat LATRES_${appendfname[$i]}.inp | sed s/gload\ =\
${appendgload[$i]}/gload\ =\ ${appendgload[$i + 1]}/g >
LATRES_${appendfname[$i + 1]}.inp

    cat LATRES_${appendfname[$i]}.qsub | sed
s/${appendfname[$i]}/${appendfname[$i + 1]}/g >
LATRES_${appendfname[$i + 1]}.qsub

Done

```

C. Residual Analysis

PSDs_and_Autocorrelation_Octave_210615.m

Page 1

```
clear
clear all

%%%%%%%%%%%%%%%%%%%%%%%%%%%%%%%%%%%%%%%%%%%%%%%%%%%%%%%%%%%%%%%%%%%%%%%%
%%
%%
%%   PSDs and Autocorrelation of Correlated Rosettes Low
%%   pass filtered at 100Hz
%%
%%
%%%%%%%%%%%%%%%%%%%%%%%%%%%%%%%%%%%%%%%%%%%%%%%%%%%%%%%%%%%%%%%%%%%%%%%%

% Some settings to easily change plot appearance
%-----
FontSize=8;
FontName='Garamond';
LineWidth=4;
LineStyle={'-k','--k','-k',':k'};
%-----

% ACF Lag Setting
MaxLag = 500000;
%-----

% Read in Data
m = dlmread("/Users/andycummings/Documents/PEAKS_DTW_AND_CROSS_CORRELATION/Correlati
on_Study/Correlated_Rosettes_Meas_and_Calc_at_100Hz.csv",",",8,1);

time = m(:,1);
r1f45 = m(:,2);
r1f90 = m(:,3);
r1m90 = m(:,4);
r1m45 = m(:,5);
r2f90 = m(:,6);
r2m90 = m(:,7);
r3f0 = m(:,8);
r3f45 = m(:,9);
r3m0 = m(:,10);
r3m45 = m(:,11);
r9f0 = m(:,12);
r9m0 = m(:,13);
r11f0 = m(:,14);
r11m0 = m(:,15);
r12f90 = m(:,16);
r12m90 = m(:,17);

MAT1 = ([r1f45, r1m45, r1f90, r1m90, r2f90, r2m90, r3f0, r3m0, r3f45, r3m45, r9f0, r
9m0, r11f0,...
        r11m0, r12f90, r12m90]);

% Calculate Residuals
res_r1_45 = r1f45 - r1m45;
res_r1_90 = r1f90 - r1m90;
res_r2_90 = r2f90 - r2m90;
res_r3_0 = r3f0 - r3m0;
res_r3_45 = r3f45 - r3m45;
res_r9_0 = r9f0 - r9m0;
res_r11_0 = r11f0 - r11m0;
res_r12_90 = r12f90 - r12m90;

% Store in Matrix for looping
MAT2 = ([res_r1_45, res_r1_90, res_r2_90, res_r3_0, res_r3_45, res_r9_0, res_r11_0,
res_r12_90]);
```

PSDs_and_Autocorrelation_Octave_210615.m

Page 2

```

for i = 1 : 8

    % Built in function for calculating autocorrelation

    [acf,lag] = xcorr(MAT1(:,((i*2)-1)),MAT1(:,(i*2)),MaxLag,"coeff");
    [acf_res,lag_res] = xcorr(MAT2(:,i),MAT2(:,i),MaxLag,"coeff");

    % Welch's method PSD

    [PSD_F,Freq_F] = pwelch(MAT1(:,((i*2)-1)),4096,0.5,4096,1200,"half","oneside
d","plot","linear");
    [PSD_M,Freq_M] = pwelch(MAT1(:,(i*2)),4096,0.5,4096,1200,"half","onesided","
plot","linear");
    [PSD_res,Freq_res] = pwelch(MAT2(:,i),4096,0.5,4096,1200,"half","onesided","
plot","linear");

    % Plot Results

    %% Set paper size
    X = 15.0;           %# A4 paper size
    Y = 12.0;           %# A4 paper size
    %xMargin = 1;       %# left/right margins from page borders
    %yMargin = 1;       %# bottom/top margins from page borders
    %xSize = X - 2*xMargin; %# figure size on paper (width & height)
    %ySize = Y - 2*yMargin; %# figure size on paper (width & height)

    %# figure size printed on paper
    set(gcf, 'PaperUnits','centimeters')
    set(gcf, 'PaperSize',[X Y])
    set(gcf, 'PaperPosition',[0 0 X Y])
    set(gcf, 'PaperOrientation','landscape')

    %set (gcf, "papersize", [6.4, 4.8])
    %set (gcf, "paperposition", [0, 0, 6.4, 4.8])

    % Plot sub plots - PSD loglog

    subplot(2,2,1)
    loglog(Freq_F, PSD_F, "linewidth", LineWidth, "Color", [0 0.5 0], "-", Freq
_M, PSD_M, "linewidth", LineWidth, ...
          "Color", "b", "--", Freq_res, PSD_res, "linewidth", LineWidth, "Colo
r", "r", "-.")
    legend("FEA", "Measured", "Residuals","location","south")
    legend boxoff
    legend left
    ax = gca();
    set(ax, "fontName", FontName, "fontSize", FontSize)
    xlabel("Frequency [Hz]", "fontName", FontName, "fontSize", FontSize)
    ylabel("[(\mum/m)^2/Hz]", "fontName", FontName, "fontSize", FontSize)
    xlim([0.1 100])
    ylim([1.0e-4 50])

```

PSDs_and_Autocorrelation_Octave_210615.m

Page 3

```

    % Plot sub plots - PSD linear scale
    subplot(2,2,2)
    plot(Freq_F, PSD_F, "linewidth", LineWidth, "Color", [0 0.5 0], "-", Freq_M,
    PSD_M, "linewidth", LineWidth, ...
    "Color", "b", "--", Freq_res, PSD_res, "linewidth", LineWidth, "Color", "r", "r", "-.")
    legend("FEA", "Measured", "Residuals", "location", "northeast");
    legend boxoff
    legend left
    ax = gca();
    set(ax, "fontname", FontName, "fontsize", FontSize)
    xlabel("Frequency [Hz]", "fontname", FontName, "fontsize", FontSize)
    ylabel("[(\mum/m)^2/Hz]", "fontname", FontName, "fontsize", FontSize)
    xlim([0 30])

    % Plot sub plots - ACF Measurements
    subplot(2,2,3)
    plot(lag,acf,"linewidth",LineWidth,"Color","b","-")
    ax = gca();
    set(ax, "fontname", FontName, "fontsize", FontSize)
    xlabel("Lag", "fontname", FontName, "fontsize", FontSize)
    set(gca, 'xtick', [-MaxLag,0,MaxLag])
    ylabel("Correlation Coefficient [\rho]", "fontname", FontName, "fontsize",
FontSize)
    ylim([-0.2 1.0])

    % Plot sub plots - ACF Residuals
    subplot(2,2,4)
    plot(lag_res,acf_res,"linewidth",LineWidth,"Color","r","-")
    ax = gca();
    set(ax, "fontname", FontName, "fontsize", FontSize)
    xlabel("Lag", "fontname", FontName, "fontsize", FontSize)
    set(gca, 'xtick', [-MaxLag,0,MaxLag])
    ylabel("Correlation Coefficient [\rho]", "fontname", FontName, "fontsize",
FontSize)
    ylim([-0.2 1.0])

    % Create Unique File Name for Results
    ResultsName = (['Rosette_1_45deg'; 'Rosette_1_90deg'; 'Rosette_2_90deg'; 'Ro
sette_3_0deg'; ...
    'Rosette_3_45deg'; 'Rosette_9_0deg'; 'Rosette11_0deg'; 'Rosette12_90
deg']);

    appendFilename = 'PSD_ACF_210615';
    filename = strjoin({ResultsName(i,:),appendFilename});
    temp = filename( filename == " " ) = "_";

    % Print Results
    print(filename, '-dpdf')

endfor

```

Max Lag = 500

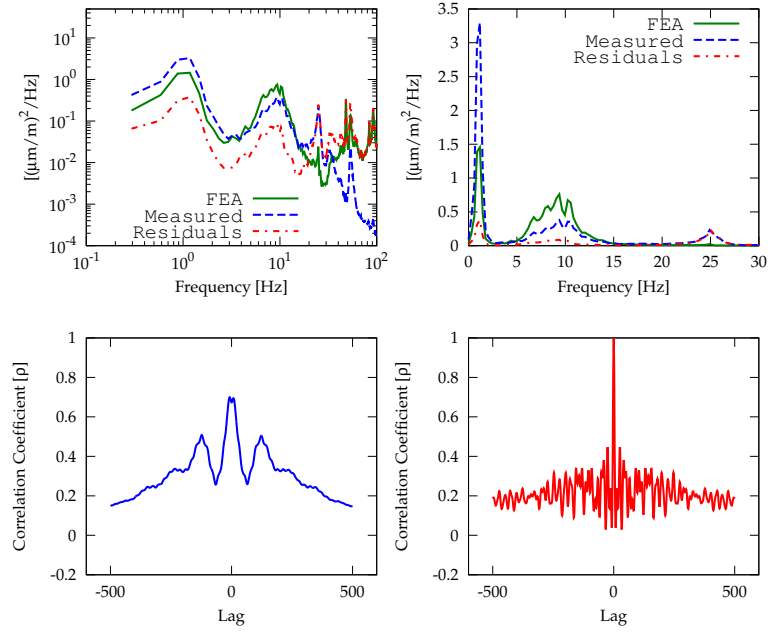


Figure 1: R1 45°

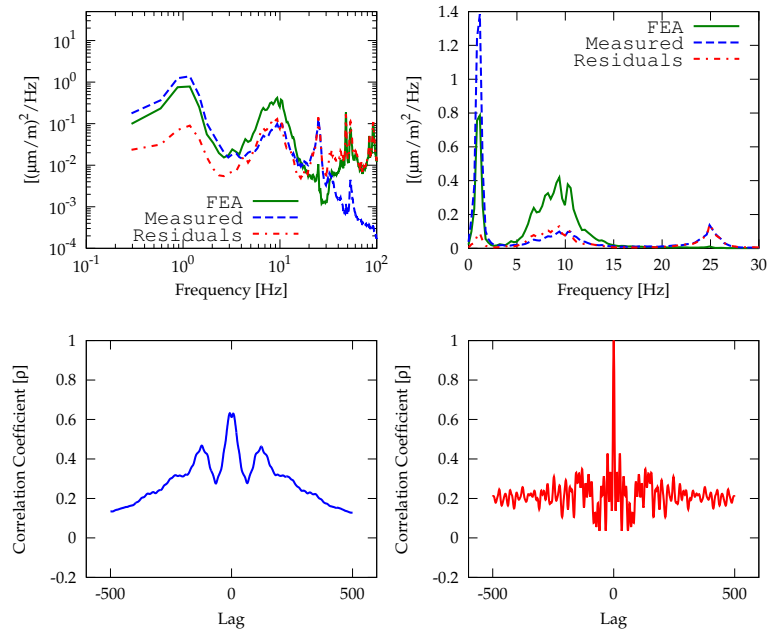


Figure 2: R1 90°

Max Lag = 500

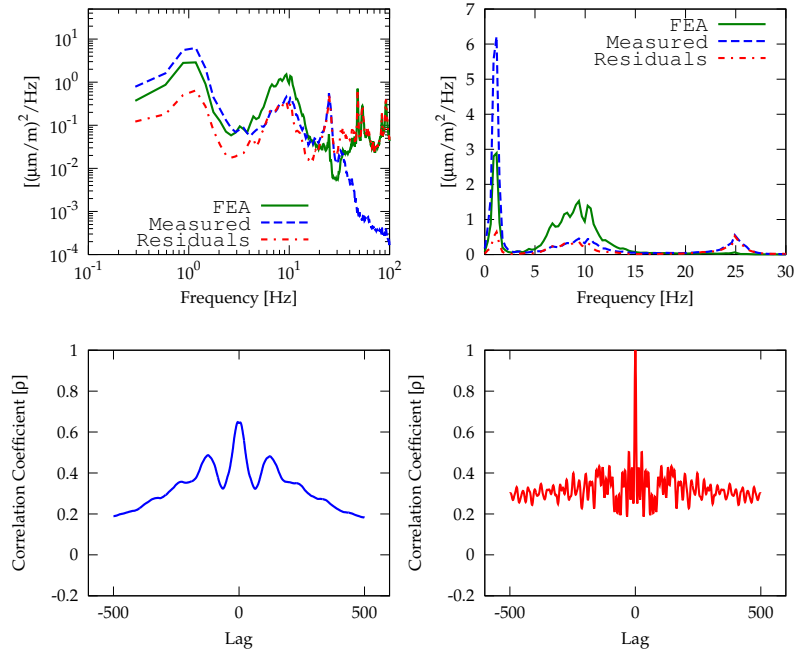


Figure 3: R2 90°

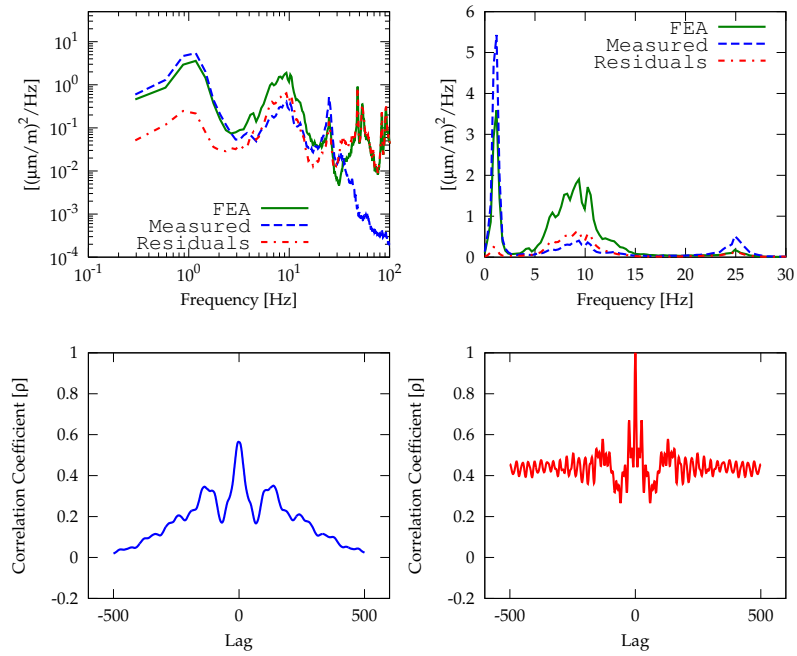


Figure 4: R3 0°

Max Lag = 500

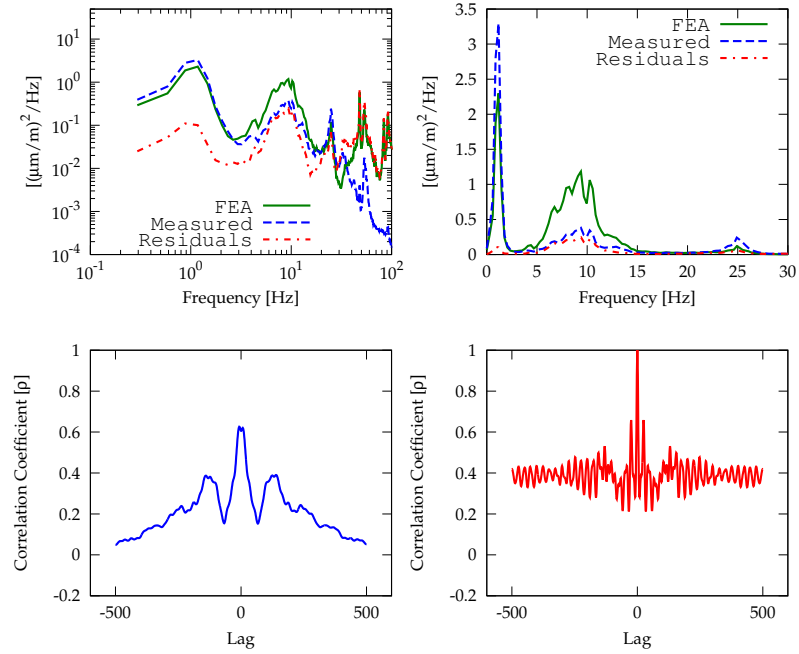


Figure 5: R3 45°

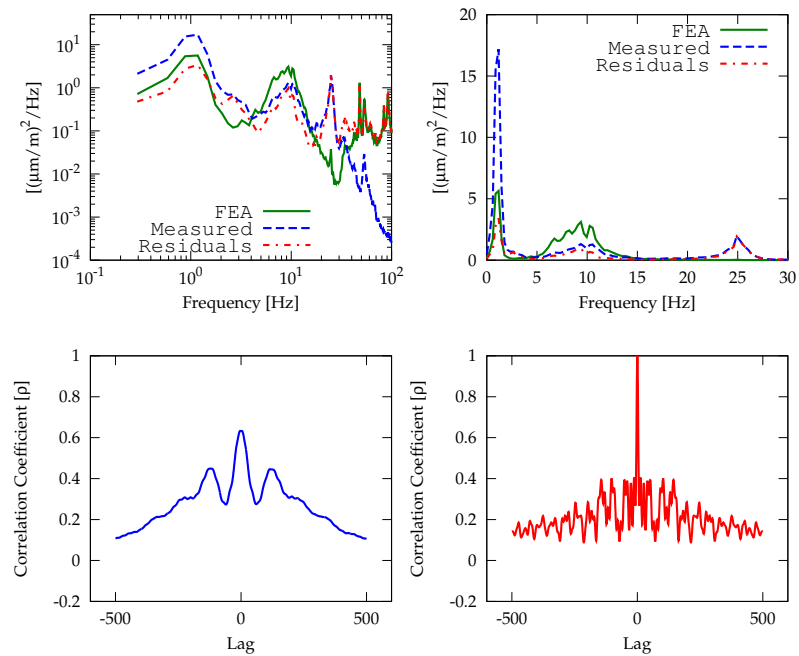


Figure 6: R9 0°

Max Lag = 500

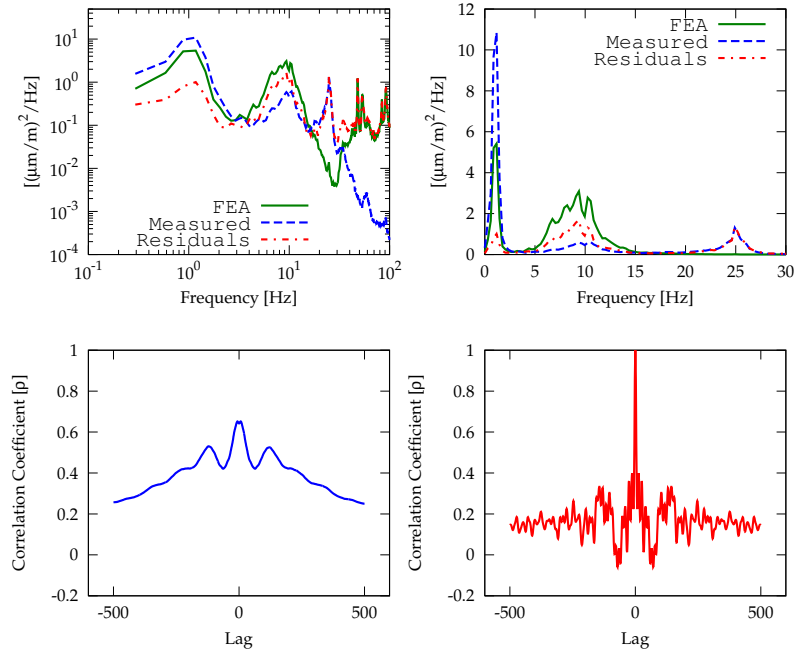


Figure 7: R11 0°

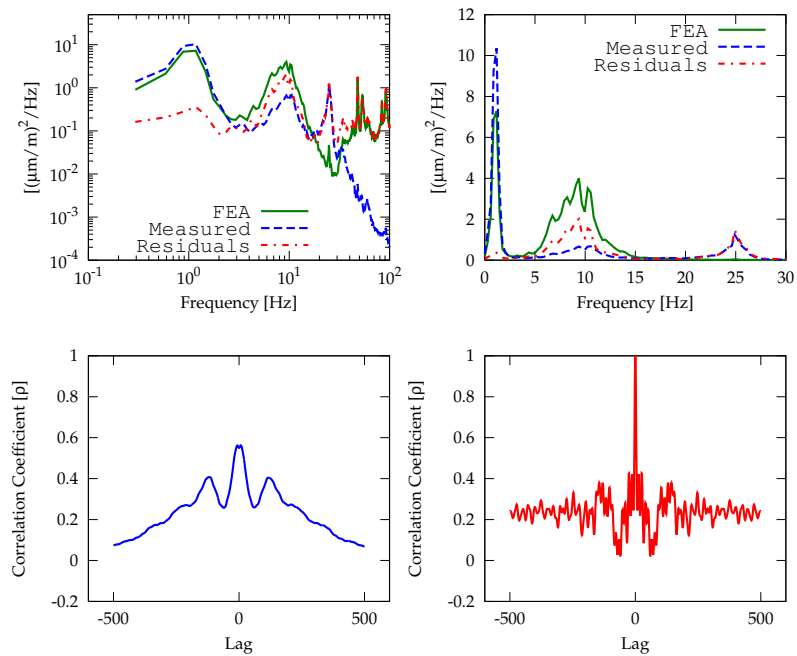


Figure 8: R12 90°

Max Lag = 5000

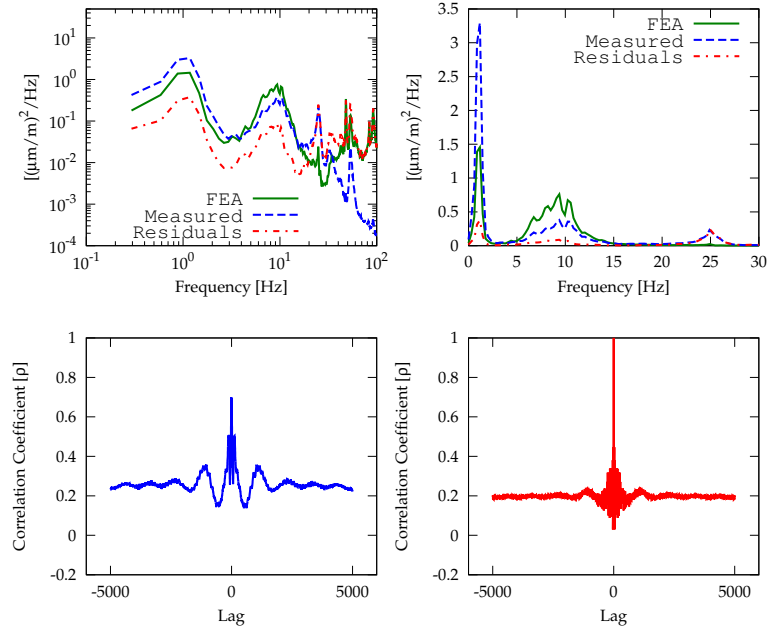


Figure 1: R1 45°

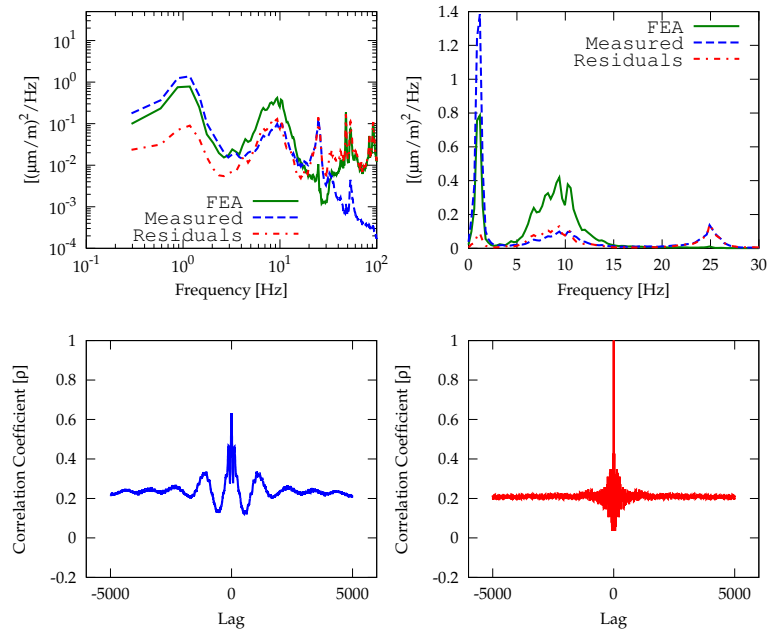


Figure 2: R1 90°

Max Lag = 5000

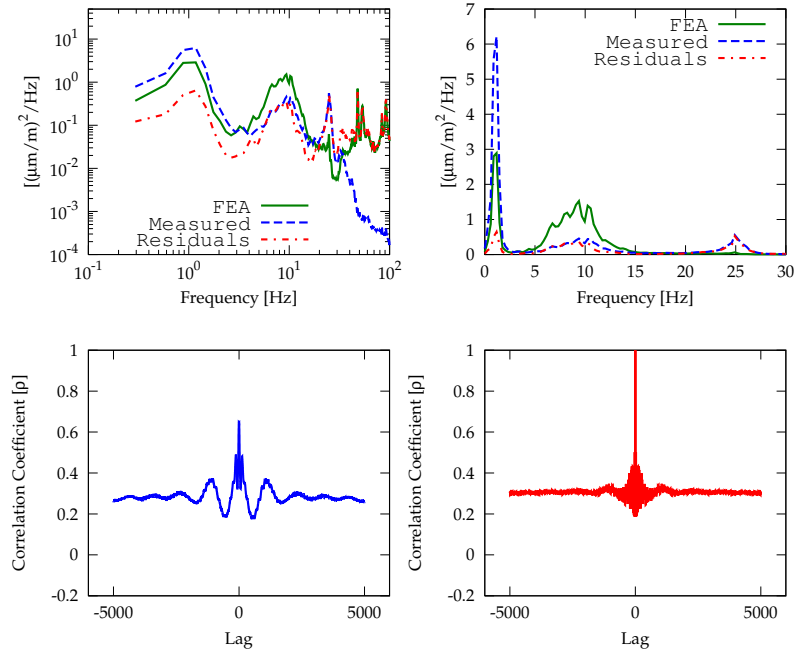


Figure 3: R2 90°

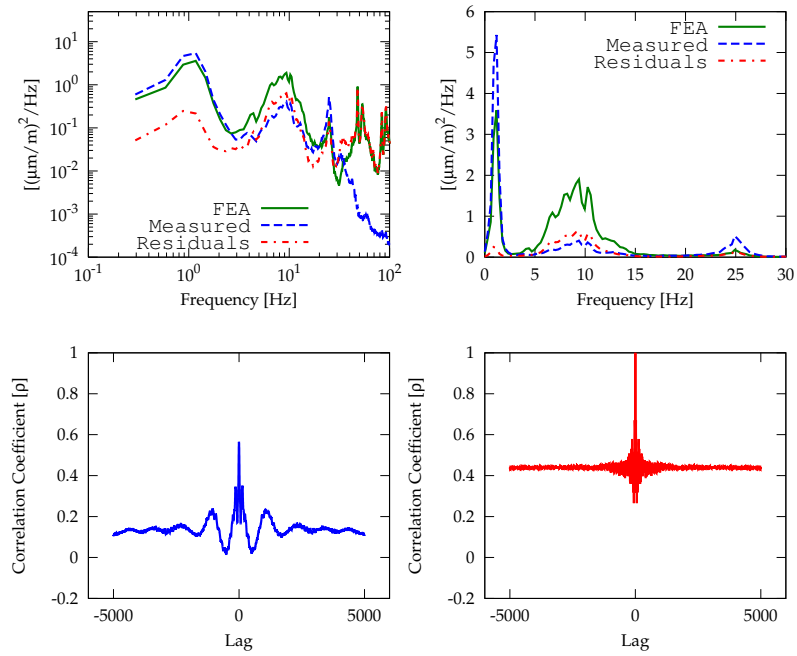


Figure 4: R3 0°

Max Lag = 5000

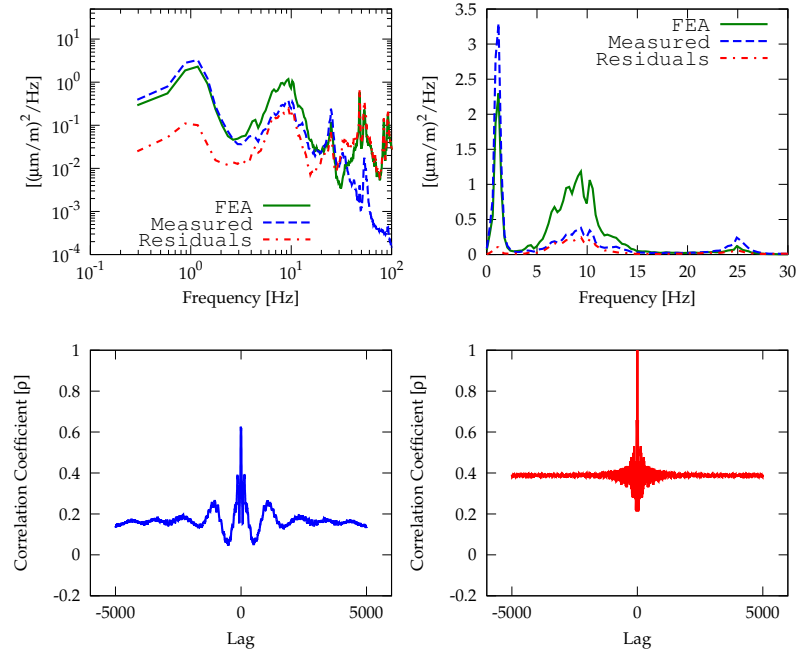


Figure 5: R3 45°

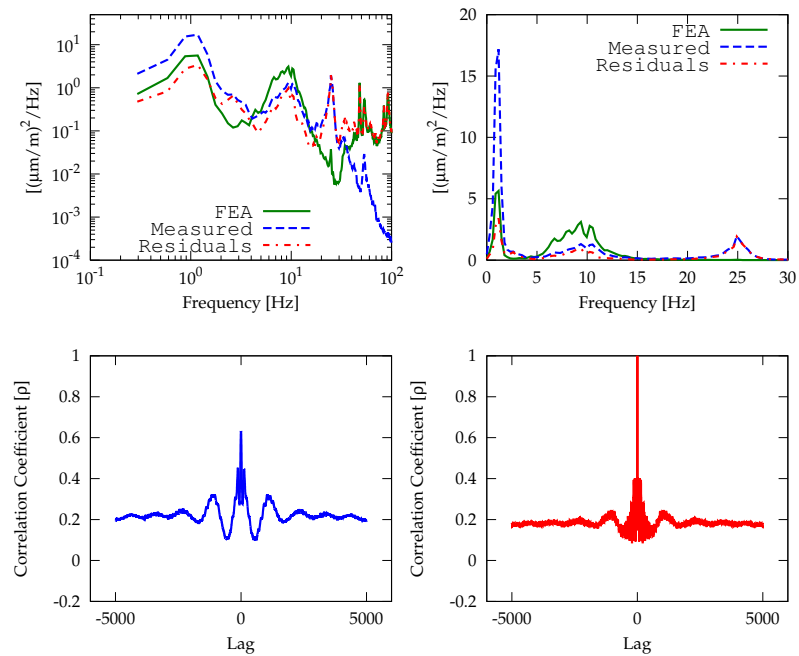


Figure 6: R9 0°

Max Lag = 5000

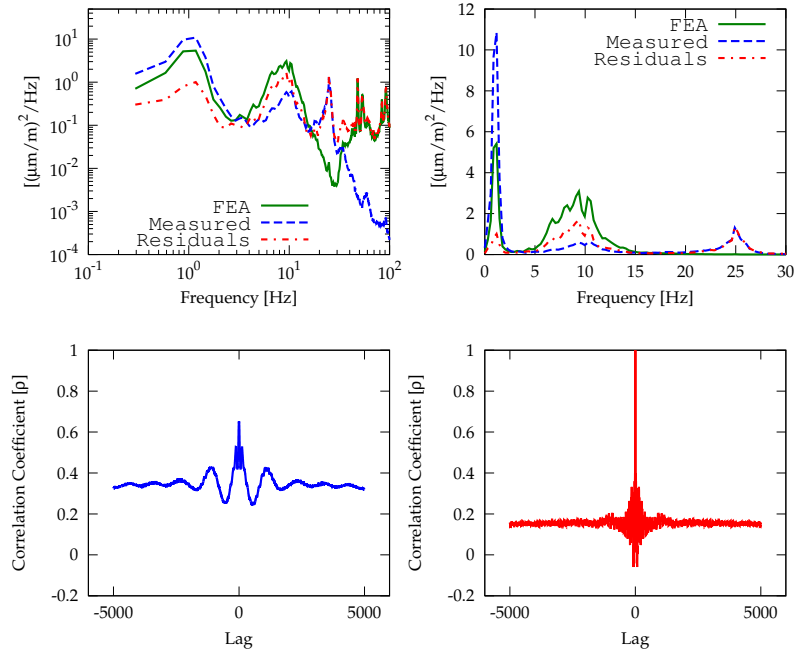


Figure 7: R11 0°

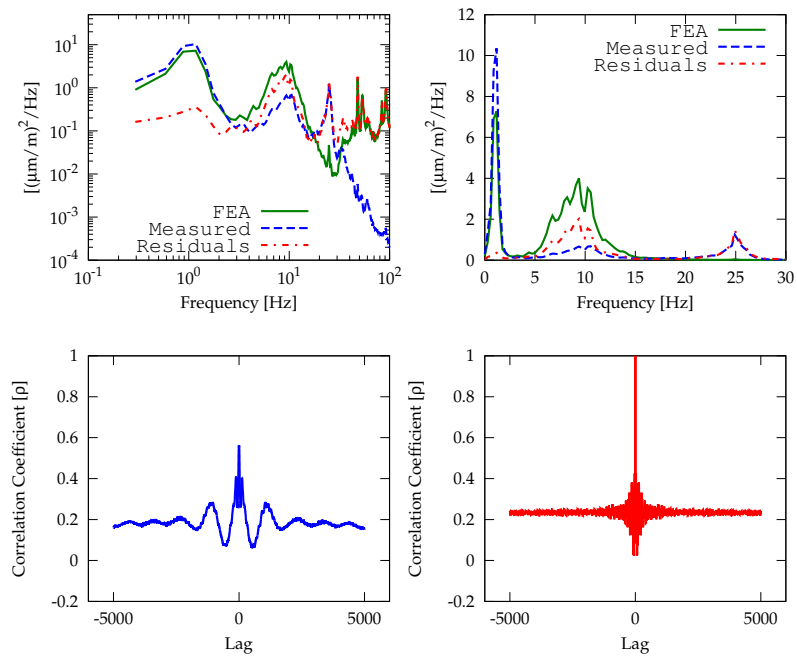


Figure 8: R12 90°

Max Lag = 500000

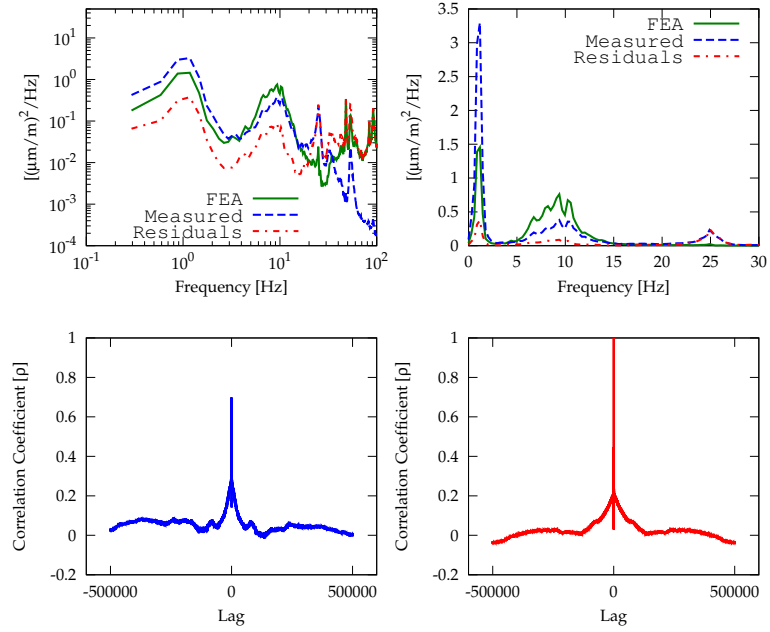


Figure 1: R1 45°

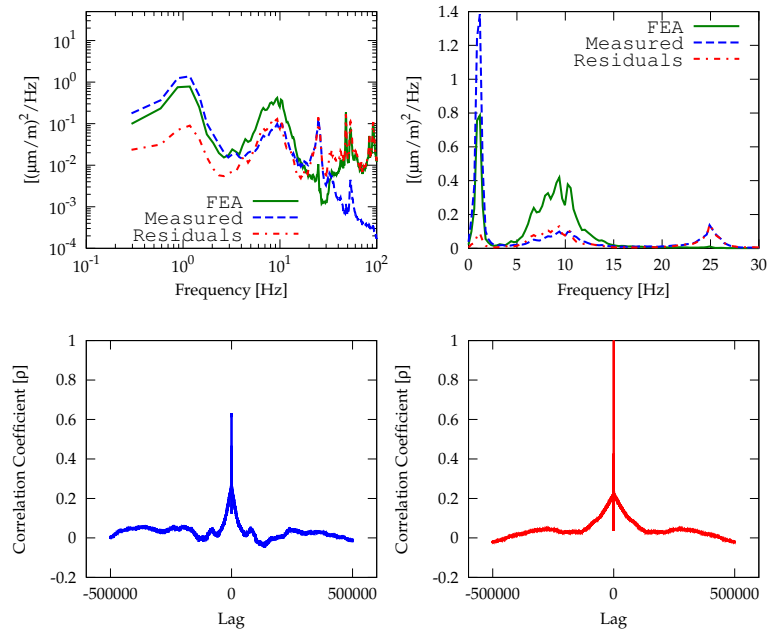


Figure 2: R1 90°

Max Lag = 500000

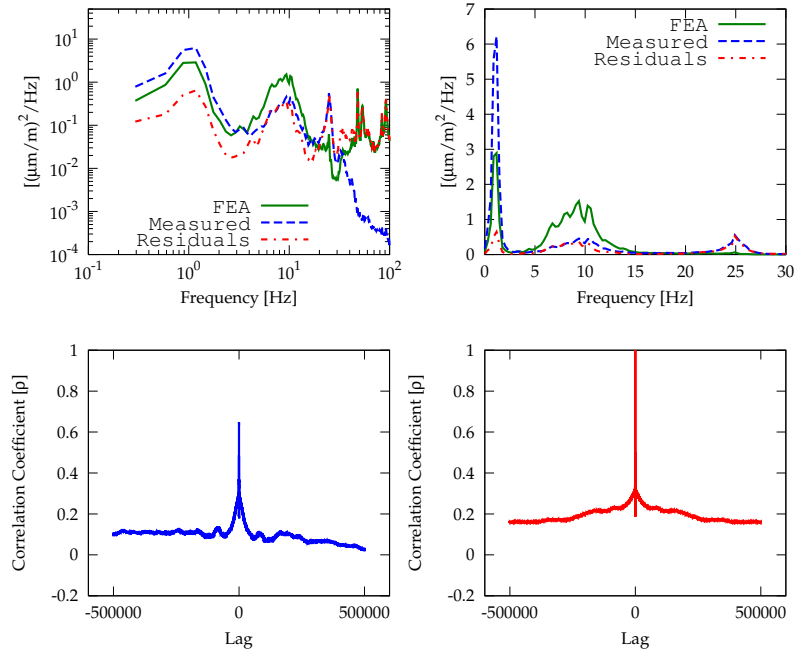


Figure 3: R2 90°

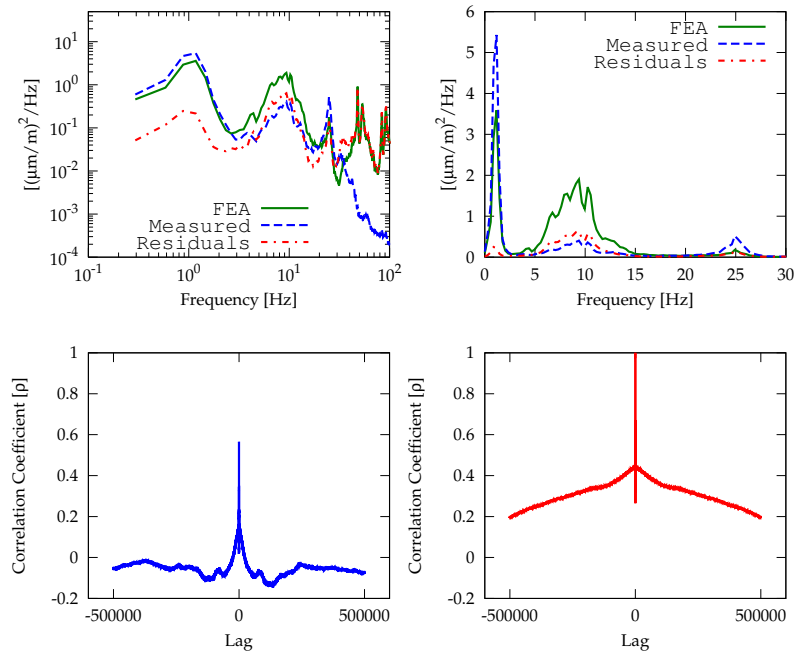


Figure 4: R3 0°

Max Lag = 500000

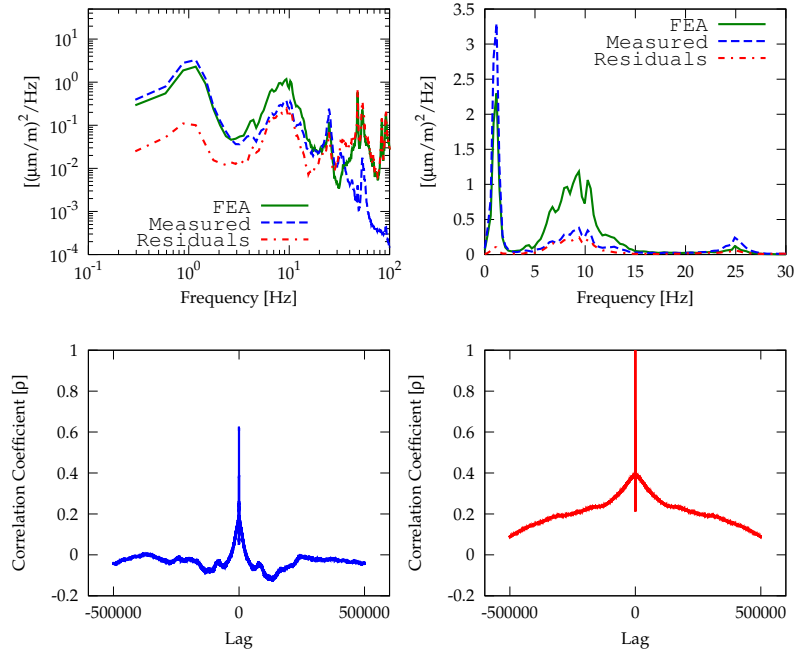


Figure 5: R3 45°

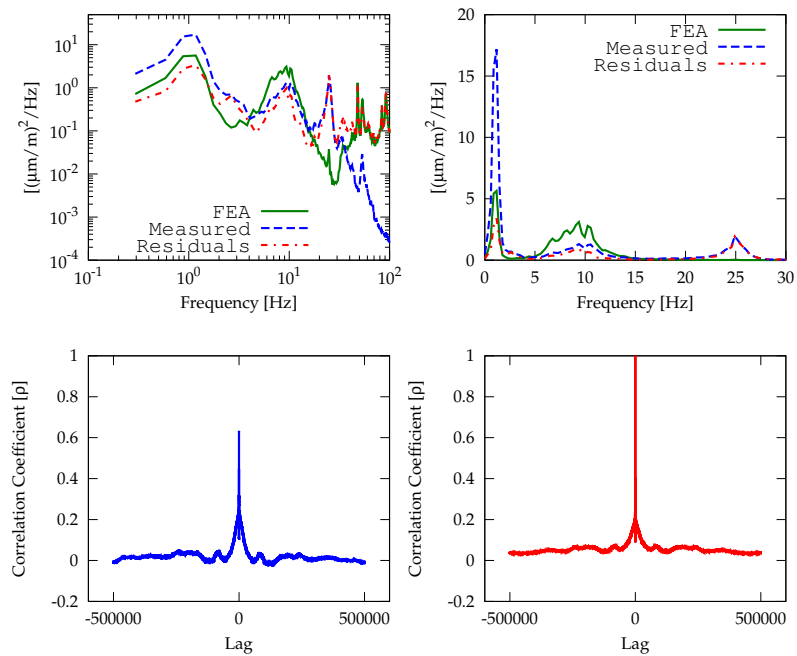


Figure 6: R9 0°

Max Lag = 500000

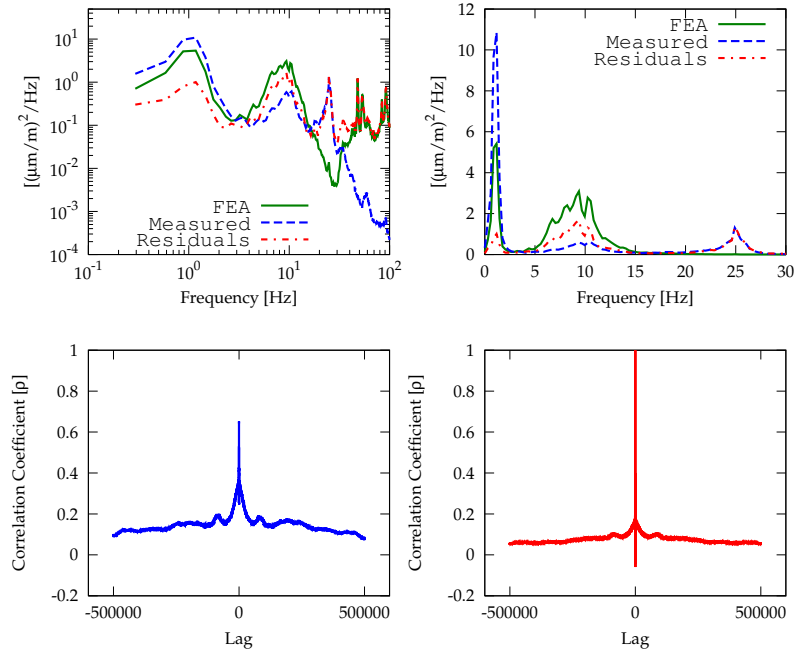


Figure 7: R11 0°

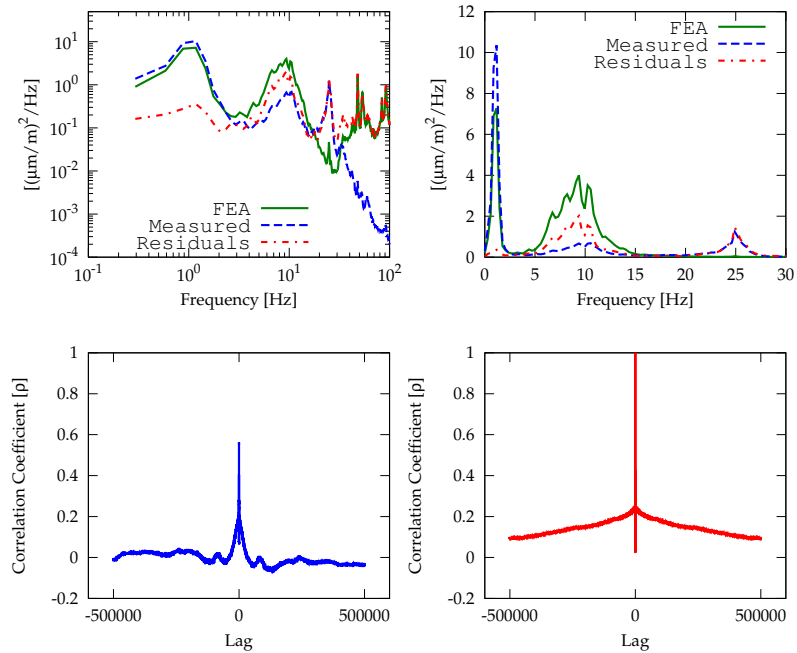


Figure 8: R12 90°

D. Peer Reviewed Journal Publications

Packaging, Transport, Stowage and Security of Radioactive Material, 2012, vol. 23, Nos. 3-4, pp 167-177

SCIENTIFIC/TECHNICAL PAPER

An experimental procedure for measuring accelerations and strains from a tie down system of a heavy nuclear transport package during a rail journey

A. D. Cummings*¹, J. Krywonos¹, P. Purcell¹, G. Rothwell² and R. English²

The transportation of nuclear waste and new nuclear fuel is an important aspect in sustaining the generation of electricity by nuclear power. The design of packages that satisfy regulatory requirements for normal operating and accident conditions is a complex engineering challenge. The ancillary equipment used to constrain the packages to their conveyance, a tie down system, is part of a multicomponent system used to transport packages. Traditionally, the individual components of the transport system have been designed in isolation. This approach does not account for the interaction between components of the system such as the conveyance, tie down system and package. The current design process for tie down systems is well established but, due to its heuristic development, suffers from uncertainties over which loading conditions should be applied. This paper presents a method for collecting measured acceleration and strain data that can be used to derive customised load cases for the design of tie down systems during rail transportation. The data was collected from a tie down system that restrained an empty TN81 package, weighing 99.7 tonnes during a routine rail journey from Barrow-in-Furness to Sellafield. Furthermore, the data can be used to validate modern computer models, allowing for the development of the previously described holistic approach to tie down system design. The results are unique because an ensemble of acceleration and strain time histories from a transport system laden with a nuclear package is unprecedented. A visual examination indicates that the loading a tie down system incurs during a rail journey consists of low magnitude accelerations. The measurement points also show that the general trend of acceleration levels is highest nearest the track and is attenuated by the package. The implications for the design of tie down systems are that two potential failure modes, fatigue and static strength, have been identified. The data provides scope for customising accurate static strength and fatigue calculations using modern computational techniques. This allows for the safety margins inherent in new designs to be determined and optimised design solutions made possible.

INS makes no representations or warranties or any kind concerning this article, express or implied, statutory or otherwise, including without limitation, warranties of accuracy or the absence of errors.

Keywords: Tie down system, Package, Fatigue, Acceleration, Strain, Rail

Introduction

The safe transportation of new fuel and irradiated nuclear waste is an essential part of the nuclear fuel cycle. Nuclear power provides a long term method of

electricity generation that is environmentally friendly. The short and long term management of nuclear waste is a complex subject with many engineering challenges. For example, the design of transportation packages that satisfy the regulatory demands for normal operating conditions and accident conditions is a major challenge. Another engineering challenge, closely related to package design, is the constraining of packages to their conveyance during transportation. The constraint mechanism is called a tie down system (Fig. 1).

¹International Nuclear Services Ltd, H260, Hinton House, Birchwood Park Avenue, Risley, Warrington WA3 6GR, UK

²Liverpool John Moores University, Liverpool, UK

*Corresponding author, email andrew.cummings@innuserv.com



1 Typical tie down system

There are four modes of transport for packages: road, rail, sea and air. In practice, the most prevalent modes of transport used in the UK are rail and sea. A tie down system can therefore be mounted to the flat bed of a trailer, to a rail wagon bed or in a ship or airplane cargo hold. The loading conditions depend on the mode of transport.

The mass of nuclear shipping packages can vary from just a few tonnes to >100 tonnes. Therefore, generic load cases must encompass all different types of packages and each mode of transport.

This paper evaluates the most pertinent points from some of the currently used design codes of practice and standards for tie down systems (in the UK) and focuses on the inconsistent load cases suggested within them. A revised methodology for obtaining experimental data suitable for design use is then presented.

Tie down system design for rail transportation

An older design procedure for tie down systems is the Oak Ridge National Laboratory Cask Tie Down Design Manual.¹ Further design guidance is available within the current Advisory Material for the International Atomic Energy Agency (IAEA) Regulations for the Safe Transport of Radioactive Material.²

The design method is to apply acceleration factors to the centre of gravity of a package, multiplying the package mass by the appropriate acceleration to derive forces to apply to the tie down system. The resulting stresses in the members of the structure are then calculated and compared to allowable stresses. The current IAEA Advisory Material states ‘the accelerations derived from routine conditions of transport should not cause any component of the package or its retention system to yield’; i.e. the yield stress of the material should be used as the allowable stress.

The current IAEA Advisory Material does not stipulate that the design of a tie down system should prevent failure by fatigue; in contrast, the 2002 Revision of the Advisory Material states ‘In addition to these quasi-static force considerations, the package designer must also account for the effects of fluctuating loads which could lead to the failure of components of the package and its retention system caused by fatigue’. Guidelines also state that suitable acceptance criteria for stresses should be agreed by the relevant competent authorities.^{2,3}

In the UK, one relevant competent authority for tie down systems is the Rail Safety Standards Board, who publishes a standard for the structural design of rail freight wagons.⁴ A further source of guidance is published by the Transport Container Standardisation Committee (TCSC).⁵ These guidance documents state

Table 1 Proof load cases

	Longitudinal/g	Lateral/g	Vertical/g
IAEA Regulations Advisory Materials TS-G-1. Radioactive material packages in Europe by rail (UIC) [IV.8]	4	0.5	1 ± 0.3
TCSC 1006 Guide to the Securing/Retention of Radioactive Material Payloads and Packages During Transport, 2012*	4	1	2(D); 1(U)
TCSC 1006 Guide to the Securing/Retention of Radioactive Material Payloads and Packages During Transport, 2012†	1	1	2(D); 1(U)
Rail Safety Standards Board – GMGN2589 Guidance on the Structural Design of Rail Freight Wagons including Rail Tank Wagons	2	1	2(D); 1(U)

*Wagons subjected to shunting.
†Combined transport.

Table 2 Fatigue load cases

	Longitudinal/g	Lateral/g	Vertical/g
TCSC 1006 and GM/GN 2589	± 0.2	± 0.2	± 0.4



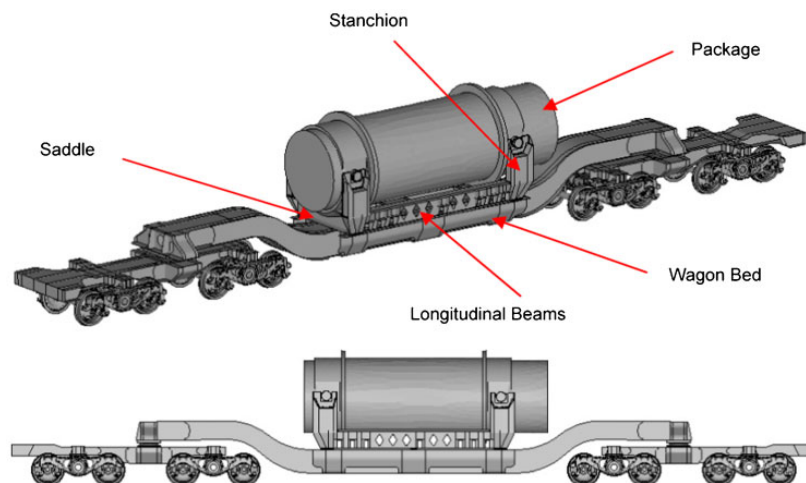
2 Map of rail journey between Barrow-in-Furness and Sellafield

that the design for prevention against fatigue failure should be considered and provide fatigue load cases to be applied. Tables 1 and 2 compare the proof and fatigue acceleration factors.^{2,4,5} These design guides place emphasis on classical hand calculation methods and not finite element analysis (FEA).

Motivation for experimental work

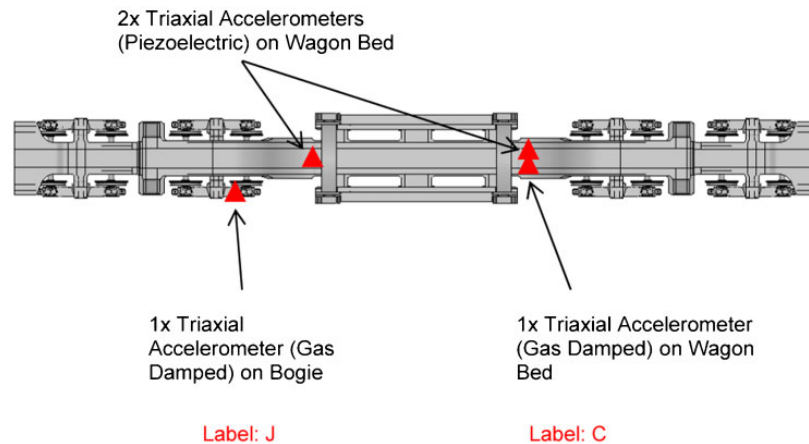
Internationally, the subject of which acceleration factors to apply and revision of acceleration factors has been

raised by several authors.⁶⁻⁸ Fourgeaud et al. argue that some of the acceleration factors in the literature, which are based upon experimental data, should be increased and rounded up to account for lack of data. Purcell suggested that reduced design criteria may be required when considering tie down systems for heavy nuclear packages as the use of the load cases enforced the need to oversize structural members, causing tie down systems to be heavier.⁷ Desnoyers recommended that the IAEA Advisory Material should be updated with a



3 Computer aided design model of rail wagon and package

Cummings et al. Measuring accelerations and strains from tie down system



4 Accelerometers positions

current list of rules, standards and guidelines for designers.⁸

In the UK, the current transportation solutions for moving waste to underground Geological Disposal Facility by rail are easier in practice if the packages can reside with the rail conveyance until they are underground. This poses an optimisation problem where constraints are imposed by the size of the rail gauge specifications and rail vehicle gross laden weight. These constraints limit the maximum size and mass of packages and their tie down systems.

Additional optimisation constraints on a tie down system are imposed by package shielding requirements and impact resistance, which constrain space and allowable mass. Therefore, the structural design of tie down systems requires a thorough understanding of the mechanical loads imposed upon them, as they will have a significant effect on the solution space available to the designer.

Despite the demanding nature of tie down system design, modern computational methods have not yet

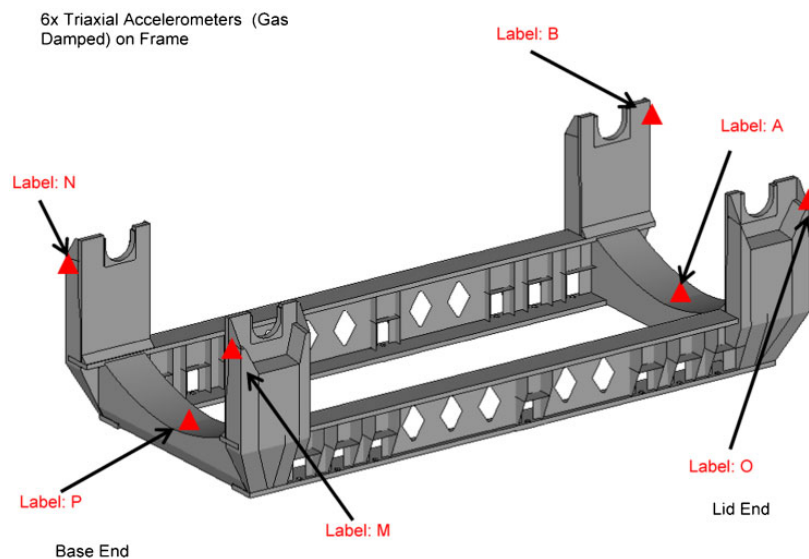
been fully utilised. With the use of FEA, the stresses and strains of an entire tie down system can be accurately calculated. The Office of Nuclear Regulation for Radioactive Materials Transport (ONR-RMT) emphasised the use of FEA for structural assessments of tie down systems as a more robust method than traditional approach.⁹

It appears that defining generic load cases for such a diverse range of transport applications causes significant difficulties. Several authors have presented arguments for revision of guidance documentation; therefore, further experimental work is required.

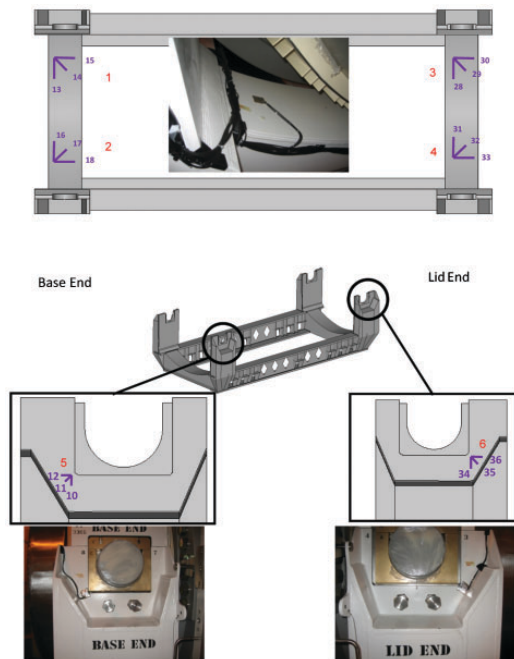
General test procedure

Test plan

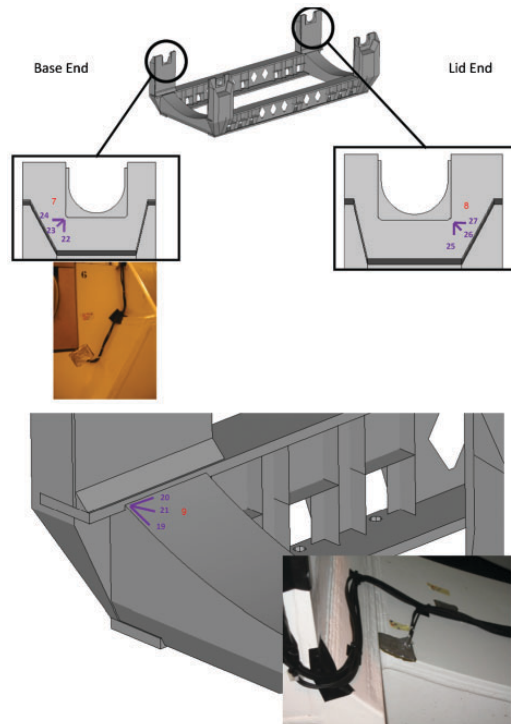
The following procedure demonstrates a method for positioning instrumentation and collecting test data that can assist in the understanding and use of acceleration factors for the design of tie down systems for transport by rail.



5 Accelerometer positions



6 Strain gauge rosettes labels and locations (numbers in red are strain gauge rosette numbers; individual legs of rosettes are numbered in purple)



7 Strain gauge rosettes labels and locations (numbers in red are strain gauge rosette number; individual legs of rosettes are numbered in purple)

The measurements were taken during a routine journey by rail from Barrow-in-Furness to Sellafield. The rail vehicle consisted of two locomotives supplied by Direct Rail Services and three rail wagons. Two of the wagons acted as spacer wagons between the locomotives and the central wagon, called a KXA-C, which transported the 99.7 tonne package, the TN81 and its tie down system. The KXA-C wagon, having previously been used for only 611 miles, was in excellent running condition, and therefore, a favourable environment for the tie down system was expected.

The first part of the test was the loading of the package onto the tie down system. The strain gauges were fitted to the frame before lifting, but during this operation, no measurements were taken. The package was lifted off the frame, and the strain gauges and accelerometers were calibrated. Strain and acceleration were measured during the reloading of the package onto the frame.

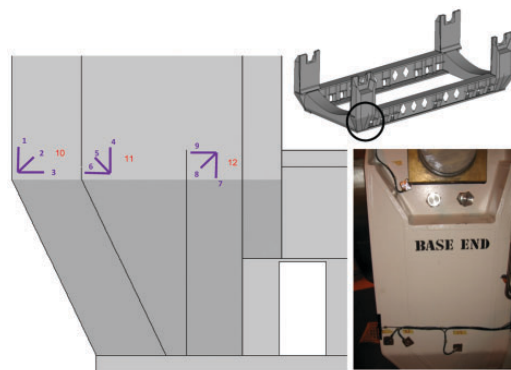
The second part of the test was the continuous measurement on all data channels. Owing to unforeseen circumstances, several minutes of data were not collected in the central section of the journey (Fig. 2).

Figure 3 shows a computer aided design model of the rail wagon and package. Figures 4 and 5 show the positions and labels of each transducer (denoted by red triangles). A total of 10 triaxial accelerometers were used, eight of which were supplied by Data Acquisition and Testing Services Ltd. One accelerometer was mounted to each stanchion of the tie down system (Fig. 5).

Two more accelerometers were mounted at the centre of each of the saddles, another on the wagon bed near

the frame to wagon interface. The final accelerometer was mounted on the bogie of the rail vehicle. The other two triaxial, piezoelectric accelerometers were mounted onto the wagon bed. These two transducers recorded peak acceleration values at 5 min intervals.

Twelve strain gauge rosettes were mounted to various locations on the frame as shown in Figs. 6–8. During the loading test, one of the strain gauge rosette legs was found to be faulty, on channel 34, rosette number 6. A new rosette was fitted for the journey measurements.



8 Strain gauge rosettes labels and locations (numbers in red are strain gauge rosette number; individual legs of rosettes are numbered in purple)

Positioning of accelerometers

Redundancy was built in to the test using duplicate accelerometers. This ensured that if an instrument failed or suffered malfunction, the test would still produce some data from the other channels. All the accelerometers were mounted on suitably stiff structures.

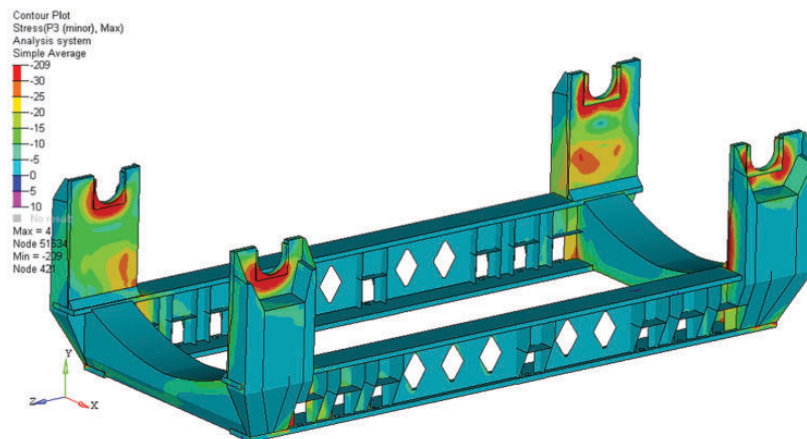
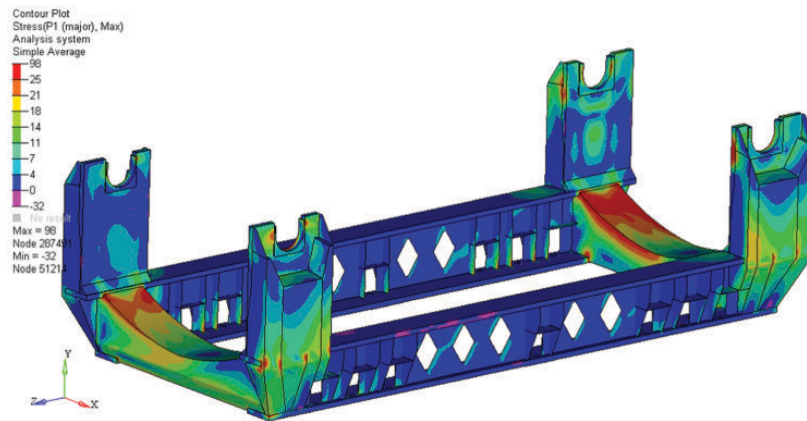
An ideal scenario would be to position the accelerometer at the centre of gravity of the package; however, at the exact position of the centre of gravity, there was no physical structure to mount an accelerometer. To identify loading on the tie down system, two alternative positions were suggested: the four stanchions and the wagon bed.

Mounting the accelerometers to the stanchions meant that they were as close to the centre of gravity of the package as possible. The wagon bed measurement was included to provide a position closest to the base of the

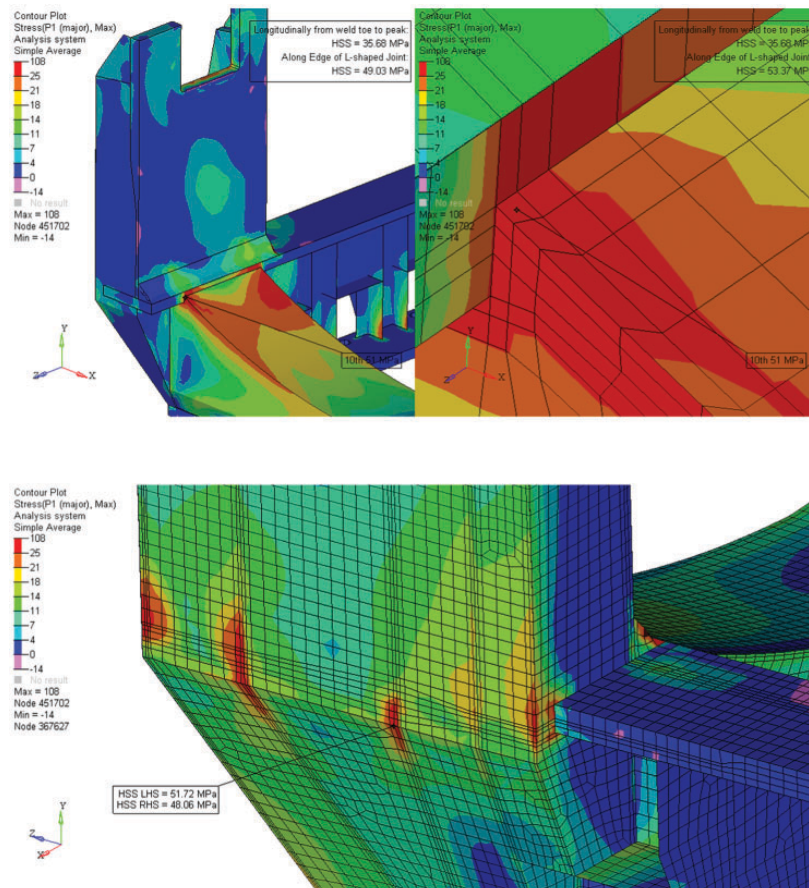
tie down system. This gives an insight into what vibration energy is transmitted through the wagon bed into the frame. This is critical to understanding the source of the accelerations that arise during freight transport and also for comparing the relative motion between the wagon bed and stanchions.

Two further accelerometers were mounted to the centre of the saddle sections between the lid stanchions and the base stanchions. These positions enabled valuable analysis when studying the transmission of vibration through the frame.

The final accelerometer was positioned on a bogie of the rail wagon, which was used to understand how much vibration was present from the wheel/track interface and how much energy contained in the signal was filtered out by the suspension. This was used as a point of reference to understand the source of the accelerations.



9 Principal stress contour plots



10 Principal stress contour plots of welded joint hot spots

Positioning of strain gauges

A mixture of nominal and local stress positions were selected for strain gauging (Figs. 6-8). Eight strain gauges were positioned to monitor nominal stresses on the stanchions and saddles of the tie down system (Figs. 9 and 10).

Four strain gauge positions were determined by FEA, which typically highlights welded joints as more highly stressed than other parts of the structure (Figs. 9 and 10). From the analysis results, the strain gauges were

positioned to monitor local stresses on three welded joints on a stanchion and one on a saddle (Figs. 8 and 10).

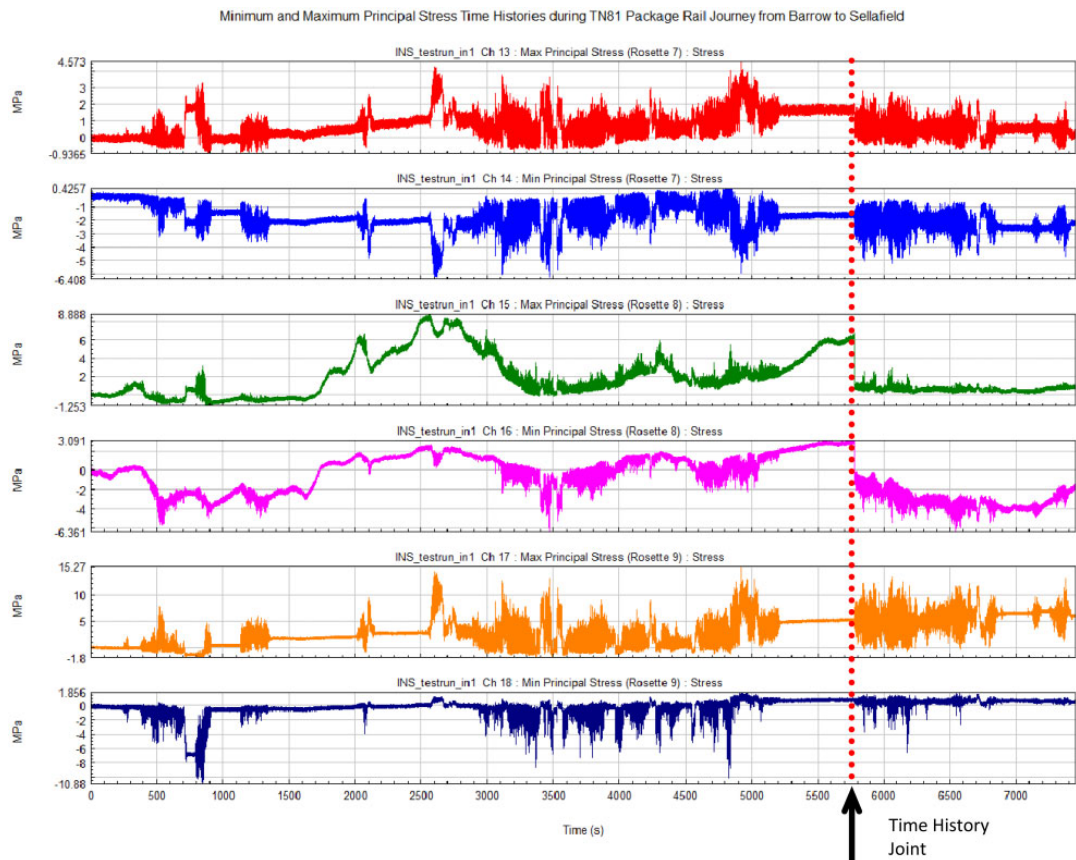
Data acquisition system and transducers

The data acquisition system used was a multichannel HBM MGCplus ML801B [Data Acquisition Services (DAQ)]. The frequency range of interest was 0–100 Hz.¹⁰ Sampling at 1000 Hz to avoiding aliasing and truncation of peaks, a sampling frequency of

Table 3 Maximum principal stresses converted from measured strains during loading test

Rosette number	Minimum principal stress/MPa	Maximum principal stress/MPa
1	-3.79	-1.28
2	-4.70	1.99
3	-2.81	-1.43
4	-2.16	1.91
5	-2.16	0.52
6	N/A	N/A
7	-1.29	0.49
8	-1.73	1.85
9	-10.26	-0.87
10	-1.77	2.45
11	3.71	4.46
12	1.92	3.27

Cummings et al. Measuring accelerations and strains from tie down system



11 Example of the strain time histories collected during the journey

1000 Hz was initially selected, but due to limitations of the DAQ, this was increased to 1200 Hz. The signal was passed through an analogue Butterworth anti-alias filter, with a cutoff frequency of 100 Hz, before digitisation.

Results

The results of the loading test are shown in Table 3 and 4. The absolute maximum principal stresses are shown in Table 3. The absolute maximum values of acceleration are shown in Table 4.

An example of the results of the journey measurements are shown in Figs. 11–12. The time histories of strains in Fig. 11 have been converted into maximum and minimum principal stresses. The absolute maximum principal stresses recorded are shown in Table 5. The absolute maximum values of acceleration are shown in Table 6. Figure 13 shows time histories of GPS coordinates and vehicle running speed. This allows identification of events in the acceleration and strain time histories to be compared to vehicle running speed and location, i.e. additional information on extreme or rarely occurring events can be extracted.

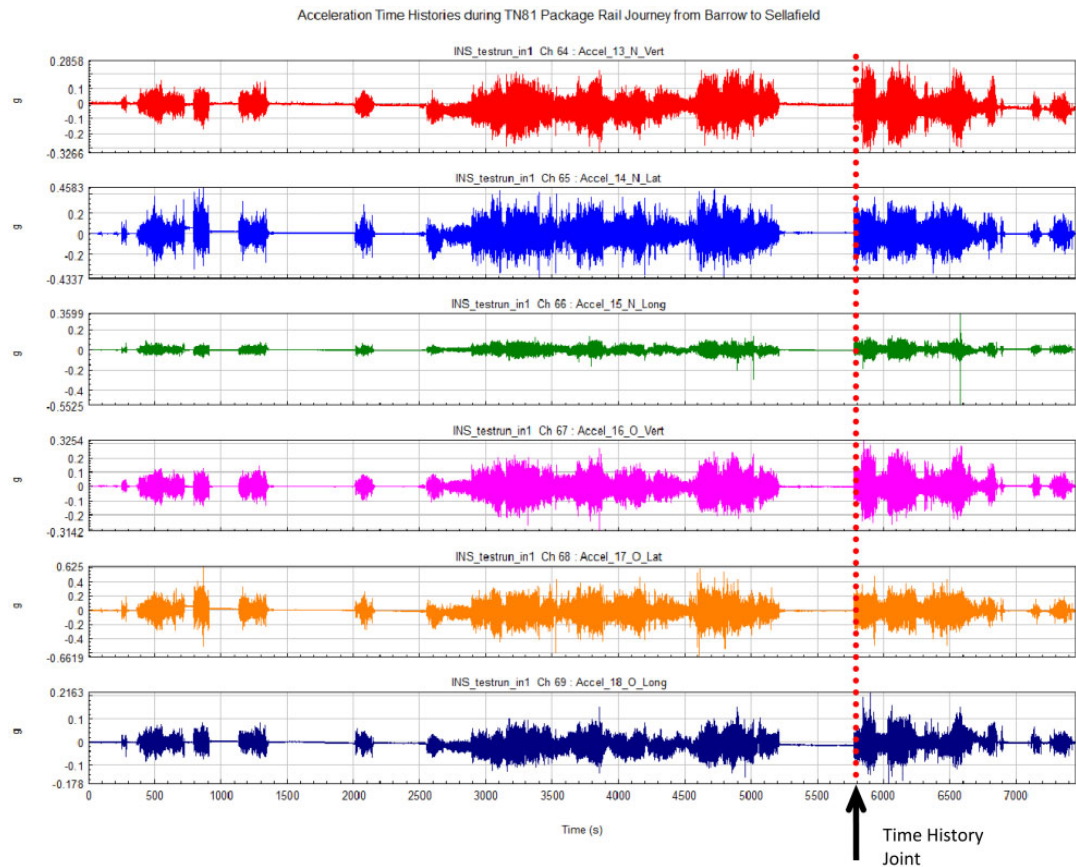
Discussion

The largest amplitude accelerations in all three axes were measured on the bogie (label J); vertical 8 g, lateral 4.8 g

and longitudinal 6.7 g. These are typical values of acceleration for a rail bogie.¹¹ On the tie down system, the lateral and vertical accelerations were generally of a similar order of magnitude to those shown in Tables 1 and 2. The measured longitudinal accelerations were found to be an order of magnitude lower than some of those recommended in the literature.^{2,4,5} This can be attributed to the documented accelerations accounting for shunting operations, which were not permitted during this transportation.^{1,5}

The measurements show that the acceleration field arises from the wheel/track interface and is attenuated by the suspension system. This is evident by the magnitude of the acceleration levels, which are highest at the bogie and attenuate upwards through the structure (Fig. 14). It is also evident that the nature of the accelerations and stresses is highly cyclic. Therefore, an underdesigned tie down system may fail due to two possible failure modes: gross yielding or fatigue. However, in this experiment, the stresses at the measured locations were very low and the methodology created indicates that the TN81 tie down system will not fail in this environment.

It is imperative that appropriate signal processing techniques and statistical methods are used for deriving load cases and that the maximum values reported here are not used as design parameters. The main reasons for this are that the peak values are the



12 Example of the acceleration time histories collected during the journey

raw measurements that require further signal processing. It is a necessity to extrapolate peak loads to account for rarely occurring values that were not measured during the test.² A digital filter may also be used to remove content in the signal, which is not appropriate for design use.

Conclusions

A review of current design practices, as prescribed by relevant regulations, standards and competent authorities, has been conducted. It is evident that there is little agreement between all parties, and further experimental work is required. Further motivation for experimental work has also been presented, and its benefit for producing optimised transport solutions has been emphasised. The ONR-RMT stated the benefits of the use of FEA for structural assessments of tie down systems as a more robust method.⁹

An experimental procedure has been created that will provide data sufficient for computational methods. The data can be used to customise tie down system design for particular applications, extend fatigue life, verify existing designs and benchmark FEA. It provides an empirical means of design and can be extended to a holistic design process.

The results show that strains in the tie down system are very low. Strain occurs as a consequence of the relative

motion between the conveyance and package. Since the magnitude of accelerations varies, a 'relative' acceleration maybe more applicable than the current design load cases, which are absolute values. This is critical for static strength and fatigue design considerations. It is evident that the careful selection of loads and boundary conditions is required during design of tie down systems.

The highest accelerations were measured at the bogie and are brought about by the harsh wheel/track interface. It is therefore overly conservative to apply the entire content of the acceleration signal to the centre of gravity of a package. Therefore, before deriving load cases, the signals should be filtered to ensure that only accelerations acting at the centre of gravity of a package are considered.

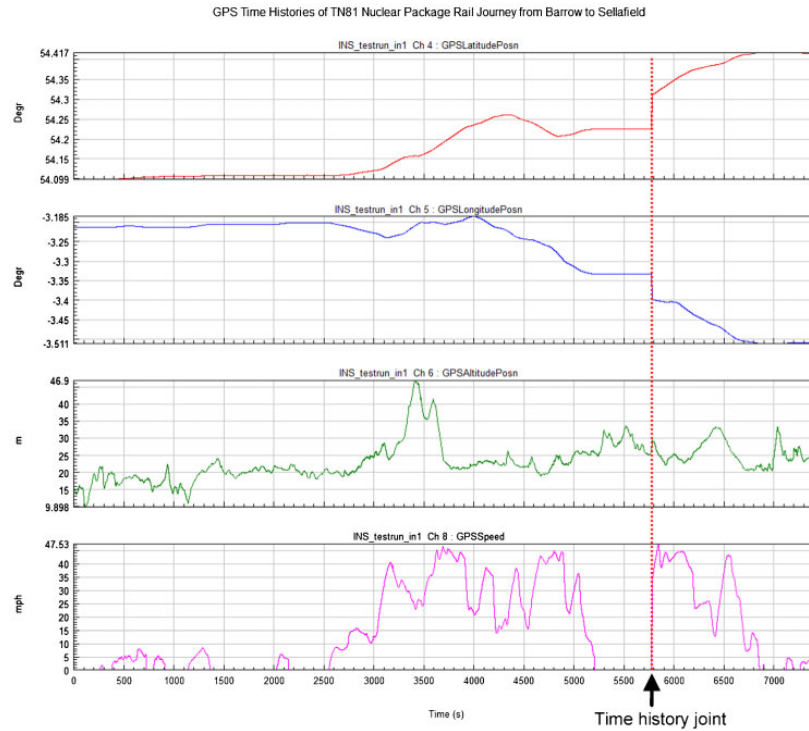
The nature of the signals is highly cyclic; therefore, there are two important failure modes to consider during tie down system design: gross yielding and fatigue.

Future work

Data analysis

A full data analysis that investigates the potential for filtering of the data and a method for deriving fatigue and proof load cases will shortly be made available for publication.

Cummings et al. Measuring accelerations and strains from tie down system



13 GPS and vehicle speed time histories

Table 4 Absolute maximum accelerations measured during loading test

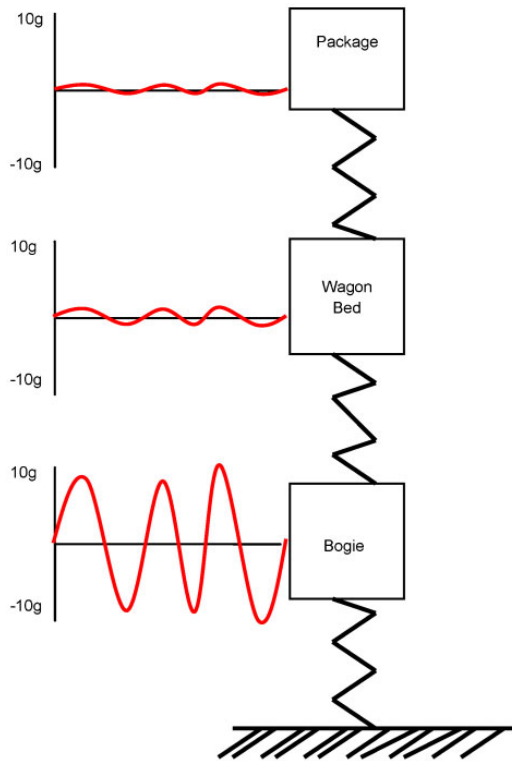
Accelerometer label	Longitudinal acceleration/g	Lateral acceleration/g	Vertical acceleration/g
A	0.04	0.06	0.08
P	0.04	0.12	0.04
B	0.07	0.08	0.12
M	0.07	0.15	0.16
N	0.18	0.07	0.18
O	0.16	0.14	0.14
C	0.02	0.03	0.02
J	0.10	0.32	0.21

Table 5 Absolute Maximum principal stresses converted from measured strain data during journey

Rosette number	Minimum principal stress/MPa	Maximum principal stress/MPa
1	11.79	12.81
2	7.54	11.95
3	-13.41	13.52
4	8.89	9.69
5	-6.04	6.21
6	-5.14	8.46
7	-6.41	4.57
8	-6.36	8.88
9	-10.88	15.27
10	-5.57	6.05
11	-12.04	9.45
12	-12.66	10.04

Table 6 Absolute maximum accelerations measured during journey

Accelerometer label	Longitudinal acceleration/g	Lateral acceleration/g	Vertical acceleration/g
A	0.38	0.48	0.62
P	0.43	0.61	0.65
B	0.16	0.48	0.29
M	0.14	0.42	0.32
N	0.55	0.46	0.33
O	0.22	0.66	0.33
C	0.43	0.58	0.87
J	6.73	4.76	8.03



14 Variation of accelerations through conveyance, tie down system and package

Computational design work

An important next step is to model the rail wagon and track profile using rigid body dynamics (RBD) and calibrate the model with these test data. This will increase confidence in the method and any derived load cases.

An RBD is a computational method that can approximate the full range of complex kinematic and

dynamic behaviour particular to rail vehicles and accurately model the influences of undulating, random track profiles, something difficult to achieve with FEA. Although not capable of reproducing stresses within a tie down system, a calibrated RBD model can be used for sensitivity studies of the mechanical loads experienced during transportation.¹⁰

Similarly, an FEA model that is calibrated with test data can provide valuable insight into the behaviour of tie down systems and a sound basis for a design by analysis methodology.

Experimental work

More studies of this kind are needed to understand the other transport environments, particularly in a ships hold. There is more uncertainty in the loads experienced at sea than any other transportation mode, and for this reason, experimental data would be an invaluable acquisition.

References

1. Oak Ridge National Laboratory: 'Structure analysis of shipping casks'. Vol. 7, 'Cask tie-down design manual', Technical Report, Rep. ORNL-TM-1312, Oak Ridge National Laboratory, TN, USA, 1969.
2. 'Advisory material for the IAEA regulations for the safe transport of radioactive material, 2008, Rev1', TS-G-1.
3. 'Advisory material for the IAEA regulations for the safe transport of radioactive material', Rev1, TS-G-1 (ST.2), 2002.
4. 'Guidance on the structural design of rail freight wagons including rail tank wagons', Issue 4, RSSB, 2010, GMGN2589.
5. 'Transport of radioactive material code of practice', 'Guide to the securing/retention of radioactive material payloads and packages during transport', TCSC 1006.
6. Fourgeaud, S., Sert, G. Ben Ouaghrem, K., Le Bars, I., 2011, 'External Loads applied to Packages during Routine Transport', Packaging, Transport, Storage and Security of Radioactive Material, Vol 22, No 2, pp 99 –103, Maney Publishing, France.
7. P. Purcell: 'Designing tie-down system for heavy RAM packages – should revised design criteria apply?'; 2010, INS, PATRAM, UK.
8. B. Desnoyers: 'Stowage and retention of radioactive packages during transport: which rules should be acceptable?'; 2012, TN International, AREVA Logistics Business Unit – Transport Oversight Division, RAMTRANS France.
9. I. Davidson: 'A discussion on the secure stowage of packages'; 2010, Department for Transport, PATRAM.
10. 'Engineering vibration environment for rail vehicle mounted equipment', RSSB.

Packaging, Transport, Stowage and Security of Radioactive Material, 2013, vol. 24, No. 1, pp 23-35

SCIENTIFIC/TECHNICAL PAPER

Filtering and analysis of accelerations and strains measured on a tie down system of a heavy nuclear transport package during a routine rail journey

A. D. Cummings*¹, J. Krywonos¹, P. Purcell¹, G. Rothwell² and C. Matthews²

The design and development of nuclear packages is critical for the safe transportation of new fuel and irradiated waste. The renaissance of the nuclear industry in recent years has increased motivation for the development of optimised transport and storage solutions. The design of mechanisms to safely constrain nuclear packages, commonly referred to as tie down systems, has become more challenging as package masses have increased. This paper focuses on characterising the loading environment that a tie down system is subjected to using signal processing techniques on previously measured acceleration and strain time histories. The measurements were taken on a tie down system for a nuclear package, weighing 99.7 tonnes, during a routine rail journey. Similar previous studies on tie downs have omitted frequency analysis of the measured signals on tie down systems. A frequency analysis has been used to determine the nature of the loading experienced by a tie down system and also the extent of vibration transmission into the package. A means for obtaining a suitable filter cutoff frequency is also presented by comparing frequency spectra from different measurement points.

To extract quasi-static accelerations from the raw data, several digital filters have been designed to study their effects on the resulting signals. By comparing the low pass and band pass filtered time histories, some insightful trends in the accelerations peaks have been found. To demonstrate what constitutes a good or bad filter design, sensitivity studies have been conducted to show how the distributions of peaks and their statistics are altered significantly with poorer filter choices.

Keywords: Tie down system, Package, Peak, Acceleration, Strain, Rail

Introduction

The transportation and storage of nuclear waste is of great importance to sustaining the generation of electricity by nuclear power. Engineers are continuously designing new, heavy, nuclear packages used to transport and store nuclear material. The design of a tie down system used to restrain a package to its conveyance during transport is an integral part of package design (Fig. 1). It is recognised by several authors that there is a paucity of experimental data for the design substantiation of tie down systems.¹⁻⁴

Cummings *et al.*⁴ presented a method for obtaining real time measured data from a tie down system suitable for design purposes. A 99.7 tonne package and its tie down system were transported by rail from Sellafield to

Barrow, in the UK. Two hours of data were measured at a sampling frequency of 1200 Hz. During data collection, an anti-alias, 100 Hz low pass, Butterworth filter was used before digitisation of the samples. A total of 24 acceleration channels from 8 triaxial accelerometers and 36 channels of strain from 12 strain gauge rosettes were collected.

The maximum values collected on each channel show that the highest accelerations were measured nearest the track and the lowest accelerations nearest the package.⁴ This paper presents a thorough analysis of the measured time history records that enhances current understanding of the behaviour of tie down systems during transit by rail specifically for large mass packages (≈ 100 tonnes).

Characterising the loading environment

A strain time history has been dissected and certain key features are highlighted (Fig. 2). Strains have been selected in preference to accelerations because the various

¹International Nuclear Services, Warrington WA3 6GR, UK
²Liverpool John Moores University, Liverpool, UK

*Corresponding author, email andrew.cummings@innuserv.com



1 Computer aided design model of rail wagon and package

types of loads are more easily detectable by visual observation of strain time histories. The time history consists of a number of sections where the measurements have reduced to the noise floor of the instrumentation. These sections are called signal dropouts.⁵ In the figure, several signal dropouts exist and are highlighted in green; these sections all correspond to time periods where the vehicle came to rest.

The strain signal commences at 0s and $0 \mu\text{m m}^{-1}$ but after 7400s +, has drifted to $\approx 25 \mu\text{m m}^{-1}$. The apparent drift is most likely due to temperature variations and is more pronounced in the strain signal than in any of the acceleration signals. Temperature compensated strain gauges were used so the drift was attributed to real temperature variations, e.g. small amounts of thermal expansion on one side of the tie down system exposed to solar insolation. The drift was considered reasonable due to the low overall values of strain and relatively high signal to noise ratio.

The structural loading imparted to tie down systems can be categorised into three main types:

- (i) quasi-static
- (ii) shock
- (iii) vibration

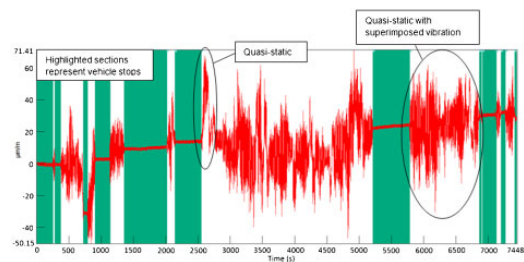
These categories of loading are evident with the exception of shock loading, which, if present, was not defined sufficiently in the signal to be highlighted (Fig. 2). The source of the loading and its effects on tie down systems is a critical consideration for their safe structural design.

Quasi-static loading

Quasi-static loads are generally slowly applied and therefore tend to appear in the lower frequency range, i.e. $< 30 \text{ Hz}$.⁶ The International Atomic Energy Agency Advisory Material⁷ does not provide a specific definition for quasi-static loading; however, it does offer guidance on filtering time histories to obtain quasi-static loading. It suggests that based on experience, 10–20 Hz is a suitable cutoff frequency for a package of 100 tonnes. For the purposes of experimental and structural analysis, two formal definitions are also provided:

- (i) structural response is time dependent if loading is time dependent; however, if loading is cyclic and of frequency less than roughly one quarter of the structure's natural frequency of vibration, dynamic response is scarcely larger than static response.⁸
- (ii) for frequencies considerably below the first resonance or slowly varying time histories, the response will be purely quasi-static and reasonable results can be obtained from a static analysis.⁹

The definitions suggest that a filter cutoff frequency should be based upon prior knowledge of a tie down systems first natural frequency. For large mass packages (where the ratio of package mass to conveyance mass is > 1), this is not a straightforward calculation. A tie down



2 Typical strain time history characteristics

system is part of a chain of dynamically coupled systems including the package and rail wagon. This means that isolating the tie down system and package to perform a modal analysis using finite element analysis (FEA), or a modal test, would not produce correct results. Therefore, to obtain an accurate natural frequency estimate, a more complex test of the complete system (i.e. vehicle and payload) is required.¹⁰ Multibody dynamics tools may also provide good estimates, but parameter identification and validation of these techniques is challenging. To circumvent these problems, a practical method of determining a suitable filter cutoff frequency has been devised.

Shock loading

The nature of shock loading is a short transient burst of energy that occurs rapidly and involves a much larger frequency range. It is a transient response that is initially low, rises to its maximum and then decays. Shock loading will typically excite many natural frequencies of a structure. The resulting structural response consists of a weighted combination of the mode shapes, causing a significantly different response than that due to a quasi-static load.^{11,12} Examples of shock loads in tie down system operations are longitudinal coupling of rail wagons or hump shunting operations. These are considered as normal conditions of transport in the advisory material⁷ and can be approximated using explicit FEA.^{13–16}

Vibration loading

Vibration can be considered as the residual loading, if quasi-static loads and shock loads are removed from the signal. Vibration is categorised into two types: deterministic and stochastic. Deterministic vibratory loads are generally created by rotating machinery such as piston engines, pumps and turbines. This kind of loading can be measured and fully quantified by test; the measurements can be reproduced exactly in a subsequent test. The loading on a tie down system during a rail journey cannot be reproduced exactly each time it is measured because it falls into the second class of stochastic or random vibration.

Random vibration can only be quantified using probabilistic methods; therefore, a repeat test will produce the same statistical measures such as the root mean square (rms) value of a signal. Depending on the tie down system's modal characteristics and the level of energy contained in the input load's, random vibrations can be treated for design in three different ways:

- (i) if the highest frequency content of the loading is less than one quarter of the fundamental natural frequency of the tie down system or is slowly

occurring, then the loading can be treated as quasi-static.

- (ii) if the vibration is of sufficient level and close to the fundamental natural frequency of the tie down system, then resonance effects should be accounted for in structural integrity calculations.
- (iii) if the level of vibration loading is insufficient to affect the tie down system or the lowest frequency of the loading is much higher than the fundamental natural frequency of the tie down system, then the influence of random vibrations can be safely neglected from structural integrity calculations.

To extract the quasi-static content from the signals, various digital filter designs have been explored.

Digital filtering

The advisory material⁷ states that digital filtering of measured acceleration time histories is necessary to define quasi-static loads and to demonstrate design compliance. Filters have been applied for two main purposes in this paper:

- (i) frequency analysis: for spectral analysis, a filter that minimises pass band ripple and has a high rolloff rate was required to refine the anti-alias filter used during measurement.
- (ii) structural analysis: for peak analysis, the filter applied should minimise time domain ringing (to avoid distorting peaks) while providing a rolloff rate sufficient to extract the quasi-static content.

Filter requirements

The design of a filter to extract low frequency content for structural analysis involves careful consideration of both its frequency and time domain characteristics. In the frequency domain, the filter behaviour in the pass band, transition band and stop band can be crucial. The filter rolloff rate dictates at what frequency the minimum stop band attenuation is achieved. Since the preservation of peaks in the pass band is of utmost importance to the structural engineer, pass band ripple should be minimised or eliminated during filter design. In addition filtering causes a phase distortion, which has been corrected using a forward-backward filtering algorithm.

Butterworth and Chebyshev type 1 filters continue to attenuate in the stop band, i.e. beyond the cutoff frequency, signal attenuation continues indefinitely. Elliptic and Chebyshev type 2 filters behave differently as they enable control over the permissible stop band attenuation. A minimum acceptable stop band attenuation was set to 1% of the original signal amplitude (-40 dB). This was considered sensible to avoid degradation of the filtered signal.

As an example, the frequency at which the minimum stop band attenuation of first, second, fourth and eighth order, low pass, Butterworth filters with a cutoff frequency of 17.5 Hz is shown in Table 1. Higher order filters provide better rolloff rates and therefore achieve the desired stop band characteristics at lower frequencies. The transition band is the frequency range between the filter cutoff frequency and the frequencies listed in Table 1. The higher the rolloff rate, the narrower this band becomes and the more accurately the filter removes content above the cutoff frequency.

Higher rolloff rates are achieved at the expense of poorer filter performance in the time domain. Increasing filter orders decreases stability, and the filter exhibits overshoot and ringing in the time domain, which can degrade its performance. This is the area of most uncertainty in this filter design: first, because the exact filter cutoff frequency is not known, and second, it is difficult to quantify the level of error that can be attributed to a filter that leaks in the transition band and a filter that overshoots and rings in the time domain.

Sensitivity studies of these filter characteristics have been carried out. Three types of infinite impulse response filters were considered for the structural analysis: the Butterworth, elliptic and Chebyshev type 1 filters. A 4th order Butterworth filter was chosen initially due to the compromise between overshoot and ringing in the time domain and rolloff rate and stop band attenuation in the frequency domain. For comparison, the bode magnitude and step response plots of the various filters used in the sensitivity study are provided (Figs. 3 and 4). For the frequency analysis, an 8th order Butterworth filter was used as it has suitable characteristics for refining the rolloff rate and stop band attenuation of the anti-alias filter.

Frequency analysis

Power spectral density

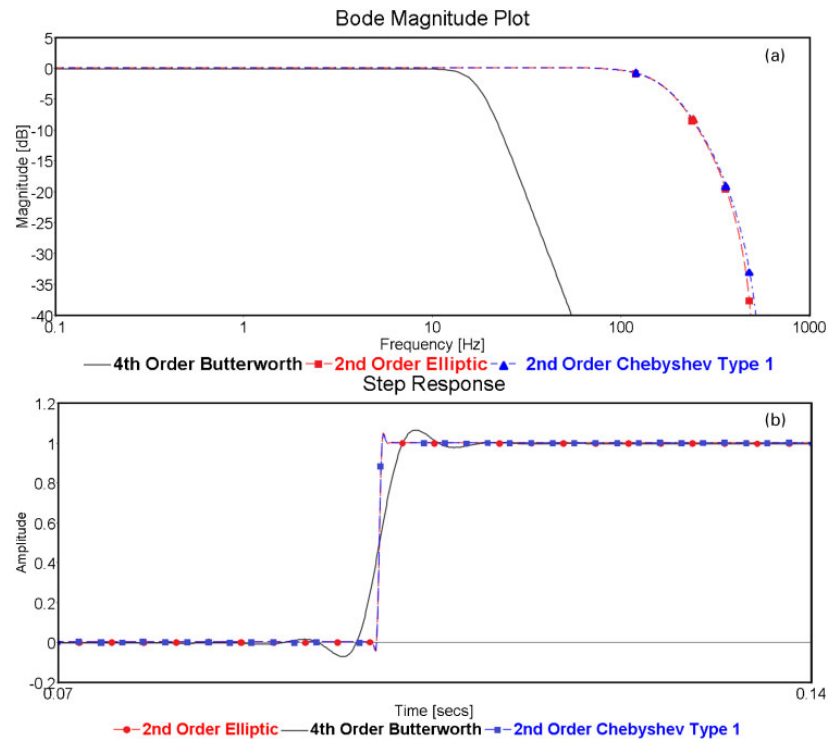
The power spectral density (PSD) enables the study of random time histories in the frequency domain. It is used to show which frequency band(s) of a signal contains the most energy and also highlights resonant frequencies as peaks. Here, the PSD is used predominantly to understand the signal content and as a guide for selecting a filter cutoff frequency. The measured time histories have been transformed to PSDs using the following calculation method:¹⁷

- (i) each time history has been low pass filtered at 100 Hz, to refine the anti-alias filter using an eighth order Butterworth filter; this filter is maximally flat in the pass band (no frequency domain ringing) and provides good rolloff characteristics and good stop band attenuation.¹⁸⁻²⁰
- (ii) the time histories were then subdivided into segments of 4096 points ($n=2182$ segments), which produced a Δf of ≈ 0.3 Hz ($T_f \approx 3.41$ s); the selection of this segment size was considered optimal to present results but was occasionally adjusted to ensure the conclusions of the frequency analysis were reasonable.
- (iii) to minimise the effects of leakage, each segment was passed through a Hanning window function and overlapped to minimise random error.
- (iv) the final PSDs were calculated using a standard fast Fourier transform method on each segment,

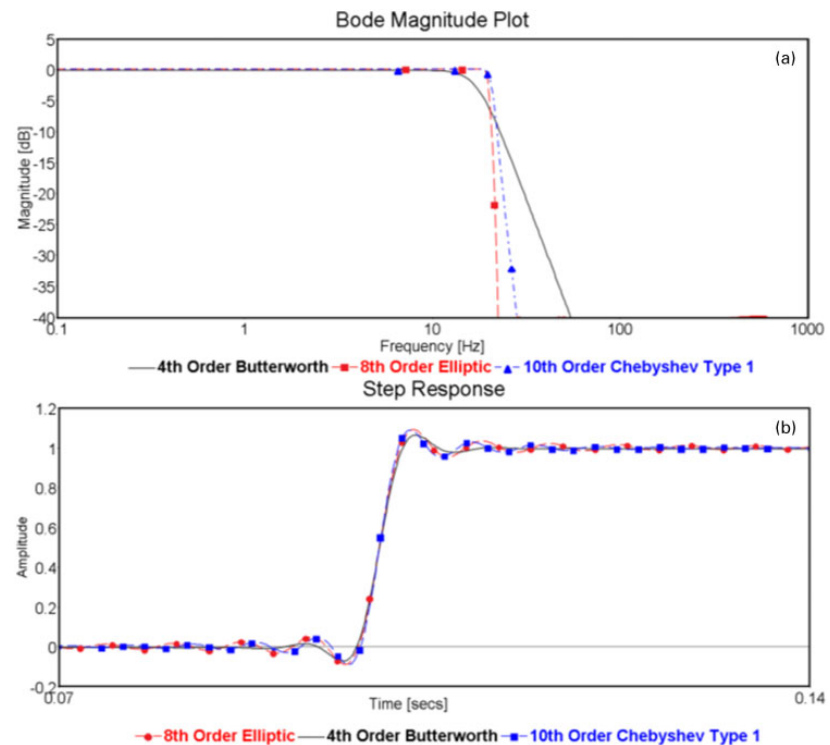
Table 1 Frequencies at which various Butterworth filters attenuate to -40 dB

Filter order	Frequency [Hz]
1	517
2	164
4	55
8	31

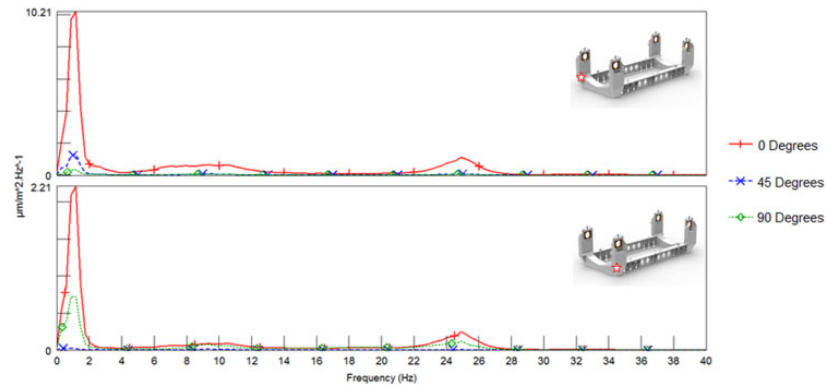
Cummings et al. Filtering and analysis of accelerations and strains



3 Filters designed to minimise time domain ringing



4 Filters designed to maximise rolloff rate



5 Example strain PSDs

and a linear average was calculated to improve their statistical properties.^{21–23}

Strain PSDs

The strain PSDs did not contain any spectral information of significance above 40 Hz, so a frequency range of 0–40 Hz was plotted. The strain PSDs were all very similar, so here an example is provided from each leg of the strain gauge rosettes from two of the welded joints (Fig. 5). Each channel exhibited similar spectral signatures; the energy is distributed in three distinct frequency bands: 0–4 Hz, 4–16 Hz and 19–29 Hz.

Acceleration PSDs

The acceleration PSDs from the tie down system were found to have similar spectral content. However, a comparison between these and the wagon bed and bogie showed differences in the PSDs. There were also differences between the lateral, vertical and longitudinal channels at each location.

The acceleration levels from the wagon bed were higher than that measured on the tie down system. The highest overall accelerations were measured at the bogie, which has a broadband spectrum that is dominated by vertical vibration energy. The difference between the overall magnitude and area under the PSD curves at the bogie and wagon bed shows how much of the vibration

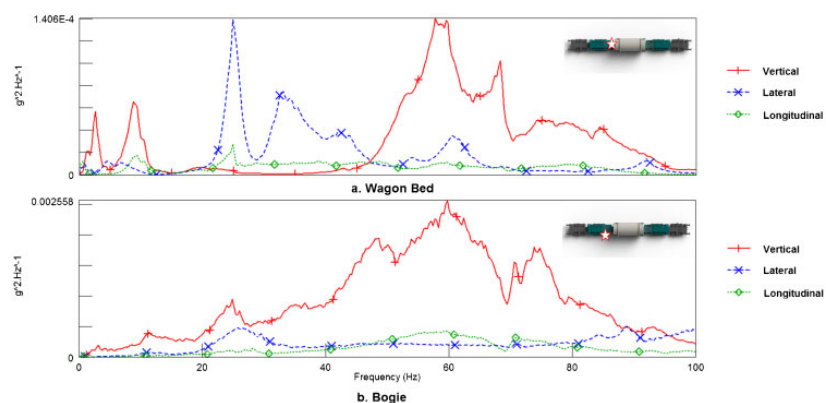
energy is attenuated by the rail vehicle suspension system, which acts as a mechanical filter (Fig. 6).

The equivalence or similarity of the acceleration PSDs at many of the locations on the tie down allowed for data reduction. The lid end accelerations have been omitted, concentrating on the slightly higher base end data. Only one of the stanchions spectra were identical.

Accelerometers from the wagon bed, the stanchion and the saddle, have been selected for comparison (Fig. 7). The wagon bed accelerometer has been included in the selection since this provides the best location to determine what relative motion occurs between the base of the tie down system and its stanchions.

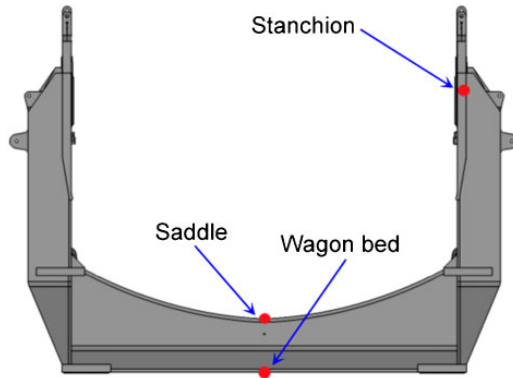
Vertical acceleration PSDs at wagon bed and tie down system

The vertical acceleration PSDs for the three accelerometers are shown (Fig. 8a). At frequencies <math><40</math> Hz, three peaks are present between 0–4 Hz, 4–16 Hz and 19–29 Hz; these frequency bands match those in the strain PSDs. At frequencies <math><40</math> Hz, the energy is marginally higher at the stanchion than at the wagon bed or saddle. Above 40 Hz, the vibration intensity is much higher at the wagon bed and saddle than it is at the stanchion.



a wagon bed; b bogie

6 Acceleration PSDs



7 Accelerometers selected for detailed analysis

Lateral acceleration PSDs at wagon bed and tie down system

The lateral acceleration PSDs for the three accelerometers are shown (Fig. 8b). Below 30 Hz peaks occur at the same frequency bands: 0–4 Hz, 4–16 Hz and 19–29 Hz. There are, however, some subtle changes in the vibration signatures.

Below 20 Hz, the stanchion vibration intensity is marginally higher than the wagon bed and saddle. Above 20 Hz, the energy levels at the stanchion are significantly reduced, whereas at the wagon bed and saddle they increase. There is also a significant peak at 25 Hz at the wagon bed and saddle, which is not present in the stanchion PSD.

Longitudinal acceleration PSDs at wagon bed and tie down system

The longitudinal acceleration PSDs for the three accelerometers are shown (Fig. 8c). Their overall vibration level is much lower than in the vertical and lateral directions. Three small peaks are evident at 9.5, 25 and

48 Hz. The energy level is very low at the stanchion across the whole frequency range with marginally higher levels of vibration existing at the wagon bed and saddle.

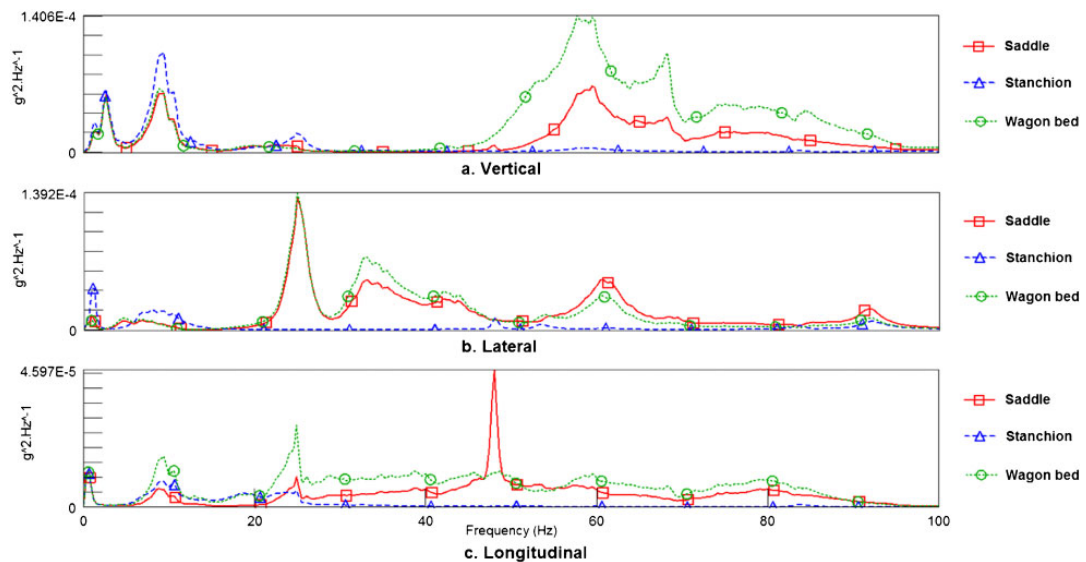
Estimating filter cutoff frequency from displacement PSDs

A method for obtaining a suitable filter cutoff frequency has been devised by comparing PSDs at the stanchion and wagon bed. The acceleration PSDs were integrated twice in the frequency domain to produce displacement PSDs. As the purpose of the filter is to obtain quasi-static loads for structural design, displacements PSDs were considered to be more closely related to structural stress and strain than accelerations. Since the standard approach used in tie down system design is to apply the loading to the centre of mass of the package, it is postulated that the cutoff frequency can be determined as the frequency at which the PSDs become lower at the stanchion than those at the wagon bed. As a first approximation, three potential cutoff frequencies have been identified from the PSDs (Figs. 9–11; Table 2). These are similar to the filter cutoff frequency recommended in Ref. 7.

Trends observed in statistics of acceleration extrema

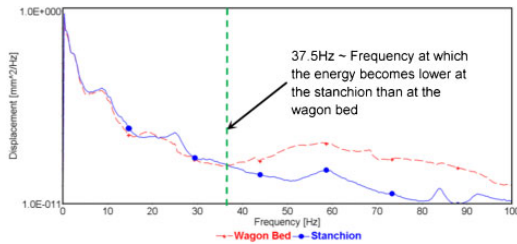
Using the filter cutoff frequencies from Table 2 and selecting a 4th order, forward-backward, Butterworth filter, the wagon bed and stanchion time history records have been filtered and the resulting signals have been compared. Three comparative filtering studies have been conducted on the signals by:

- (i) low pass filtering with a cutoff frequency of 100 Hz.
- (ii) low pass filtering with the cutoff frequencies from Table 2.
- (iii) band pass filtering, where the lower cutoff frequencies have been taken from Table 2 and the upper cutoff frequency was set to 100 Hz.



a vertical; b lateral; c longitudinal

8 Power spectral densities of acceleration time history



9 Vertical displacement PSD from wagon bed and stanchion

Some statistics from the resulting time histories are presented (Tables 3–5).

On the wagon bed, the largest peak acceleration of -0.87 g (highlighted with a red circle) was measured in the vertical direction (Table 3). The signal is shown in a close-up of this peak, and the low pass and band pass filtered signals are also shown for comparison (Fig. 12). It is evident that the peak is a high frequency oscillation. To understand how this peak transmits through the package, a similar figure has been created for the stanchion time history during the corresponding time period (Fig. 13). Following the trend identified by Cummings *et al.*,⁴ the overall level of acceleration is lower at the stanchions than the wagon bed (Figs. 12a and 13a), and the low frequency content is similar at the wagon bed and stanchions (Figs. 12b and 13b). The peaks in Figs. 12 and 13 are summarised in Table 6.

The high frequency peaks measured at the wagon bed have been attenuated by an order of magnitude at the stanchions, from -0.79 to -0.02 g (Figs. 12c and 13c). These results are emphasised in overlaid time history plots of the peak at both the stanchion and wagon bed (Fig. 14). Figure 14a is low pass filtered at 37.5 Hz, and

Table 2 Possible filter cutoff frequencies

	Longitudinal	Lateral	Vertical
Frequency [Hz]	20	15.5	37.5

Table 3 Statistics of acceleration signals low pass filtered at 100 Hz

	Wagon bed [g]			Stanchion [g]		
	rms	Max.	Min.	rms	Max.	Min.
Longitudinal	0.03	0.31	-0.43	0.02	0.12	-0.32
Vertical	0.07	0.78	-0.87	0.04	0.26	-0.32
Lateral	0.05	0.57	-0.56	0.03	0.22	-0.18

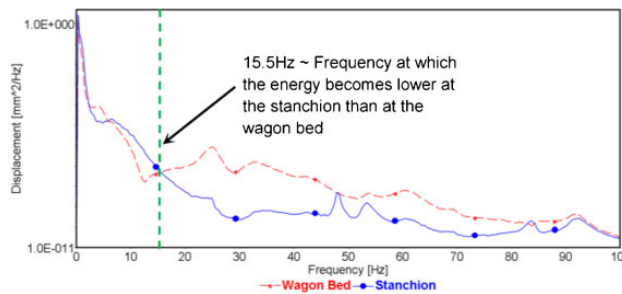
Table 4 Statistics of acceleration signals low pass filtered at cutoff frequencies from Table 2

	Wagon bed [g]			Stanchion [g]		
	rms	Max.	Min.	rms	Max.	Min.
Longitudinal	0.02	0.12	-0.12	0.01	0.09	-0.11
Vertical	0.03	0.22	-0.19	0.04	0.23	-0.31
Lateral	0.02	0.11	-0.15	0.02	0.16	-0.16

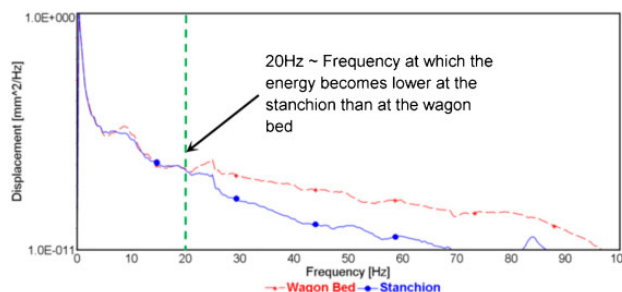
Fig. 14b is band pass filtered between 37.5 and 100 Hz. It is evident that the signals are in phase and therefore at low frequency, a state of near rigid body motion exists.

Sensitivity of acceleration extrema due to filter design

For this part of the study the triaxial accelerations measured by accelerometer N at the base end stanchion have been used. This accelerometer was chosen because it was closest to the centre of mass of the package.

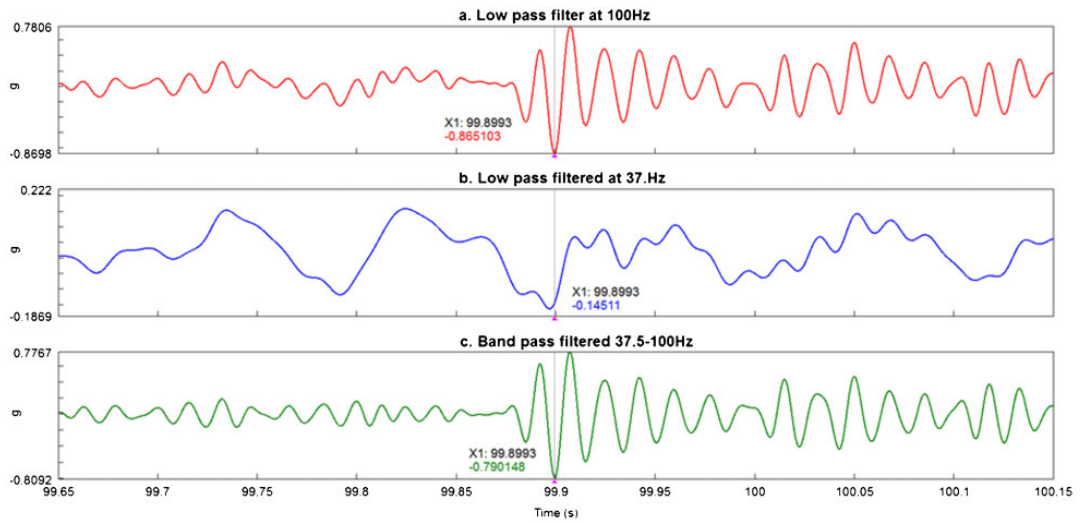


10 Lateral displacement PSD from wagon bed and stanchion

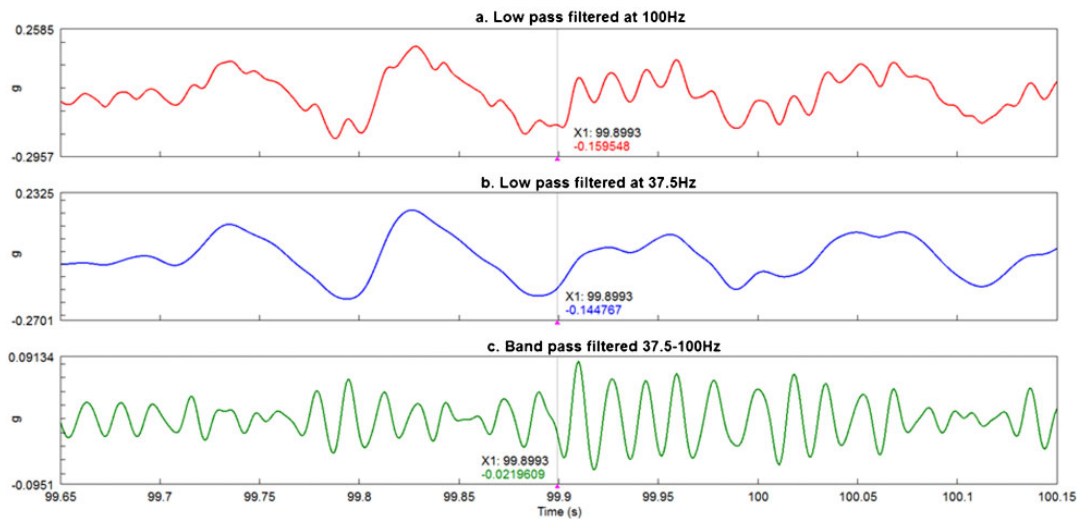


11 Longitudinal displacement PSD from wagon bed and stanchion

Cummings et al. Filtering and analysis of accelerations and strains



a low pass filtered at 100 Hz; b low pass filtered at 37.5 Hz; c band pass filtered at 37.5–100 Hz
 12 Peak vertical acceleration measured at wagon bed



a low pass filtered at 100 Hz; b low pass filtered at 37.5 Hz; c band pass filtered at 37.5–100 Hz
 13 Vertical acceleration corresponding to wagon bed peak at stanchion

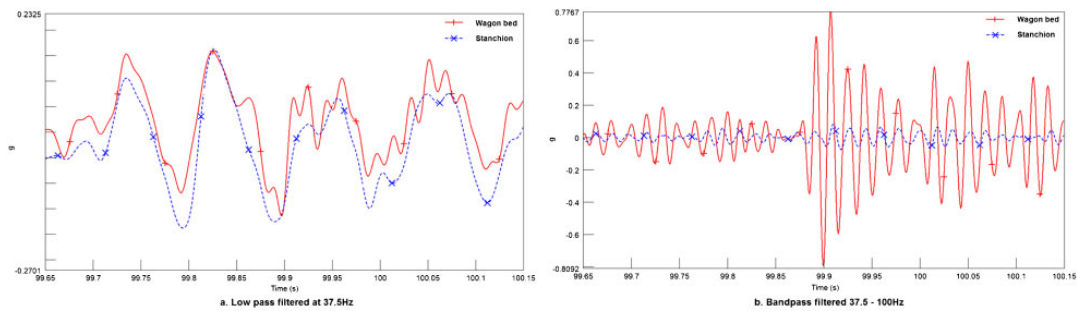
Table 5 Statistics of acceleration signals band pass filtered, lower cutoff frequencies from Table 2 and upper cutoff frequency of 100 Hz

	Wagon bed/g			Stanchion/g		
	rms	Max.	Min.	rms	Max.	Min.
Longitudinal	0.03	0.33	-0.37	0.01	0.17	-0.25
Vertical	0.06	0.78	-0.81	0.01	0.09	-0.10
Lateral	0.04	0.54	-0.56	0.01	0.14	-0.16

To assess the sensitivity of the acceleration extrema, the filter cutoff frequency was set to 17.5 Hz. The signals were first filtered with a 4th order, forward-backward, low pass Butterworth filter (Figs. 3 and 4). Four other forward-backward, low pass filters were also used to compare the effects of filter rolloff rates and time domain ringing on the extrema. To minimise time domain ringing, a second order Chebyshev type 1 and a second order elliptic filter were selected (Fig. 3). To maximise rolloff rate, a 10th order Chebyshev type 1 and

Table 6 Transmission of peak vertical acceleration from wagon bed into package

	Low pass (100 Hz)	Low pass (37 Hz)	Band pass (37.5–100 Hz)
Wagon bed/g	-0.87	-0.15	-0.79
Stanchion/g	-0.16	-0.14	-0.02



a low pass filtered at 37.5 Hz; b band pass filtered 37.5–100 Hz

14 Filtered peak vertical acceleration measured at stanchion and wagon bed

an 8th order elliptic filter were selected (Fig. 4). The allowable passband ripple of all the Chebyshev and elliptic filters was set to -0.0001 dB, which tends towards a flat passband response at the expense of rolloff rate. The poorer rolloff rate is particularly prominent in the lower order Chebyshev and elliptic filters. The elliptic filters stopband attenuation was set to a minimum of -40 dB.

The results of the two studies using Chebyshev type 1 and elliptic filters are provided for comparison with those from the 4th order Butterworth filter (Tables 7–9). The statistics in Tables 7–9 provide some clues about the distributions that the data sets produce. They also show some discrepancy between the lower order filters designed to minimise time domain ringing and the higher order filters designed to maximise rolloff rate.

To understand the likelihood of seeing larger peaks, histograms were constructed from the various filtered signals by carrying out a level crossing analysis. A level crossing analysis is used to count the number of occasions a signal exceeds a given level.²⁴ By setting intervals and counting the number of crossings within each interval, a histogram of the results is obtained. The level crossing histogram is often a precursor for probabilistic analysis on extreme values.^{22–25}

An example of all the lateral acceleration histograms is shown in Fig. 15. The abscissa of the histograms is set to the range of -0.165 to 0.165 , and the ordinate shows the number of crossings. It is evident that the shape and size of the histograms due to the higher order filtered signals are all similar, but those due to the lower order filtered signals are significantly different. In particular, the number of

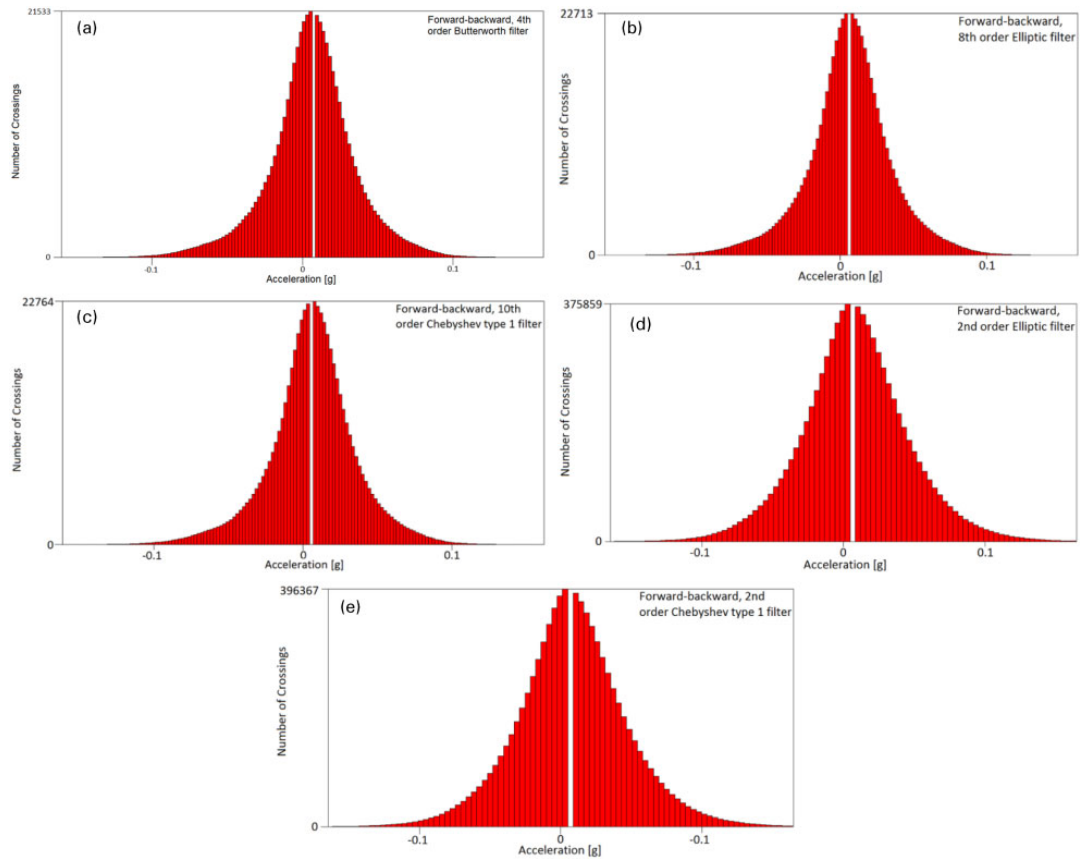
Table 7 Statistics of filtered lateral accelerations

Filter designed to maximise rolloff rate				
Filter type	Mean [g]	SD	Min [g]	Max [g]
Fourth order Butterworth	0.0065	0.0213	-0.1590	0.1590
Eighth order elliptic	0.0065	0.0214	-0.1595	0.1612
Tenth order Chebyshev type 1	0.0064	0.0214	-0.1604	0.1609
Filter designed to minimise time domain ringing				
Filter type	Mean [g]	SD	Min [g]	Max [g]
Fourth order Butterworth	0.0065	0.0213	-0.1590	0.1590
Second order elliptic	0.0065	0.0283	-0.2692	0.2713
Second order Chebyshev type 1	0.0065	0.0289	-0.2817	0.2840

Table 8 Statistics of filtered vertical accelerations

Filter designed to maximise rolloff rate				
Filter type	Mean [g]	SD	Min [g]	Max [g]
Fourth order Butterworth	-0.0195	0.0259	-0.2434	0.2086
Eighth order elliptic	-0.0195	0.0262	-0.2540	0.2189
Tenth order Chebyshev type 1	-0.0194	0.0264	-0.2605	0.2190
Filter designed to minimise time domain ringing				
Filter type	Mean [g]	SD	Min [g]	Max [g]
Fourth order Butterworth	-0.0195	0.0259	-0.2434	0.2086
Second order elliptic	-0.0195	0.0295	-0.3239	0.2702
Second order Chebyshev type 1	-0.0195	0.0295	-0.3242	0.2715

Cummings et al. Filtering and analysis of accelerations and strains



15 Level crossing histograms of lateral accelerations with various filters applied

crossings increases dramatically for the lower order filters because these filters allow far more of the lower amplitude content of the signal through the transition band.

The statistical properties of the higher order filtered signals were very similar and comparable to the results from the 4th order Butterworth filter. The lower order filters produced vastly different histograms due to the leaky nature of the filters in the frequency domain (Fig. 3). This demonstrates the importance of a high rolloff rate and shows that some overshoot and ringing in the time domain is permissible.

In all cases, the distributions indicate clearly that peak accelerations occur rarely and the larger the peaks, the

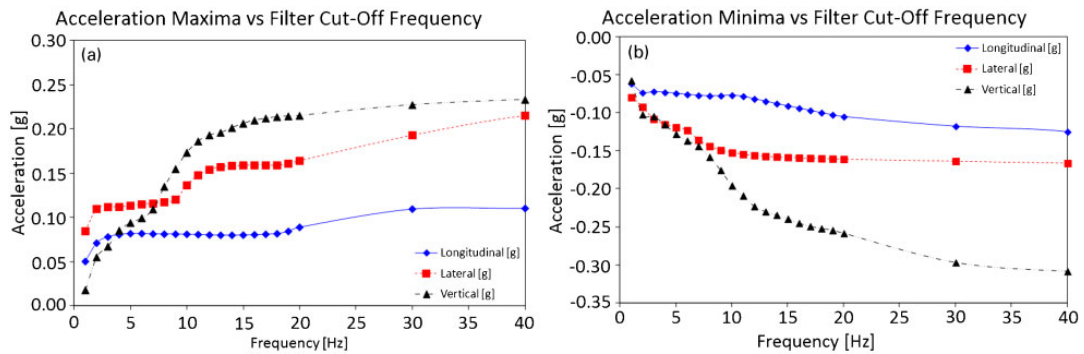
less likely they are to occur. This is because the tails of the distributions are exponentially decreasing; therefore, the likelihood of larger accelerations gets smaller as the peaks get larger.

Effect of filter cutoff frequency on acceleration extrema

This final part of the study was carried out using a low pass, forward-backward, 4th order Butterworth filter. The cutoff frequencies <4 Hz produced marginally stable filters but were adequate for the purposes of this assessment. The cutoff frequency was varied in increments of 1 Hz from

Table 9 Statistics of filtered longitudinal accelerations

Filter designed to maximise rolloff rate				
Filter type	Mean [g]	SD	Min [g]	Max [g]
Fourth order Butterworth	-0.0010	0.0106	-0.0932	0.0804
Eight order elliptic	-0.0010	0.0111	-0.0951	0.0816
Tenth order Chebyshev type 1	-0.0010	0.0114	-0.1051	0.0825
Filter designed to minimise time domain ringing				
Filter type	Mean [g]	SD	Min [g]	Max [g]
Fourth order Butterworth	-0.0010	0.0106	-0.0932	0.0804
Second order elliptic	-0.0010	0.0132	-0.4091	0.2130
Second order Chebyshev type 1	-0.0010	0.0132	-0.4134	0.2247



16 Acceleration extrema versus filter cutoff frequency

1–20 Hz and then in increments of 10 Hz from 20–100 Hz. The resulting acceleration extrema showed an increasing trend as the filter cutoff frequency increased (Table 10).

The trend in the extrema is not linear, and no simple mathematical relation exists between cutoff frequency and acceleration peaks. In general, the difference between extrema of the low pass filtered signals between 10–20 Hz is small and the largest changes observed are in the vertical minima (Fig. 16).

Discussion and conclusions

Frequency analysis

The high frequency oscillations (>25 Hz) of the wagon bed are attenuated at the stanchions by the large package mass, which does not have time to respond to the motion due to inertia. The energy at the wagon bed

in the lateral and vertical acceleration PSDs appears to be the cause of the peak at 25 Hz in the strain PSDs. If a tie down design was produced using reduced accelerations factors compared with current guidance material, this could influence fatigue life due to the larger number of cycles that occur at high frequencies. It should be noted that no fatigue damage was calculated from any of the measured strain channels for this tie down system.

In general, the loading expected to affect tie down system design is low frequency, i.e. <25 Hz. Two main frequency ranges of interest were identified, between 0–4 Hz and 4–16 Hz. In the range of 0–4 Hz, the strain peak was quite pronounced and corresponded with both lateral and vertical accelerations. In the range of 4–16 Hz, there was no distinct peak in the strain PSD, just marginally higher spectral content. The acceleration PSDs differed; the vertical PSD exhibited a distinct

Table 10 Acceleration extrema due to different filter cutoff frequencies*

Stanchion	Vertical [g]		Lateral [g]		Longitudinal [g]	
	Max.	Min.	Max.	Min.	Max.	Min.
1	0.018	-0.058	0.085	-0.080	0.050	-0.062
2	0.055	-0.102	0.110	-0.093	0.071	-0.074
3	0.067	-0.105	0.112	-0.108	0.078	-0.072
4	0.085	-0.115	0.112	-0.115	0.081	-0.073
5	0.094	-0.128	0.113	-0.119	0.082	-0.075
6	0.099	-0.137	0.115	-0.123	0.082	-0.076
7	0.109	-0.144	0.116	-0.136	0.081	-0.077
8	0.135	-0.158	0.117	-0.144	0.081	-0.078
9	0.155	-0.176	0.120	-0.149	0.081	-0.078
10	0.173	-0.196	0.136	-0.152	0.081	-0.077
11	0.186	-0.209	0.148	-0.155	0.081	-0.079
12	0.193	-0.223	0.154	-0.156	0.080	-0.082
13	0.196	-0.230	0.157	-0.157	0.080	-0.085
14	0.201	-0.234	0.158	-0.158	0.080	-0.088
15	0.206	-0.239	0.159	-0.159	0.080	-0.091
16	0.210	-0.245	0.159	-0.159	0.081	-0.094
17	0.212	-0.249	0.159	-0.160	0.081	-0.097
18	0.213	-0.252	0.159	-0.160	0.082	-0.100
19	0.214	-0.254	0.161	-0.161	0.084	-0.103
20	0.215	-0.258	0.164	-0.161	0.089	-0.105
30	0.227	-0.297	0.193	-0.164	0.110	-0.118
40	0.233	-0.308	0.215	-0.166	0.110	-0.125
50	0.237	-0.312	0.225	-0.168	0.112	-0.149
60	0.248	-0.315	0.223	-0.172	0.114	-0.181
70	0.254	-0.317	0.217	-0.175	0.115	-0.217
80	0.256	-0.318	0.214	-0.178	0.117	-0.253
90	0.257	-0.319	0.217	-0.181	0.121	-0.287
100	0.258	-0.320	0.225	-0.184	0.123	-0.316

*The International Atomic Energy Agency Advisory Material⁷ states a frequency range of 10–20 Hz to use as a cutoff frequency relative to defining quasi-static loads.

peak, while the lateral PSD displayed a band of increased energy, similar to the strains.

Filter design

Throughout the study, different filters and their characteristics have been assessed to ensure the robustness of the analysis. When designing a filter to obtain quasi-static accelerations where the main concern is preserving the acceleration extrema, the results showed that the rolloff rate of the filter was the most influential characteristic. For this reason, when applying higher order, forward-backward filters, the resulting signals all possessed similar statistical properties, but for second order filters, the statistical properties differed.

An estimate of the filter cutoff frequency was based on the postulate that the frequency at which the energy levels at the stanchion fall below those at the wagon bed is the most suitable to use as a cutoff frequency. This is logical since current design practice of tie down systems is to apply loads at the centre of mass of the package. The results also suggested that the cutoff frequencies were, in general, close to those suggested in the advisory material.⁷ As this method is not directly based on the natural frequencies of the tie down system and package, it is not necessarily the most accurate way of separating quasi-static content from the signals.

Peak analysis

Comparing the quasi-static acceleration factors quoted in the advisory material to the results of this study from the stanchion accelerometer highlights two main differences.⁷ The measured accelerations are quoted as approximate as their actual value depends on which filter is used:

- (i) the longitudinal acceleration factor of 1g for dedicated movements with special rail wagons is an order of magnitude higher than those measured ($\approx 0.1g$).
- (ii) the lateral acceleration factor of 0.5g is also considerably larger than the measured accelerations ($\approx 0.16g$).

The vertical acceleration factor of $1 \pm 0.3g$, where 1g is assumed to be the force of gravity, appears to agree with the measured accelerations (downwards $\approx 0.26g$ and upwards $\approx 0.22g$). A summary of this comparison is shown in Table 11.

The quasi-static accelerations at the wagon bed were similar to those at the stanchion, and the signals were in phase. However, the acceleration peaks at the wagon bed at higher frequencies were much larger.

The level crossing histograms are approximately bell shaped, but an attempt to achieve a good fit to several statistical distributions failed. From their shape, the histograms exhibit an exponentially decaying process, and therefore, the likelihood of higher accelerations peaks is small.

Table 11 Comparison of measured versus advisory acceleration factors

	TS-G-1 (Table IV.2)/g	Measured/g
Lateral	0.5	0.16
Longitudinal	1.0	0.1
Vertical	1.0 ± 0.3	0.22 (U) 0.26 (D)

It is acknowledged that the data set examined is limited due to the length of journey and relatively low vehicle speed; however, this is representative of a real routine journey by rail in the UK. The results indicate that there are very large margins of safety between current design parameters and the actual strains and accelerations measured during this test. In conclusion, the current acceleration factors for routine conditions of transport used for the design of tie down systems for heavy packages are adequate and appear to be conservative.

Further work

If the design parameters for tie down system designs for heavy packages were lowered based on the results presented here, then an investigation into fatigue loading on tie down systems would become necessary. Filtered accelerations may not be appropriate as the fatigue life would depend not only on the quasi-static loading but also on the residual vibratory and shock loading. To optimise package and tie down system design, which has many benefits to the future of the nuclear transport industry, the expected fatigue life of auxiliary equipment needs to be fully understood. This is particularly true in the UK where rail gauge constraints place limitations on the rail wagon design, which severely restrict the size of tie down systems.

A better method to separate quasi-static loading would also be beneficial. The underlying process of the quasi-static loading is likely to be attributed to rail curvature and undulation and vehicle speed and manoeuvres. The residual shock and vibratory processes that occur during routine conditions of transport would depend more on the vehicle suspension, the wheel/track interface and track irregularities. The track irregularities could be considered as superimposed on the curvature and undulating profile of the rail, which is largely responsible for the quasi-static response. It may be possible to extract improved acceleration data for tie down system design by careful modelling of these characteristics of the rail environment. This would also assist in understanding the variation in accelerations that arise when nuclear packages of different masses and geometric configurations are transported by rail, thereby allowing for the selection of design parameters to suit a particular tie down system and package configuration.

Using modern computer modelling, a parametric study of package mass, vehicle running speed and tie down system stiffness, in conjunction with a measurement programme for validation, would allow for a more scientific basis for revising existing design criteria.

References

1. S. Fourgeaud, G. Sert, K. Ben Ouaghrem and I. Le Bars: 'External loads applied to packages during routine transport', in 'Packaging, transport, storage and security of radioactive material', Vol. 22, No. 2, 99-103; 2011, Maney Publishing, UK.
2. P. Purcell: 'Designing tie-down system for heavy RAM packages—should revised design criteria apply?'; 2010, PATRAM, UK.
3. B. Desnoyers: 'Stowage and retention of radioactive packages during transport: which rules should be acceptable?'; 2012, TN International, AREVA Logistics Business Unit – Transport Oversight Division, RAMTRANS, France.
4. A. D. Cummings, J. Krywonos, P. Purcell, G. Rothwell and R. English: 'An experimental procedure for measuring accelerations and strains from a tie down system of a heavy nuclear transport package during a rail journey', in 'Packaging, transport, storage and

- security of radioactive material', Vol. 23, No. 3; 2013, Maney Publishing, UK.
5. BS EN 15433-3: 'Transportation loads—measurement and evaluation of dynamic mechanical loads—part 3: data validity check and data editing for evaluation'.
 6. K. B. Smith and W. C. Shust: 'Bounding natural frequencies in structures I: gross geometry, material and boundary conditions', 2004 IMAC-XXII: Conference & Exposition on Structural Dynamics Southwest Research Institute; Objective Engineers, US.
 7. TS-G-1: 'Advisory material for the IAEA regulations for the safe transport of radioactive material', 2008, Rev1.
 8. R. D. Cook, D. S. Malkus, M. E. Plesha and R. J. Witt: 'Concepts and applications of finite element analysis', 4th edn; 2002, John Wiley and Sons Ltd, US.
 9. D. Hitchings: 'A finite element dynamics primer'; 1992, NAFEMS, UK.
 10. S. Iwnicki: 'Handbook of railway vehicle dynamics'; 2006, Taylor and Francis Group, UK.
 11. R. J. Scavusso and H. C. Pusey: 'Naval shock analysis and design', 5th edn; 2009, The Shock and Vibration Information Analysis Centre HI-TEST Laboratories, Inc, US.
 12. N. Jones: 'Structural Impact'; 2003, Cambridge University Press, UK.
 13. R. Bartholomew: 'Cargo response to rail car impact tie-down load analysis'; 1978, Los Alamos Scientific Laboratory, US.
 14. S. R. Fields: 'Dynamic analysis to establish normal shock and vibration environments experienced by radioactive shipping packages', Quarterly Report, NUREG/CR-2146, NEDL-TME 81-15, Hanford Engineering Laboratory, 1980, US.
 15. M. A. Elbestawi and D. F. Lau: 'Irradiated fuel shock and vibration environment during off-site transportation'; 1983, Ontario Hydro Reserach Division, US.
 16. J. Read, S. Owen and C.-F. Tso: 'Tie-down assessment of radioactive material packages on conveyances: approach to competent authority approval applications in accordance with TS-R-1 (July 2004) and TS-G-1:1 (June 2002)', Vol. 16, No. 2, 109-124; 2005, Ramtrans Publishing, UK.
 17. A. Brandt: 'Noise and vibration analysis – signal analysis and experimental procedures'; 1st edn; 2011, John Wiley and Sons Ltd, Denmark.
 18. R. Allred: 'Digital filters for everyone'; 2010, Creative Arts and Sciences House, US.
 19. S. Smith: 'The scientists and engineers guide to digital signals processing', 1st edn; 1997, California Technical Publishing, US.
 20. F. Kihm: 'How to choose between Butterworth and fast Fourier filters?'; 2005, nCode International, UK.
 21. P. H. Wirsching, T. L. Paez and K. Ortiz: 'Random vibrations – theory and practice'; 1995, Dover Publications, US.
 22. D. E. Newland: 'An introduction to random vibrations, spectral and wavelet analysis', 3rd edn; 2005, Dover Publications, US.
 23. J. S. Bendat and A. G. Piersol: 'Random data—analysis and measurement procedures', 4th edn; 2010, New York, Wiley Series in Probability and Statistics, US.
 24. S. O. Rice: 'Mathematical analysis of random noise', *Bell Syst. Tech. J.*, 1944-1945, **23**, 282-332.
 25. S. Krenk, H. O. Madsen and N. C. Lind: 'Methods of structural safety'; 2006, Dover Publications, US.

Publisher - Journal of Rail and Rapid Transit

How well does a Linear Static Finite Element Analysis Predict Measured Strains from a Nuclear Package Tie Down System during Rail Transportation?

Journal Title
 XX(X):1-13
 ©The Author(s) 2015
 Reprints and permission:
 sagepub.co.uk/journalsPermissions.nav
 DOI: 10.1177/ToBeAssigned
 www.sagepub.com/


Andrew Cummings¹, Dr. Glynn Rothwell² and Dr. Christian Matthews²

Abstract

Freight rail is often the preferred method for transportation of dangerous goods. One particular application is the use of rail to convey radioactive material in purpose built packages. During transit, packages are secured to a rail wagon bed with a tie down system. The design of tie down systems vary considerably depending on package type and rail vehicle, for example shackles, turnbuckles, tie-rods, gravity wells or transport frames are all commonly used. There are also a large number of different packages in existence that all vary in size and mass; typically 1 - 7 m in length and 100 kg - 100 tonnes in mass. Despite the uniqueness of many transport configurations the design of tie down systems is always carried out using a limited set of design load cases as defined in the appropriate Codes of Practice and Standards. Many authors have suggested that the load cases within the standards need revision or question which load cases should apply to which scenario.

In a previous experiment accelerations and strains have been measured on a freight wagon and transport frame of a heavy package during a routine rail journey. From these data new insight into the magnitude and nature of loading has been gained.

In the present study the measured accelerations have been used as input to a Finite Element Model (FEM) of the transport frame and a method based on correlation between predicted and measured strains has been developed to determine an appropriate low pass filter cutoff frequency, f_c , which separates quasi-static loading from raw dynamic data. The residual dynamic measurements have been assessed using signals processing techniques to understand their significance. The FEM has also been used to assess the presence of contact and boundary nonlinearities and how they affect the agreement between measured and predicted strains.

Keywords

Tie down system, package, acceleration, strain, rail

Introduction

The conventional safety record for transport of heavy packages by rail is very good with very few incidents or accidents reported. One important aspect of achieving and maintaining this level of safety is the thorough design of tie down systems.

A broad spectrum of load cases due to the transportation environment are addressed during the development phase. Tie downs are required to withstand everyday operational usage including package loading/unloading, lifting, tilting and loads that arise during transportation. These requirements are satisfied by designing the system to possess sufficient strength.

The cyclic nature of the loads and the dynamic transportation loads require that the system also possesses sufficient fatigue resistance. Additionally, in the event of an accident the tie down system must not damage the package in such a way that impairs its safety. This requirement has led to the design of weak links in some tie downs, ensuring that in an impact accident condition the package safety is not compromised.

Cummings *et al*¹ described methods for filtering measured accelerations during a rail journey of a 99.7 tonne nuclear package. They estimated quasi-static accelerations for comparison with the current design parameters. In the present study dynamic acceleration and strain data is systematically passed through a low pass filter, whilst varying its cutoff frequency between 1 Hz - 100 Hz. The filtered tri-axial acceleration time histories are used to scale the results of a linear static Finite Element Model (FEM) at specific elements in the model corresponding to strain gauge locations. The scaled vertical, lateral and longitudinal accelerations are then summed to calculate strain time histories. The calculated strain time histories are compared with actual measurements.

¹International Nuclear Services

²Liverpool John Moores University

Corresponding author:

Andrew Cummings, International Nuclear Services Hinton House, Birchwood Park Avenue, Risley, Warrington, WA3 6GR, UK.
 Email: andrew.cummings@innuserv.co.uk

A linear mathematical model has been used to predict the response of the tie down to the transportation loading. By studying correlation between measured and predicted strains it is possible to assess the limits of such a model and establish when the response of the tie-down is no longer linear. A successfully validated computer model has several key benefits:

- (i) Safety margins based on experimental results can be quantified.
- (ii) Provides an opportunity to assess other areas of the structure where no measurements were taken.
- (iii) Improves interpretation of experimental results i.e. provides a justification for choice of filter cutoff frequency (f_c) to obtain loads for design.
- (iv) Presents the possibility of reconstructing acceleration time histories from the measured strains i.e. inversely determine tie down loading based on material response not structural motion.

A FEM of the tie down system has been constructed and its idealisation explained. Methods for simplifying the complex frame to package interface are emphasised. Linearisation of the interaction between contacting parts enables a scaling and superposition method to calculate strain time histories. This requires careful analysis to determine the validity or error caused by omitting nonlinear effects.

Correlation between measured accelerations and strains

For linear static analysis to be applicable a linear dependency between the measured accelerations and strains must exist. If the strains are linearly dependent on the accelerations then, in theory, they can be predicted using a suitable mathematical model which relates them.

The Pearson correlation coefficient (ρ) is calculated as follows:-

$$\rho = \frac{C_{xy}}{\sigma_x \sigma_y}$$

where:-

C_{xy} = Covariance between two random variables x and y

σ_x = Standard deviation of x

σ_y = Standard deviation of y

The correlation coefficient provides a measure of linear dependency between two sets of random data². When comparing acceleration and strain signals $\rho = \pm 1$ for perfect linear dependency and $\rho = 0$ when the strains and accelerations are independent of each other.

Assessing the Strength of the Correlation

Wirsching *et al*² provide guidance on interpreting intermediate values of ρ however it is useful to first highlight some of the sources of random error or noise that weaken correlation. In signals analysis the terminology "strength" or "weakness" indicate the degree of dependence between one signal and

another. Three main sources of error are proposed in **Figure 1**.

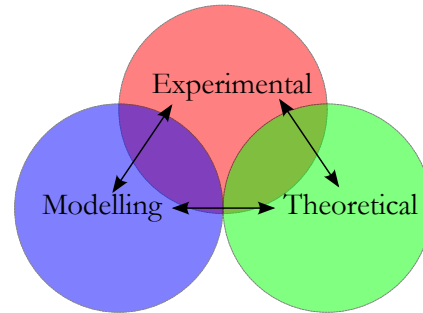


Figure 1. Sources of Error

When ρ deviates from ± 1 at least one or more of these sources are the cause of the weakened correlation. The total error can be described as follows:-

$$\epsilon_{total} = \epsilon_{experimental} + \epsilon_{modelling} + \epsilon_{theoretical}$$

Breaking down these sources of error further, to pinpoint root causes of weak correlation:-

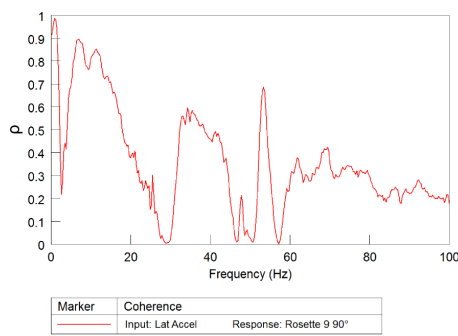
$$\begin{aligned} \epsilon_{experimental} &= \epsilon_{electrical} + \epsilon_{temperature} + \epsilon_{procedural} \\ \epsilon_{modelling} &= \epsilon_{modelling\ assumptions} + \epsilon_{numerical\ (rounding)} \\ \epsilon_{theoretical} &= \epsilon_{nonlinearities} + \epsilon_{dynamic\ effects} \end{aligned}$$

Each of these error sources consist of a number of different variables that degrade the strength of the correlation. Wirsching² suggests that if the total random error is $1/2$ the strength of the signal then $\rho \approx 0.9$ and the dependency between the signals is considered strong.

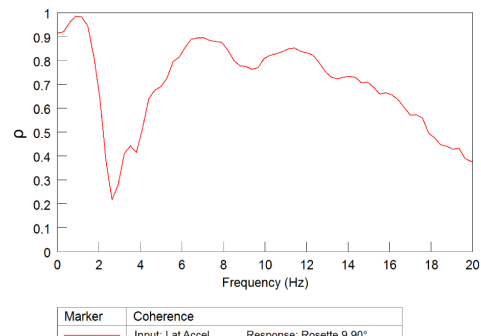
If the error is about the same strength as the signal then $\rho \approx 0.7$ and the dependency between the signals is considered moderate. When $\rho < 0.7$ this is an indication of weak dependence of strains on accelerations.

The Coherence function calculates the correlation coefficient across a range of frequencies for a given input and output time history or channel. Based on an examination of the magnitude and direction of each strain channel it was evident that the strain response was dominated by lateral loading. Therefore the coherence function for each strain channel was calculated using the lateral acceleration measurements from the tie down system base end stanchion as the input channel. **Figure 2a** shows an example of a coherence function with the frequency axis set to 0 - 100 Hz.

Figure 2b shows the same coherence plot between 0 - 20 Hz. This frequency range has been chosen because the anticipated quasi-static content of the signal is < 20 Hz. The coherence function shows that all the signals are at least moderately correlated between 0 - 2 Hz and 5 - 15 Hz. This suggests that a linear model is appropriate, at least for this frequency range.



(a) 0 - 100 Hz



(b) 0 - 20 Hz

Figure 2. Example of Coherence between Measured Acceleration and Strain

This simple coherence analysis treats the tie-down as a single input, single output system, however in reality there are multiple inputs that influence the output. Therefore, the combination of multi-axial accelerations, should increase the coherence in the 2 - 5 Hz range.

Data Cleansing

Data cleansing is a necessary process to make a comparison between calculated and measured peak strains. It is common practice to carry out some basic data cleansing normally to remove any DC offset and very low frequency content (drift) 3;4.

The acceleration data was visually examined and not corrected further. However it was observed that the strains were very low, close to the noise floor of the instrumentation in some cases. Because of this any small amount of drift and offset that is present is evident visually.

The drift present may be due to real physical loading such as thermal expansion. It may also be attributed to thermal errors, however this was minimised by the use of temperature compensated strain gauges 3. Where necessary an attempt to remove drift was made using 1st or 2nd order polynomial curves (Figure 3). The removal of drift does not affect correlation, it just allows better comparison of peaks.

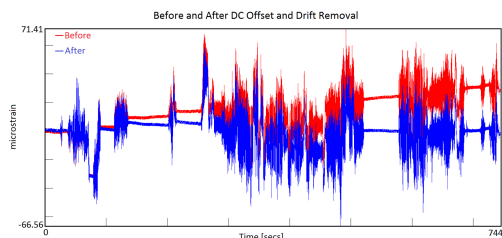


Figure 3. An Example of Data Cleansing used on some of the Measured Strain Time Histories

Prepared using sagej.cls

Tie Down System - General Arrangement

Figure 4 shows an exploded 3-D CAD model of the tie down system (inset is the assembled structure). The main structural members are the saddles, longitudinal beams and stanchions, all manufactured from high strength stainless steel plates and joined by welding. The trunnion bushes are made of a phosphor bronze (Figure 5).

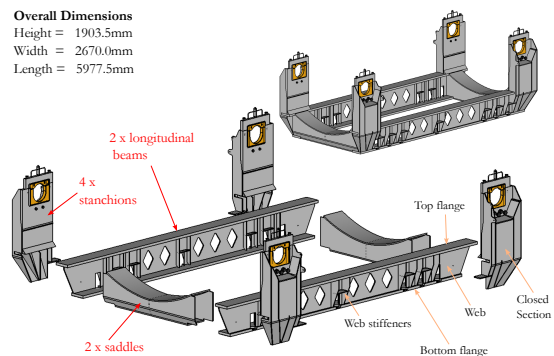


Figure 4. Details of the Tie Down System Construction

A mixture of partial and full penetration butt welds are used for joining the plates. Where possible the welds are double sided, however many closed sections exist and the welds are often, by necessity, single sided. Additionally due to its large size the welds are all manual and therefore stop/start sections are expected.

Figure 5 shows a close up of the package trunnion interface at the lid end stanchion of the tie down system. The trunnion bush is designed to allow ± 20 mm of longitudinal sliding due to package thermal expansion/contraction. This is an area of analytical complexity for two reasons. The first is that this area consists of many contacting parts (some omitted here for clarity). The second is the geometrical configuration of the stanchion which enforces modelling simplifications, often in areas that warrant detail.

For example the backing plate (Figure 5) is a compound section, consisting of a 50 mm thick section at the trunnion bushes, a tapered section and 15 mm thick section at its

base. The lateral restraint bolts combined with the irregular welded structure on the backing plate outward facing surface and the keep plates and their bolts are difficult to mesh with brick elements, but not suitable for shell element idealisation, therefore some modelling compromises are necessary.

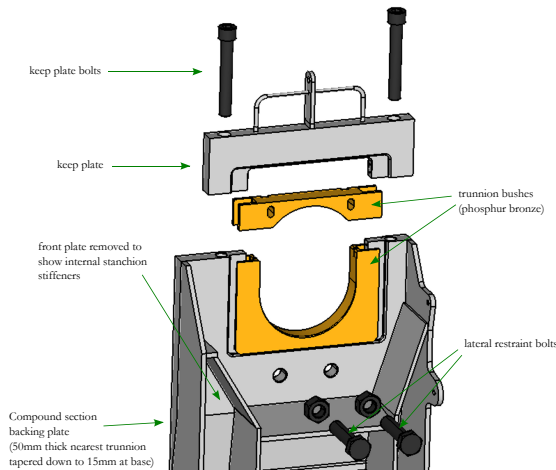


Figure 5. Detail of Lid End Trunnion Bushes and Upper Stanchion

The overarching compromise arises when connecting a hybrid shell and brick element mesh together. There is a disparity in nodal degrees of freedom between the two element types and the usual method of eliminating unwanted mechanisms due to this is by adding an extra row of shell elements "painted" over the surface of the connecting bricks. This method approximates load transfer across the joints but predicted stresses and strains at this type of interface are often in doubt.

Finite Element Model

The model was pre-processed using Hyperworks 12.0⁵. All solutions were obtained using the sparse, direct, linear solver in Abaqus 6.13⁶. **Figure 6** shows a wireframe view of the entire tie down system and a "dummy" package. As only limited information on the package was available it was modelled, excluding shock absorbers, with 4-noded tetrahedral elements and the density of the linear elastic material model was adjusted to obtain a mass of 99.7 tonnes.

Details of the finite element mesh of the tie down are shown in **Figure 7**. The mesh consists of a mixture of 8-node brick elements and 4-node shell elements (C3D8 and S4). To maintain good element shape a small number of wedge and triangular elements have been used. A total of 568,416 elements: 135,696 quadrilaterals, 108 triangles, 394,340 bricks and 258 wedges were used in the model.

A global element size of 15 mm was selected, although smaller elements were used in some areas to resolve intricate details properly.

The mesh of the trunnion interface has retained most of the original design detail however the keep plate bolts and wear plates beneath the sliding lid end trunnion bush have been omitted. The interacting parts have been meshed with a finer, solid element mesh (≈ 5 mm) this allows

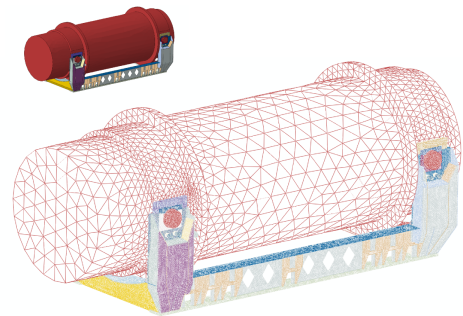


Figure 6. Finite Element Model of Tie Down System and Dummy Package (Shock Absorbers Omitted from Package)

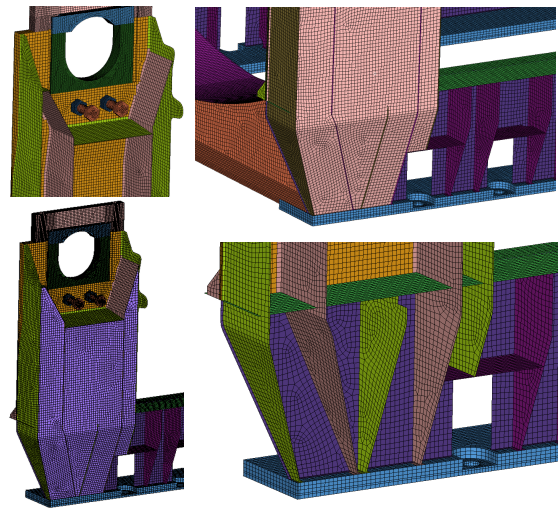


Figure 7. Details of Finite Element Mesh of Tie Down System

obvious definition of master and slave surfaces in nonlinear sensitivity studies. Included in the model are the lateral restraint bolts represented with solid elements; their threaded portions are modelled by merging the nodes at the interface between the bolts, nuts and the stanchion back plates. **Figure 8** shows the mesh of the lid end trunnion attachments and lateral restraint bolts.

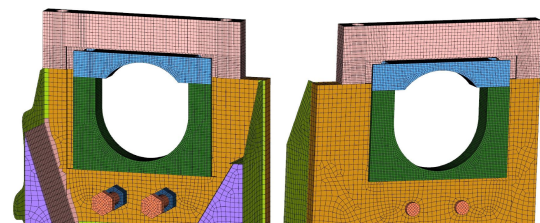


Figure 8. Finite Element Mesh of Lid End Trunnion Attachments and Restraint Bolts

Material	Grade	ρ [kg/m ³]	E [GPa]	ν	$\sigma_{0.2\%}$ [MPa]	References
High Strength Stainless Steel	S890Q	7,800	200	0.3	960	7
Phosphur Bronze		7,600	121	0.3	123	8
Carbon Bolt Steel	BS898	7,800	192	0.3	1100	9
	12.9					

Table 1. Material Properties applied to Finite Element Model

Materials Modelling

During the rail journey the tie down system was not subjected to loads sufficient to cause nonlinear material behaviour. Therefore in this model all the materials have been modelled with a linear elastic material model, the properties used are listed in Table 1 and the 0.2% yield stress is provided for reference.

Boundary Conditions and Loads

The package is mounted to the tie down system which is bolted to the rail wagon (Figure 9). The configuration of the rail wagon is an 8-axle wagon with four bogies connected to two sub frames with centre bowls and sidebearers. The subframes are connected to the superstructure with a centre pivot and sidebearers.

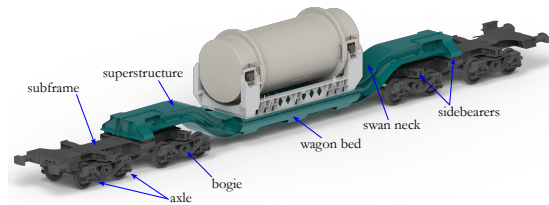


Figure 9. Major Components and Features of the Rail Wagon, Package and Tie-Down (Package Shock Absorbers removed for Clarity)

The tie down system is connected to the swan neck wagon bed with 14 x M45 bolts. To isolate the tie down from the wagon it is necessary to constrain the model to eliminate any rigid body motion. In this analysis the tie down bolts are omitted and the entire lower surface of the bottom flange of the longitudinal beams is constrained (Figure 10). This overconstrains the structure slightly but sensitivity analysis showed that alternative methods, such as constraining only the nodes at the bolt holes, produced minor differences in structural response.

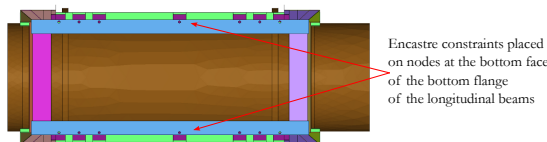


Figure 10. Boundary Conditions Applied to the Model

The unit load model was run in three uncoupled, linear perturbation steps, with a different load cases for each

step (Figure 11). Distributed loads were used to apply an acceleration of 1 g to the whole model in the lateral, longitudinal and vertical directions. A comparison of the total computation time for the model is shown for 1, 2, 4, 6 and 8 CPUs (Table 2).

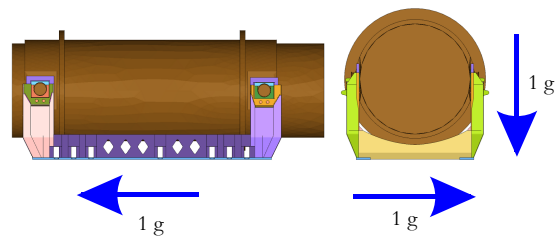


Figure 11. 3 x 1g Load Cases (Unit Loads)

CPUs	Wall Clock Time [min:secs]	RAM [Gbytes]
1	11:30	13
2	10: 5	13
4	9:28	13
6	8:47	13
8	8:48	13

Table 2. Run Times to Completion for Linear Model

Calculating Strain Time Histories

To obtain strain time histories a combination of scaling and superposition of the FEA results was used with the measured acceleration time histories as follows^{10,11}:-

$$\varepsilon_{ij}(t) = \sum_{k=1}^N \varepsilon_{(ij,k)} L_k(t)$$

$\varepsilon_{ij}(t)$ = the strain tensor at a time t
 $\varepsilon_{ij,k}$ = the strain tensor due to unit load
 $L_k(t)$ = the acceleration time history

where

k = lateral, vertical or longitudinal loading

Elements were selected that correspond to the measured strain locations and their strain tensors used in the scaling and superposition algorithm (**Figure 12**). This method accounts for multi-axial loading of the structure. A 30-minute section of the measurements during the journey were low pass filtered with a 4th order, forward-backward, Butterworth filter. Strain time histories were calculated using the filtered accelerations measured at the base end stanchion. This process was repeated for 28 different filter cut-off frequencies 1 Hz - 20 Hz in 1 Hz increments and 20 Hz - 100 Hz in 10 Hz increments. These calculations were carried out in nCode DesignLife¹².

Contact Modelling

Modelling the contacting parts has been achieved by either, meshing parts congruently and merging the nodes at the mating interfaces or by modelling with a contact pair, which is then "tied", effectively bonding the parts together and achieving the desired linearisation.

Both methods require several important assumptions to hold or they will produce inaccurate results due to load path variations caused by sliding between contacting surfaces. Sensitivity analysis has been carried out to confirm the validity and effect of the major assumptions. There is a lot of contact present between the parts of the tie down system, rail wagon and package; the two most important contact interactions for this study are now identified and discussed.

Contact at the Trunnion Attachments

There are several contacting parts in the trunnion attachments of the tie down system (**Figure 5**). The floating lid end trunnion bush could cause sliding and nonlinear geometric effects which may affect the strain results in the stanchions. A hand calculation, assuming a coefficient of friction $\mu = 0.35$ which is typical of steel to phosphur bronze contact, shows that an acceleration of 0.1 g would be enough to overcome friction, resulting in sliding of the trunnion bush. This could arise due to heavy braking or cornering at speed. Lateral sliding of the trunnion bush is prevented due to the lateral restraint bolts, however only frictional forces prevent the floating trunnion bush from sliding due to longitudinal loading.

Lateral Restraint Bolts

The lateral restraint bolts are fitted to the tie down system through threaded holes in the stanchion back plates. They are adjusted to make contact with the package prior to transportation and held in place with a locking nut. This will produce a small bearing stress between the package side wall and the end of the bolt shank. Under lateral loading a change in the load paths may occur, as one stanchion will bend away from the restraint bolts, causing them to experience a compressive force exerted by the package and transmitted through to the stanchion. The opposite stanchion will bend towards the package, therefore any bearing stress between the end of the restraint bolt and the package side wall will decrease or in the limiting case, contact will be lost, resulting in differences in stanchion stresses and strains under reversed loading.

Sensitivity Analysis

A preliminary review of the modelling assumptions and loading was carried out to assess the validity of the scaling and superposition approach. Low pass filtering of measured accelerations with a cutoff frequency of 20 Hz produced the following load ranges:-

$$\begin{aligned} \text{Lateral} &= [-0.16g, 0.16g] \\ \text{Longitudinal} &= [-0.11g, 0.09g] \\ \text{Vertical} &= [-0.26g, 0.22g] \text{ (excluding gravity)} \end{aligned}$$

Accelerations in the frequency range 0 - 100Hz, produced larger load ranges:-

$$\begin{aligned} \text{Lateral} &= [-0.18g, 0.23g] \\ \text{Longitudinal} &= [-0.32g, 0.12g] \\ \text{Vertical} &= [-0.32g, 0.26g] \text{ (excluding gravity)} \end{aligned}$$

In the frequency range 0 - 100 Hz the longitudinal accelerations are large enough to cause sliding of the trunnion bushes. In this paper it is postulated that these peak accelerations occur too rapidly to introduce noticeable nonlinearity in the response of the tie-down system. The lateral and vertical load ranges do not vary significantly with f_c , however, the lateral loading may be enough to cause contact loss between the package and restraint bolts.

In the following section FEA results are compared by reviewing stresses at elements corresponding to the strain gauge positions. These elements are called the virtual strain gauge rosettes (**Figure 12**).

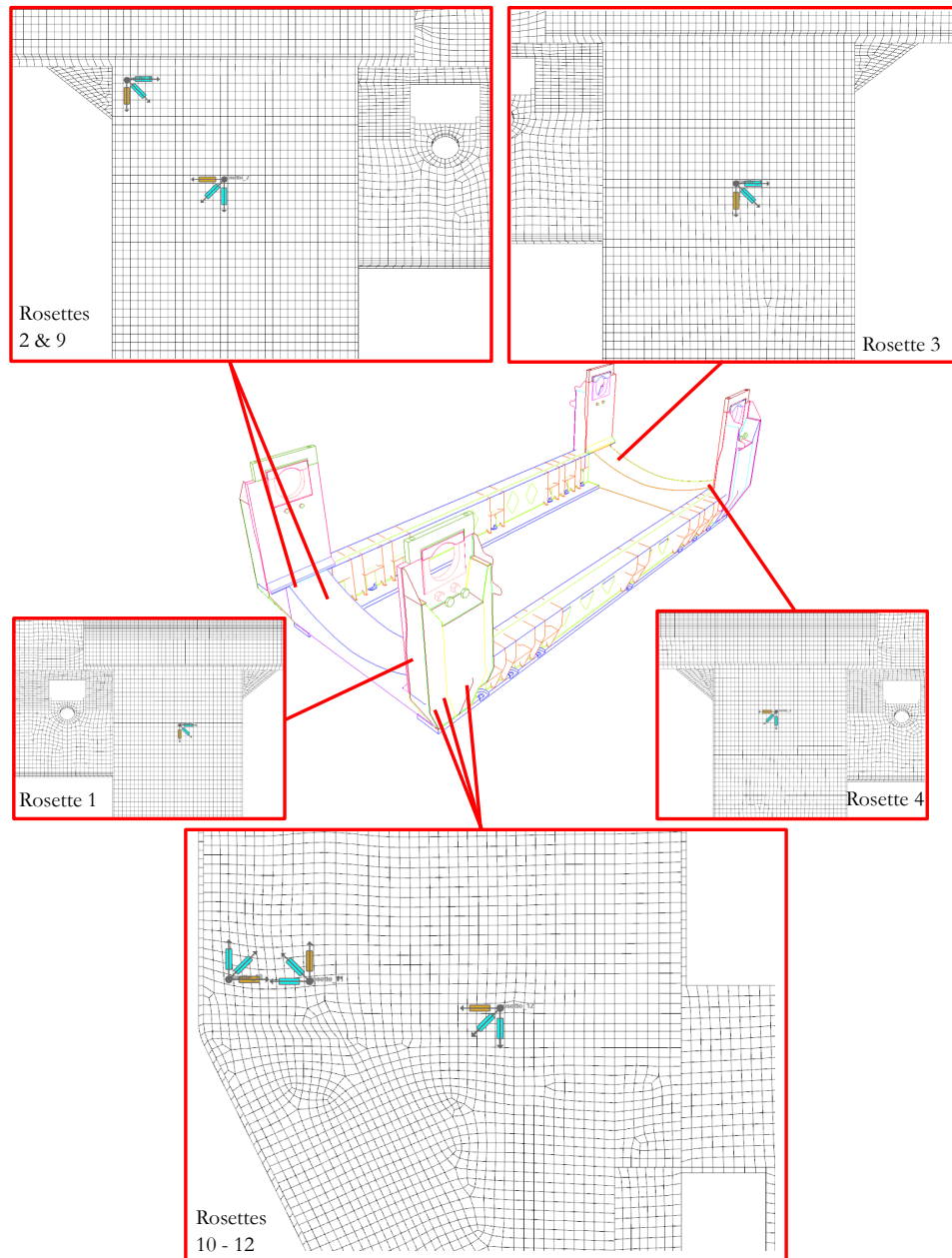


Figure 12. Locations and Orientations of the Virtual Strain Gauges

Nonlinear Effects during Longitudinal Loading

To assess the effects of using a tied contact at the "floating" lid end trunnion bushes, a half symmetry model was created for nonlinear analysis. The symmetry model retained five of the virtual strain gauge rosettes. The package was remodelled in brick elements with a refined mesh at the lateral restraint bolt contact areas and the trunnions (**Figure 13**).

Speckert published a method for calculating time histories on a rail vehicle ball joint based on a set of nonlinear analyses that represent various combinations of load direction and

magnitude¹³. Here a nonlinear analysis has been carried out to assess the contact effects of the trunnion bushes and lateral restraint bolts on the FEA results.

The analysis is run in two sequential load steps; the first to calculate a vertical preload due to gravity and also include the range of vertical loading. In the second step, a range of longitudinal loads have been prescribed, a matrix of runs is provided in **Table 3**. Consideration of the combined vertical and longitudinal load cases is necessary to obtain contact

Vertical	Load Cases - Longitudinal Acceleration [g]									
	Longitudinal					Longitudinal				
-1.32	-0.32	-0.27	-0.22	-0.17	-0.12	-0.07	-0.03	0.03	0.07	0.12
-1.0	-0.32	-0.27	-0.22	-0.17	-0.12	-0.07	-0.03	0.03	0.07	0.12
-0.74	-0.32	-0.27	-0.22	-0.17	-0.12	-0.07	-0.03	0.03	0.07	0.12

Table 3. Combination of Loading in Nonlinear Analysis

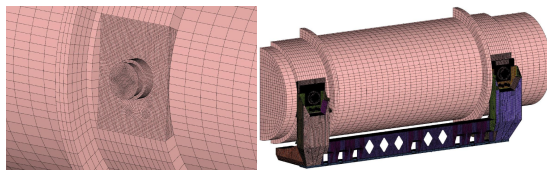


Figure 13. Detailed Mesh of Package Required for Nonlinear Studies

forces between the trunnion bushes, tie down and package that resist longitudinal motion.

The half symmetry model consisted of 414,535 elements and produced 1.7×10^6 degrees of freedom. A single model ran in approximately 1.5 hours on 8 CPUs and used 23 gigabytes of RAM. The 30 nonlinear runs were solved on a Linux server.

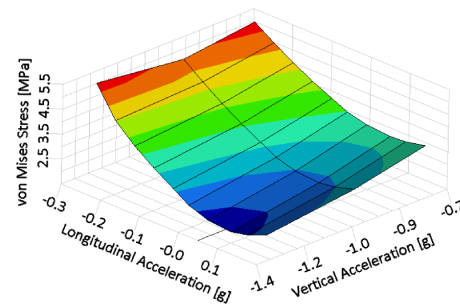
To reduce the overall solution time the first step was run only once per vertical load and a restarted analysis was then used to vary the longitudinal load cases. The line search method was used which provided additional computational efficiency. These techniques reduced the overall computation time from (an estimated) two days to approximately 5 hours. Both the pre and post processing were automated with a combination of shell scripts and HyperMath programming⁵.

Figure 14 shows that the von Mises stress response is nonlinear in the load space analysed (i.e. lateral acceleration set to zero). The predicted stresses are very low for all five of the virtual rosettes, which is in agreement with the strain measurements that did not appear to be influenced by longitudinal loading. The Finite Element results do demonstrate that nonlinearity is present and significant in this tie-down system, however it will have a diminishingly small effect on this study because of the negligible influence of longitudinal loading during the experiment.

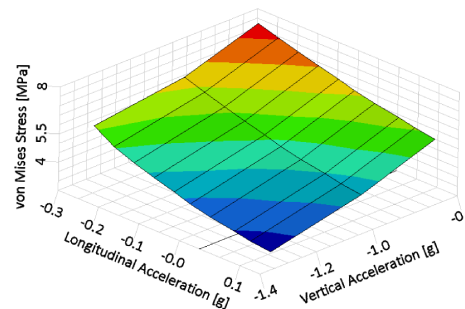
Nonlinear Effects during Lateral Loading

The half symmetry tie-down model and remodelled package were reflected and combined by merging the nodes on the symmetry plane to produce a complete FEA model for nonlinear analysis of lateral loading. The potential for nonlinear effects arising during lateral loading was considered to be independent of the other loading directions. This is because the contact pressure that develops between the lateral restraint bolts and the package side wall is not due to gravitational effects. This analysis was also carried out in two steps. Gravity was applied in the first step, to make the stresses comparable to the nonlinear longitudinal study and the results of this step were restarted for 10 lateral load cases in the range -0.23 g to 0.18 g.

Figure 15 provides a schematic to show the effects of the lateral restraint bolts contacting the package side wall



(a) Rosette 10



(b) Rosette 12

Figure 14. Example of von Mises Stress Results from Virtual Strain Gauges during Combined Longitudinal and Vertical Loading

during lateral loading. It is clear that the effective bending moment arm changes during load reversals, something that the linearised unit load model cannot account for.

At all the virtual strain gauges the von Mises stresses due to lateral loading are much larger than those predicted due to longitudinal loading.

The virtual strain gauges 10 - 12 are most likely to be effected by the bending response of the stanchion due to the presence of contact nonlinearity. (Figure 16) presents the results from rosette 10 and 12 for both the non-linear and unit load analyses.

The stress results called "Nonlinear contact opened" are due to positive lateral loads which cause the contact between the trunnion restraint bolts and package to open. Those called "Nonlinear contact closed" are due to negative lateral loads (or a reversal) that causes the gap between the trunnion restraint bolts and the package to close and contact pressure to develop. The unit load model results are called "Linear bonded", the lateral restraint bolts are effectively glued to the side wall of the package.

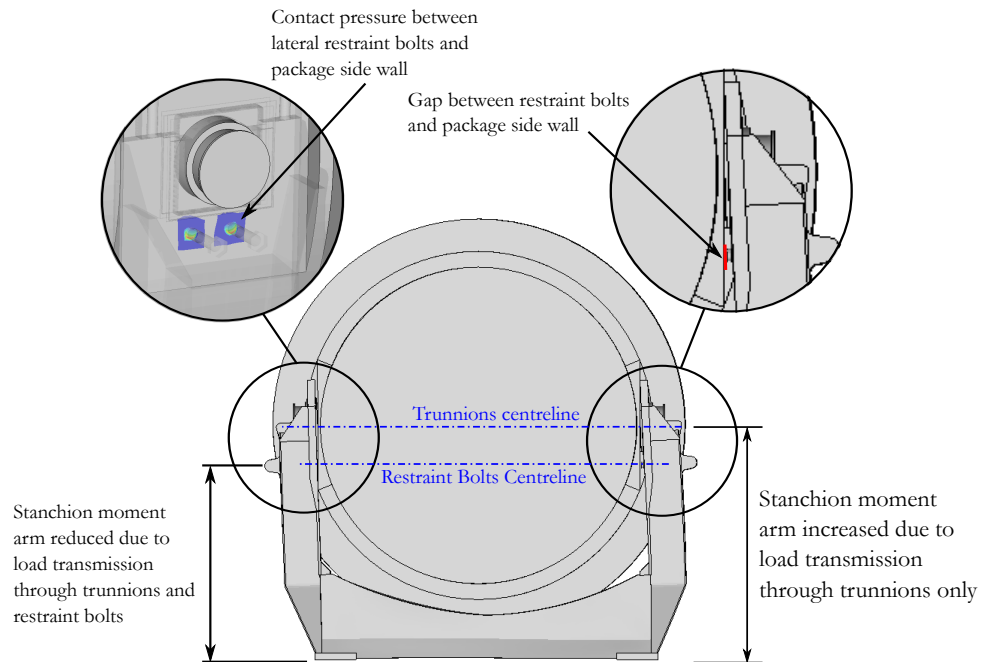


Figure 15. Sensitivity Analysis, Non-Linear Lateral Load Case to Assess the Effects of Discontinuous Contact Behaviour between the Package Side Walls and Tie-Down Lateral Restraint Bolts

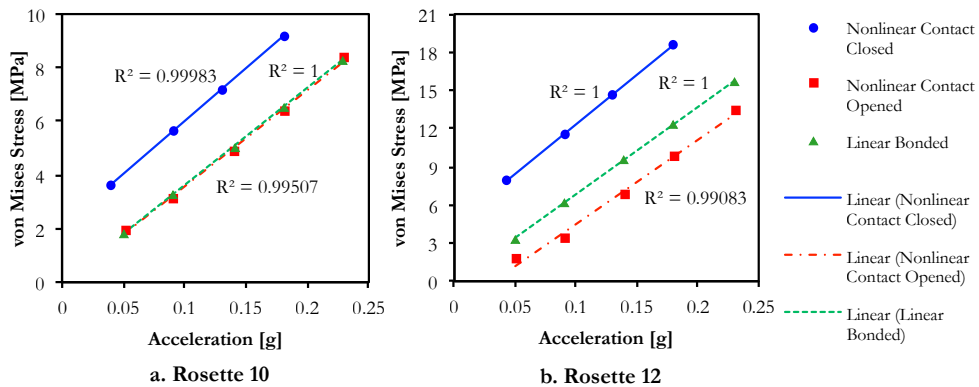


Figure 16. Sensitivity Analysis, Example of Nonlinear and Linear Load Case Stress Results from two Virtual Strain Gauges and a Linear Curve Fitting Trend Analysis which demonstrates the Linear Relationship between Increasing Lateral Load and Stress Response

The results are fitted with trend lines and their coefficient of determination is annotated. This provides a measure of how linear the stress response is to increased loading.

The R^2 values are all very close to 1, confirming the applicability of scaling the linear lateral results. Also the stresses due to the nonlinear load reversals tend to bound those from the linear model. The difference in all the stress results was small, so the unit load model was considered a suitable candidate for comparison with the experiment.

Vertical Load Application

The presence of gravity causes the load range to be offset by -1 g. When applying the unit load this has been neglected because during the experimental procedure the strains and

accelerations were measured during the loading of the package onto the tie down system and then zeroed prior to the journey. Therefore both positive and negative, measured vertical accelerations and tensile and compressive measured strains result from vertical loading.

The tensile strains due to vertical loading are offset by the compressive preload on the structure due to gravity. In reality the strains resulting from vertical loading will remain compressive unless a vertical acceleration > 1 g is experienced. If this does occur then the package is essentially weightless and the load path changes significantly. In this case the unit load model will not predict the load reversal correctly, however in the experiment the largest upwards, vertical acceleration was 0.26 g.

The direction of load applied to the model is also important as it changes the sign of the predicted stresses. It was necessary to account for this in the superposition procedure by pre-multiplying the acceleration time history by -1.0.

Correlation between Predicted and Measured Strains

For a quantitative assessment of the correlation between the measured and calculated strain time histories a script was written to calculate the correlation coefficient for each of the signals generated at different filter cutoff frequencies in HyperMath. The results are plotted as correlation coefficient vs filter cutoff frequency for each of the strain gauge rosettes (Figure 17).

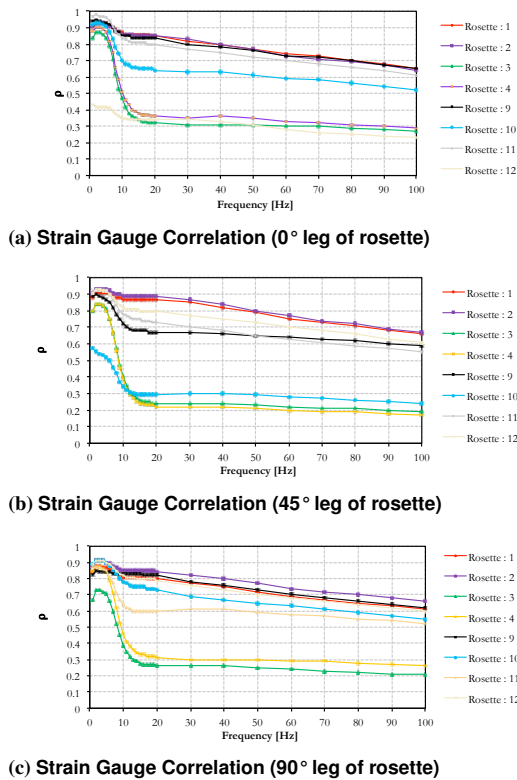


Figure 17. Preliminary Correlation Results

It is evident that a number of the channels produced poor agreement particularly at frequencies > 5 Hz. Visual examination of the signals with weak correlation indicated that some of the channels contained strain content <10] μmm/mm. These channels were discarded from any further processing because they were considered small enough to be structurally insignificant and also too small to be accurately represented by the finite element model. The remaining results were collated and are shown in Figure 18.

At filter cutoff frequencies < 5 Hz all the channels achieve at least moderate correlation (rho > 0.7) and in many cases strong correlation (rho > 0.9). Figure 18 shows that there are 2

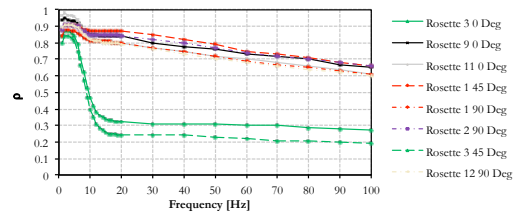


Figure 18. Correlation Results with Channels < 10 μ mm/mm Removed

channels that still produce very weak correlation > 5 Hz. The anomalous results were found on two legs of rosette 3 (the third leg was previously discarded due to low strains levels). This was the only rosette, in the collated results, that was situated at the lid end of the structure. Therefore rosette 3 was re-run using the acceleration time histories from a lid end accelerometer. This was the subject of further investigation discussed later. The final correlation results are shown in Figure 19.

Five of the eight channels display strong correlation between 2 Hz - 5 Hz. At frequencies above 5 Hz the correlation is moderate and constant between 10 - 20 Hz, rho ≈ 0.8. As the fc increases above 20 Hz the correlation becomes weaker.

Due to the large size of each time history, which contained 2 x 10^6 points, smooth scatter cross plots and time history slices have been used to provide a visual indication of the correlation (Figure 20)^14. Rosette 12 was selected for use in Figure 20 because it provided a typical example consistent with the results from the other virtual strain gauges. The most extreme outliers in the data are shown in the cross plots as small black points and a smoothing contour kernel used to blend the colours to distinguish densely populated areas of the cross plot from sparsely populated areas. The colour blue indicates the highest density of points and as the density decreases blue changes to red and then from red to white. The results indicate that as the fc is reduced the outliers become more clustered and the scatter reduces.

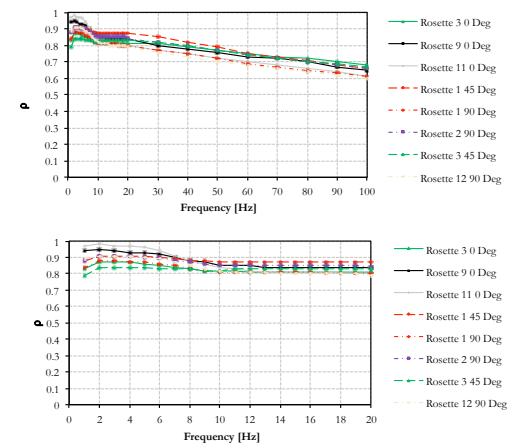


Figure 19. Final Correlation Results

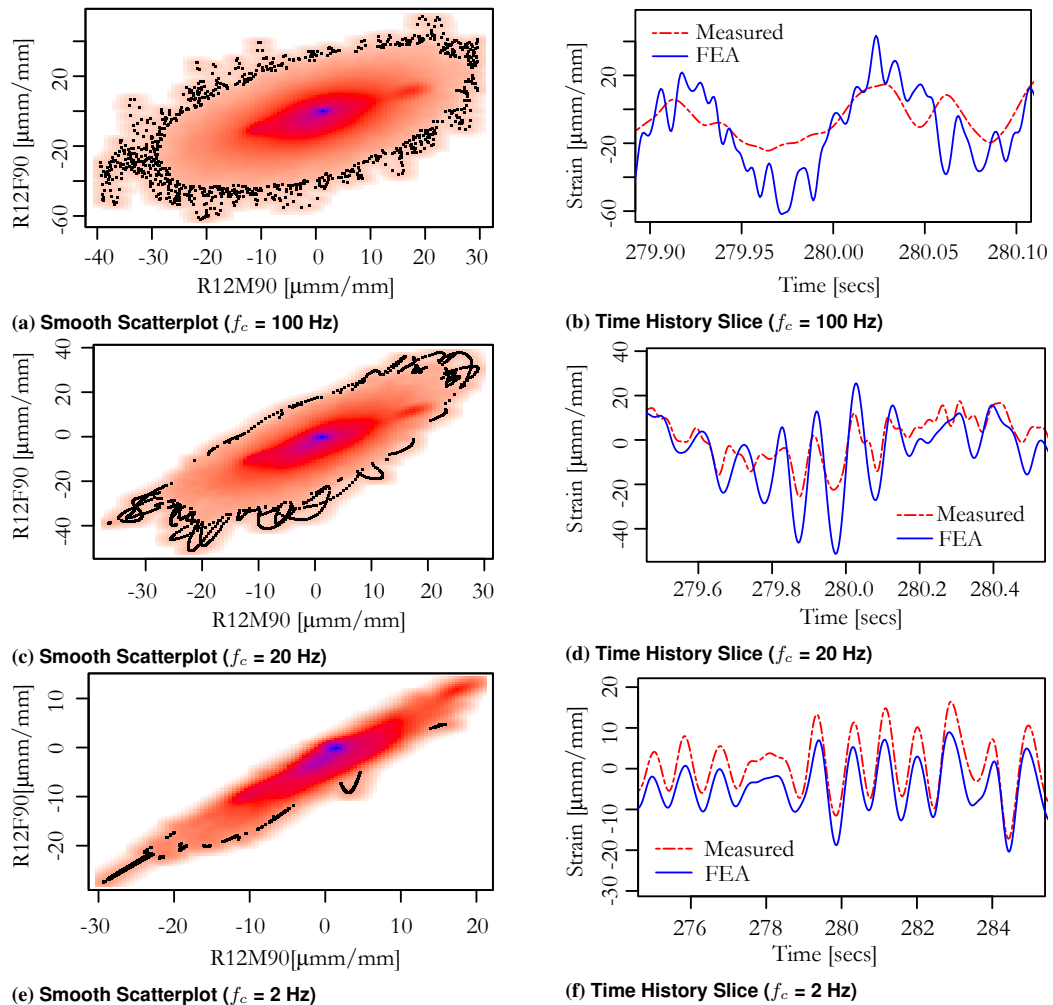


Figure 20. Effects of (f_c) on Correlation of Strain Gauge Rosette 12

The time history slices were produced by setting a time window that displayed approximately 10 cycles based on the f_c . Several different starting points were analysed, here an example is shown at 280 seconds that illustrates the effects of the filters in the time domain. The weak correlation obtained with $f_c = 100$ Hz is characterised by small high frequency oscillations in the FEA strains which arise due to the noisy acceleration measurements at high frequency.

The weakest correlation was found on rosette 12, filtered at 100 Hz, $\rho = 0.6$ (Figures 20a & 20b). Moderate correlation was achieved on rosette 12, filtered at 20 Hz, $\rho = 0.79$ (Figures 20c & 20d). Very strong correlation was achieved on rosette 12, filtered at 2 Hz, $\rho = 0.91$ (Figures 20e & 20f). The strongest correlation achieved was $\rho = 0.98$ on Rosette 11.

Analysis of Residuals

The residuals between the correlated and measured time histories have been compared using spectral analysis and

autocorrelation functions. All computations were carried out using the open source, high level interpreted language GNU Octave and verified with the commercial software nCode Glyphworks^{12,15}.

Initially the PSDs of the measured and predicted signals were overlaid. This pinpoints which frequencies match between experiment and analysis. To quantify the level of agreement the residuals were calculated by subtracting corresponding measured time histories from those predicted. The residual PSDs were included as a third overlaid plot. An example is shown in log-log axes over the full frequency range for the 90° leg of rosette 12, Figure 21. The same PSD is also plotted on linear axes over the narrower frequency range of 0 - 30 Hz (Figure 22).

The results indicate that the predicted and measured strain PSDs are similar at frequencies < 40 Hz. At frequencies > 40 Hz the predicted strains are significantly over predicted.

To verify these results autocorrelation functions have been used. The autocorrelation function (ACF) calculates

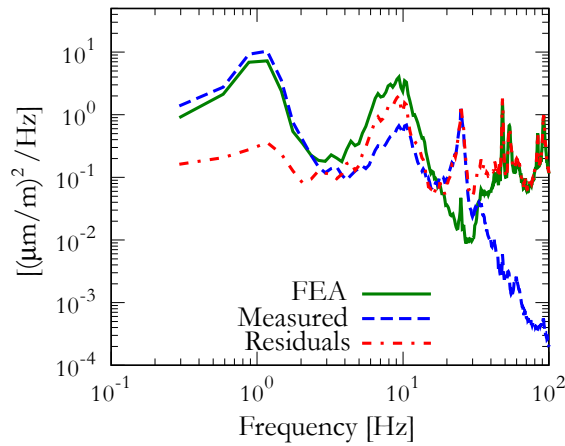


Figure 21. Comparison between Predicted and Measured Strain Time Histories, Converted into PSDs, Log-Log Scale, Full Bandwidth

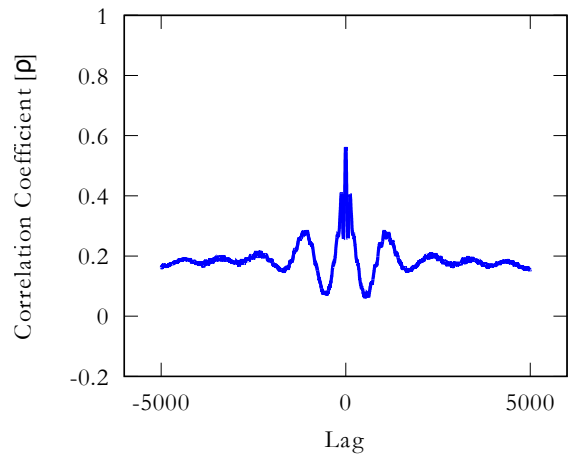


Figure 23. Correlogram of the Measured Strain Signal from the 90° Leg of Rosette 12

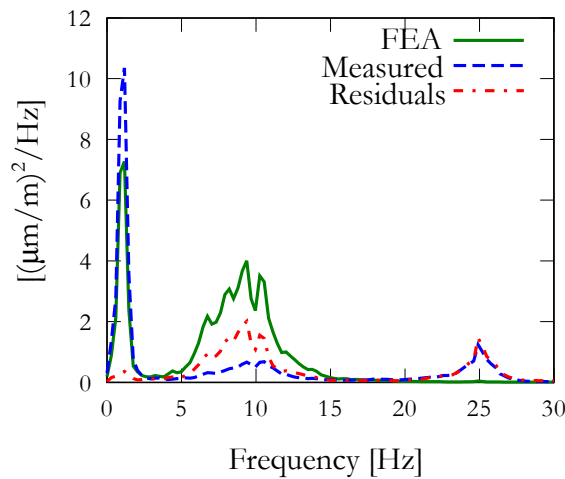


Figure 22. Comparison between Predicted and Measured Strain Time Histories, Converted into PSDs, 0 - 25 Hz

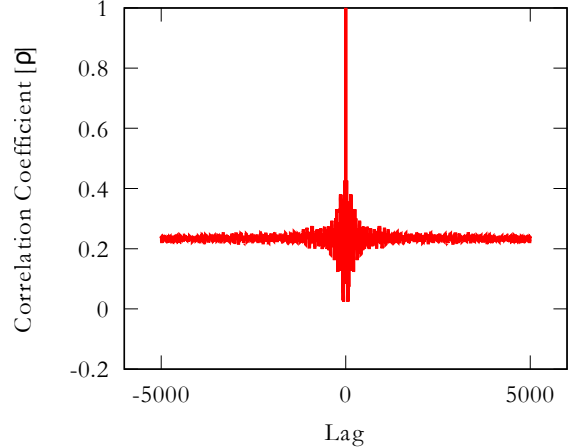


Figure 24. Correlogram of the Residuals between the Measured and Predicted Strain Signal from the 90° Leg of Rosette 12

the correlation coefficient, ρ , of the signal by continuously shifting the signal relative to itself to build a plot of ρ vs lag, called the correlogram. An ACF has been calculated for each correlated, measured strain signal and also for each residual time history.

Figures 23 & 24 show correlograms from the measured strains of the 90° leg of rosette 12 and the residuals. The correlogram of the measurements possesses a narrow band signature, which is due to the peak between 0 - 3.5 Hz. The residuals on the other hand tend towards a white noise signature, demonstrating that the model successfully predicts the dominant trend in the measured strains.

Discussion

Data for fatigue load cases are currently in shortage for tie down design. This is due to the wide variation of packages and transport systems, difficulties in collecting experimental data and limited usage schedules. The type of data presented

here is ideal for fatigue assessments, but larger measured strains would be necessary to calculate fatigue life and perform comparative fatigue analysis. A rainflow cycle count of the acceleration signals would produce conservative data for fatigue load cases by selecting a low pass filter cutoff frequency > 3.5 Hz.

A dynamic model would be more suitable for predicting response > 3.5 Hz. The results of this study have shown that the small strains at higher frequencies are unlikely to cause fatigue damage and therefore no attempt to produce a dynamic model has been made.

Examining the lower frequency range more closely it is clear that the agreement between 0 - 3.5 Hz is very good. In the range 3.5 Hz - 15 Hz the predicted energy content in the strain signals is higher than in the measured signals. This concurs with expectations; a linear static model is only really suited to predicting very low frequencies.

To improve agreement the linear scaling and superposition procedure could be adapted to handle contact nonlinearities.

One method to achieve this is to fit polynomial response functions of finite element stresses at each rosette location, based on a set of nonlinear analysis results that consider the measured load ranges and various combinations of loading. The scaling can then proceed by calculation of the strain time histories based on the fitted polynomials.

The analysis showed that the mean square of the signals were often underpredicted at very low frequencies, possibly as a result of the chosen finite element discretization size. However at frequencies greater than 3.5 Hz treating measured accelerations as quasi-static tends to overpredict the spectral content and therefore the fatigue damage and peaks. This is attributed to the large inertia of the package which attenuates any high frequency strain response.

At higher frequencies the acceleration response measured nearest the package is also attenuated, this model demonstrates that a linear relationship between measured accelerations and strains does not exist at higher frequencies, i.e. the linear model tends to overpredict higher frequencies strains because it does not include inertial dynamic effects.

Conclusions

- A linear static FEM of a tie down system of a 99.7 tonne nuclear package has been successfully validated using strain and acceleration measurements with weak signal content.
- It was demonstrated that at least moderate correlation can be achieved with a properly prepared, linear static FEM.
- Spectral and residual analysis highlighted that the dominant source of loading occurred as a narrow band process between 0 - 3.5 Hz and the FEM correlation was strong at these frequencies.
- This level of agreement between FEA and a field experiment, which is highly uncontrollable, is very satisfactory.

References

1. Cummings AD, Krywonos J, Purcell P et al. "Filtering and Analysis of Accelerations and Strains Measured on a Tie Down System of a Heavy Nuclear Transport Package during a Routine Rail Journey". *Packaging, Transport, Storage & Security of Radioactive Material* 2013; 24(1): 23–35. DOI:10.1179/1746510913Y.0000000027. URL <http://www.maneyonline.com/doi/full/10.1179/1746510913Y.0000000027>.
2. Wirsching PH, Paez TL and Ortiz K. "Random Vibrations: Theory and Practice". Mineola, NY: Dover Publications Inc., 2006. ISBN 9780486450155.
3. Bendat JS and Piersol AG. "Random Data: Analysis and Measurement Procedures". 4th edition edition ed. Wiley-Blackwell, 2010. ISBN 9780470248775.
4. BS EN 15433-3:2007 "Transportation Loads - Measurements and Evaluation of Dynamic Mechanical Loads - Part 3: Data Validity Check and Data Editing for Evaluation". BSI Standards Limited, 2007.
5. Altair. Hyperworks 12.0.
6. Systemes D. Abaqus 6.13.
7. BS EN 10025-6:2004 "Hot rolled products of structural steels Technical Delivery Conditions for Flat Products of High Strength Structural Steels in Quenched and Tempered Condition". BSI Standards Limited, 2004.
8. Carvill J. "Mechanical Engineers Data Handbook". Butterworth-Heinemann, 2012.
9. BS EN ISO 898-1:2013 "Mechanical Properties of Fasteners made of Carbon Steel". BSI Standards Limited, 2013.
10. Lee YL. "Metal Fatigue Analysis Handbook: Practical Problem-solving Techniques for Computer-aided Engineering". Butterworth-Heinemann, 2011. ISBN 9780323165006.
11. Heyes P, Dakin J and StJohn C. The Assessment and Use of Linear Static FE Stress Analyses for Durability Calculations. In *9th International Conference on Vehicle Structural Mechanics and CAE*. Warrendale, PA: SAE International. URL <http://papers.sae.org/951101/>.
12. nCode H. Design Life 9.1.
13. Speckert M. "Calculation of Stress Time Signals of Multi Bolted Joints Located at a Ball Joint of a Railway Vehicle". Technical report, Idealisation of Bolted Joints, NAFEMS, 2010.
14. Team RC. "R: A Language and Environment for Statistical Computing. R Foundation for Statistical Computing", 2014. URL <http://www.R-project.org/>.
15. Eaton JW, Bateman D and Hauberg S. *GNU Octave version 3.0.1 manual: a high-level interactive language for numerical computations*. CreateSpace Independent Publishing Platform, 2009. URL <http://www.gnu.org/software/octave/doc/interpreter>. ISBN 1441413006.